

Multiple-inlet Building Integrated Photovoltaics: Modeling and Design including Wind Effects

Efstratios-Dimitrios Rounis

A Thesis

In the Department

of

Building, Civil and Environmental Engineering

Presented in Partial Fulfillment of the Requirements

for the Degree of Master of Applied Science (Building Engineering) at

Concordia University

Montreal, Quebec, Canada

September 2015

© Efstratios Dimitrios Rounis, 2015

CONCORDIA UNIVERSITY
School of Graduate Studies

This is to certify that this thesis prepared

By: Efstratios Dimitrios Rounis

Entitled: Multiple-inlet Building Integrated Photovoltaics: Modeling and Design including Wind Effects

and submitted in partial fulfillment the requirements for the degree of

Master of Applied Science (Building Engineering)

complies with the regulations of the University and meets the accepted standards with respect to originality and quality.

Signed by the final Examining Committee:

<u>Dr. L. Wang</u>	Chair
<u>Dr. G. Vatisas</u>	Examiner External (to program)
<u>Dr. H. Gue</u>	Examiner
<u>Dr. A. Athienitis</u>	Supervisor
<u>Dr. T. Stathopoulos</u>	Supervisor

Approved by _____
Chair of Department or Graduate Program Director

Dean of Faculty

Date _____

Abstract

Multiple-inlet Building Integrated Photovoltaics: Modeling and Design including Wind Effects

Efstratios Dimitrios Rounis

Air-based, open loop Building Integrated Photovoltaic/Thermal (BIPV/T) systems have proven to be an efficient means for generating renewable energy. They produce electrical energy, converting part of the incident solar radiation, and recover part of that radiation that turns to heat, while acting as the outer shell of the building. However, for the typical BIPV/T design with air entering at the bottom of the installation, flowing within a continuous air channel and exiting at the outlet of the system high PV temperatures may still occur. This is due to the fact that as air moves inside the air channel it accumulates heat and the heat exchange efficiency between the PV panels and the flowing air drops along the flow path of the air channel. In large building integrated PV installations, high PV temperatures may lead to quicker PV panel degradation, as well as lower electrical efficiency.

A multiple-inlet BIPV/T system aims to increased heat extraction from the PV panels, with the introduction of several intakes of fresh air along the height of the installation. This may lead to lower and more uniform PV temperatures, enhanced PV panel durability and higher electrical and thermal performance.

This study presents the development of a methodology for the modelling and design of multiple-inlet systems, as well as a numerical study of such a system. The modelling component consists of two aspects, namely, the fluid mechanics and the energy balance of the system. A flow model was developed, based on flow networking techniques, in order to assess the inlet flow distributions. The flow model incorporates wind effects in the form of exterior pressures, acquired through wind tunnel testing. The inlet flow distributions were used in a modified energy balance model that accounts for the flow conditions of the inlets and the air channels of the system. This was an improvement on the assumption of uniform flow from all the openings of the system, which has been common in the limited number of studies of multiple-inlet systems so far.

The developed models were applied for the numerical investigation of variations of multiple-inlet BIPV/T systems for a potential retrofit project on an office building in Montreal. The

investigation was carried out assuming summer and winter conditions, as well as several cases of wind direction and velocity. A multiple-inlet system with optimized geometric features of the inlets was found have up to 1% higher electrical efficiency and 14% to 25% higher thermal efficiency than that of a single-inlet system, also resulting in lower and more uniform PV operating temperatures. The latter can be a crucial factor for the durability of large building integrated PV installations.

Acknowledgements

I would like to express my utmost gratitude to my supervisors, Dr. Andreas Athienitis and Dr. Theodore Stathopoulos, first of all for giving me the opportunity to work with them and for their expert guidance throughout this effort.

I made great friends of my office colleagues, from whom I had great help during various stages of my time at Concordia. Dear tenants of EV.16.117, thank you all. A special thanks to my friend Sam Yip, who took the time and effort to review my thesis.

I would like to acknowledge the financial support from the NSERC/Hydro Quebec Research Chair and the faculty of Engineering, as well as the scholarship awarded by Concordia University. I would also like to thank Joe Hrib for his technical support and sharp wit in times of distress.

Starting my graduate studies at Concordia University would not have been possible without the support from my family in Greece. I also owe a lot to my exquisite Professors from Democritus University of Thrace, Dr. Minas Papadopoulos and Dr. Konstantinos Chalioris for their encouragement and support.

Most importantly, I would like to thank my wonderful Christina for her endless love and motivation. This one goes to you.

Table of Contents

List of Figures	viii
List of Tables	xi
Nomenclature	xii
1. Introduction	1
1.1 Overview	1
1.2 Solar technologies	2
1.3 Building-integrated solar technologies	2
1.4 Multiple-inlet Building-Integrated Photovoltaic/Thermal systems.....	3
1.5 Purpose of this investigation.....	4
1.6 Thesis Outline	4
2. Literature review.....	6
2.1 BIPV/T	6
2.2 BIPV/T modelling.....	9
2.3 Thermal efficiency enhancement	14
2.4 Multiple-inlet BIPV/T.....	17
2.5 Flow modelling	22
2.5.1 Forced flow in single inlet systems.....	22
2.5.2 Natural ventilation in single inlet systems	23
2.6 Multiple-inlet flow network modelling.....	25
2.6.1 Flow networks.....	26
2.6.2 Resistance approach and the Hardy Cross method	28
2.7 Wind effects on solar collectors.....	35
3. Experimental procedure	39
3.1 Multiple-inlet BIPV/T concept and initial design.....	39
3.2 Solar Simulator testing.....	40
3.3 Wind tunnel testing	41
3.3.1 Concordia University Boundary Layer Wind Tunnel	42
3.3.2 Wind tunnel model.....	43
3.3.3 Experimental results and discussion	45
4. Multiple-inlet BIPV/T modelling.....	49
4.1 Flow distribution model.....	49

4.1.1 Pressure drops	51
4.1.2 Frictional and secondary losses.....	52
4.1.3 Electrical analogy.....	53
4.1.4 Solution matrix.....	54
4.2 Wind effects and energy balance	56
4.2.1 Flow distributions due to wind effects	56
4.2.2 Measured and simulated results	57
4.3 Modified energy balance model.....	58
4.3.1. Positive channel flow (towards the air collector).....	60
4.3.2. Negative channel flow (reversed flow).....	62
4.4 Modelling assumptions	64
5. Simulations and results	66
5.1 Systems considered.....	66
5.2 Numerical procedure.....	69
5.3 Results and discussion	71
5.3.1 Flow modelling.....	71
5.3.2 Energy balance.....	77
6. Summary and conclusions	91
6.1 Contributions.....	92
6.2 Future work.....	93
REFERENCES	94
APPENDIX I Flow distribution and PV temperatures of the optimized multiple-inlet systems (Systems V and VI)	100

List of Figures

Figure 2.1: The Eco Terra house (Chen, 2009).	8
Figure 2.2: BIPV/T system of the JMSB Building, Concordia University.	9
Figure 2.3: Air based BIPV/T basic components: PV layer, air channel and back wall with insulation.	10
Figure 2.4: BIPV/T energy balance.	10
Figure 2.5: Single pass PV/T configurations (Hegazy, 1999).	14
Figure 2.6: Double pass PV/T configurations (Hegazy, 1999).	15
Figure 2.7: Plot of daily overall collector efficiency with respect to mass flow rate of the PV/T configurations studied by Hegazy (1999).	16
Figure 2.8: Cross sectional view of PVT/Air collector models studied by Tonui & Tripanagnostopoulos (2006).	16
Figure 2.9: Hybrid UTC-PV/T system installed at Concordia University (Athienitis et al, 2010).	18
Figure 2.10: UTC and BIPV/T equivalent efficiency versus mass flow rate (Athienitis et al, 2010).	19
Figure 2.11: Two-inlet BIPV/T system connected in series with glazed air collector (Yang et al, 2014).	20
Figure 2.12: Stepped roof BIPV/T configuration studied by Mizraei (2014).	21
Figure 2.13: Box double-skin façade with multiple openings (Lou et al, 2012).	27
Figure 2.14: Strip type DSF with multiple venting holes in the zonal approach (Lou et al, 2012).	28
Figure 2.15: Typical loop formation analyzed by the Hardy Cross method.	30
Figure 2.16: Example of a 3 x 3 set of pipe junctions connected to form a pipe network (Dymond & Kutscher, 1996).	32
Figure 2.17: Example of a loop of the pipe network (Dymond & Kutscher, 1996).	34
Figure 2.18: Convective heat transfer-wind velocity relations for vertical building surfaces (Vasan, 2014).	36
Figure 2.19: Wind tunnel mean pressure coefficients ($C_{p_{mean}}$) distribution over a solar panel scaled 1:20 (Aly & Bitsuamlak, 2013).	7
Figure 3.1: 3-inlet BIPV/T prototype tested at Concordia University Solar Simulator.	40
Figure 3.2: 3-inlet BIPV/T prototype tested at Concordia University Solar Simulator (dimensions in mm).	40
Figure 3.3: The Montreal Courthouse (left) and its orientation (right).	42
Figure 3.4: Schematic of the boundary layer wind tunnel at Concordia University (Stathopoulos, 1984).	43
Figure 3.5: 1:400 scale model of the Courthouse building made by 3D printer.	43
Figure 3.6: Face with pressure taps of the wind tunnel model.	44

Figure 3.7: Building orientation, wind diagram for Montreal and wind directions tested.	44
Figure 3.8: Mean pressure coefficient (C_{P_mean}) for 0° wind direction (top) and wind tunnel model placement (bottom).	45
Figure 3.9: Mean pressure coefficient (C_{P_mean}) for 45° wind direction (top) and wind tunnel model placement (bottom).	46
Figure 3.10: Mean pressure coefficient (C_{P_mean}) for 90° wind direction (top) and wind tunnel model placement (bottom).	46
Figure 3.11: Mean pressure coefficient (C_{P_mean}) for 135° wind direction (top) and wind tunnel model placement (bottom).	46
Figure 3.12: Mean pressure coefficient (C_{P_mean}) for 180° wind direction (top) and wind tunnel model placement (bottom).	47
Figure 4.1: Resistance-circuit representation of the flow network of the multiple-inlet system.	50
Figure 4.2: Possible flow paths for the inlets and channels of the multiple-inlet system.	57
Figure 4.3: Normalized mass flows at the back of each panel of the 3-inlet prototype, for three angles of placement in the solar simulator.	58
Figure 4.4: BIPV/T control volume energy balance.	59
Figure 4.5: Multiple-inlet BIPV/T control volume energy balance.	60
Figure 4.6: Positive channel flow with positive flow from the previous channel and positive inlet flow.	60
Figure 4.7: Positive channel flow with negative (reverse) flow from the previous channel and positive inlet flow.	61
Figure 4.8: Positive channel flow with positive flow from the previous channel and negative inlet flow (outflow).	62
Figure 4.9: Negative (reverse) channel flow with negative (reverse) flow from the next channel and positive flow from the next inlet.	63
Figure 4.10: Negative (reverse) channel flow with positive flow from the next channel and positive flow from the next inlet.	63
Figure 4.11: Negative (reverse) channel flow with negative flow from the next channel and negative flow from the next inlet (outflow).	64
Figure 5.1: System I: Single inlet system with channel gap size: 0.1m.	67
Figure 5.2: System II: Single inlet system with channel gap size: 0.15m.	67
Figure 5.3: System III: Multiple-inlet system with equally sized inlets (1% of the PV module area) and channel gap size of 0.1m.	67
Figure 5.4: System IV: Multiple-inlet system with equally sized inlets (1% of the PV module area) and channel gap size of 0.15m.	68

Figure 5.5: System V: Multiple-inlet system with optimized inlets (porosities as shown in Table 5.1) and channel gap size of 0.1m.	68
Figure 5.6: System VI: Multiple-inlet system with optimized inlets (porosities as shown in Table 5.1) and channel gap size of 0.15m.	68
Figure 5.7: Maximum daily PV temperatures for Systems I and II (single inlet) for summer conditions at total air mass flow rate of 400 kg/h and 800 kg/h.	78
Figure 5.8: Maximum daily PV temperatures for Systems I and II (single inlet) for winter conditions at total air mass flow rate of 400 kg/h and 800 kg/h.	79
Figure 5.9: Maximum daily PV temperatures for Systems III and IV (multiple-inlet, equal inlets) for summer conditions at total air mass flow rate of 400 kg/h and 800 kg/h.	80
Figure 5.10: Maximum daily PV temperatures for Systems III and IV (multiple-inlet, equal inlets) for winter conditions at total air mass flow rate of 400 kg/h and 800 kg/h.	81
Figure 5.11: Maximum daily PV temperatures for Systems III and IV (multiple-inlet, optimized inlets) for summer conditions at total air mass flow rate of 400 kg/h and 800 kg/h.	82
Figure 5.12: Maximum daily PV temperatures for Systems III and IV (multiple-inlet, optimized inlets) for winter conditions at total air mass flow rate of 400kg/h and 800 kg/h.	83
Figure 5.13: Maximum daily PV temperatures comparison for all systems, for summer conditions and 0m/s, 1m/s and 2m/s wind velocities at total air mass flow rate of 400kg/h and 800kg/h.	85
Figure 5.14: Maximum daily PV temperatures comparison for all systems, for winter conditions and 0m/s, 1m/s and 2m/s wind velocities at total air mass flow rate of 400 kg/h and 800kg/h.	86
Figure 5.15: Electrical efficiency of the six systems for summer and winter conditions, with or without wind and at total air mass flow rate of 400 kg/h and 800 kg/h.	88
Figure 5.16: Combined electrical and thermal efficiency of the six systems for summer and winter conditions, with or without wind and at total air mass flow rate of 400 kg/h and 800 kg/h.	89

List of Tables

Table 5.1: Inlet porosities for the optimized multiple-inlet systems.	69
Table 5.2: Flow distributions of the multiple-inlet systems at no wind conditions, for total mass flow rates of 400kg/h and 800kg/h.	71
Table 5.3: Inlet flow rate distributions for System III (equal inlets, gap: 0.1m), with or without wind.	73
Table 5.4: Inlet flow rate distributions for System IV (equal inlets, gap: 0.15m), with or without wind.	73
Table 5.5: Inlet flow rate distributions for System IV (optimized inlets, gap: 0.1m), with or without wind.	74
Table 5.6: Inlet flow rate distributions for System VI (optimized inlets, gap: 0.15m), with or without wind.	74
Table 5.7: Flow distributions and PV temperatures for 45°, 2m/s wind for windward edge PV string of System V.	76
Table 5.8: Flow distributions and PV temperatures for 45°, 2m/s wind for windward edge PV string of System VI.	76

Nomenclature

Symbols

A	Orifice area (m^2)
A_I	cross-sectional area of the DSF cavity (m^2)
A_E	effective flow area of the opening (m^2)
A_{face}	collector section area (m^2)
c_p	Specific heat of air ($\text{J/kg}\cdot^\circ\text{C}$)
C	Flow coefficient ($\text{m}^3/\text{s Pa}^n$)
C_D	Discharge coefficient for the orifice
C_p	Pressure coefficient
C_{pe}	External pressure coefficient
C_{PEj}	External pressure coefficient of the j-th cell
C_{pi}	Internal pressure coefficient
C_{PIj}	Internal pressure coefficient of the j-th cell
$C_{P\text{mean}}$	Mean pressure coefficient
D	BIPV/T air channel depth (m)
D_h	Hydraulic diameter (m)
f	The Darcy friction factor
g	Gravitational constant (9.81 m/s^2)
h	Convective heat transfer coefficient ($\text{W/m}^2\cdot^\circ\text{C}$)
h_{c1}	Convective heat transfer coefficient for the PV layer ($\text{W/m}^2\cdot^\circ\text{C}$)
h_{c2}	Convective heat transfer coefficient for the insulation layer ($\text{W/m}^2\cdot^\circ\text{C}$)
h_f	Head loss (m)
h_o	Exterior film coefficient (combined radiation and convection) ($\text{W/m}^2\cdot^\circ\text{C}$)

h_{rad}	Radiative heat transfer coefficient ($\text{W}/\text{m}^2 \cdot ^\circ\text{C}$)
h_{y_pipe}	Length of y-directional pipe (m)
h_w	Wind induced heat transfer coefficient ($\text{W}/\text{m}^2 \cdot ^\circ\text{C}$)
I	Electric current (A)
I_{incident}	Solar radiation incident on the BIPV/T surface (W)
k	Thermal conductivity of air ($\text{W}/(\text{m} \cdot ^\circ\text{C})$)
k'	Head loss per unit flow ($\text{s}^n/\text{m}^{3n-1}$)
K	Local loss coefficient for flow through an orifice
K'	Coefficient for pressure drop ($\text{kg}/\text{m}^4 \cdot \text{s}$)
K'_{absorber}	Coefficient for pressure drop across the absorber ($\text{kg}/\text{m}^4 \cdot \text{s}$)
L	Characteristic length of the flow (m)
m	Mass flow rate (kg/h)
M	Mass flow rate of the air collector (kg/h)
n	Flow exponent
Nu	Nusselt number
Nu_{top}	Nusselt number for the top part of the air collector
Nu_{bottom}	Nusselt number for the bottom part of the air collector
P	Pressure (Pa)
P_e	Wind induced external static pressure (Pa)
P_i	Wind induced internal static pressure (Pa)
P_p	Fan power (W)
Pr	Prandtl number
P_s	Surface pressure (Pa)
Q	Volumetric flow rate (m^3/s)
Q_{channel}	Air channel volumetric flow (m^3/s)

$Q_{\text{extracted}}$	Thermal energy extracted from the PV panels (W)
Q_{face}	Flow through the collector (m^3/s)
Q_i	Flow through the i-th branch (m^3/s)
Q_{inlet}	Inlet volumetric flow (m^3/s)
Q_j^E	Flow through the j-th hole (m^3/s)
Q_j^I	Flow through the j-th cell (m^3/s)
$Q_{j,j+1}^I$	Flow from j-th cell to (j+1)-th cell (m^3/s)
R	Electrical resistance (Ω)
R'	Airflow resistance (kg/m^7)
R_{channel}	Channel flow resistance ($\text{kg}/(\text{m}^4 \cdot \text{s})$)
Re	Reynolds number
R_{eq}	Equivalent resistance (Ω)
R_{inlet}	Inlet flow resistance ($\text{kg}/(\text{m}^4 \cdot \text{s})$)
S_{PV}	Radiation absorbed by the PV layer (W)
T_i	Entrance air temperature ($^{\circ}\text{C}$)
T_{ins}	Temperature of the insulation on the back wall of the BIPV/T ($^{\circ}\text{C}$)
T_{ma}	Temperature of air inside the BIPV/T air channel ($^{\circ}\text{C}$)
T_o	External temperature ($^{\circ}\text{C}$)
T_{PV}	Temperature of the PV module ($^{\circ}\text{C}$)
T_R	Temperature of the adjacent room to the BIPV/T ($^{\circ}\text{C}$)
T_{STC}	PV module cell temperature at standard testing conditions ($^{\circ}\text{C}$)
V	Fluid average velocity (m/s)
V_G	Wind velocity at gradient height (m/s)
V_{loc}	Wind velocity at the height of measurements (m/s)
V_Z	Mean wind velocity at height Z (m/s)

Z	Reference height for wind velocity (m)
Z_G	Gradient height (m)

Greek Letters

β_{PV}	PV module temperature coefficient
δ	absorber porosity
$\Delta\rho$	Density difference (kg/m^3)
ΔP	Pressure drop (Pa)
$\Delta P_{\text{absorber}}$	Pressure drop across the absorber (Pa)
$\Delta P_{\text{buoyancy}}$	Pressure drop due to buoyancy (Pa)
ΔT	Temperature difference ($^{\circ}\text{C}$)
η_{PV_theo}	PV module theoretical electrical efficiency (%)
η_{stc}	PV module efficiency at standard test conditions (%)
η_{thermal}	Thermal efficiency of the collector (%)
μ	Air dynamic viscosity ($\text{kg}/(\text{m}\cdot\text{s})$)
ν	Air kinematic viscosity (m^2/s)
ρ	Air density (kg/m^3)
ρ_{ambient}	Ambient air density (kg/m^3)
ρ_{y_pipe}	Air density in the y-directional pipe (kg/m^3)

Abbreviations

BIPV	Building Integrated Photovoltaic
BIPV/T	Building Integrated Photovoltaic/Thermal
CFD	Computational Fluid Dynamics
CHTC	Convective Heat Transfer Coefficient

COP	Coefficient of Performance for heat pump
DSF	Double Skin Façade
HVAC	Heating, Ventilation and Air Conditioning
PV	Photovoltaic
STC	Standard Testing Conditions
STPV	Semi Transparent Photovoltaic
UTC	Unglazed Transpired Collector

1. Introduction

1.1 Overview

The need for sustainable technologies has become more than a reality in recent years. The established methods of energy production are based on limited resources (fossil fuels, nuclear) and have byproducts that are hazardous for the environment and human health. A pursuit to replace these methods with resources that are “cleaner” as well as limitless has been ongoing during the last decades and is most prominent nowadays.

Resources such as solar and wind energy, hydropower and geothermal energy are essentially inexhaustible, while posing minimal environmental or health threat. According to the Global Status Report for Renewables of 2014, a growing number of cities, states and regions, such as Djibouti, Scotland, have set goals for 100% transition to renewable energy by the year 2020, while many regions in Germany have already achieved this goal. Denmark banned the use of fossil fuel-fired boilers in 2013 with an aim for renewables to provide approximately 40% of the total heat supply by 2020.

Buildings are high energy consumers. In Canada residential and commercial buildings account for 30% of total energy consumption (NRCan, 2015), while in the United States and Europe the corresponding percentage exceeds 40% (US Energy Information Administration, Balaras et al, 2007). In all cases, the amount of energy used for space heating is about half of the total building energy requirements.

Building codes started including energy efficiency standards in late ‘60s, however, in recent years these have become stricter, lowering the threshold of power consumption per unit area, while providing incentives for energy efficiency through characterization and certification of the buildings. Most energy efficiency requirements in building codes have followed local, state or national standards, however, according to the IEA information paper on energy efficiency requirements and policies in building codes, during the past decade, there has been a trend for international collaboration for the development of energy efficiency requirements and standards. The United States of America and Canada follow the IECC and ASHRAE standards, while in the European Union standards are established according to the European Energy Performance in Buildings Directive.

1.2 Solar technologies

Of the total global energy production of 2011, about 19% was produced by renewables, 9% being from biomass and 10% from modern renewables, with renewable energy development being mainly positive for Europe and the United States. Hydropower is the driving force in renewable energy production, followed by wind power. Solar energy accounts for only 0.9% of the total energy production, although there has been significant development in its application in recent years, with an ever growing rate, mainly due to the ever decreasing cost of solar technologies.

Solar energy, reaching the earth in the form of radiation, is an unlimited source of clean energy which may be gathered by photovoltaic (PV) systems and solar collectors and be converted to electricity and heat respectively, or both with photovoltaic/thermal systems. These technologies have been successfully applied to buildings for many decades and in various forms. Closed-loop, water-based flat plate solar collectors are widely used in Europe as a heat source for domestic hot water, or in conjunction with heat storage tanks, while air-based unglazed transpired collectors (UTC) are widespread in North America and can be combined with the heating, ventilation and air conditioning (HVAC) system of the building for space conditioning or in other formations, such as in combination with heat pumps. The latter is an example of a building integrated solar technology. PV panels have also been used in buildings, mainly as an independent element of the building, most often racked on roofs, forming either a stand-alone system, or a grid-connected one.

1.3 Building-integrated solar technologies

Experience and technological development, as well as the ongoing requirement for energy efficient buildings have dictated that a highly efficient way of employing sustainable technologies is by integration with the building itself. Buildings can this way include efficiency measures from their original design, while making optimal use of the technologies employed, which now comprise a part of the building itself, rather than an added external feature.

Building-Integrated Photovoltaic/Thermal systems (BIPV/T) are an example of the above concept, which combines the features of a solar collector and a PV system, while acting as the exterior layer of a building. There are numerous application of such a system, such as roof BIPV/T, especially for residential cases, wall-mounted or double skin facades that can be

extensively applied on commercial buildings, as well as use of semi-transparent PV windows (STPV) for the incorporation of natural illumination and shading control. The main concept is that the PV panels form the external layer, also acting as a rain screen cladding, while a channel is formed between the PV layer and the internal skin of the building. In that channel a liquid medium (water, glycol, air) may circulate in an open or closed-loop formation, extracting excess heat from the PV panels via convection and part of this heat can be recovered and used through various means. Moreover, this has a positive effect on the PVs, since their electrical efficiency is affected by their temperature.

A main advantage of BIPV/T over solar collectors, apart from the energy generation along with useful heat, is that in moderate climates, during the summer season, heating is not required. Unless the collector is used for hot water or some application other than space heating, it is essentially obsolete during the hot season.

1.4 Multiple-inlet Building-Integrated Photovoltaic/Thermal systems

Water-based closed-loop BIPV/T systems have generally higher heat exchange efficiency between the PV panels and the liquid medium, however they are more expensive, have higher installation cost and cannot have extensive application due to weight and maintenance issues. On the other hand air-based systems are more easily installed and can be used in larger applications; however they have lower heat exchange efficiency that can lead to PV overheating issues, as well as lower efficiency-to-cost ratios. In order to counter that, several techniques have been adopted, such as double-pass BIPV/T or the use of fins. This study focuses on the introduction of multiple inlets along the PV surface for the intake of fresh air as a means to enhance the heat extraction from the PV layer to the air channel. Without the use of any means other than PV panel spacing, or use of inlets on the PV frames, this method aims to break the thermal boundary layer formed on the PV layer and increase the heat exchange efficiency with the introduction of several air streams with a much lower temperature than air circulating in a long continuous channel as is the case of typical BIPV/T installations.

The aim of a multiple-inlet BIPV/T system is the uniform, or near uniform, heat extraction from all the PV modules that comprise a PV string, so that the PV panels may operate at a lower temperature, while the heat extraction from them will be maximized. In typical single inlet BIPV/T systems, the part of internal convection can be modified by the air channel flow rate, as

well as the channel width to height ratio. However, as air moves through the continuous channel, it accumulates heat resulting to higher PV temperatures of the higher PV modules, as well as decreasing heat exchange efficiency along the air channel.

With the introduction of multiple inlets, the internal convection part of the energy balance can be further modified by the amount of air entering each PV module in combination with the fact that an additional air stream is introduced per module at exterior air temperature. Apart from the flow, the entrance air temperature is accordingly modified, depending on the flow conditions, as described later on.

1.5 Purpose of this investigation

The purpose of this investigation is the development of a flow model that can calculate the inflow through each opening of a multiple-inlet BIPV/T system, given the total air collection rate of the system, the channel and opening geometry and wind effects in the form of exterior pressures over the area of interest. This flow model will be integrated with a modified energy balance model, where the flows calculated will be used as inputs and relationships for convection given in literature will be used.

The modelling procedure described in this study comprises the first attempt for performance assessment of multiple-inlet BIPV/T systems. Furthermore, the inclusion of wind effects on the inlet flow distributions will provide design insight for such systems, especially for large-scale installation.

The above tool will be used for the performance investigation of multiple-inlet system variations compared to a single inlet system, for a potential retrofit project at the Montreal Courthouse, as a theoretical case study.

1.6 Thesis Outline

This study consists of six chapters, the first being the introduction. The rest of the chapters are summarized as follows:

Chapter 2: Review of BIPV/T technology and thermal efficiency enhancement methods. Multiple-inlet BIPV/T systems are introduced and the background theory and studies, upon which the modelling of such systems is based, are presented.

Chapter 3: The experimental procedure carried out for this research in a solar simulator and a boundary layer wind tunnel is described. The experimental results have to do with the flow distributions of a 3-inlet BIPV/T prototype tested in a solar simulator facility and the external pressure distributions caused by wind over the potential retrofit area of a multi-storey institutional building, studied in a scaled version of the building in a boundary layer wind tunnel facility.

Chapter 4: In this chapter the development of a flow distribution model for multiple-inlet systems is described, as well as how it is integrated with a modified energy balance model.

Chapter 5: The models developed in the previous chapter are used for the simulation of several versions of multiple-inlet systems to be compared with single inlet designs in terms of electrical and thermal performance and PV temperature uniformity, for summer and winter design days with and without wind.

Chapter 6: In the final chapter, the main findings and contributions of this research are presented.

2. Literature review

This chapter reviews the main literature on BIPV/T technology, concerning design considerations and limitations, as well as methods that have been adopted in order to enhance its performance, and the theory that may lead to the appropriate modelling of multiple-inlet BIPV/T. Flow and internal convection inside the air channel of a BIPV/T system is addressed while the concept of a multiple-inlet BIPV/T system, as a means of heat exchange enhancement, is introduced. A large part of this chapter is dedicated to the flow modelling of a BIPV/T system, the focus being on the use of flow networking techniques and resistance-circuit analogy to create a flow distribution model of a multiple-inlet system. Finally, there is a review of the research on wind effects on PV/T systems and wind tunnel experimentation, as well as on the combination of experimental data and mathematical models.

2.1 BIPV/T

Building-Integrated Photovoltaic/Thermal systems are created by the architectural integration of the PV panels into the building envelope (roof, walls and windows). By doing so, the PV system becomes an integral element of the building rather than a stand-alone system. A BIPV/T system has a twofold role: electricity production, making use of the photovoltaic effect of the PV panels, and recovery of part of the excess heat from the radiation that is absorbed by the PV panels and is not converted to electricity or reflected back to the environment. To remove the excess heat from the PV panels, a channel is formed behind the PV layer, where a fluid medium circulates and extracts the heat from the panels via convection.

Depending on the fluid medium, BIPV/T systems are divided into air-based and water-based (combination of water with an anti-freezing medium), while depending on the fluid circulation, there are open and closed-loop systems. Most water based systems are closed-loop, while air-based systems can be both open and closed-loop. Due to high specific heat capacity and circulating fluid density, water-based BIPV/T systems have higher heat exchange efficiency in general. The amount of heat transferred to the moving fluid is given by:

$$q_{thermal} = m \cdot c_p \cdot \Delta T \quad (2.1)$$

where:

- q_{thermal} : the thermal energy transferred to the moving fluid (J)
- m : the mass flow rate inside the channel (kg/s)
- c_p : the specific heat capacity of the moving fluid (J/kg/°C)
- ΔT : the temperature difference between the collector and the fluid (°C)

Air-based systems suffer from a low heat exchange efficiency (Yadav and Bhagoria, 2014), due to the much lower density of air. However, air-based systems have structural and maintenance advantages over water-based systems:

- There are no leakage issues through ducts and joints, as well as the resulting corrosion effects
- There is no need for addition of anti-freezing fluids in order to withstand freezing conditions
- They are lighter, easier to install and to maintain, while far less complicated (Bambara, 2010)

There is a double benefit from the extraction of excess heat from the PV panels; one being the useful heat gained and the other is the enhancement of the electrical performance of the system, since the electrical efficiency of a PV module is related to its surface temperature as follows (Florschuetz, 1979):

$$\eta_{PV_theo} = \eta_{stc} \cdot (1 - \beta_{PV} \cdot (T_{PV} - T_{STC})) \quad (2.2)$$

where:

- β_{PV} : the PV module temperature coefficient (%/°C)
- η_{stc} : the PV module efficiency at standard test conditions (%)
- T_{STC} : the PV module cell temperature at standard test conditions (25°C)

Several values have been calculated experimentally for β_{pv} , 0.006 (Tonui & Tripanagnosotopoulos, 2006), 0.005 (Anderson et al, 2008; Green, 1998), 0.004 (Hegazy, 1999; Bergene et al, 1996), 0.004-0.005 (Skoplaki & Palyvos, 2009).

It becomes clear that a low operating PV temperature can be crucial for the performance of the systems, especially in large installations.

The potential of full scale applications of BIPV/T systems has been studied in both residential and commercial/institutional buildings, as well as experimentally. Chen et al (2010) studied an air-based open-loop BIPV/T system installed in a prefabricated low-energy residential construction in Quebec, Canada (Figure 2.1). The system was coupled with a ventilated concrete slab, so that the warm air coming from the air channel of the BIPV/T system could be passed through a tubing system formed inside the slab thus preheating it and making use of the thermal storage properties of concrete. A finite difference model was developed for this system and validated through field experiments. It was found that the PV panels' temperature was significantly lower, while the system had the potential to greatly assist in space heating.



Figure 2.1: The EcoTerra house (Chen, 2009).

Athienitis et al (2010) developed a hybrid prototype PV/T system coupled with an unglazed transpired collector (UTC). This system consisted of a layer of UTC 70% of the area of which was covered with PV panels. Taking into account that electric energy is about 4 times more valuable than heat (considering the average COP of a heat pump), it was found the this prototype system could generate 7%-17% more energy than a typical UTC installation covering the same

area. This prototype BIPV/T was realized as a demonstration project at the JMSB building of Concordia University in Montreal, Canada, as shown in Figure 2.2:



Figure 2.2: BIPV/T system of the JMSB Building, Concordia University.

The prototype BIPV/T system is architecturally integrated in the building's south-west façade and it can produce 25 kW of electricity and 75 kW of heat which can be used for preheating ventilation fresh air.

There have been various studies, including full scale (Chen, 2010; Athienitis, 2010), experimental (Bambara, 2013; Yang, 2014), numerical (Charron & Athienitis, 2005) and computational fluid dynamics (CFD) (Yadav & Bhagoria, 2013), dealing with the modelling of the performance of BIPV/T systems. However, for the time being, there is a lack of standards and specifications on the design of BIPV/T systems, the choice of system per case, their maintenance, as well as design issues such as mechanical stresses due to live loads and structural capacity of a building to carry such a system (Yang, 2014).

2.2 BIPV/T modelling

As previously mentioned, open-loop air-based BIPV/T systems suffer from low heat exchange efficiency due to the low specific heat capacity of air, as well as the low density of the fluid medium. Typically, BIPV/T systems consist of the PV layer, the air channel, or plenum where air circulates, structural attachments to link the PV to the insulation and the interior wall layers (Candanedo et al, 2011) as shown in Figure 2.3.

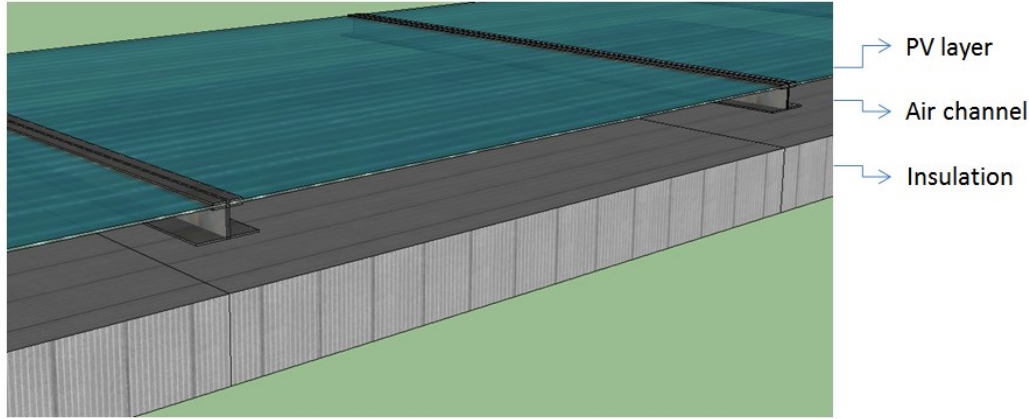


Figure 2.3: Air based BIPV/T basic components: PV layer, air channel and back wall with insulation.

The energy balance of such a system, using the method of finite control volumes is shown in Figure 2.4:

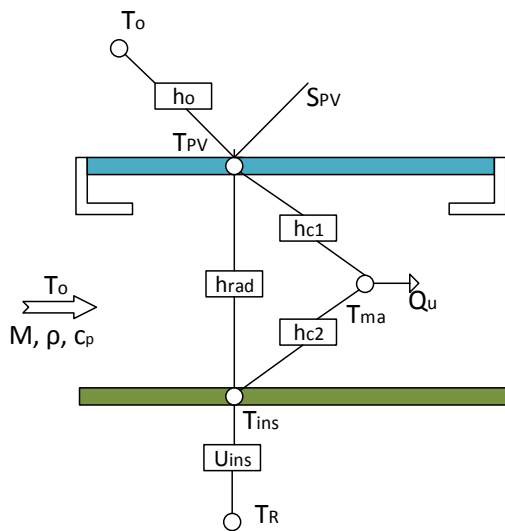


Figure 2.4: BIPV/T energy balance.

where:

- T_o : the external temperature ($^{\circ}\text{C}$).
- h_o : the exterior film coefficient (combined radiation and convection, $\text{W}/\text{m}^2\cdot^{\circ}\text{C}$).
- T_{PV} , T_{ma} , T_{ins} and T_R : the temperatures of the PV (average), the air inside the air channel, the surface of the insulation and the adjacent room respectively ($^{\circ}\text{C}$).
- h_{c1} , h_{c2} : the convective heat transfer coefficients from the PV and the insulation surface to the flowing air respectively ($\text{W}/\text{m}^2\cdot^{\circ}\text{C}$).

- h_{rad} : the radiative heat transfer between the PV and the insulation surfaces ($W/m^2 \cdot ^\circ C$).
- S_{PV} : the net heat absorbed by the PV layer (total absorbed-electric produced) (W/m^2)
- ρ : the density of air (assumed constant), $1.2kg/m^3$
- c_p : the specific heat capacity of air (assumed constant), $1000j/kg/^\circ C$
- M : the mass flow rate inside the collector (kg/hr)

The above is a simplified energy balance model, where the long wave radiative heat exchange between the PV layer and the environment (sky, ground) is included in an external combined heat transfer coefficient.

The system consists of a continuous air channel, typically with an inlet at the bottom of the installation and a fan placed on top, which draws the warm air to a manifold, to be either used directly in the HVAC system or driven to a heat pump. As the air moves inside the air channel, it accumulates heat and its temperature rises along the flow path. This leads to a decreasing heat exchange efficiency, as well as an increasing PV temperatures, which can be as high as $70^\circ C$ (Yang, 2014), as it reaches the outlet.

The internal convection part of the above energy balance is affected by two main parameters; the temperature difference between the PV panels and the circulating air, and the local Nusselt number, which defines the convective heat transfer coefficient. The above can be summarized as follows:

$$\text{Convection} = f(\Delta T, Nu)$$

where:

- ΔT : the temperature difference between the PV panels and the circulating air
- Nu : the Nusselt number of the local flow

The Nusselt number is a dimensionless number which gives the ratio of convective to conductive heat transfer across the boundary of the flow. It is defined as follows:

$$Nu = \frac{h \cdot L}{k} \quad (2.3)$$

where:

- h : the convective heat transfer coefficient (W/(m² K))
- L : a characteristic length of the flow, namely the length of the flow path (m)
- k : the thermal conductivity of air (W/(m K))

In the case of forced convection, the Nusselt number is empirically expressed as a function of the Reynolds and the Prandtl number:

$$Nu = f(Re, Pr)$$

The Reynolds number of the flow is the ratio of viscous over inertia forces of the flow and is defined as:

$$Re = \frac{\rho \cdot V \cdot D_h}{\mu} \quad (2.4)$$

where:

- ρ : the air density (kg/m³)
- V : the fluid average velocity (m/s)
- D_h : the hydraulic diameter of the duct, defined as four times the flow area over the wetted perimeter (m)
- μ : the dynamic viscosity of the fluid (air) (kg/m/s)

The Prandtl number is defined as the ratio of momentum over thermal diffusivity and is given as:

$$Pr = \frac{\nu}{\alpha} = \frac{C_p \cdot \mu}{k} \quad (2.5)$$

where:

- ν : the kinematic viscosity (m²/s)
- α : the thermal diffusivity of air (m²/s)

- C_p : the specific heat capacity of air (J/(kg K))
- μ : the dynamic viscosity of the fluid (air) (kg/m/s)
- k : the thermal conductivity of air (W/(m K))

The most common empirical relationship for the Nusselt number is the Dittus-Boelter Correlation for developed turbulent flow ($Re > 10000$):

$$Nu = 0.023 \cdot Re^{0.8} \cdot Pr^n \quad (2.6)$$

with $n=0.4$ when the surface temperature is higher than the medium temperature and $0.6 < Pr < 160$

However, depending on experimental measurements for various system configurations, as well as the flow regime, several correlations have been developed (Warren et al, 1998; Tonui & Tripanagnostopoulos, 2006; Ghani et al, 2012, Candanedo, 2011)

The Nusselt number, and as a result the convective heat transfer coefficient (CHTC), is affected by the aspect ratio of the air channel, while the CHTC is highly affected by the air stream velocity. Several studies have shown that increased air flow rate inside the air channel result in higher heat extraction and lower PV temperatures, though lower outlet air temperatures (Hegazy, 1999). A very high air collection rate may result in very effective PV panel cooling; however, it may result in increased fan consumption and to a lower net electricity production.

Several common assumptions adopted in order to simplify BIPV/T thermal modeling are the following:

1. The heat flow is one-dimensional. For each control volume of the energy balance, the heat path is assumed perpendicular to the layers comprising the control volume and not parallel in the horizontal or vertical sense, along the plane of each layer. This results in an average temperature for each layer of the control volume. However, Ghani (2012) showed that due to the non-uniform flow distribution of the medium circulating within the channel, hot spots may form over the area of a PV panel.

2. The fluid medium is assumed to have a uniform velocity profile and an average fluid velocity is assumed throughout the channel. Therefore, in most numerical and CFD studies (Yadav & Bhagoria, 2013), a two-dimensional model of the system is assumed.
3. Since the PV layer, as well as the back insulation layer, is considered to have no thermal storage capacity, it is common to assume a steady state analysis. There have also been studies where transient modelling is adopted (Candanedo et al, 2011), especially for cases of combined BIPV/T and phase changing materials (PCM) (Aelenei et al, 2013).

2.3 Thermal efficiency enhancement

A common definition of the thermal efficiency of a solar system is given as the total thermal energy extracted from the absorber layer and transferred to the fluid medium over the total incident solar radiation on the absorber:

$$\eta_{thermal} = q_{extracted} / I_{incident} \quad (2.7)$$

In order to enhance the system's thermal performance, either the thermal losses from the front and the back of the system must be controlled, or the internal convection and resulting heat extraction needs to be boosted, or a combination of both can be adopted.

Thermal losses from the front part of the system, namely the one affected by the climatic conditions, may be regulated with the use of a glazing part installed over the PV layer. Hegazy (1999) studied variations of a glazed system, two of which are shown in Figure 2.5:

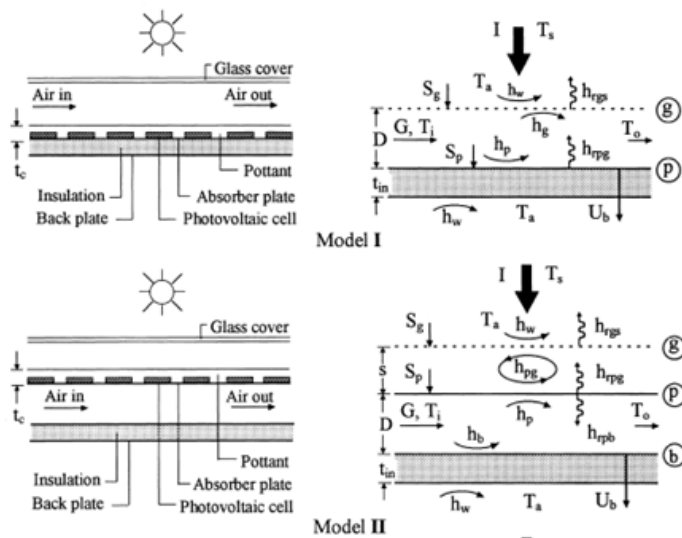


Figure 2.5: Single pass PV/T configurations (Hegazy, 1999).

The concept was to set the PV layer behind a glazing in order to minimize the external convection, resulting in a system much less susceptible to wind effects. In the first design, the PV layer was set on the back surface with the air stream moving on top of it and on the second design it was set in the middle, with air circulating behind it. Although both variations led to a higher thermal efficiency, the second variation performing better, they also resulted in a much higher PV temperature and a decreased electrical efficiency. By increasing the air mass flow rate, the PV temperature dropped, however, the fan energy consumption was greatly increased, resulting only to a slight increase in electrical efficiency.

Two other designs studied included a case where the PV panels are set in the middle of the air channel and air passes both in front of and behind them, to be collected at the outlet, or a continuous channel was formed, creating a double pass configuration, thus doubling the length of the flow path, as shown in Figure 2.6

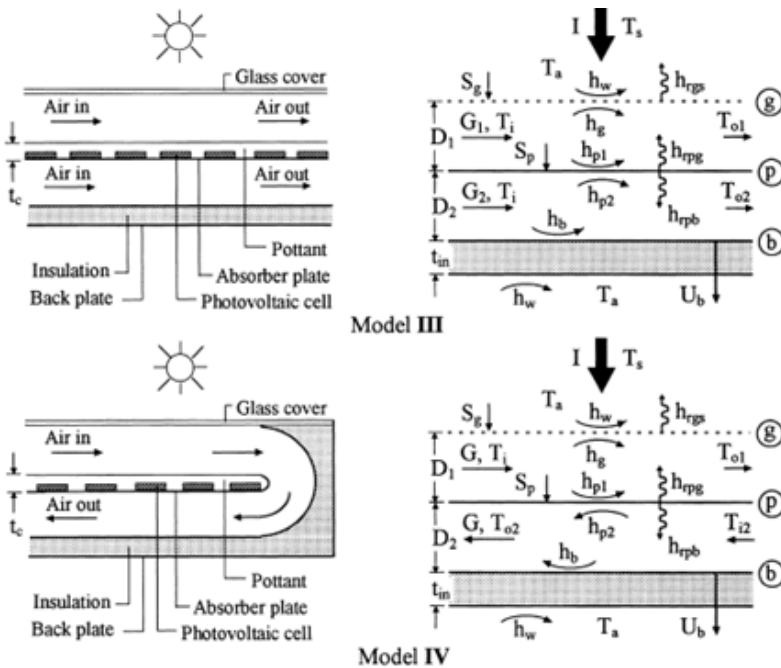


Figure 2.6: Double pass PV/T configurations (Hegazy, 1999).

Model III was found to have the best overall performance, followed by model IV. However, it was found that for each model type, there exists a critical mass flow rate, beyond which, the overall collector performance decreases. This can be seen in Figure 2.7:

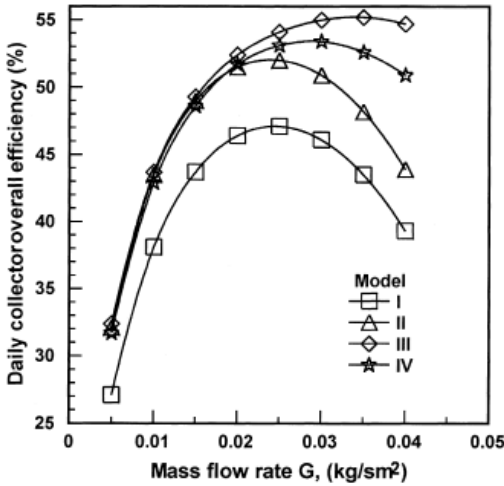


Figure 2.7: Plot of daily overall collector efficiency with respect to mass flow rate of the PV/T configurations studied by Hegazy (1999).

Tonui and Tripanagnostopoulos (2006) studied experimentally similar design variations, adding two cases: one where fins were installed along the flow path in order to induce turbulence and thus enhance convection inside the air channel and another where a thin metal sheet is placed behind the PV layer, within the air channel. The variations studied are shown in Figure 2.8:

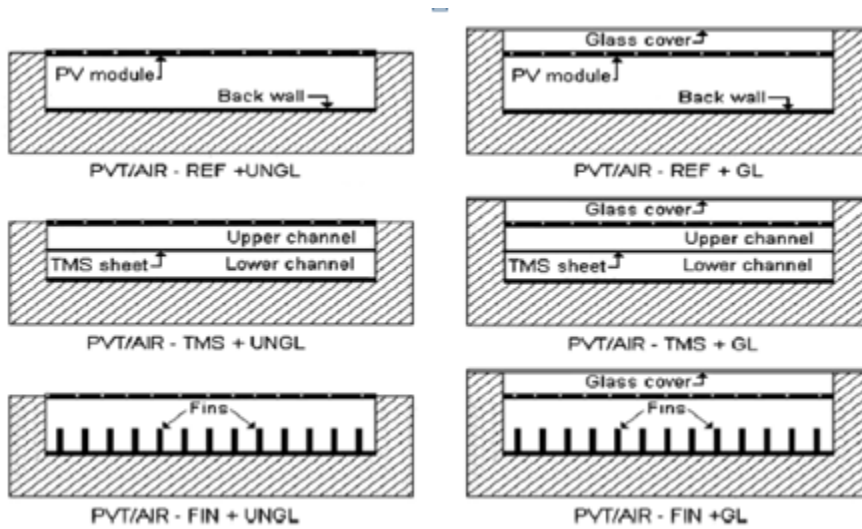


Figure 2.8: Cross sectional view of PVT/Air collector models studied by Tonui & Tripanagnostopoulos (2006).

It was shown that both the thin metal sheet and the fins highly increased the performance of the system, both for buoyancy driven flow and for forced flow, the fin system being superior. It was

also observed that the optimum channel depth was between 5 and 10cm and that the thermal efficiency increases with increasing exit area of the air channel.

A system combining BIPV and PCM was studied by Aelenei et al (2013). The system has been installed on the main façade of Solar XXI office building in Lisbon and was found to have a thermal efficiency of 10% and a combined electrical and thermal efficiency of about 20%.

2.4 Multiple-inlet BIPV/T

The methods referred to in section 2.3, aim to improve the thermal efficiency of a BIPV/T system by modification of the flow in a continuous air channel, that is, improvement of the Nusselt number of the flow. However, even if the heat extraction is enhanced, the issue of accumulated heat and temperature stratification over the PV layer along the collector remains. PV panels operating at considerably varying temperatures, especially along the height of large installations may result in failure of the attachment with the supporting structure due to differential expansion, as well as quicker degradation of the top panels operating at higher temperatures (Yang, 2014). Also, depending on the strings and arrays' configurations (in series or in parallel), the electrical efficiency of the panels operating at higher temperatures could undermine that of the whole system.

The introduction of more than one opening, namely one per PV module, along the height of a PV string aims to the combined regulation of the two factors affecting the internal convection in the air channel:

- The flow rate of each control volume and
- The temperature difference between the PV panels and the circulating fluid

The goal is to achieve uniform heat extraction, as well as uniform temperature distribution for the whole system. This can be achieved by studying and modelling the flow distributions, namely the inflow from each inlet of the system, the regulation of which can be achieved by the geometric modification of the inlets. The flow modelling and the expected effects of the regulation of the flow distributions are discussed in detail in Chapter 4.

A multiple-inlet BIPV/T is a rather new concept and there are few references in literature. Athienitis et al (2010) designed a prototype PV/T combined with unglazed transpired collector (UTC) which is shown in Figure 2.9:

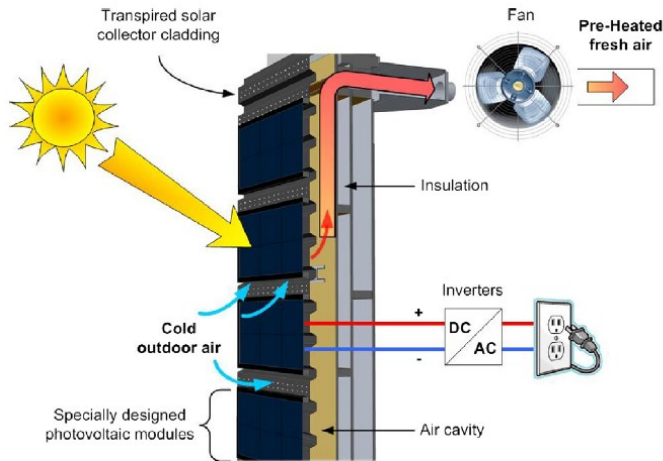


Figure 2.9: Hybrid UTC-PV/T system installed at Concordia University (Athienitis et al, 2010).

This hybrid PV/T-UTC prototype consisted of a layer of UTC upon which custom made PV modules were fixed with supports, covering 70% of the total UTC area. The concept of the system was that the solar collector could also produce electrical energy, increasing its cost-effectiveness, especially in the summer months, during which space heating is not needed (except for domestic water heating use). UTC is a proven efficient solar collector and the system would benefit from heat extraction from both the UTC and the PV covered area, the latter resulting in an increased electrical efficiency of the PV system.

The overall thermal performance of the hybrid system was lower than that of a UTC, however, if the electrical energy produced was expressed in terms of equivalent thermal energy, the overall efficiency of the hybrid system was found to be 7-17% higher than that of the UTC (Athienitis et al, 2010; Bambara et al, 2012). The term “equivalent thermal energy” was developed for that specific study in order to be able to compare different systems, with the assumption that one unit of electrical energy equals to four units of thermal energy, if the average COP of a heat pump (4) is taken into account.

For the comparison, a UTC and a hybrid prototype of the same area were studied experimentally side by side under the same climatic conditions. The performance of the two systems in respect to the air collection rate measured is shown in Figure 2.10:

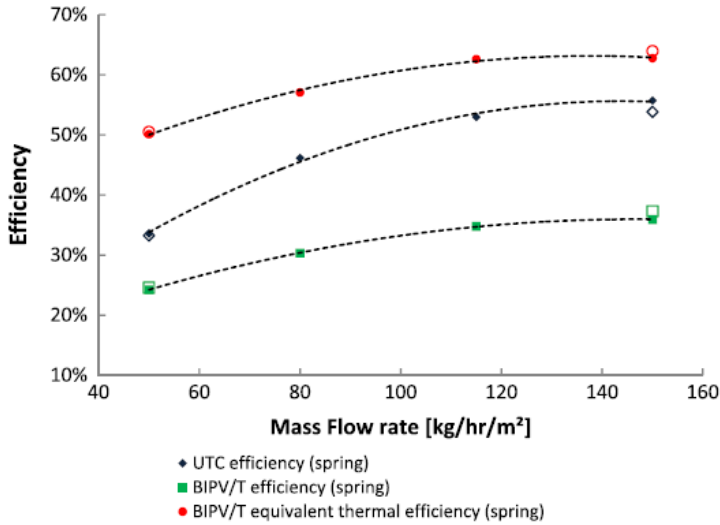


Figure 2.10: UTC and BIPV/T equivalent efficiency versus mass flow rate (Athienitis et al, 2010).

The above is a form of a multiple-inlet system, since air is entering from the pores of the UTC from the whole installation area, while for each PV module, the stream of air passing under is at ambient temperature and not preheated inside the air channel.

The system was modelled assuming uniform suction from the UTC perforations, according to Kutscher (1994), considering the mass flow entering the exposed UTC area and the PV covered area for the energy balance.

Yang et al (2014) studied experimentally a BIPV/T prototype, previously studied outdoors by Candanedo et al (2011), in the Solar Simulator facility of Concordia University. The single-inlet prototype was a scaled version of the system installed in EcoTerra (Chen, 2010) and an explicit finite difference control volume model was developed for its modelling. The flow rate inside the air channel was controlled by an air collection unit, while the Reynolds number was kept below 10,000 in order to keep frictional losses low. The following Nusselt number correlations were developed for the PV layer and the back insulation, for the turbulent and the laminar region:

- In the turbulent region ($2300 < Re < 9500$):

$$Nu_{top}(x) = 8.188 \cdot Re^{0.77} \cdot Pr^{3.85} \cdot e^{\frac{-x^{0.2}}{2.8 \cdot D_h}} + 0.061 \cdot Re^{0.77} \cdot Pr^{3.85} \quad (2.8)$$

$$Nu_{bottom}(x) = 4.02 \cdot Re^{1.09} \cdot Pr^{19.3} \cdot e^{\frac{-x^{0.2}}{14 \cdot D_h}} + 0.005 \cdot Re^{1.09} \cdot Pr^{19.3} \quad (2.9)$$

- In the laminar region ($1190 < Re < 2300$)

$$Nu_{top}(x) = 0.6883 \cdot Re^{0.7} \cdot Pr^{0.8} \cdot e^{\frac{-x^{0.3}}{6.45 \cdot D_h}} + 0.0124 \cdot Re^{0.7} \cdot Pr^{0.8} \quad (2.10)$$

$$Nu_{bottom}(x) = 50 \cdot Re^{0.5} \cdot Pr^{0.2} \cdot e^{\frac{-x^{0.2}}{1.37 \cdot D_h}} + 0.428 \cdot Re^{0.5} \cdot Pr^{0.2} \quad (2.11)$$

An improved design with two inlets, intended for inclined roof applications, was studied and modelled according to the developed mathematical model. The original single-inlet prototype, which was 2.8m long, was divided into two equal length sections. In order to further enhance the thermal performance of the system, a vertical glazed solar collector part added to the BIPV/T system was also modelled. The combination of the two-inlet system and the vertical glazed collector part are shown in Figure 2.11:

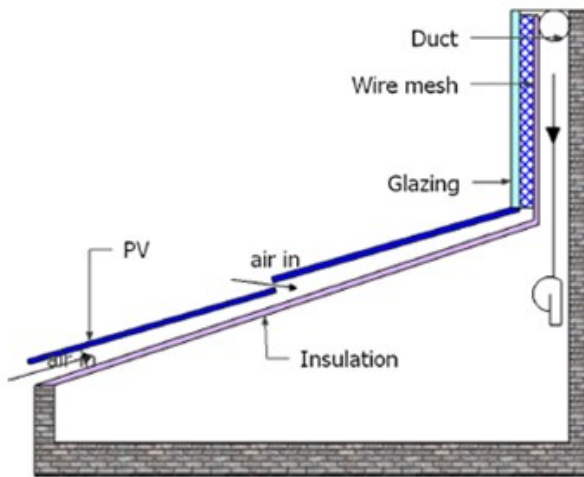


Figure 2.11: Two-inlet BIPV/T system connected in series with glazed air collector (Yang et al, 2014).

The Nusselt number for the second section was calculated based on the assumption that the thermal boundary layer that forms over the PV surface restarts at the second inlet. For the

modelling part, it was also assumed that the inflow through the two inlets was equal. It was found that the thermal efficiency of the two inlet system was 5% higher than that of the single-inlet prototype. Furthermore, there was a 1.5°C decrease in the peak PV temperature, as well as a marginal increase in the electrical efficiency of the system. It was expected that for larger roof installations of 5-6m the temperature decrease would be from 5-10°C, depending on the flow rate and the wind conditions. Such a reduction in peak PV temperature would also mean slower PV degradation.

Mirzaei et al (2014) investigated experimentally the role of cavity flow on the performance of BIPV/T panels placed on inclined roofs. A scaled building model was developed with BIPV/T set on the roof section and the model was tested inside a closed loop atmospheric wind tunnel. A small scale solar simulator was also placed inside the wind tunnel, while a part of the coating at the center of the BIPV/T was scraped in order to facilitate a Particle Image Velocimetry (PIV) test arrangement.

An infra-red camera was used for the assessment of the temperature field on the PV area. The purpose of this novel experimental set-up was to simultaneously assess the effects of flow over and below the PV panels on their temperature, while investigating the flow field.

For the experiments, the configurations considered consisted of a flat and a stepped PV arrangement, with open and closed cavity settings, as shown in Figure 2.12 and for three upstream wind velocities.

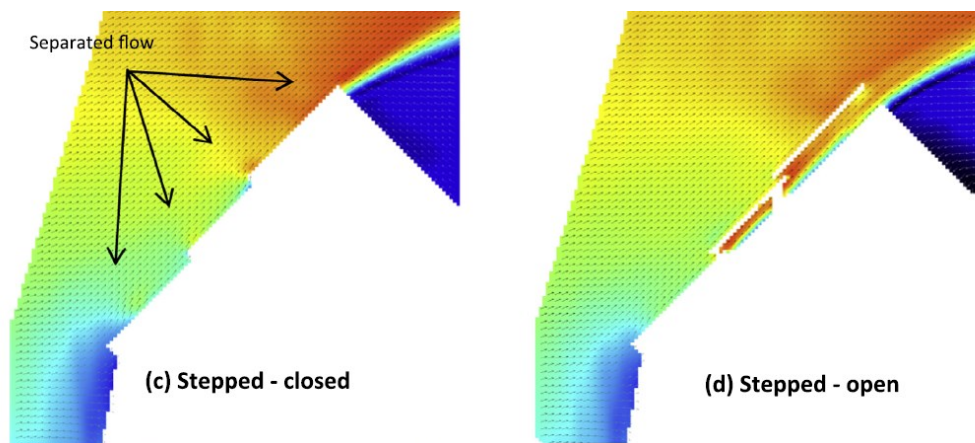


Figure 2.12: Stepped roof BIPV/T configuration studied by Mizraei (2014).

The stepped configuration is essentially a multiple-inlet system. However, the designs of the BIPV/T air channel did not include an air collector and only focused on wind induced air flow. For the cases with the closed cavity, the wind effects on exterior convection were investigated, while with the open cavity cases, the ratio of flow over and flow below the PV panels was measured. It was assumed that the mean flow was two-dimensional due to the shape of the cavity and the nature of the air flow.

From the experimental findings, it was shown that:

- For the cases of closed cavity, the temperature distribution over the PV area, for both the flat and stepped configurations, was similar, indicating that the effect of wind on the external convection was approximately the same.
- When the cavity was open, the air velocity below the PV panels was found to be higher than that over the PV panels, mainly due to the flow resistance caused by separation at the edges of the system. However, it was also found that the airflow at the top of the PV was similar to that of the closed cavity cases. This would mean that the presence of openings does not highly affect the external flow field over the PV plane.
- It was found that the PV temperatures were much lower for the cases with open cavity, and most importantly, they were considerably lower for the case of stepped configuration, namely the multiple-inlet configuration.

2.5 Flow modelling

2.5.1 Forced flow in single inlet systems

The flow inside the air channel is the factor that determines the internal convection. In order to regulate internal convection, the flow has to be properly modelled. In almost all literature on BIPV/T, airflow modelling is done in the same manner. Since in almost all cases air enters from a single inlet and exits at the outlet, in a single continuous channel, the flow is essentially known and regulated by the fan. If the flow is known, one can obtain experimentally correlations for the Nusselt number, by measuring the temperature of the PV surface and the air channel. In addition, the pressure drop along the air collector due to the frictional losses can be calculated according to the Darcy-Weisbach equation:

$$\Delta P = f \cdot \frac{L}{D_h} \cdot \frac{\rho \cdot V^2}{2} \quad (2.12)$$

where:

- ΔP : the pressure drop across the air collector (Pa)
- f : the Darcy friction factor (dimensionless)
- L : the length of the air collector (m)
- D_h : the hydraulic diameter of the air channel, defined as four times the cross sectional area over the wetted perimeter of the duct (m)
- ρ : the air density (kg/m^3)
- V : the average air velocity inside the air channel (m/s)

The above pressure drop is used for the calculation of the fan power consumption according to the following:

$$P_p = \frac{m \cdot \Delta P}{\rho} \quad (2.13)$$

where:

- P_p : the fan power (W)
- m : the mass flow rate of the air collector (kg/s)
- ΔP : the pressure drop along the collector
- ρ : the density of the fluid (kg/m^3)

A common assumption in BIPV/T modelling is the two-dimensional nature of the flow, which means that the flow changes along the height and the length of the air collector, but not along the width of the PV module. This is most common within CFD studies on the performance of BIPV/T and flow and CHTC relations (Yadav & Bhagoria, 2013, Getu et al, 2014).

2.5.2 Natural ventilation in single inlet systems

On the other hand, the case is not the same when dealing with natural ventilation, which may be wind driven or due to buoyancy. In this case, the flow is not known and has to be calculated

based on pressure measurements for the case of wind-driven ventilation, or according to temperature differences in the case of buoyancy.

When dealing with wind driven flow, in most cases a flow network is formed making use of the pressure drop across the opening of the collector, the pressure drop along the air channel and the measured discharge coefficients, or flow coefficients. The general equation of flow through an opening, as a function of the pressure difference across the opening is the following:

$$Q = C \cdot (\Delta P)^n \quad (2.14)$$

where:

- Q: the flow rate (m^3/s)
- C: the flow coefficient ($\text{m}^3/\text{s Pa}^n$)
- ΔP : the pressure drop across the opening (Pa)
- n: the flow exponent of the opening (dimensionless)

The most commonly used form of the above is the orifice equation:

$$Q = C_D \cdot A \cdot (2\Delta P / \rho)^{0.5} \quad (2.15)$$

which is derived from the pressure drop across an orifice equation:

$$\Delta P = 0.5 \cdot K \cdot \rho \cdot Q^2 / A^2 \quad (2.16)$$

where:

- Q: the flow rate (m^3/s)
- ΔP : the pressure drop across the orifice (Pa)
- A: the orifice area (m^2)
- ρ : the density of the fluid (kg/m^3)
- C_D : the discharge coefficient for the orifice (dimensionless)
- K: the loss coefficient for flow through an orifice (dimensionless)

The relationship between the discharge and the loss coefficient is the following:

$$C_D = (1/K)^{0.5} \quad (2.17)$$

The pressure difference across the opening due to wind driven flow is given by the following:

$$P_e - P_i = \Delta P = 0.5 \cdot (C_{pe} - C_{pi}) \cdot \rho \cdot V_{loc}^2 \quad (2.18)$$

where:

- P_e, P_i : the external and internal static pressure respectively due to wind (Pa)
- C_{pe} : the external pressure coefficient
- C_{pi} : the internal pressure coefficient
- V_{loc} : the wind velocity at the height of measurements

The pressure coefficients show the ratio of the static pressure measured at a specific location over the dynamic pressure of wind at the height of that location.

2.6 Multiple-inlet flow network modelling

Throughout most studies of systems with more than one opening, such as UTC and multiple-inlet systems, the main assumption is that of uniform flow through all the openings of the system. However, this may not be the case for multiple-inlet systems, as the resistance to the flow is not the same for all the openings of the system and as a consequence the amount of air entering through each inlet. This can be even more complicated when wind effects are taken into account. Wind induced pressure on the openings of a large installation will not be uniform, resulting in different pressure differences between the openings and the fan, again resulting in different intakes of air. The actual inflow distributions for multiple-inlet systems have not been modelled yet and no standard exists for the time being.

However, there are several concepts such as the orifice flow, wind induced flow and flow networks, as well as numerical methods used for calculation of flow distributions in pipe networks, such as the Hardy-Cross method, which can be used for the development of a model that describes the flow distributions of a multiple-inlet system. These concepts are presented below.

2.6.1 Flow networks

Flow networks are created with the nodal representation of the flow path. The pressure is evaluated at each node and the branches linking each node represent the segments of the airflow between nodes. Branch flows merge at the nodes and if more than 2 branches are connected to a node, these nodes are referred to as junctions. For each node the summation of flows entering and those exiting is equal to zero, according to the mass conservation principle. Flow networks make use of the known correlations linking flow and pressure drop, such as the orifice equation, the Darcy-Weisbach frictional pressure drop equation, as well as other secondary loss relationships.

Asfour & Gadi (2006) compared the predictions of CFD and flow network models for cases of natural cross ventilation in a generic rectangular building with two openings. The flow network model was based upon the orifice flow equation, using wind tunnel measurements for external and internal pressure coefficients. It was found that there was a good agreement between the CFD and the flow network model results, the maximum discrepancy being around 11%.

Karava (2003) studied the validity of the orifice equation in the full scale experimental investigation of trickle ventilators. Two types of ventilator were installed in an outdoor test room. An exhaust fan was used to create negative pressure and expel air from the room to the outside, with a valve installed to control the exhaust air flow rate. Differential pressure was applied across the building envelope and the total air leakage of the room was measured. Subsequently, the ventilators were sealed and thus, the envelope leakage was determined. The difference between the total flow and the envelope air leakage gave the flow at a specific differential pressure from the trickle ventilator.

Comparing the measured and the predicted air flow, it was found that the orifice equation overestimated the flow by a factor near 2. The actual C_D value that should be used for openings such as trickle ventilators (the two cases tested had opening area of 19 and 40 cm² respectively) was calculated to be approximately 0.34.

Lou et al (2012) applied a zonal approach for the modelling of the inner gap pressures for various double-skin façade (DSF) layouts in tall rectangular buildings. One of the layouts studied consisted of a strip type DSF with multiple venting holes, as shown in Figure 2.13:

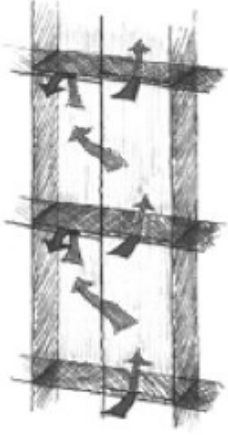


Figure 2.13: Box double-skin façade with multiple openings (Lou et al, 2012).

A model of a generic rectangular building was created and tested in a boundary layer wind tunnel and pressure coefficients were obtained for three surfaces: the outer and inner surface of the external skin and the surface of the internal skin. A zonal model was developed according to the measurements to describe the relation between wind pressure distribution and the volumetric flow rates through all the openings of the DSF. The model was validated against the wind tunnel results.

For the zonal flow model, the flows through the ventilating holes were described by the general equation for flow through an opening (2.14), which for wind driven flow takes the form of:

$$Q_j^E = C \cdot A_E \cdot \left(\frac{\rho \cdot v_0^2}{2}\right)^n \cdot (C_{pe,j} - C_{pi,j}) \cdot \left(|C_{pe,j} - C_{pi,j}|\right)^{n-1} \quad (2.19)$$

with Q_j^E the flow through the j -th hole, C the flow coefficient, v_0 , the wind speed at the datum level and C_{PEj} , C_{PIj} , the external and internal pressure coefficient of the j -th hole and A_E the effective flow area of the opening.

The frictional pressure drop along the cavity was calculated by the Darcy-Weisbach equation (2.12), according to which the airflow inside the DSF from the $(j+1)$ -th cell to the j -th cell was expressed as:

$$Q_{j+1,j}^I = \frac{A_I \cdot v_0}{\sqrt{(f \cdot L / D_h)}} \cdot (C_{pi,j+1} - C_{pi,j}) \cdot \left(|C_{pi,j+1} - C_{pi,j}|\right)^{0.5} \quad (2.20)$$

where A_I is the cross sectional area of the cavity of the DSF. The mass conservation equation for incompressible flow, for the j -th cell was expressed as:

$$\sum Q_j = Q_j^E + Q_{j-1,j}^I - Q_{j,j+1}^I = 0 \quad (2.21)$$

where: Q_j the flow through the j -th cell (m³/s), Q_j^E the flow through the opening of the j -th cell, $Q_{j-1,j}^I$ the flow from the $(j-1)$ -th cell to the j -th cell and $Q_{j,j+1}^I$ the flow from the j -th cell to the $(j+1)$ -th cell.

By solving the mass equation for the first cell, the wind driven flow across the opening should equal the flow within the cavity from the first to the second cell. That way the pressure coefficient for the internal skin of the second cell could be evaluated and so on and so forth for the rest of the cells. Thus, a zonal flow network was created, relating the wind pressure and flow to the frictional pressure drop and flow inside the DSF as shown in Figure 2.14:

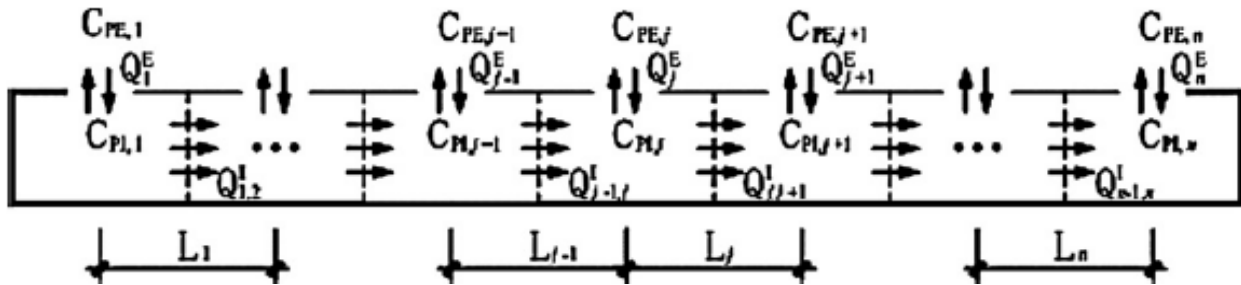


Figure 2.14: Strip type DSF with multiple venting holes in the zonal approach (Lou et al, 2012).

The flow coefficient used was $K=1$ and the flow exponent $n=1$ according to Inculet (1994).

2.6.2 Resistance approach and the Hardy Cross method

A useful representation of flow networks is with the electrical analogy, especially when dealing with complex flows with multiple inlet and outlet openings which are interconnected through a network of alternating branch flows (Aynsley, 1997). Pressure drop is related through a proportionality constant, or flow resistance, to the flow in an equivalent manner as voltage is linked to electrical current.

When flow passes through a number of resistances in series, as i.e. a sequence of openings, an equivalent resistance, R_{eq} , equal to the sum of the resistances, R_1, R_2, \dots, R_n , can be used in exactly the same manner as in electric circuits:

$$R_{eq} = R_1 + R_2 + \dots + R_n \quad (2.22)$$

When the flow passes through a number of parallel branches, the equivalent resistance can be calculated as:

$$1/R_{eq} = 1/R_1 + 1/R_2 + \dots + 1/R_n \quad (2.23)$$

From the known equations relating pressure drop to the volumetric flow (2.11, 2.14, 2.15, 2.16) it is clear that the relationship between the flow and the pressure drop is non-linear. The pressure drop is actually proportional to the square of the flow and, conversely, flow is proportional to the square root of the pressure drop.

Flows in networks with parallel or in series branches can be analyzed directly using the electrical analogy (or resistance–circuit analogy). However there might be cases where flow branches overlap, or are interconnected, forming a complex flow network, the direct solution of which may be impossible.

A well-established method for solving complex flow networks, the branches of which form closed loops, is the Hardy Cross method, or moment-distribution method, which was originally proposed by Hardy Cross for framed structure analysis, but has since found extensive application in flow and pipe networking problems. The method has been found to converge for all known examples and was afterwards proven to be a Jacobi iterative scheme (Volokh, 2001). The Hardy-Cross method can calculate the flow through an infinite number of loops, number of nodes or number of input nodes (Brkic, 2008). The first two laws of Kirchoff are used:

- The quantity of air entering a junction must be equal to the quantity of air exiting the junction (mass continuity)
- The summation of pressure drops around any closed path is zero (potential/energy continuity)

The method is based upon the relation between head loss and flow:

$$h_f = k' \cdot Q^n \quad (2.24)$$

where:

- h_f : the loss of head (m), from the relationship

$$\Delta P = h_f \cdot \rho \cdot g \quad (2.25)$$

ρ being the air density (kg/m^3) and g the gravitational acceleration (9.81m/s^2)

- k' : the head loss per unit flow ($\text{s}^n/\text{m}^{3n-1}$)
- n : the flow exponent (dimensionless)

The factors k' and n can be defined according to the appropriate relationship between flow and pressure drop or head (Darcy-Weisbach, orifice flow etc.). The Hardy Cross method assumes that the flow entering and exiting the system is known, as well as the geometric and roughness features of the branches, according to which the k factors may be calculated.

There are two ways of applying the Hardy Cross method:

- The method of balancing heads, where there is an initial guess of branch flows that satisfies continuity at each junction of the system and then iteratively balances the flows until continuity of potential is reached.
- The method of balancing flows, which uses an initial guess that satisfies continuity of potential over each loop of the system and then balances the flows, until continuity of flow is achieved in each junction.

A typical form of a flow network set in loops solved by the Hardy Cross method is shown in Figure 2.15:

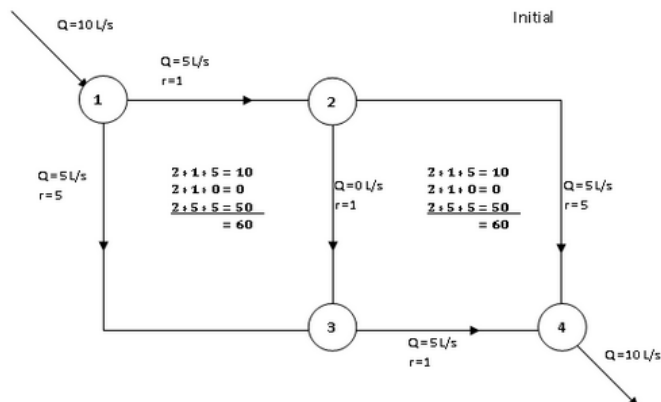


Figure 2.15: Typical loop formation analyzed by the Hardy Cross method.

Aynsley (1997) used a resistance approach for the analysis of natural ventilation air-flow networks in buildings with a limited number of openings in series. This approach made use of the orifice flow, based on estimates of pressure differences and discharge coefficients of openings. The Hardy-Cross method was used for the iterative calculation of flows through the nodes of the network. The orifice equation used employs a discharge coefficient of $C_D=0.65$ for flow through sharp edged rectangular objects. For the case of flow through wall openings on buildings it would be between the total pressure at the windward opening and the static pressure near the wall beside the leeward opening. The kinetic energy represented by the dynamic pressure of the air jet issuing from the leeward opening would be dissipated downstream of the building and therefore would not contribute to the head loss between windward and leeward opening.

Since the study dealt with multiple inlet and outlet openings, as well as internal flows, an electrical circuit analogy was used, according to Atkinson's equation which relates the pressure drop to the square of the discharge Q (m^3/s), with a constant of proportionality, R' , which is the equivalent of an electrical resistance:

$$\Delta P = R' \cdot Q^2 \quad (2.26)$$

The airflow resistance through the wall openings was expressed in terms of their discharge coefficients, the air density and the area of the opening:

$$R' = (\rho / 2) / (C_D^2 \cdot A^2) \quad (2.27)$$

The Hardy-Cross method, along with the resistance analogy was used as simple flow modelling approach as opposed to three dimensional CFD calculations. This method did not provide detailed information on airflow outside the main air streams, it could, however, produce adequate estimation in terms of the flow through the openings of the system.

Dymond & Kutscher (1997) used pipe networking methods to develop a simple computer algorithm for the calculation of the flow distributions in transpired solar collectors, in an effort to create a design guideline to counter the poor flow distribution occurring in large building installations.

Addressing it as a flow distribution problem, pipe networking techniques were adopted instead of developing a CFD case, since it was noted that the Navier-Stokes equations need not be solved, as long as the pressure drop across the absorber and in the plenum were known empirically.

The absorber was modelled with a three-dimensional set of fictitious pipes, the x and y-dimensional pipes representing flow within the plenum and the z-directional pipes flow across the absorber, as shown in Figure 2.16:

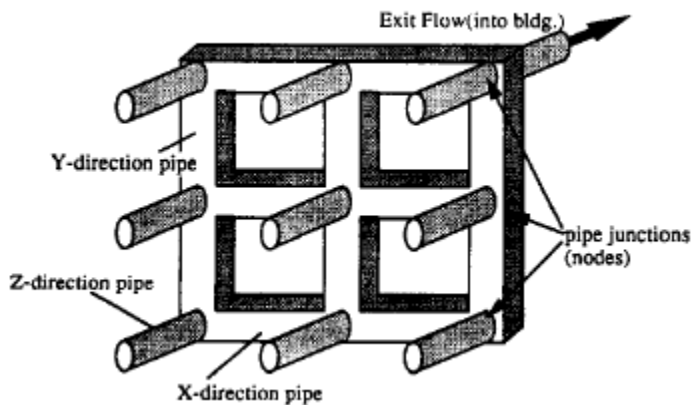


Figure 2.16: Example of a 3 x 3 set of pipe junctions connected to form a pipe network (Dymond & Kutscher, 1996).

The model consisted of M horizontal nodes and N vertical nodes. This resulted in $M \cdot N$ z-directional pipes representing flow across the absorber, $(M - 1) \cdot N$ horizontal, x-directional pipes and $(N - 1) \cdot M$ vertical, y-directional pipes. The model also assumed one outlet for the flow placed at the top right corner and that, due to that, the flow could move only to the right and upwards.

The flow distribution problem consisted, thus, of a total $M \cdot N + M \cdot (N - 1) + N \cdot (M - 1)$ pipes with unknown flows. Modelling was based upon the principles of mass continuity and conservation of mechanical energy for each loop of the system.

Mass continuity was applied to the $M \cdot N$ nodes/junctions of the system, expressed with the following equation:

$$\sum_{i=1}^{Noofflows} (\rho_i \cdot Q_i) = 0 \quad (2.28)$$

Conservation of mechanical energy was applied to the $(N-1) \cdot M$ x-directional and $(M-1) \cdot N$ y-directional loops of the system by setting the sum of pressured drops around any closed loop to zero, assuming steady state incompressible flow.

The types of pressure drop considered are the following:

- Pressure drop across the absorber (z-directional pipes), defined according to Kutscher (1994) as:

$$\Delta P_{absorber} = 0.5 \cdot \rho \cdot \frac{Q_{face}^2}{A_{face}^2} \cdot [6.82 \cdot \left(\frac{1-\delta}{\delta}\right) \cdot \text{Re}^{-0.236}] \quad (2.29)$$

δ being the porosity of the absorber.

- Frictional pressure drop inside the collector plenum (Darcy-Weisbach, eq. 2.11)
- Pressure drop due to buoyancy:

$$\Delta P_{buoyancy} = (\rho_{ambient} - \rho_{y-pipe}) \cdot g \cdot (h_{y-pipe}) = \Delta \rho \cdot g \cdot h_{y-pipe} \quad (2.30)$$

$\Delta \rho$ being the difference between external and internal air density due to the temperature difference. It was assumed that the local variation of temperature resulted in a vertical buoyancy force positive in the y-direction and, thus, zero for the x-direction.

- Acceleration pressure drop, due to mass addition and geometric convergence as the flow reaches the outlet.

A loop of the system had the form shown in Figure 2.17:

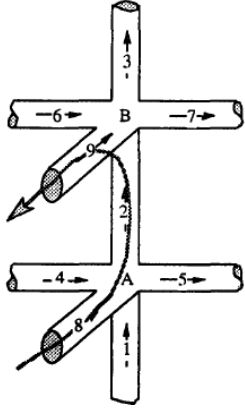


Figure 2.17: Example of a loop of the pipe network (Dymond & Kutscher, 1996).

For the loop of Figure 2.16, the mechanical energy conservation equation yields:

$$\Delta P_8 + \Delta P_2 - \Delta P_9 = 0 \quad (2.31)$$

where ΔP_8 and ΔP_9 were the pressure drops across the absorber for two consecutive z-directional pipes, the negative sign for ΔP_9 indicating that the flow in pipe 9 was in the opposite direction of the loop path and ΔP_2 consisted of the pressure drop due to friction, buoyancy and acceleration.

The relationships for pressure drop due to friction in a turbulent regime as well as for flow across the absorber and acceleration friction were linearized in the form of:

$$\Delta P = K' \cdot Q \quad (2.32)$$

For example, the coefficient for pressure drop across the absorber was the following:

$$K'_{absorber} = 0.5 \cdot \rho \cdot \frac{Q_{face}}{A_{face}^2} \cdot [6.82 \cdot (\frac{1-\delta}{\delta}) \cdot Re^{-0.236}] \quad (2.33)$$

so that:

$$\Delta P_{absorber} = K'_{absorber} \cdot Q_{face} = K'_{absorber} \cdot Q_{z-pipe} \quad (2.34)$$

The continuity equations and the linearized pressure drop equations were set in a matrix solution form for the flow distribution calculation:

$$K' \cdot Q = C \quad (2.35)$$

where K is the coefficient matrix, Q the matrix containing the unknown flows and C the solution vector. After the iterative solution of the flow distributions, the flows were then used to calculate the temperature distribution over the UTC area. The energy balance included radiation losses to the sky and to the ground and convectional losses due to external wind. The solutions of the temperature distributions were then again used as initial values for the flow model and the procedure was repeated until a defined convergence threshold was reached.

A major assumption of the model was that wind effects were considered insignificant and were not modeled based on the fact that if the pressure difference across the absorber is more than 25 Pa, wind does not affect the flow across the absorber.

2.7 Wind effects on solar collectors

Although the effect of wind on the flow distributions through the multiple-openings of such systems has been poorly addressed, such an investigation can benefit from parts of studies dealing with velocity and pressure distributions over an area of interest, as well as studies dealing with combination of wind tunnel exterior pressure results used as boundary conditions for CFD simulations. This will form the basis for the part of this investigation dealing with wind effects on the flow distribution over a multiple-inlet BIPV/T system, where the external pressures measured in a boundary layer wind tunnel over the BIPV/T area will be used as input to the mathematical flow model.

Wind effects have been studied extensively in terms of wind-induced convection on solar applications such as solar collectors, PV racks and BIPV/T, as well as in terms of wind loads concerning the structural stability of such systems. Wind forms a velocity boundary layer over the earth's surface, the velocity being lower near the earth's surface due to ground friction. After a specific height, called the gradient height, wind has its maximum velocity, termed gradient speed, which for all practical purposes is assumed constant after this height (Simiu & Scanlan, 1996). The in-between values of wind speed are calculated according to the following power law:

$$\frac{V_Z}{V_G} = \left(\frac{Z}{Z_G}\right)^a \quad (2.36)$$

where:

- V_Z : the mean wind velocity at a given height, below the gradient height (m/s)
- V_G : the gradient wind speed (m/s)
- Z : the height of interest (m)
- Z_G : the gradient height of the boundary layer (m)
- a : a power law exponent, which depends on the type of upstream exposure (open field, suburban, urban) (dimensionless)

Wind determines the external convective part of the collector's energy balance and thus the convective losses. In literature the external convective heat transfer coefficient, h_w , has been related linearly to the wind speed at a reference height, V_{loc} , depending on the direction of wind, the exposure settings and the geometric features of the test subject. There are considerable differences throughout these relationships, which makes it very difficult to have a general approach to include wind in the energy balance (Kaldellis et al, 2013). The relationship between h_w and V_{loc} is of the following format:

$$h_w = a \cdot V_{loc} + b \quad (2.37)$$

with a and b constants.

Vasan (2014) performed an extensive literature review of the above correlations, some of which are presented in Figure 2.18:

Study	h_c - V_{loc} relation	Equation number	Applicable wind direction	Distance of V_{loc} measurement from building surface
Ito et al., 1972	$h_c = 18.6 V_{loc}^{0.605}$	(10)	All	0.3 m
Sharples (1984)	$h_c = 1.7 V_{loc} + 5.1$	(11)	All	1 m
CIBSE Guide Book (2006)	$h_c = 4 V_{loc} + 4$	(12)	All	Not available
Liu and Harris (2007)	$h_c = 5.90 V_{loc} + 3.95$	(13)	0°	0.5 m
	$h_c = 6.42 V_{loc} + 3.17$	(14)	45°	
	$h_c = 7.42 V_{loc} + 2.98$	(15)	90°	
Blocken et al. (2009) [CFD study]	$h_c = 10.2 V_{loc}^{0.93}$	(16)	0°	1 m
	$h_c = 9.2 V_{loc}^{0.82}$	(17)	45°	
	$h_c = 7.7 V_{loc}^{0.77}$	(18)	90°	

Figure 2.18: Convective heat transfer-wind velocity relations for vertical building surfaces (Vasan, 2014).

Vasan investigated the effect of using the actual velocity distributions over a UTC installation versus assuming a uniform wind velocity over the whole area, on the estimation of the UTC performance. It was found that assuming that wind acts uniformly over the whole area lead to an overestimation of the heat exchange effectiveness of the collector up to 50%, as well an underestimation of the wind induced convective heat transfer coefficient by up to 20%. In a similar study concerning wind velocity distributions on roofs, Ladas (2014) found that there were considerable differences between wind velocities in the windward and the leeward part of the roof and that reflected upon the performance of solar collectors placed on each location.

Similarly, wind induced pressure over a large vertical surface is not distributed evenly, especially with varying wind direction. Aly & Bitsuamlak (2013) performed a sensitivity analysis on wind tunnel model scaling for ground-mounted solar panels. It was found that mean pressure coefficients were not affected by the size of the model, while for peak pressure coefficients the results were very consistent for scales 1:20 and 1:30. From the measurements over a PV installation with full scale dimensions 1.336m x 9.144m, a considerable variation of pressure coefficients was found over the test area, as shown in Figure 2.19:

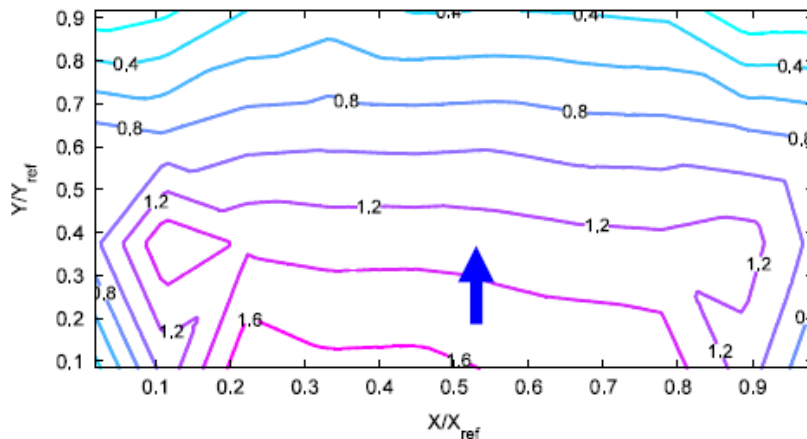


Figure 2.19: Wind tunnel mean pressure coefficients ($C_{p,mean}$) distribution over a solar panel scaled 1:20 (Aly & Bitsuamlak, 2013).

The study also suggested the combined use of wind tunnel measurements and CFD, with which, a full scale model could be simulated.

Kato et al (1997) introduced a hybrid approach combining wind tunnel measurements and CFD for the estimation of cross ventilation. A wind tunnel was used to simulate the external airflow

and CFD was used for the internal airflow distributions. This method aimed to reduce the computational cost of CFD for simulation of the outdoor wind while still providing detailed indoor air distribution. Lo et al (2013) improved on Kato's hybrid method with the inclusion of wind fluctuations, as well as change in wind directionality.

The aforementioned hybrid approach consisted of wind tunnel pressure measurements conducted on the façade of the building, specifically by placing sets of pressure taps at the locations where the openings were supposed to be and averaging the measurements. The acquired pressure measurements could afterwards be used as pressure boundary conditions for the CFD model.

This method was based upon the note that since the façade openings were of less than 2% wall porosity, pressure driven flows could be assumed. It was found that although the flow distribution predictions in the interior were not that accurate, the coupled wind tunnel-CFD method could provide more accurate predictions of the total cross ventilation flow rates.

3. Experimental procedure

3.1 Multiple-inlet BIPV/T concept and initial design

The concept of a multiple-inlet BIPV/T system has its origins in the hybrid PV/T-UTC design developed by Athienitis (2010), as a project of the Solar Buildings Research (SBRN), and was applied to the JMSB building of Concordia University as a demonstration project. As described in the previous chapter, this prototype consisted of a layer of UTC of 1% porosity, with PV panels placed on 70% of its surface area. With this configuration, this system was able to produce energy, while heat was extracted from both the absorber plate of the UTC and the PV panels.

An evolution of the above was to make maximum use of the given area with 100% PV coverage, but assigning inlets to the frames of each PV, the area of each inlet being 1% of the total PV area. The UTC would not be needed as a racking system, as the framed PV panels could be set directly on the side bearing elements.

An experimental design of a multiple-inlet BIPV/T prototype was developed by Bigaila and Athienitis (Bigaila et al, 2015), while the author of this thesis assisted in its construction and the experimental measurements out carried upon it, focusing on the flow measurements. The prototype, which can be seen in Figure 3.1, consisted of three PV panels, two opaque and a semi-transparent module. The PV panels were set within frames, while holes were cut on the front part of the frame of each panel. The framed panels were set in an overlapping configuration, the cross section of which can be seen in Figure 3.2

Two side buffer zones were created with use of aluminum plates painted black, to represent adjacent PV strings and eliminate heat transfer to the sides of the PV set-up. The back part of the PV frame protruded by 4cm into the air channel, leaving an opening of 0.04m x 1m for the air to pass through.

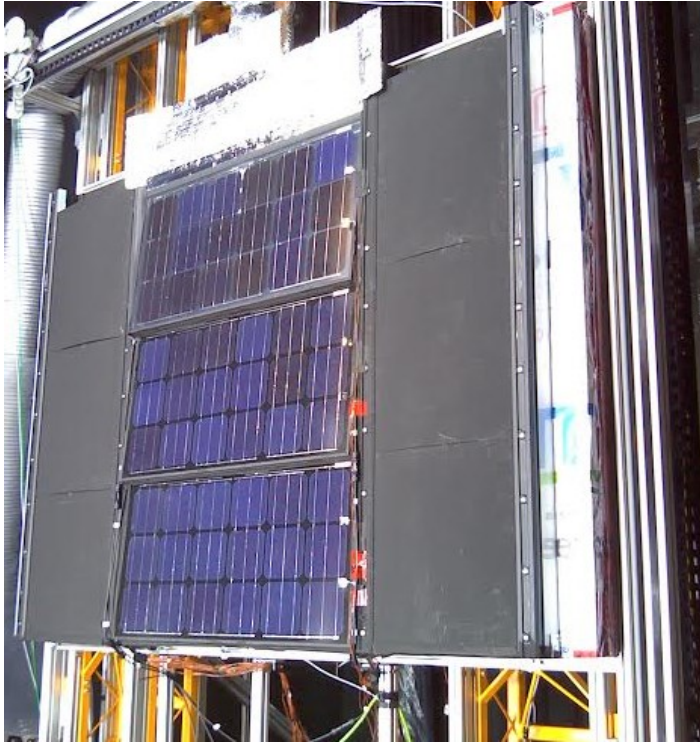


Figure 3.1: 3-inlet BIPV/T prototype tested at the Concordia University Solar Simulator.

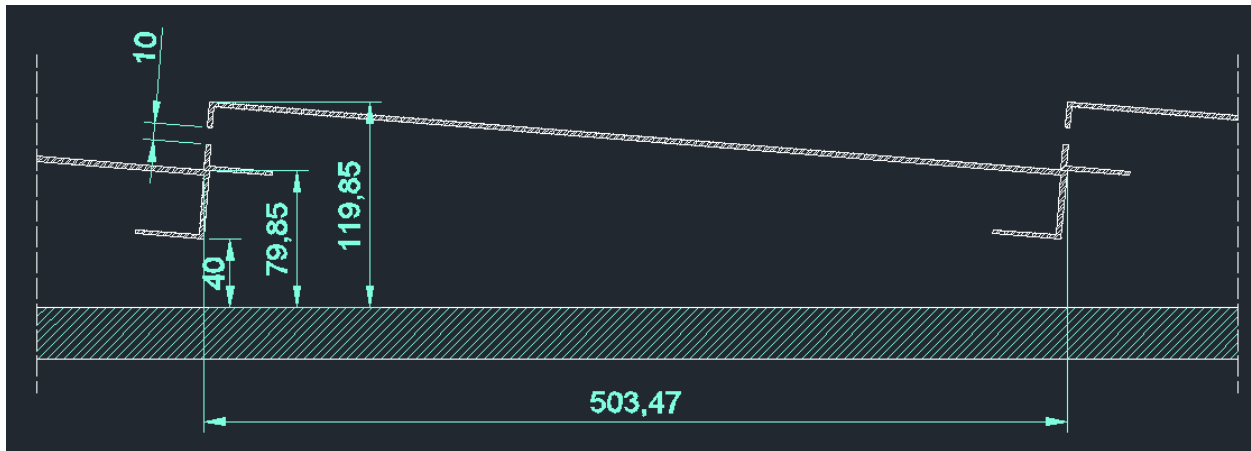


Figure 3.2: 3-inlet BIPV/T prototype tested at the Concordia University Solar Simulator (dimensions in mm).

3.2 Solar Simulator testing

The experimental prototype was tested at the Concordia University Solar Simulator. This research facility is designed to simulate solar radiation and wind-induced convection at ambient temperature of 20-25°, thus providing controlled environmental testing conditions. The solar simulator consists of a test platform, upon which test specimens may be mounted and a lamp

field that can emulate the sun light. The test platform may be tilted at any angle between the horizontal and the vertical position (Bambara et al, 2012).

The lamp field consists of a set of 8 metal halide global lamps which can be moved individually on a 2-axis system to provide an irradiance uniformity of up to $\pm 5\%$ on test surfaces of different sizes. The irradiance intensity may vary from 700 W/m^2 to 1100 W/m^2 . To eliminate the infrared radiation from the hot lamps, an artificial sky is placed in front of the lamp field, which also simulates sky temperature.

In order to simulate wind-induced convection, a centrifugal fan is set at the bottom edge of the platform blowing wind parallel to the test specimen.

When testing air-based systems such as BIPV/T, an air collector unit can be connected to the test specimen in an open- or closed-loop formation to cause the circulation of air with use of a multiple speed fan creating negative pressure (suction). An orifice plate is set within the air collector, for which the relationship between pressure drop across the plate and air flow is known and thus the air collection rate can be set manually.

The three-inlet prototype was tested for its electrical and thermal performance and flow measurements were carried out with a hot wire flow meter. The flow measurements were taken at the back part of the frames of each PV panel. The various flow rates were set by the air collector and for three angles of placement of the test specimen (horizontal, 45° and vertical). From the measurements it was found that the inclination of the subject did not affect the flow distributions of the three inlets. However, the flow measurements were limited due to the available equipment and were performed at one single location for each panel, namely, in the middle of the gap created by the back part of the frame of each panel and the back insulation, where the air flow was expected to converge. The results of the measurements and the comparison to the numerical model for the inlet flow distributions are presented in Chapter 4.

3.3 Wind tunnel testing

The multiple-inlet prototype tested in the Solar Simulator would form the base for a potential BIPV/T retrofit project, for an institutional office building application, namely the Montreal Courthouse. This particular building is located in the Old Port location of Montreal, Canada, facing 58° east of south (azimuth -58°), as shown in Figure 3.3:

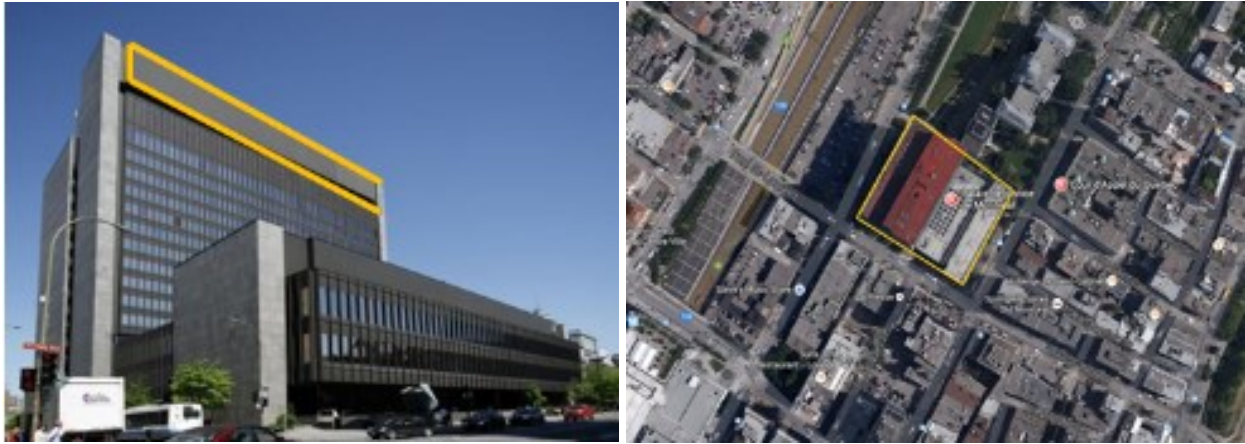


Figure 3.3: The Montreal Courthouse with potential BIPV/T installation in yellow (left) and its orientation (right).

The highlighted area in Figure 3.3 (left) shows the top part of the south east façade where the BIPV/T system could be installed.

In order to account for the wind effects on the flow distributions of a multiple-inlet system installed over such a large area (81.2m x 11m), the pressure distributions over the BIPV/T area needed to be assessed. These pressures would be used as inputs in the flow distribution model, described in detail in Chapter 4.

These pressure distributions were studied experimentally at the Boundary Layer Wind Tunnel facility of Concordia University, on a 1:400 scale model of the actual building.

3.3.1 Concordia University Boundary Layer Wind Tunnel

The BLWT of Concordia University is an open loop wind tunnel with a width of 1.8 m, height ranging from 1.4-1.8m due to an adjustable ceiling and a length of 12.2 m. It can produce wind velocities from 3 m/s to 14 m/s, while test specimens can be placed on a turntable located at the test section, which allows them to be tested for various wind directions (Vasan, 2013). A schematic of the facility is shown in Figure 3.4:

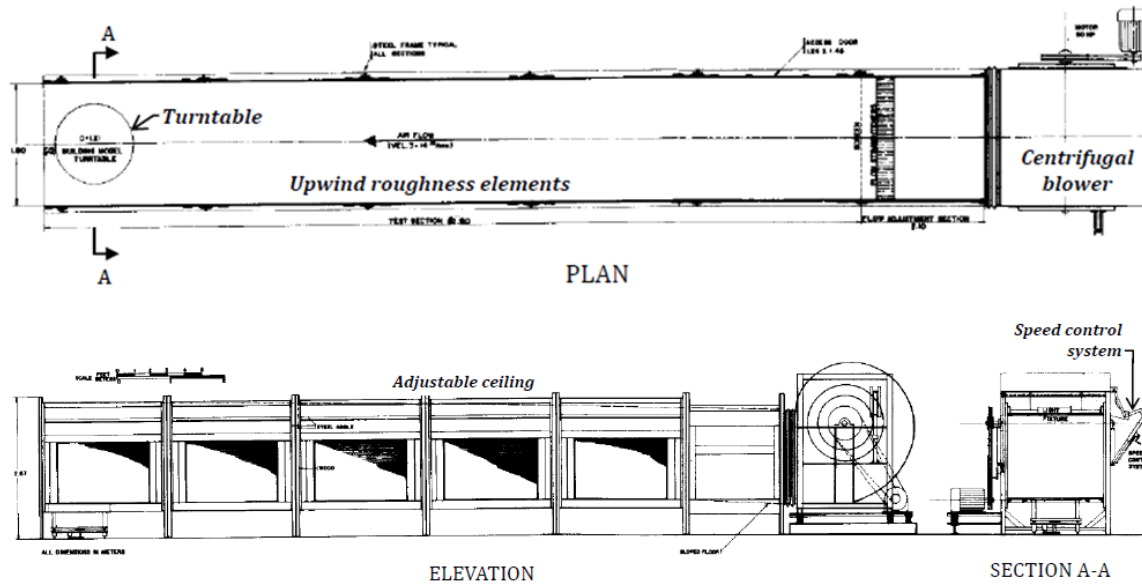


Figure 3.4: Schematic of the boundary layer wind tunnel at Concordia University (Stathopoulos, 1984).

3.3.2 Wind tunnel model

Stathopoulos (1984) found that based on the wind tunnel dimensions and flow characteristics, a model scale of 1:400 resulted in the best agreement for the actual and modelled spectrum of wind and thus provided the best measurement results. A model of the Courthouse building was designed and built to that scale by using 3D printers. The model, shown in Figure 3.5, was designed as a 3mm thick shell and was printed out of a rigid polymer.



Figure 3.5: 1:400 scale model of the Courthouse building made by 3D printer.

A 203 mm x 27.5 mm Plexiglas face was created to represent the retrofit area. 28 pressure taps were embedded in that face as shown in Figure 3.6:



Figure 3.6: Face with pressure taps of the wind tunnel model.

It is the author’s opinion that wind measurements cannot be generalized and that for each particular building an exact representation of the surroundings should be employed for accurate measurements of either the velocity or the pressure field over the test area.

However, a general assessment of pressure distributions over a retrofit area, for various angles of incidence of oncoming wind, may provide input on the expected performance of a multiple-inlet system, as well as design insight concerning the amount and placement of the inlets, based on the prevailing local winds.

The model was, therefore, tested in an open field exposure, with a flow exponent of $\alpha=0.23$, and for 5 directions of oncoming wind, as shown in Figure 3.7:

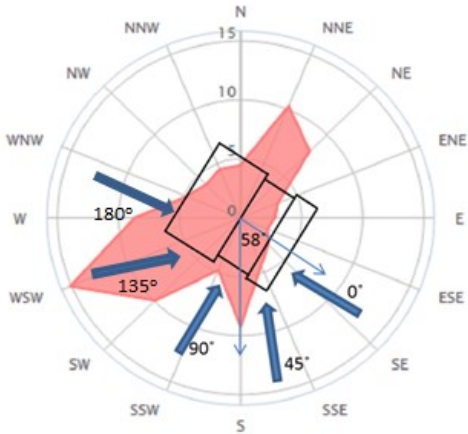


Figure 3.7: Building orientation, wind diagram for Montreal and wind directions tested.

A pitot tube was placed at the simulated gradient height (60 cm), from which the dynamic pressure of wind was acquired. The static pressures over the retrofit area were measured for the five wind directions. Finally, the ratios of the static pressures measured over the dynamic pressure of wind were calculated in order to form the dimensionless pressure coefficients, C_p . These coefficients are independent of the wind velocity, but vary according to the wind direction over the given surface, and can be used to calculate surface pressures as follows:

$$P_s = C_p \cdot \frac{1}{2} \cdot \rho \cdot V_{loc}^2 \quad (3.1)$$

where:

- P_s : the surface pressure (Pa)
- C_p : the pressure coefficient for a given wind direction (dimensionless)
- ρ : the air density (kg/m^3)
- V_{loc} : the velocity of wind at the height of measurement (m/s)

3.3.3 Experimental results and discussion

The results of the measurements are presented in the form of contours of the mean pressure coefficients over the retrofit surface. Each case, classified according to the angle of incidence of oncoming wind to the test area, is presented in Figures 3.8 through 3.12:

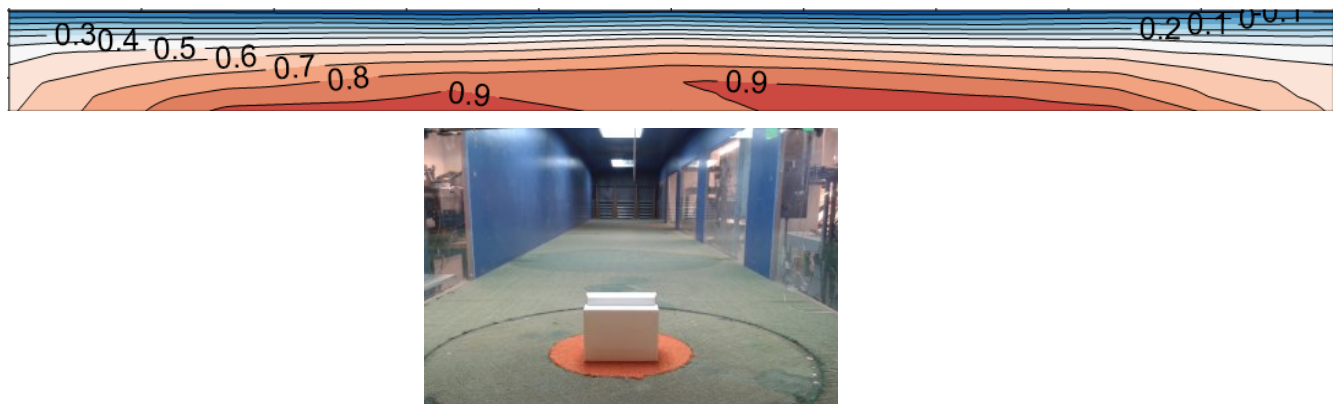


Figure 3.8: Mean pressure coefficient (C_{p_mean}) for 0° wind direction (top) and wind tunnel model placement (bottom).

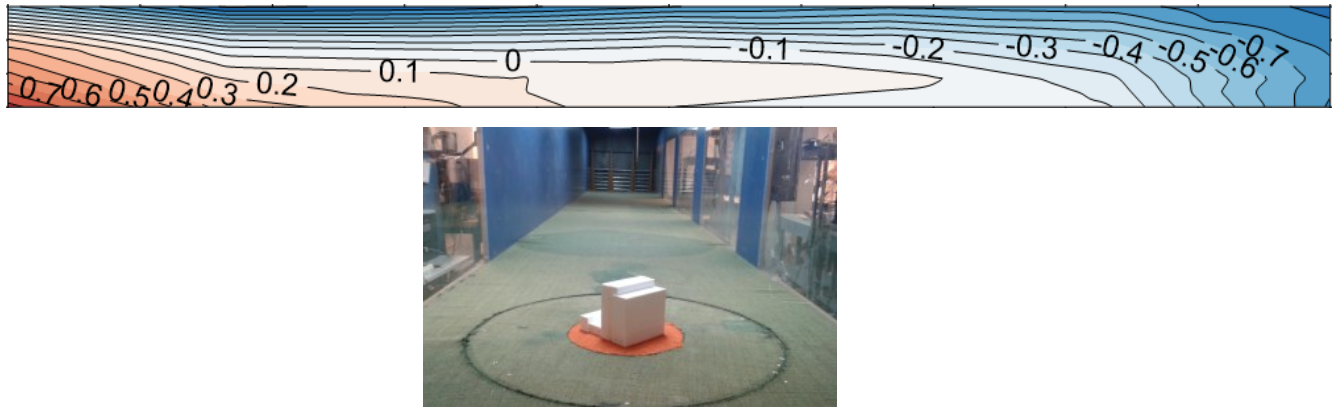


Figure 3.9: Mean pressure coefficient (C_{p_mean}) for 45° wind direction (top) and wind tunnel model placement (bottom).



Figure 3.10: Mean pressure coefficient (C_{p_mean}) for 90° wind direction (top) and wind tunnel model placement (bottom).



Figure 3.11: Mean pressure coefficient (C_{p_mean}) for 135° wind direction (top) and wind tunnel model placement (bottom).

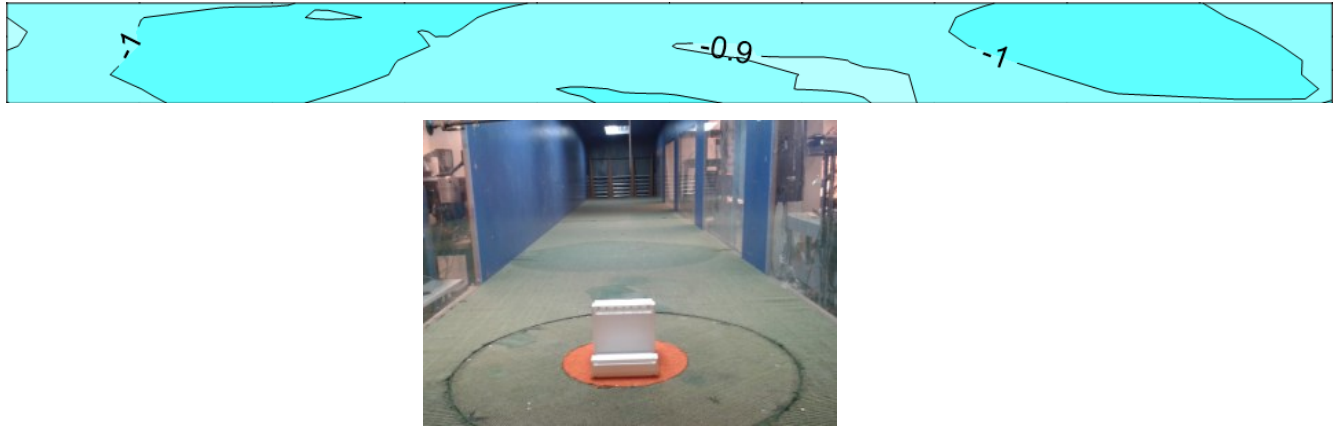


Figure 3.12: Mean pressure coefficient (C_{p_mean}) for 180° wind direction (top) and wind tunnel model placement (bottom).

Negative pressure coefficients mean that suction occurs at the specific location. In order for the results to be more visual, scales of red were used to signify positive pressure, the darker shades denoting the highest values and vice versa for negative pressure, for which shades of blue were used, white implying zero pressure.

As expected, for the first case of 0° wind, the pressure distribution is almost symmetric about the y-axis of the retrofit area. Highest positive pressure coefficients occur at the central bottom part of the surface, while suction is present at the top edge where the airflow separates and accelerates, creating a negative pressure zone.

The first and the second case, that of 45° wind, seem to create the highest pressure coefficient distributions in the vertical sense. For a PV string, placed along the installation height, this would mean highly varying pressure values at each inlet of the system which could lead to outflow at the locations under suction for an improperly designed system.

For the case of 90° wind, regions under the same pressure coefficient are almost vertically discretized. This means that PV strings would lie under the same pressure regime along the height of the string and the flow distributions would be affected the same way as in no wind conditions. The negative pressure, however, would reflect upon the fan consumption by increasing it to achieve the same air collection rate. In this case, the BIPV/T surface is parallel to the oncoming wind and with separation occurring at the building's edge, it is under extreme suction regime. The highest suction occurs at the windward part, within the separation zone.

For the cases of 135° and 180° wind, the BIPV/T surface is essentially located at the wake of the airflow. For both cases, the BIPV/T area is under suction which is approximately uniform throughout.

4. Multiple-inlet BIPV/T modelling

As stated in section 2.2, heat transfer via convection from the PV layer to the air stream is mainly dependent upon two factors: the air flow rate inside the air channel and the temperature difference between the circulating air and the PV panels.

The purpose of a multiple-inlet system is the regulation of both of the above parameters. With the introduction of more openings for the intake of fresh air, the temperature difference between circulating air and the PV panels is increased for the upper PV modules, due to the addition of an air stream that is cooler than the preheated air coming from the previous control volume below. The temperature of air entering each control volume is determined by the nature of the flow through the corresponding inlet, as well as by that of the previous control volume, as described in section 4.2.1.

The amount of flow coming from each inlet and as a result the weighted air temperature and the flow rate of each control volume is regulated according to the geometric features of the openings and the air channel. These geometric features determine the resistance to the flow and as a consequence the flow distributions from the inlets of the system.

The modelling of a multiple-inlet BIPV/T consists of two parts; one is the flow model, dealing with the amount of air entering from each opening of the system, and the other is the energy model which uses the flow rates calculated from the flow model for the internal convection part.

4.1 Flow distribution model

Flow distributions in a multiple-inlet system result in a complex flow network that could be described with an electrical analogy, as discussed in section 2.6.1. A set of exterior sources, outside the system's openings, or inlets, represents the exterior pressures over the BIPV/T area, while the interior nodes represent the internal pressure of the air channel. The branches connecting exterior sources to interior nodes show the flow through the inlets, while the branches connecting interior nodes, the flow through the air channel. A schematic of the general flow network of multiple-inlet BIPV/T is shown in Figure 4.1:

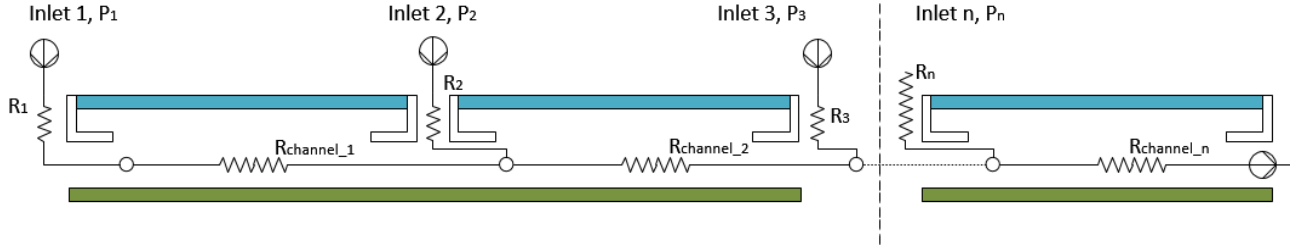


Figure 4.1: Resistance-circuit representation of the flow network of the multiple-inlet system.

The exterior sources and interior nodes of two consecutive inlets form a closed loop, similar to the ones of pipe networks, also adopted by Dymond and Kutscher (1996) for the modelling of UTC flow distributions.

The main principles upon which the flow modelling is based are mass continuity and conservation of mechanical energy.

Mass continuity is expressed as follows:

$$\sum_{i=1}^n Q_{opening(i)} = Q_{tot} \quad (4.1)$$

where:

- $Q_{opening(i)}$: the flow through the i -th opening of the system (m^3/s)
- Q_{tot} : the total air collection rate from the system's fan (m^3/s)

Conservation of mechanical energy is applied to each of the closed loops formed in the flow network in the form of pressure drop. The sum of pressure drops in a closed loop should be equal to zero, as expressed by the following relationship:

$$\Delta P_{opening(i)} + \Delta P_{channel(i)} - \Delta P_{opening(i+1)} + P_{(i+1)} - P_{(i)} = 0 \quad (4.2)$$

where:

- $\Delta P_{opening(i)}$: Pressure drop from flow across the i -th inlet (flow through an orifice) (Pa)
- $\Delta P_{channel(i)}$: Frictional pressure drop from flow within the i -th air channel, as well as from flow through the back frame of the PV panels (Pa)

- $P_{(i)}$: Pressure exterior to the i-th inlet, defined by the local wind effects (Pa)

4.1.1 Pressure drops

- Flow across the inlet

The system's inlets will be less than 2% of the BIPV/T area, therefore, according to Lo et al (2012), pressure driven flow may be assumed. The flow through an orifice (equation 2.16) could be employed to describe the pressure drop from flow across the system's inlets.

- Flow through the air channel

The flow through the air collector is not continuous, since new air streams, entering through the inlets, interfere with the internal stream, interrupting its continuous flow. For practical purposes, it can be assumed that between openings, separate channels are formed for each module, which are interconnected. The flow of these channels is a sum of the air entering from the previous channel and that from the inlet, resulting to a different Reynolds number for each channel and different frictional losses.

The pressure drop from flow within the air channel is a combination of frictional losses, as well as pressure drop from flow across the back part of the air channel, due to the resistance caused by the frame of the PV panels, in case of a framed configuration.

The relationship used to describe the frictional losses of these channels is the Darcy-Weisbach equation (2.12), which can be replaced by equation 4.3 as follows:

$$\Delta P = f \cdot (L / D_h) \cdot \frac{1}{2} \cdot \rho \cdot (Q^2 / A^2) \quad (4.3)$$

where Q and A are the volumetric flow rate inside the air channel and the cross sectional area of the air channel respectively.

The pressure drop due to flow across the back part of the air channel is also described by this orifice equation.

- External pressure

The local pressure exterior to the inlets of the system is a result of the local wind effects. The pressure caused by wind on the BIPV/T area, depending on its direction and velocity, was measured at the Boundary Layer Wind Tunnel of Concordia University for a test model of the Montreal Courthouse building, as described in sections 3.3.2 and 3.3.3. In order to acquire the external pressure distribution, the dynamic pressure of wind needs to be calculated as:

$$P_{wind} = \frac{1}{2} \cdot \rho \cdot V_{loc}^2 \quad (4.4)$$

where V_{loc} is the wind velocity at the installation height. Then the dynamic pressure will be multiplied by the measured pressure coefficients, depending on the direction of oncoming wind and thus provide the local pressure distribution. When acquired, these pressures can be used as input in the mechanical energy conservation equations of the flow loops described above, in a similar way as Lo et al (2012).

4.1.2 Frictional and secondary losses

The friction factor f , used in the Darcy-Weisbach equation (2012) for the calculation of the frictional pressure drop in a pipe, is calculated from the Moody chart, according to the Reynolds number of the flow and the relative roughness of the material of the pipe walls. In the case of laminar flow ($Re < 2300$) an empirical formula used is:

$$f = 64 / Re \quad (4.5)$$

For the turbulent regime, several empirical relationships have been suggested (Hegazy, 1999; Balocco, 2001; Ghani et al, 2012). The one used in this study is the one also used by Ghani (2012), as it also has good agreement of results with equation 4.5 for the laminar region:

$$f = (0.79 \cdot \ln(Re) - 1.64)^{-2} \quad (4.6)$$

The flow factors of secondary, or local, losses due to flow across the inlets and the opening formed by the back frame of the PV and the back wall, namely the K_{inlet} and the $K_{b.frame}$ were calculated according to the Duct Design section (Ch.21) of the ASHRAE Fundamentals. For each opening the local losses are due to flow through a sharp opening with a $K=0.5$ and a sudden

expansion of the flow, or exit loss, with a $K=1$. As a result both the K_{inlet} and the $K_{b.frame}$ were assumed equal to 1.5. This was an approximation to be used in the numerical procedure; however, further experiments should be carried out to establish more accurate coefficients from the measured relationship between the flow through the designed openings and the pressure drop across them.

4.1.3 Electrical analogy

The complex flow network of a multiple-inlet BIPV/T is modelled in this study employing an electrical circuit analogy, in accordance with Aynsley (1997). In an electrical circuit the relationship linking the voltage, V , the current, I , and the electrical resistance R is:

$$V = I \cdot R \quad (4.7)$$

For the flow network, the volumetric flow rate Q (m^3/s) is the equivalent to current, the pressure drop (Pa) between two nodes is the equivalent to voltage and the resistance to the flow is defined according to the geometric features of the flow path. The equivalent relationship to equation (4.57) is the following:

$$\Delta P = Q \cdot R \quad (4.8)$$

There are two types of resistances formed from the linearization of equations (2.16) and (4.3) in order for them to take the form of equation (4.8):

- Inlet Resistance

$$R_{inlet} = \left(\frac{K_{inlet}}{A_{inlet}^2} \right) \cdot \frac{Q_{inlet}}{2} \cdot \rho \quad (4.9)$$

- Channel resistance

$$R_{channel} = \left(f \cdot \frac{L}{D_h} + K_{b.frame} \right) \cdot \frac{Q_{channel}}{2 \cdot A_{b.frame}^2} \cdot \rho \quad (4.10)$$

where:

- $R_{opening}$, $R_{channel}$: the resistances of the inlet and the air channel respectively ($kg/(m^4 s)$)

- K_{inlet} , $K_{b.frame}$: the K factors of the inlet and the back part of the PV frame, as defined in section 4.1.2
- A_{inlet} , $A_{channel}$: the cross sectional area of the inlet and the air channel respectively (m^2)
- L : the length of the air channel (m)
- D_h : the hydraulic diameter of the air channel (m)
- f : the friction factor as defined in 4.1.2
- Q_{inlet} , $Q_{channel}$: the volumetric flow rate through the inlet and the air channel respectively
- ρ : the air density (kg/m^3)

The pressure drops due to flow across an inlet and through an air channel can now be written as follows:

- Inlet pressure drop:

$$\Delta P_{inlet} = Q_{inlet} \cdot R_{inlet} \quad (4.11)$$

- Channel pressure drop:

$$\Delta P_{channel} = Q_{channel} \cdot R_{channel} \quad (4.12)$$

By substituting (4.9) and (4.10) into (4.2), it becomes:

$$Q_{inlet(i)} \cdot R_{inlet(i)} + Q_{channel(i)} \cdot R_{channel(i)} - Q_{inlet(i+1)} \cdot R_{inlet(i+1)} + P_{(i+1)} - P_{(i)} = 0 \quad (4.13)$$

4.1.4 Solution matrix

A system with n-inlets will consist of n-1 loops. This system will be described by a set of n-1 equations of conservation of mechanical energy in the form of (4.13), one per loop, as well as one mass conservation equation. This results in a system of n-equations with n-unknown flows through the inlets.

The resulting equations are of the following form:

Mechanical energy conservation:

- First loop:

$$Q_{\text{inlet}(1)} \cdot R_{\text{inlet}(1)} + Q_{\text{channel}(1)} \cdot R_{\text{channel}(1)} - Q_{\text{inlet}(2)} \cdot R_{\text{inlet}(2)} + P_2 - P_1 = 0 \quad (4.14)$$

- Second loop:

$$Q_{\text{inlet}(2)} \cdot R_{\text{inlet}(2)} + Q_{\text{channel}(2)} \cdot R_{\text{channel}(2)} - Q_{\text{inlet}(3)} \cdot R_{\text{inlet}(3)} + P_3 - P_2 = 0 \quad (4.15)$$

- (n-1)-th loop:

$$Q_{\text{inlet}(n-1)} \cdot R_{\text{inlet}(n-1)} + Q_{\text{channel}(n-1)} \cdot R_{\text{channel}(n-1)} - Q_{\text{inlet}(n)} \cdot R_{\text{inlet}(n)} + P_n - P_{n-1} = 0 \quad (4.16)$$

Mass continuity equation:

$$Q_{\text{inlet}(1)} + Q_{\text{inlet}(2)} + \dots + Q_{\text{inlet}(n)} = Q_{\text{total}} \quad (4.17)$$

The flow of each channel equals to the sum of the flow from the previous channel and the flow through the module's inlet:

$$Q_{\text{channel}(i+1)} = Q_{\text{channel}(i)} + Q_{\text{inlet}(i+1)} \quad (4.18)$$

Given the equations (4.17) and (4.18), the mechanical energy conservation equations (4.14) through (4.16) may be transformed as follows:

- First loop:

$$Q_{\text{inlet}(1)} \cdot (R_{\text{inlet}(1)} + R_{\text{channel}(1)}) - Q_{\text{inlet}(2)} \cdot R_{\text{inlet}(2)} = P_1 - P_2 \quad (4.19)$$

- Second loop:

$$Q_{\text{inlet}(1)} \cdot R_{\text{channel}(2)} + Q_{\text{inlet}(2)} \cdot (R_{\text{inlet}(2)} + R_{\text{channel}(2)}) - Q_{\text{inlet}(3)} \cdot R_{\text{inlet}(3)} = P_2 - P_3 \quad (4.20)$$

- (n-1)-th loop:

$$Q_{inlet(1)} \cdot R_{channel(n-1)} + \dots + Q_{inlet(n-2)} \cdot R_{channel(n-1)} + Q_{inlet(n-1)} \cdot (R_{inlet(n-1)} + R_{channel(n-1)}) - Q_{inlet(n)} \cdot R_{inlet(n)} = P_{n-1} - P_n \quad (4.21)$$

All the above equations can be rewritten in a matrix form as follows:

$$[R] \cdot \{Q\} = [P] \quad (4.22)$$

where:

- [R]: the matrix containing the coefficients of the flows; the resistances for the mechanical energy conservation equations and those for the continuity of mass equation
- {Q}: the vector with the unknown inlet flows
- [P]: the vector containing the constants of the right part of the equations; the external pressure differences and the total air collector volumetric flow

It is clear that the relationship between pressure difference and flow is non-linear. Inlet and channel flows are used within the resistances in order to produce a system of equations with a linear form for the matrix solution.

4.2 Wind effects and energy balance

4.2.1 Flow distributions due to wind effects

The following modelling part, dealing with flow distributions due to wind effects and the energy balance, is done with the assumption that the total outflow, through each PV string's outlet to the manifold, is the same.

Investigation of flow distributions of the manifold is not an object of the current study. It is also assumed that the fan provides a constant suction rate. This means that if the pressure difference is higher, the fan will provide the desired total flow rate, but at higher consumption. Furthermore, if in case of wind, there are differential external pressures along a PV string, the outflow due to suction at some of the inlets of the system will be compensated for by increased flow through some other inlets.

As shown in section 3.3.3, wind may cause varying pressure distributions over the BIPV/T area, depending on its direction. The angles of incidence of 0° (perpendicular wind) and 45° may cause the most varying differential pressures along the height of a PV string. For the rest of the cases

(angles of incidence 90° , 135° and 180°), due to the nature of the pressure distributions, it could be assumed that areas are formed with the same pressure regime along the PV string height.

For the first two cases (see Figures 3.8 and 3.9) varying pressures may cause both compression and suction through the system inlets. In Figure 4.2 the possible flow paths through the inlets and within the air channels are shown:

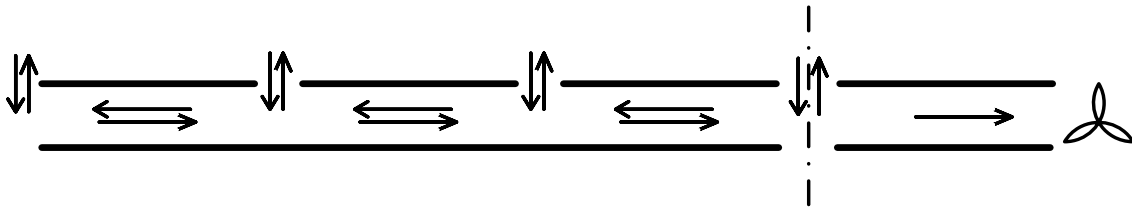


Figure 4.2: Possible flow paths for the inlets and channels of the multiple-inlet system.

The convention for the flow paths is as follows: The flow within the channel is considered positive if it is directed towards the fan and negative otherwise. The flow through the inlets is considered positive if it is entering the collector and negative otherwise. The flow distributions of the multiple-inlet system are of utmost importance for its energy balance, since the flows within each channel define the internal convection, while the direction of the inlet and the channel flow determines the entrance temperature of air, as will be shown in detail in the energy balance part.

4.2.2 Measured and simulated results

The flow distribution model was applied to the three inlet prototype described in sections 3.1 and 3.2. The measured and simulated results are shown in Figure 4.3. The flow distribution model was applied for the experimental case of the three-panel BIPV/T described in sections 3.1 and 3.2. The results of the model were compared to the measurements taken with the hot wire velocity meter at three flow points, at the back part of each panel. The measured and simulated results are shown in Figure 4.3. All measured flows are normalized by the total outflow of the air collector.

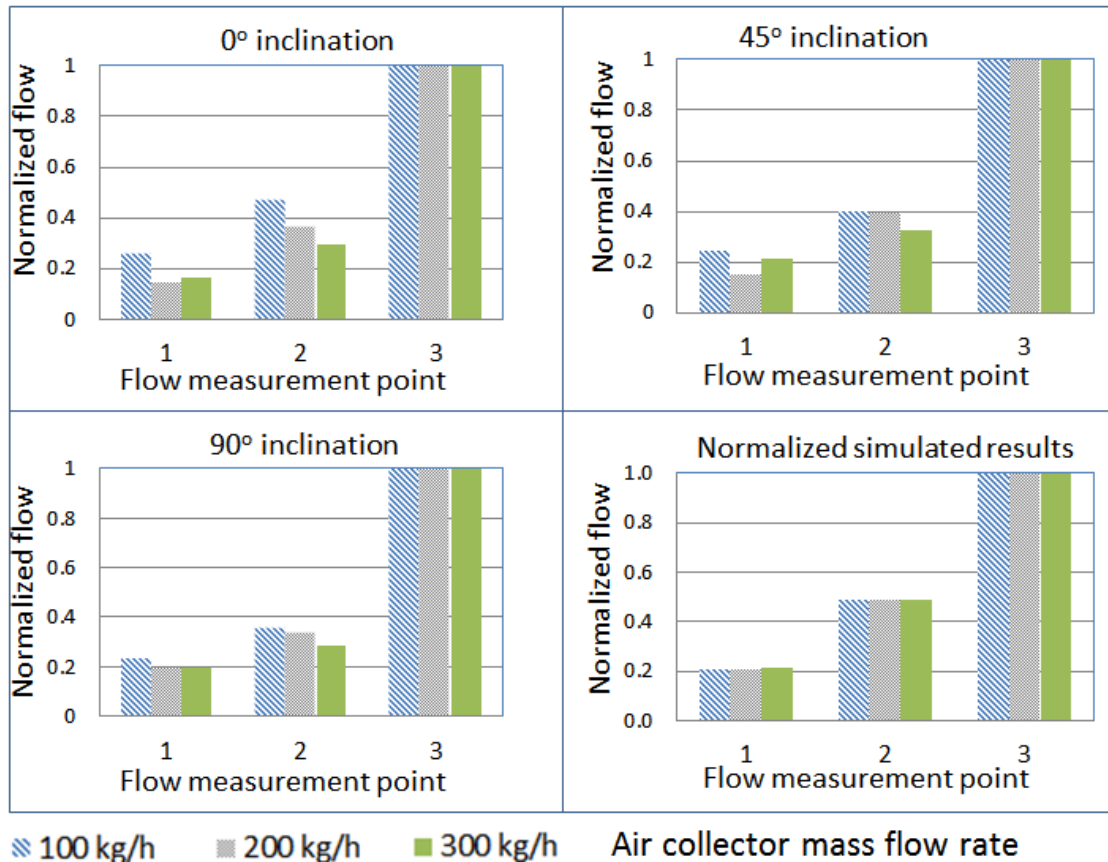


Figure 4.3: Normalized mass flows at the back of each panel of the 3-inlet prototype, for three angles of placement in the solar simulator.

The specific results were for cases where no external wind and no irradiation were involved, as the representation of wind effects in the Solar Simulator is not accurate, while the effects of fan induced suction and the plenum’s geometry were under investigation. The measurements were carried out for three total mass flow rates 100kg/h, 200kg/h and 300kg/h for each angle of placement. The model requires further calibration, however, the results of the simulations were within a 25% error range from the measured results, which would be a reasonable threshold for flow measurements (Rounis et al, 2015)

4.3 Modified energy balance model

The energy balance for a BIPV/T, assuming that each PV module comprises a control volume (CV), is shown in Figure 4.4:

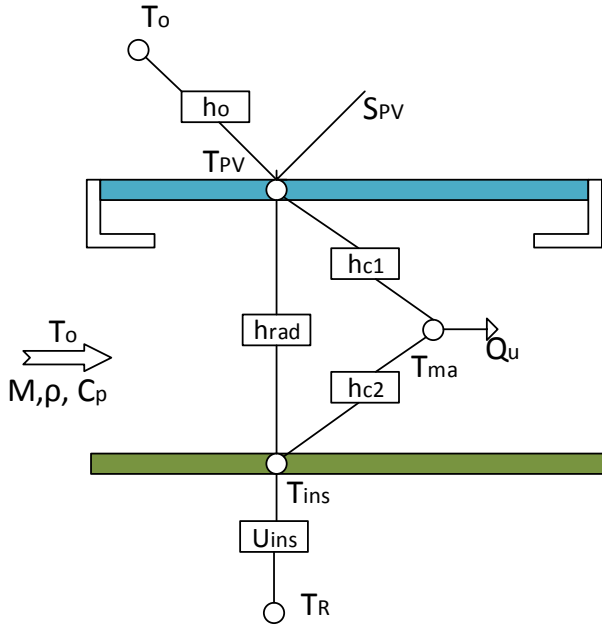


Figure 4.4: BIPV/T control volume energy balance.

where:

- T_o : the external temperature ($^{\circ}\text{C}$)
- h_o : the exterior film coefficient ($\text{W}/\text{m}^2\text{ }^{\circ}\text{C}$)
- T_{PV} , T_{ma} , T_{ins} and T_R : the temperatures of the PV the air inside the air channel, the surface of the insulation and the adjacent room respectively
- h_{c1} , h_{c2} : the convective heat transfer coefficients from the PV and the insulation surface to the flowing air respectively ($\text{W}/\text{m}^2\text{ }^{\circ}\text{C}$)
- h_{rad} : the radiative heat transfer between the PV and the insulation surfaces ($\text{W}/\text{m}^2\text{ }^{\circ}\text{C}$)
- S_{PV} : the net heat absorbed by the PV layer (total absorbed-electric produced) (W/m^2)
- ρ : the density of air (assumed constant), ($1.2\text{kg}/\text{m}^3$)
- C_p : the specific heat capacity of air, assumed constant ($1000\text{j}/\text{kg }^{\circ}\text{C}$)
- M : the mass flow rate inside the collector, assumed constant (kg/s)

The flow rate within the air channel is constant and therefore so is Reynolds number. As the air enters from a single opening, the temperature of air at the entrance of the first control volume (CV) is assumed equal to the ambient air temperature and for each new CV, the entering air temperature is assumed the same as that of air exiting the previous CV.

The energy balance for a multiple-inlet BIPV/T is very similar and is shown in Figure 4.5:

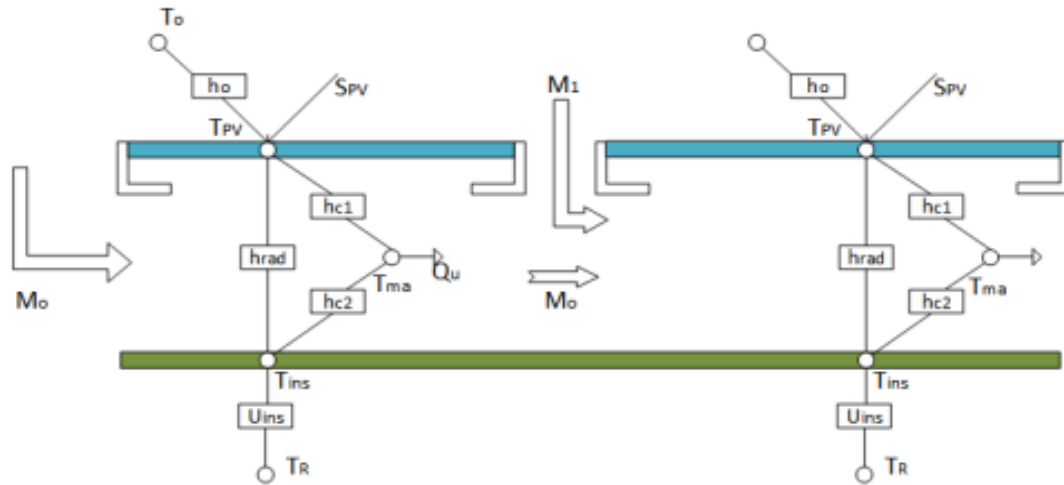


Figure 4.5: Multiple-inlet BIPV/T control volume energy balance.

The main difference is that each CV has a different air flow rate and Reynolds number, and there are various cases concerning the entrance temperature of air entering a CV. For the case of no wind, the flow rate of the n-th control volume is the sum of the flows from the previous CV and that of the n-th inlet, while the entrance air temperature is a weighted temperature of the exterior air and that exiting the previous CV.

For the instances of varying exterior pressure as discussed in 4.3.1 the following cases are created concerning inlet and channel flows and how these are going to be used in the energy balance:

4.3.1. Positive channel flow (towards the air collector)

I. Positive flow from previous CV and positive inlet flow

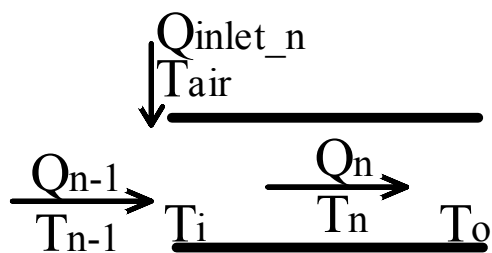


Figure 4.6: Positive channel flow with positive flow from the previous channel and positive inlet flow.

where:

- Q_{inlet_n} : the flow through the n-th inlet (m^3/s)
- Q_{n-1} : the flow from the (n-1)-th CV (m^3/s)
- Q_n : the flow of the n-th CV (under investigation) (m^3/s)
- T_{air} : the ambient air temperature ($^{\circ}C$)
- T_{n-1} : the temperature of air from the (n-1)-th channel ($^{\circ}C$)
- T_i, T_o : the air temperature at the entrance and at the exit of the air channel respectively ($^{\circ}C$)

For each channel/CV, the subscript I denotes the end of the n-th CV closer to the n-th inlet, while the subscript o, the end closer to the system's outlet. In the case of reversed flow, as will be seen later on, these subscripts are not reversed.

For this case, the stream from the inlet joins the stream from the previous channel resulting in an entrance air temperature weighted by the respective flows:

$$T_i = \frac{T_{air} \cdot Q_{inlet_n} + T_{n-1} \cdot Q_{n-1}}{Q_{inlet_n} + Q_{n-1}} \quad (4.23)$$

II. Positive inlet flow, negative flow from previous CV

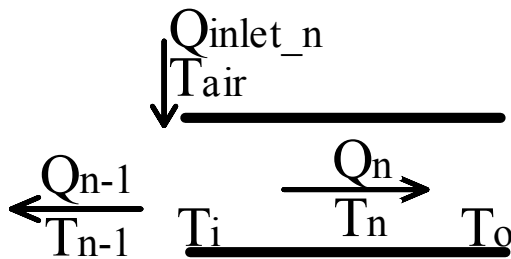


Figure 4.7: Positive channel flow with negative (reverse) flow from the previous channel and positive inlet flow.

In this case, flow reversal occurs in the previous channel, so, part of the flow entering from the n-th inlet is directed there and part enters the n-th CV. This means that the air circulating in the n-th CV enters at ambient temperature:

$$T_i = T_{air} \quad (4.24)$$

III. Negative inlet flow, positive flow from the previous CV

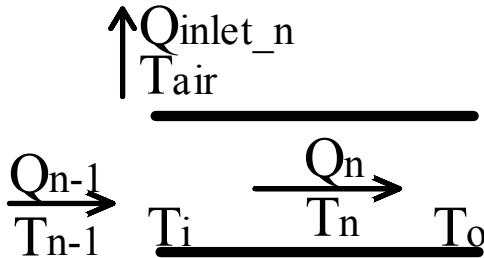


Figure 4.8: Positive channel flow with positive flow from the previous channel and negative inlet flow (outflow).

In this case, part of the flow from the previous channel escapes from the inlet and as a consequence the air entering the new air channel is at the same temperature as air leaving the previous channel:

$$T_i = T_{n-1} \quad (4.25)$$

4.3.2. Negative channel flow (reversed flow)

In the case of reversed flow within a channel, the heat extracted from the PV panels is released to the atmosphere. The flow may exit from the corresponding inlet of that particular CV, or from a previous one, denoting reversed flow in the previous CV as well. Although the heat escapes to the exterior, the modelling must be done properly in order to assess the PV temperature of that particular CV/module. The following are the possible cases for the instance of reverse flow. Here, the air enters the CV at point “o”:

I. Positive flow from the (n+1)-th inlet, negative flow from the (n+1)-th channel:

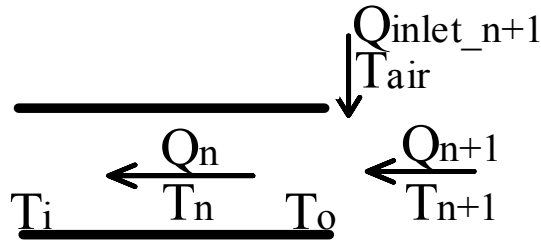


Figure 4.9: Negative (reverse) channel flow with negative (reverse) flow from the next channel and positive flow from the next inlet.

This is the exact reverse of the first case of positive channel flow. In this case, flow reversal occurs also at the (n+1)-th CV and that air stream is joined with that from the (n+1)-th inlet and passes through the n-th channel. The entrance air temperature (at point “o”) is:

$$T_o = \frac{T_{air} \cdot Q_{inlet_n+1} + T_{n+1} \cdot Q_{n+1}}{Q_{inlet_n+1} + Q_{n+1}} \quad (4.26)$$

II. Positive flow from the (n+1)-th inlet and positive flow from the (n+1)-th channel:

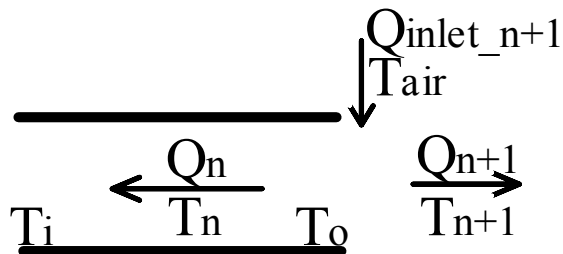


Figure 4.10: Negative (reverse) channel flow with positive flow from the next channel and positive flow from the next inlet.

This is the reverse of the second case of positive flow. Part of the air entering from the (n+1)-th inlet goes to the (n=1)-th channel and part in reverse to the n-th channel. The entrance air temperature at point “o” is equal to the ambient:

$$T_o = T_{air} \quad (4.27)$$

III. Negative flow from the (n+1)-th inlet and positive flow from the (n+1)-th channel:

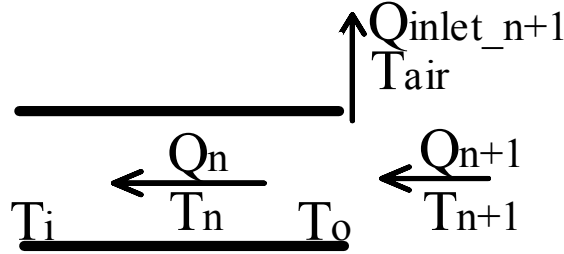


Figure 4.11: Negative (reverse) channel flow with negative flow from the next channel and negative flow from the next inlet (outflow).

This is the reverse of the third case of positive channel flow. Part of the reverse flow of the (n+1)-th channel exits from the (n+1)-th inlet and the rest enters the n-th CV at point “o”, the result being that the entrance air temperature is that of the air channel of the (n+1)-th CV:

$$T_o = T_{n+1} \quad (4.28)$$

4.4 Modelling assumptions

Several assumptions have been made in this numerical study for simplicity purposes, since its main purpose is the introduction of a methodology for multiple-inlet BIPV/T modelling. Several of these assumptions have either been the subject of previous studies or could be further investigated in the future, as suggested in Chapter 6.

As mentioned in section 4.1.2, the secondary loss factors (K) used in the flow distribution model were assumed from the literature on duct design. Furthermore, the Nusselt number correlation used in this study were those developed by Yang (2014), who studied a similar system with 2 inlets and performed a numerical study on a four-inlet system.

The wind effects investigated in this study concerned the effect of wind induced pressure distributions on the inlet flow distributions and not wind induced convection on the exterior of

the BIPV/T. An average relationship connecting local wind velocity and external convection was used, similar to the ones developed by Liu & Harris (2007):

$$h_{wind} = 6 \cdot V_{loc} + 4 \quad (4.29)$$

For simplicity, only one wind reference speed is considered and not the actual velocity distributions over the BIPV/T area. This, according to Vasan (2014) may lead to overestimation of the heat exchange efficiency and underestimation of the wind-induced losses.

5. Simulations and results

The models developed in the previous chapter were used for the numerical investigation of the performance of several single and multiple-inlet BIPV/T systems considered for an office building application, namely the Montreal Courthouse, which was described in section 3.3. The available 80 m x 10 m retrofit area was assumed to be covered by 2 m x 1 m PV modules, thus forming 40 PV strings of 10 modules each.

The electrical and thermal performance of six BIPV/T systems, described in section 5.1, were investigated for a typical summer and a typical winter day, for two total mass flow rates and for three different wind directions and two wind velocities per direction.

The goal of these simulations was twofold:

1. Investigate the flow distributions of the multiple-inlet systems in relation to the system's geometry, total flow rate and wind effects.
2. Investigate the performance of a multiple-inlet system against a single-inlet, for typical Montreal weather conditions, as well as study the potential of optimizing its performance by modifying the flow distributions of the inlets. The systems were compared in terms of electrical and combined electrical-thermal efficiency, as well as PV temperature uniformity, which is a major factor of consideration for the durability of large PV installations.

5.1 Systems considered

In total six different systems were compared, every two had the same inlet opening geometry but varied in the distance between the PV layer and the back wall, or gap size. The main features of these systems are the following:

- All the systems are based on framed PV modules 2m wide and 1m long along the flow path of air inside the air channel. This means that the PV strings created have a width of 2 m and a total length of 10 m.
- Systems I and II (Figures 5.1 and 5.2) are single inlet systems, with a gap size of 0.10 m and 0.15m respectively and a bottom opening of 2 m x 0.1 m and 2 m x 0.15 m, for each PV string.

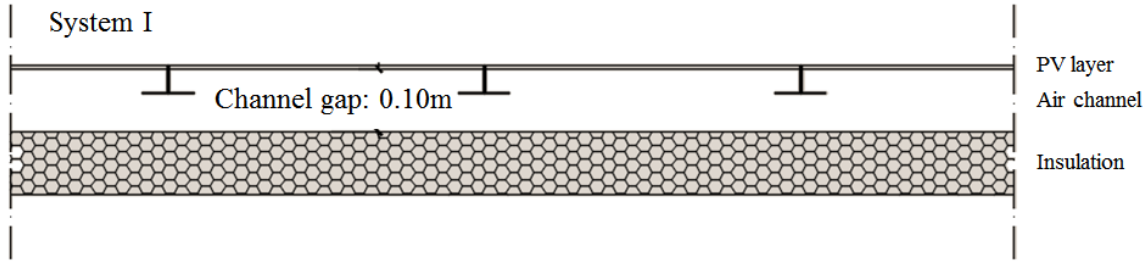


Figure 5.1: System I: Single inlet system with channel gap size: 0.1 m.

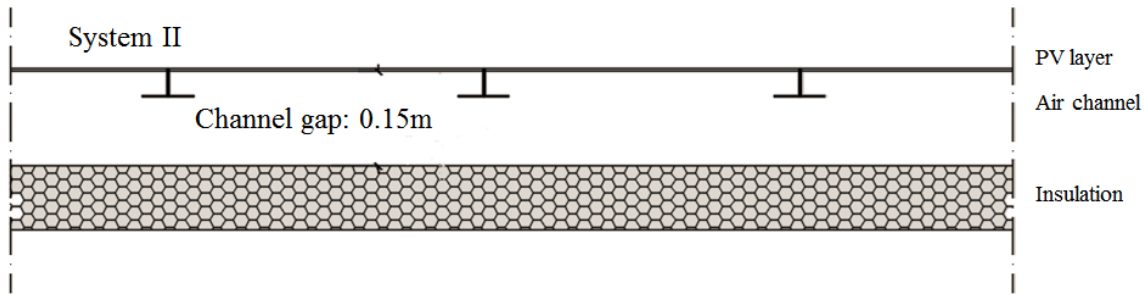


Figure 5.2: System II: Single inlet system with channel gap size: 0.15 m.

- Systems III and IV (Figures 5.3 and 5.4) are multiple-inlet systems with equally sized inlets and of the same gap sizes as above. The inlet areas for these systems were 0.02 m^2 corresponding to a porosity of 1% of the PV module area, same as the system described in Athienitis et al (2010). The inlet area could be modified by either PV spacing or with adjustable covers. It is also assumed that the part of the frame protruding from the PV inside the air channel is 4 cm long. The latter is used for the flow model calculations.

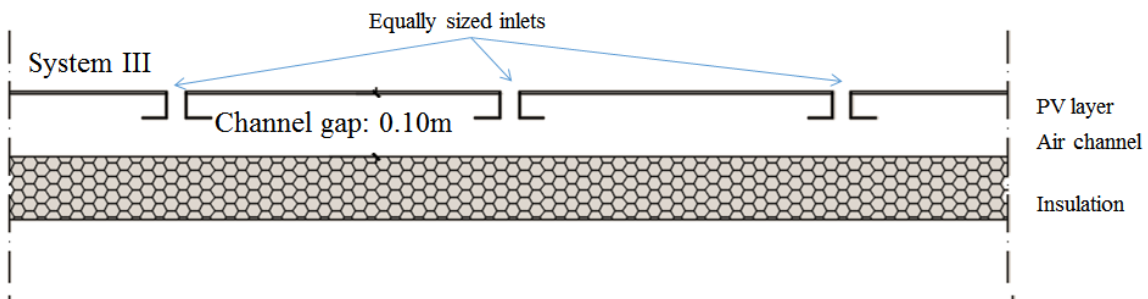


Figure 5.3: System III: Multiple-inlet system with equally sized inlets (1% of the PV module area) and channel gap size of 0.1 m.

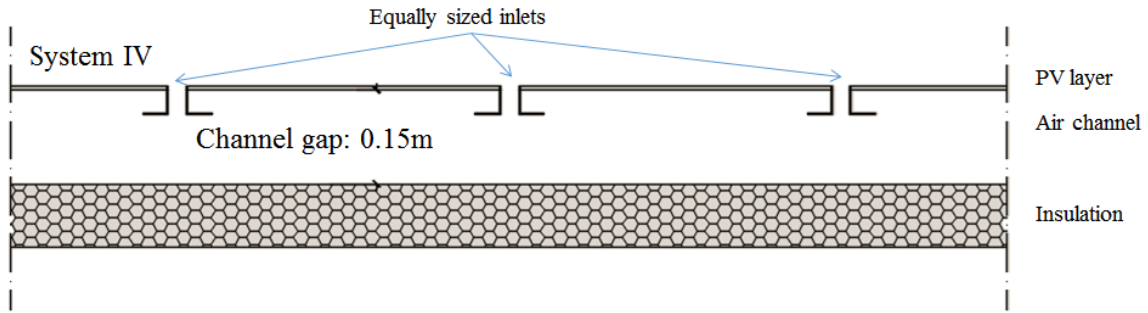


Figure 5.4: System IV: Multiple-inlet system with equally sized inlets (1% of the PV module area) and channel gap size of 0.15 m.

- Systems V and VI (Figures 5.5 and 5.6) are multiple-inlet systems, again with 0.10 m and 0.15 m respective gap sizes. The inlet areas, given in the form of PV module area porosities are presented in Table 5.1:

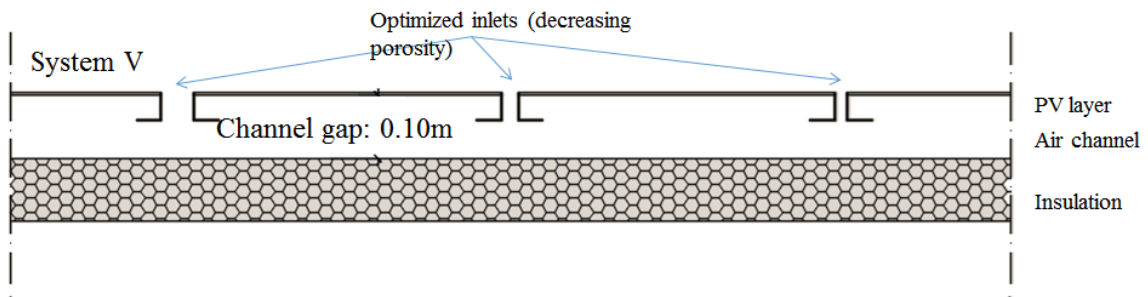


Figure 5.5: System V: Multiple-inlet system with optimized inlets (porosities as shown in Table 5.1) and channel gap size of 0.1 m.

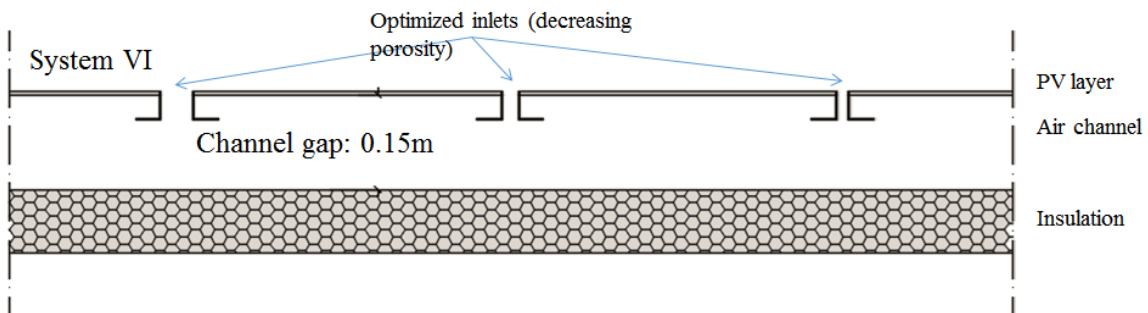


Figure 5.6: System VI: Multiple-inlet system with optimized inlets (porosities as shown in Table 5.1) and channel gap size of 0.15 m.

Table 5.1: Inlet porosities of the optimized multiple-inlet systems.

Inlet	Porosity (%)
1	10
2	1
3	0.5
4	0.5
5	0.3
6	0.2
7	0.1
8	0.01
9	0.01
10	0.01

The porosities shown in Table 5.1 were the result of a trial and error procedure. This is described in more detail in section 5.2.

5.2 Numerical procedure

The steps of the numerical procedure are summarized as follows:

1. The first step was the investigation of flow distributions for the multiple-inlet systems with equally sized inlets. First, a no wind case was tested, in order to study the effect of the total air collector mass flow on the inlet flow distribution. Following, two wind directions were considered, based on the prevailing wind conditions for Montreal, as shown in Figure 3.7, in order to investigate the effect of wind on the flow distribution. All cases were studied for two air collector flow rates, 400 kg/h and 800 kg/h and all cases with wind were studied for two typical wind velocities, 1m/s and 2m/s.
2. The energy balance model was used for the assessment of the performance of the above systems for every case. The results for each system include the daily electrical and combined efficiency for the summer and winter days assumed, as well as the maximum PV temperatures for each day. An average temperature was calculated for each PV module of the string.
3. The multiple-inlet system was optimized through a trial and error procedure as follows: In the energy balance model, several flow distributions were assumed until the maximum PV temperature distributions along the PV string were near uniform. This was done

assuming no wind conditions, since wind would result in further uniform temperature distributions, with external convection dominating, as well as summer conditions, as the highest PV temperatures would be expected then. It is noted that the systems could be further optimized, however, for the frame of this study, the results achieved were considered satisfactory.

4. Given the required flows for optimized performance, the flow model was used in order to size the inlets, or inlet porosities to achieve these flows. Again a trial and error method was followed until the resulting flows were sufficiently close enough to the required ones.
5. Finally, the modified multiple-inlet systems were investigated for the wind cases mentioned above, plus an additional wind direction, that of 45° , since it was found to produce the highest variations of pressure coefficients and would be expected to cause the most significant effect in the flow distributions and as a result on the energy performance.

5.3 Results and discussion

5.3.1 Flow modelling

- Effect of flow rate

The flow distributions of the multiple-inlet systems at no-wind conditions and for the two flow rates considered are shown in Table 5.2:

Table 5.2: Flow distributions of the multiple-inlet systems at no wind conditions, for total mass flow rates of 400kg/h and 800kg/h.

Inlet flows (kg/h)	System III		System IV		System V		System VI	
	400 kg/h	800 kg/h	400 kg/h	800 kg/h	400 kg/h	800 kg/h	400 kg/h	800 kg/h
1	20.0	40.2	29.0	58.1	215.4	431.7	260.5	521.5
2	20.3	40.8	29.1	58.4	42.7	85.3	37.2	74.4
3	21.5	43.2	29.7	59.6	30.7	61.3	24.1	48.0
4	24.0	48.2	31.1	62.3	39.5	78.8	29.2	58.3
5	28.2	56.5	33.4	66.9	28.0	55.9	20.0	39.8
6	34.3	68.8	36.9	73.8	23.6	47.0	16.0	31.8
7	42.9	85.5	41.7	83.3	17.7	35.2	11.5	22.9
8	54.2	107.7	48.0	95.6	0.6	1.1	0.4	0.8
9	67.2	136.0	55.7	111.6	0.9	1.8	0.6	1.2
10	87.4	173.0	65.4	130.4	0.9	1.9	0.6	1.3

Table 5.2 shows clearly that the ratios of the inlet flows, over the total air collector flow rate, remain the same when the latter is varied. For example, if the total flow rate of the air collector is doubled, the flows of each inlet are doubled as well. This is consistent for both equal-sized inlet and modified-inlet configurations, as well as for both gap sizes of each configuration.

- Effect of gap size

Table 5.2 also demonstrates that the reduced gap size increases the resistance to the flow both in terms of increased friction, as well as reduced flow area, since the opening created by the back part of the PV frame and the back wall becomes smaller. For both multiple-inlet system configurations, equal-sized and modified inlets, the inlets have the same geometric features and

the reduced gap size results in reduced inflow from the inlets that are farther away from the outlet.

- Effect of wind velocity and direction

As described in section 5.2, two wind directions were investigated, based on the prevailing wind conditions for Montreal, those of 90° and 135° angle of incidence. Additionally, the direction of 45° was also investigated for the optimized system, since it was expected to create the highest differences in the flow distributions. Each direction was tested at 1m/s and 2m/s wind velocities.

Tables 5.3 to 5.6 show the results for the flow distributions of an average PV string. This means that the flow of each inlet is the weighted average of the 40 PV modules comprising a horizontal array. This was done in order to show the average effect of wind on the system's flow distributions. The extreme cases of individual PV strings are also presented separately. The flow distributions of the entire system, containing all 40 PV strings per case, are included in Appendix I.

Table 5.3: Inlet flow rate distributions for System III (equal inlets, gap: 0.1m), with or without wind.

Total flow rate		400 kg/h					800 kg/h						
Wind direction		-		90°		135°		-		90°		135°	
Wind velocity (m/s)		0		1		2		0		1		2	
Inlet flow rates (kg/s)	1	20.0	20.1	17.1	20.4	20.9	40.2	40.2	39.8	40.5	41.2		
	2	20.3	19.5	15.0	20.2	19.5	40.8	40.2	38.6	40.8	40.7		
	3	21.5	21.0	25.1	21.9	23.1	43.2	43.5	44.8	43.3	43.9		
	4	24.0	24.9	27.6	24.2	25.0	48.2	48.5	49.7	48.2	48.5		
	5	28.2	29.0	31.6	28.0	27.3	56.5	56.8	57.9	56.4	56.1		
	6	34.3	35.2	37.7	33.8	32.2	68.8	69.1	70.1	68.4	67.5		
	7	42.9	42.2	40.1	42.4	41.6	85.5	85.2	84.2	85.3	84.7		
	8	54.2	53.7	53.1	53.8	53.8	107.7	107.5	107.1	107.6	107.4		
	9	67.2	68.0	67.3	68.4	68.9	136.0	136.1	135.6	136.3	136.4		
	10	87.4	86.4	85.3	87.0	87.7	173.0	172.8	172.2	173.1	173.4		

Table 5.4: Inlet flow rate distributions for System IV (equal inlets, gap: 0.15m), with or without wind.

Total flow rate		400 kg/h					800 kg/h						
Wind direction		-		90°		135°		-		90°		135°	
Wind velocity (m/s)		0		1		2		0		1		2	
Inlet flow rates (kg/s)	1	29.0	29.2	28.5	29.2	28.5	58.1	58.3	58.6	58.3	58.6		
	2	29.1	28.7	27.2	29.2	28.8	58.4	58.2	57.5	58.5	58.6		
	3	29.7	29.5	28.8	29.9	30.6	59.6	59.5	59.2	59.7	60.0		
	4	31.1	31.9	34.8	31.3	32.3	62.3	62.7	64.0	62.4	62.7		
	5	33.4	34.2	37.1	33.3	33.1	66.9	67.3	68.5	66.8	66.6		
	6	36.9	37.7	40.5	36.4	35.2	73.8	74.2	75.4	73.6	72.9		
	7	41.7	41.1	38.9	41.3	40.5	83.3	83.0	82.1	83.1	82.6		
	8	48.0	47.6	46.8	47.9	48.0	95.6	95.6	95.1	95.7	95.6		
	9	55.7	55.3	54.3	55.8	56.3	111.6	111.1	110.4	111.3	111.4		
	10	65.4	64.8	63.1	65.6	66.5	130.4	130.2	129.2	130.6	131.0		

Table 5.5: Inlet flow rate distributions for System V (optimized inlets, gap: 0.1m), with or without wind.

Total flow rate		400 kg/h							800 kg/h								
Wind direction		-		45°		90°		135°		-		45°		90°		135°	
Wind velocity (m/s)		0	1	2	1	2	1	2	0	1	2	1	2	1	2		
Inlet flow rates (kg/s)	1	215.4	218.3	227.4	215.7	217.3	215.7	217.4	431.7	433.1	437.5	437.5	432.4	431.6	432.6		
	2	42.7	42.6	42.8	42.1	39.9	42.5	41.6	85.3	85.3	85.2	85.2	84.1	85.2	84.8		
	3	30.7	30.6	29.9	30.8	31.1	30.7	30.6	61.3	61.3	61.0	61.0	61.6	61.1	61.3		
	4	39.5	39.0	37.6	39.5	39.7	39.4	39.3	78.8	78.5	77.6	77.6	78.9	78.6	78.7		
	5	28.0	27.5	26.2	28.1	28.2	28.0	27.9	55.9	55.7	55.0	55.0	56.0	56.1	55.8		
	6	23.6	22.8	20.3	23.8	23.8	23.7	23.4	47.0	46.6	45.8	45.8	47.1	47.6	46.9		
	7	17.7	16.8	12.9	17.6	17.6	17.6	17.5	35.2	34.8	33.4	33.4	35.1	35.2	35.2		
	8	0.6	0.5	0.7	0.6	0.6	0.6	0.6	1.1	1.1	1.1	1.1	1.1	1.1	1.1		
	9	0.9	0.9	1.0	0.9	0.9	0.9	0.9	1.8	1.8	1.7	1.7	1.8	1.7	1.8		
	10	0.9	0.9	1.1	0.9	0.9	0.9	0.9	1.9	1.9	1.8	1.8	1.9	1.8	1.9		

Table 5.6: Inlet flow rate distributions for System VI (optimized inlets, gap: 0.15m), with or without wind.

Total flow rate		400 kg/h							800 kg/h								
Wind direction		-		45°		90°		135°		-		45°		90°		135°	
Wind velocity (m/s)		0	1	2	1	2	1	2	0	1	2	1	2	1	2		
Inlet	1	260.5	265.3	283.3	260.9	264.3	261.0	263.9	521.5	523.8	521.7	522.7	432.4	521.8	522.8		
	2	37.2	37.2	37.8	36.5	32.5	36.9	35.4	74.4	74.5	74.1	72.7	84.1	74.3	73.8		
	3	24.1	23.8	22.7	24.2	24.4	24.0	23.8	48.0	47.9	48.1	48.3	61.6	48.0	47.9		
	4	29.2	28.4	25.2	29.3	29.6	29.1	28.7	58.3	57.9	58.3	58.5	78.9	58.2	58.1		
	5	20.0	19.2	15.7	20.0	20.4	19.9	19.8	39.8	39.4	39.9	40.0	56.0	39.8	39.6		
	6	16.0	14.7	10.4	16.0	15.8	15.9	15.3	31.8	31.2	31.8	31.7	47.1	31.7	31.6		
	7	11.5	9.9	4.6	11.5	11.3	11.6	11.3	22.9	22.2	22.9	22.7	35.1	22.9	22.8		
	8	0.4	0.4	0.2	0.4	0.4	0.4	0.4	0.8	0.7	0.8	0.8	1.1	0.8	0.8		
	9	0.6	0.6	0.5	0.6	0.6	0.6	0.6	1.2	1.2	1.2	1.2	1.8	1.2	1.2		
	10	0.6	0.7	-0.4	0.6	0.7	0.6	0.7	1.3	1.3	1.3	1.3	1.9	1.3	1.3		

From these results, as well as from the full results of systems V and VI, presented in Appendix I, the following comments are noted:

- If the pressure distributions along a PV string are uniform (the pressure outside each inlet is the same) the flow distributions of the PV string are identical with the no-wind condition case, regardless of the wind velocity.
- For the cases of parallel wind (90°) and wind approaching at an angle from the back side of the BIPV/T installation (135°) the PV string flow distributions are of similar magnitude as for the no-wind case. For the first case, this happens because the pressure coefficients form vertical zones and most PV strings are under the same external pressure conditions. This also happens for most part of the 130° case, aided by the fact that the pressure coefficients vary by 0.1 or 0.2, creating very uniform external pressure conditions.
- Higher wind velocity results in higher differences of the string flow distributions than the no-wind distributions, while the higher the total mass flow rate of the air collector the less wind affects the flow distributions. However, these differences for the wind velocities considered are still quite low.

In order to understand the end result of the wind effects on the flow distributions of the system, which is the final effect on the PV temperatures and efficiency, the following extreme cases have been considered. These are the cases of 45° wind with 2m/s velocity, which was found to create the highest differences in the flow distributions, as compared to the no-wind case. These effects are localized to the PV strings located in the windward edge.

Tables 5.7 and 5.8 contain the flow distributions for the no-wind case (uniform external pressure) and those caused by the aforementioned wind conditions. They also contain the PV temperatures that would be expected on the PV string for the uniform pressure distribution and that caused by the localized uneven pressure distribution for a 2m/s wind velocity.

Table 5.7: Flow distributions and PV temperatures for 45°, 2m/s wind for windward edge PV string of System V.

System V, 2m/s wind							
400 kg/h total mass flow				800 kg/h total mass flow			
Flow distributions (kg/h)		PV temperatures (°C)		Flow distributions (kg/h)		PV temperatures (°C)	
Uniform pressure	45°wind pressures	Uniform pressure	45°wind pressures	Uniform pressure	45°wind pressures	Uniform pressure	45°wind pressures
215.4	273.4	39.2	38.2	431.7	459.1	36.1	35.8
42.7	29.2	38.5	37.8	85.2	78.4	35.2	35.1
30.7	19.0	37.0	36.6	61.3	55.8	34.2	34.1
39.5	24.4	37.4	37.1	78.8	71.8	34.1	34.0
28.0	23.0	37.0	36.9	55.9	52.9	33.7	33.6
23.6	17.6	36.7	36.6	47.0	44.6	33.3	33.3
17.7	10.0	36.5	36.5	35.3	33.0	33.1	33.1
0.6	1.1	36.9	36.7	1.1	1.0	33.5	33.5
0.9	1.0	36.8	36.7	1.8	1.6	33.4	33.4
0.9	1.1	36.8	36.7	1.9	1.7	33.3	33.4

Table 5.8: Flow distributions and PV temperatures for 45°, 2m/s wind for windward edge PV string of System VI.

System VI, 2m/s wind							
400 kg/h total mass flow				800 kg/h total mass flow			
Flow distributions (kg/h)		PV temperatures (°C)		Flow distributions (kg/h)		PV temperatures (°C)	
Uniform pressure	45°wind pressures	Uniform pressure	45°wind pressures	Uniform pressure	45°wind pressures	Uniform pressure	45°wind pressures
260.3	364.1	39.3	38.0	521.5	563.4	36.4	36.0
37.2	25.1	38.8	37.7	74.4	66.2	35.7	35.5
24.0	5.7	37.4	36.7	48.0	40.0	34.7	34.6
29.2	-9.0	38.1	39.1	58.3	47.3	35.0	34.9
19.9	10.5	37.9	37.6	39.8	35.9	34.7	34.6
15.9	5.3	37.7	37.6	31.8	26.7	34.5	34.5
11.8	2.6	37.6	37.6	22.9	15.8	34.4	34.4
0.4	0.0	38.1	40.4	0.8	0.9	34.8	34.8
0.6	-1.5	38.0	42.2	1.2	1.9	34.7	34.6
0.6	-2.6	37.9	43.4	1.3	1.9	34.7	34.6

From these results, the following are noted:

- Although this particular wind direction may result in considerable deviation of the inlet flows from the designed distribution, the final effect on the PV temperatures is very small. This is attributed to the fact that with increasing wind speed, the external (and not the internal) convection dominates. Also, the effect of wind on the PV electrical efficiency is insignificant.
- The increased inflow from the bottom inlet and the outflow from the top inlets is due to the pressure distributions for this particular case. For the bottom part there is considerable pressure, whereas for the top part there is suction.
- The higher PV temperatures that occur for the top panels are due to the suction mentioned above. The outflow from the top inlets results in only warm air from the preceding air channel entering the new one, without the mixing of fresh air.
- As previously mentioned, increased total mass flow of the air collector results in wind affecting less the inlet flow distributions.

It is clear that a system properly designed for uniform pressure conditions will behave similarly for all wind conditions. Although wind may cause considerable deviations of the flow distributions from the designed values, increasing wind velocity also results to more uniform temperature distributions. The results of the cases considered on the temperatures and the performance of the systems considered are investigated in more detail in the following section.

5.3.2 Energy balance

- Temperatures

The PV temperatures for the average string of each system studied and each case tested are displayed in Figures 5.7 through 5.12. The full results for all the PV strings are presented in Appendix I. The variations of temperature of the extreme cases of PV string flow distributions due to wind were shown in Tables 5.7 and 5.8.

The temperatures are plotted per system, for summer and winter conditions and for every wind direction and velocity:

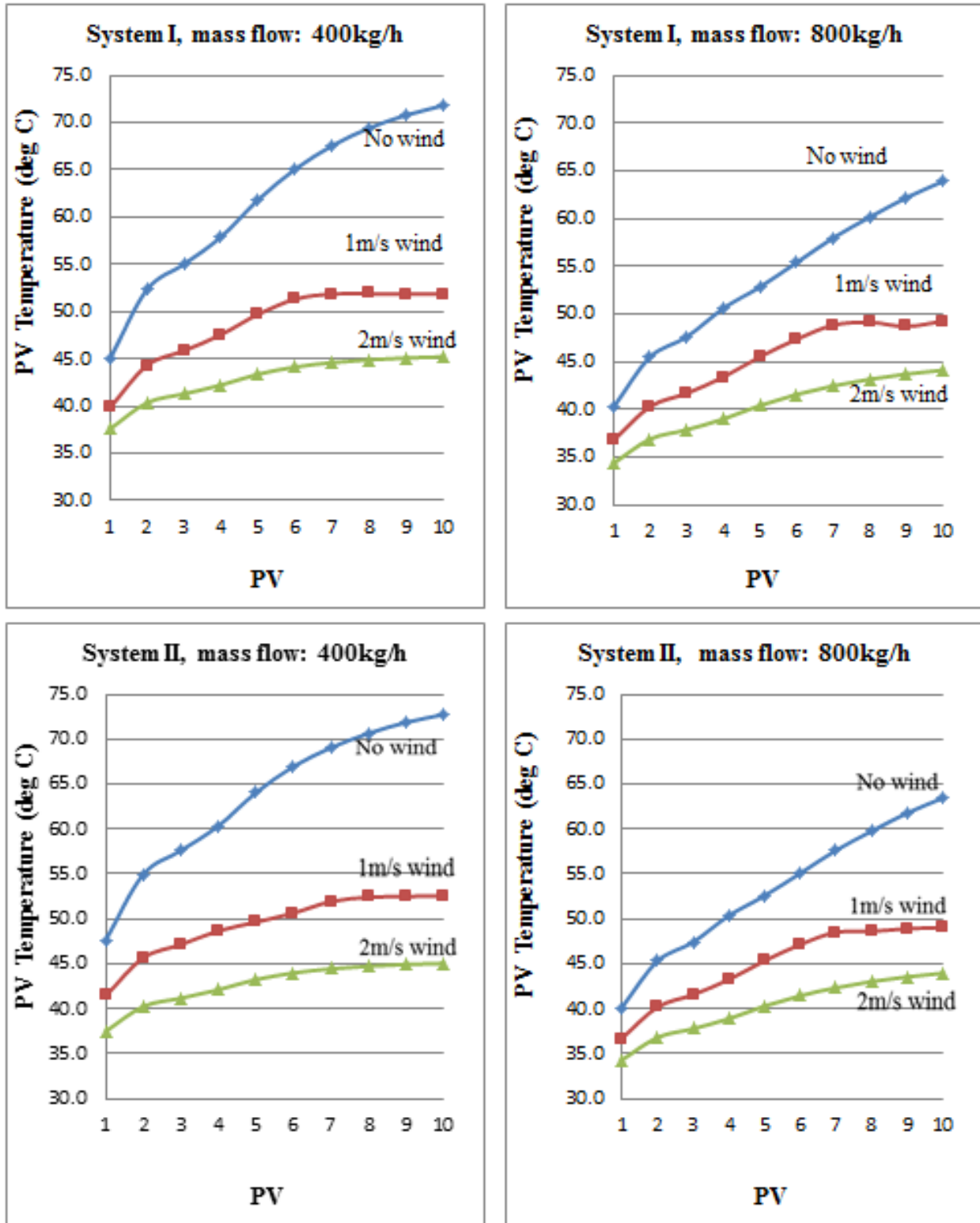


Figure 5.7: Maximum daily PV temperatures for Systems I and II (single inlet) for summer conditions at total air mass flow rate of 400 kg/h and 800 kg/h.

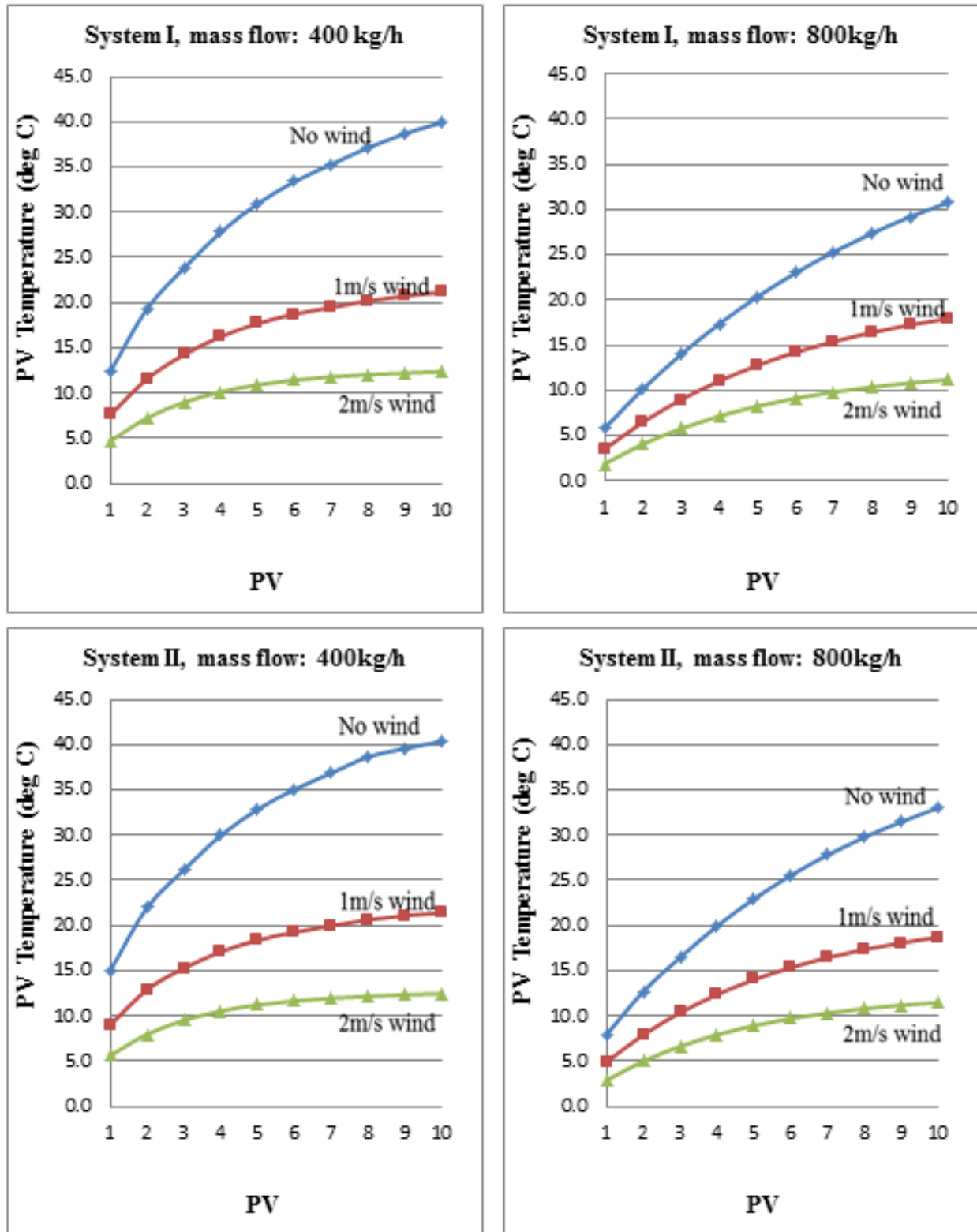


Figure 5.8: Maximum daily PV temperatures for Systems I and II (single inlet) for winter conditions at total air mass flow rate of 400 kg/h and 800 kg/h.

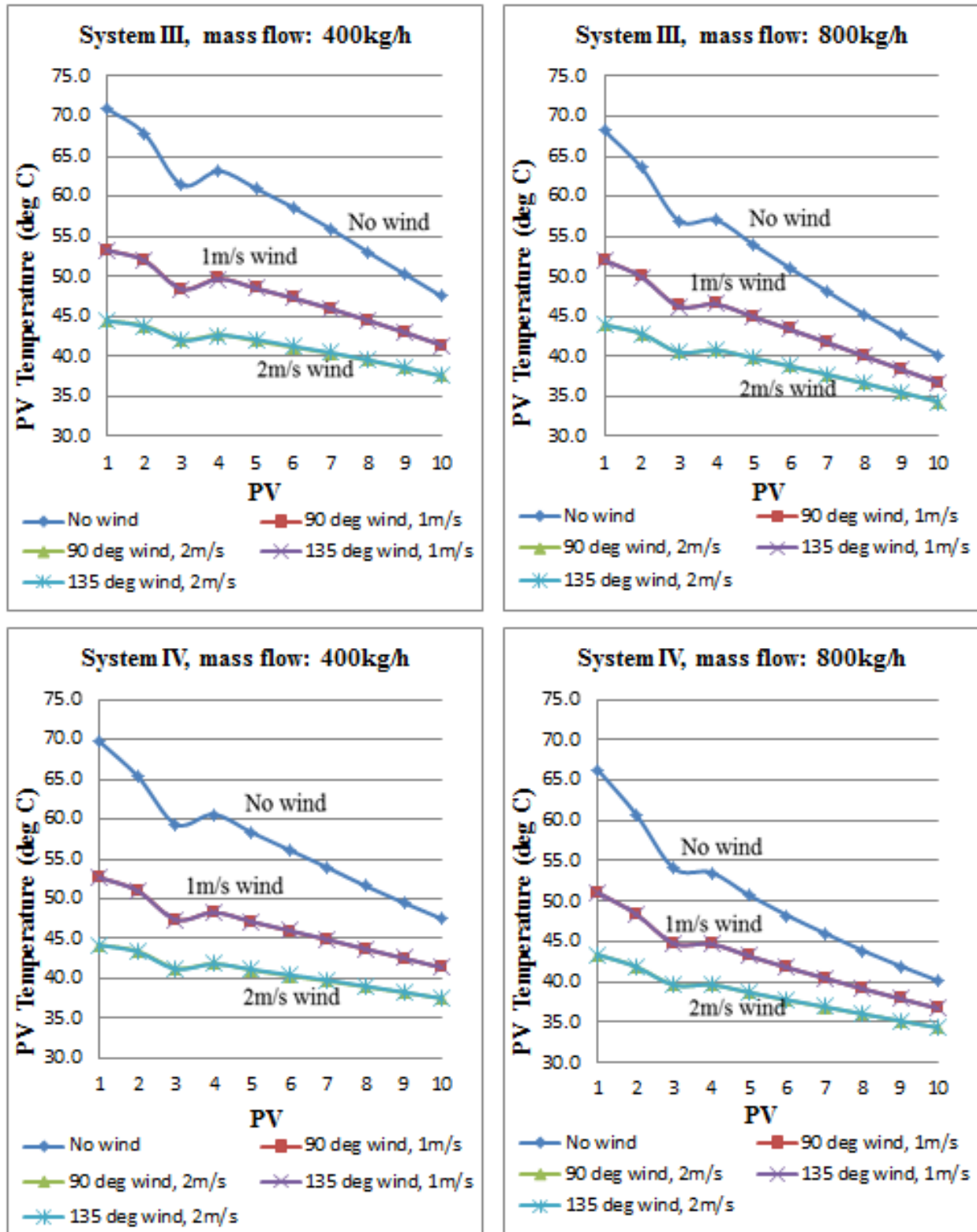


Figure 5.9: Maximum daily PV temperatures for Systems III and IV (multiple-inlet, equal inlets) for summer conditions at total air mass flow rate of 400 kg/h and 800 kg/h.

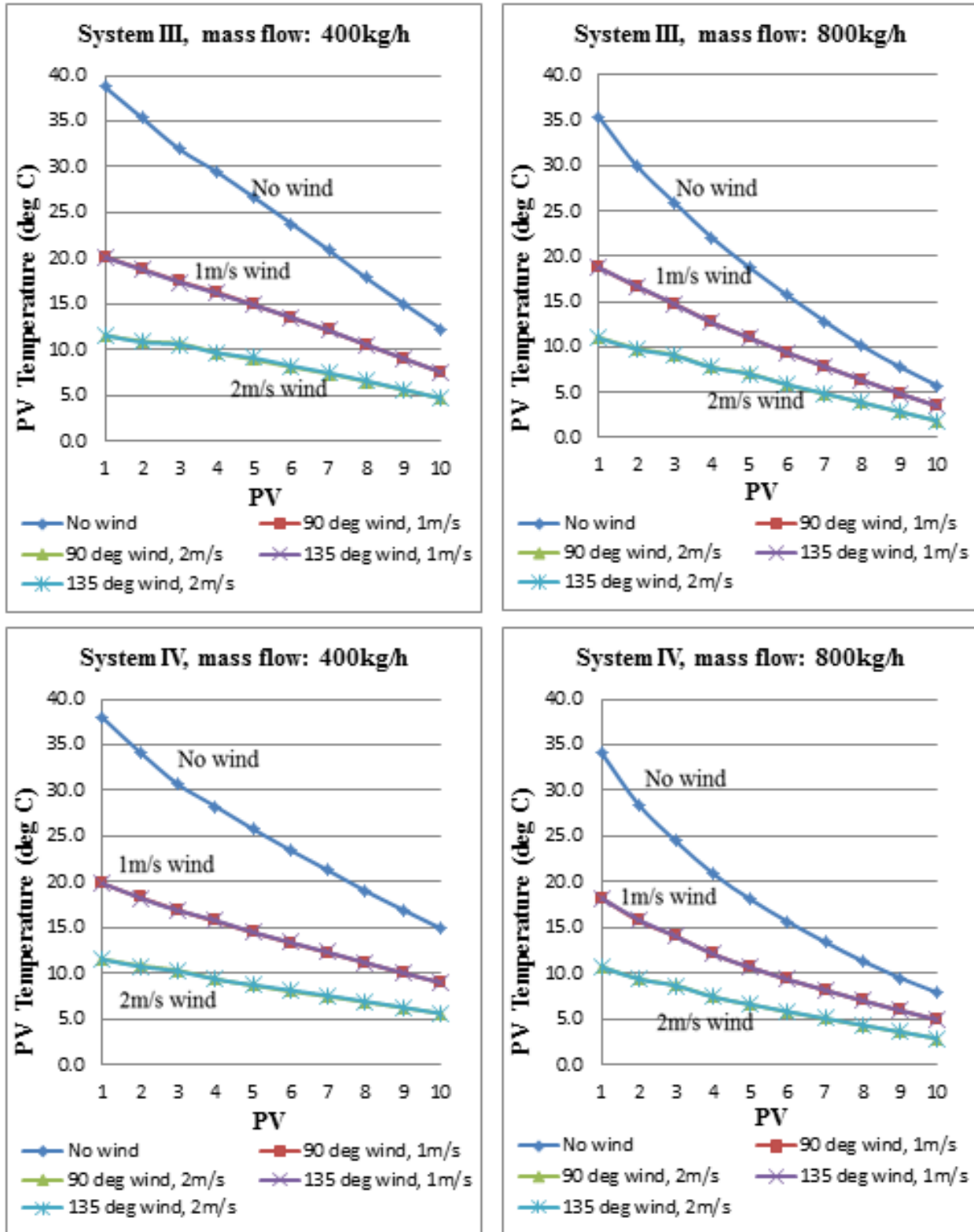


Figure 5.10: Maximum daily PV temperatures for Systems III and IV (multiple-inlet, equal inlets) for winter conditions at total air mass flow rate of 400 kg/h and 800 kg/h.

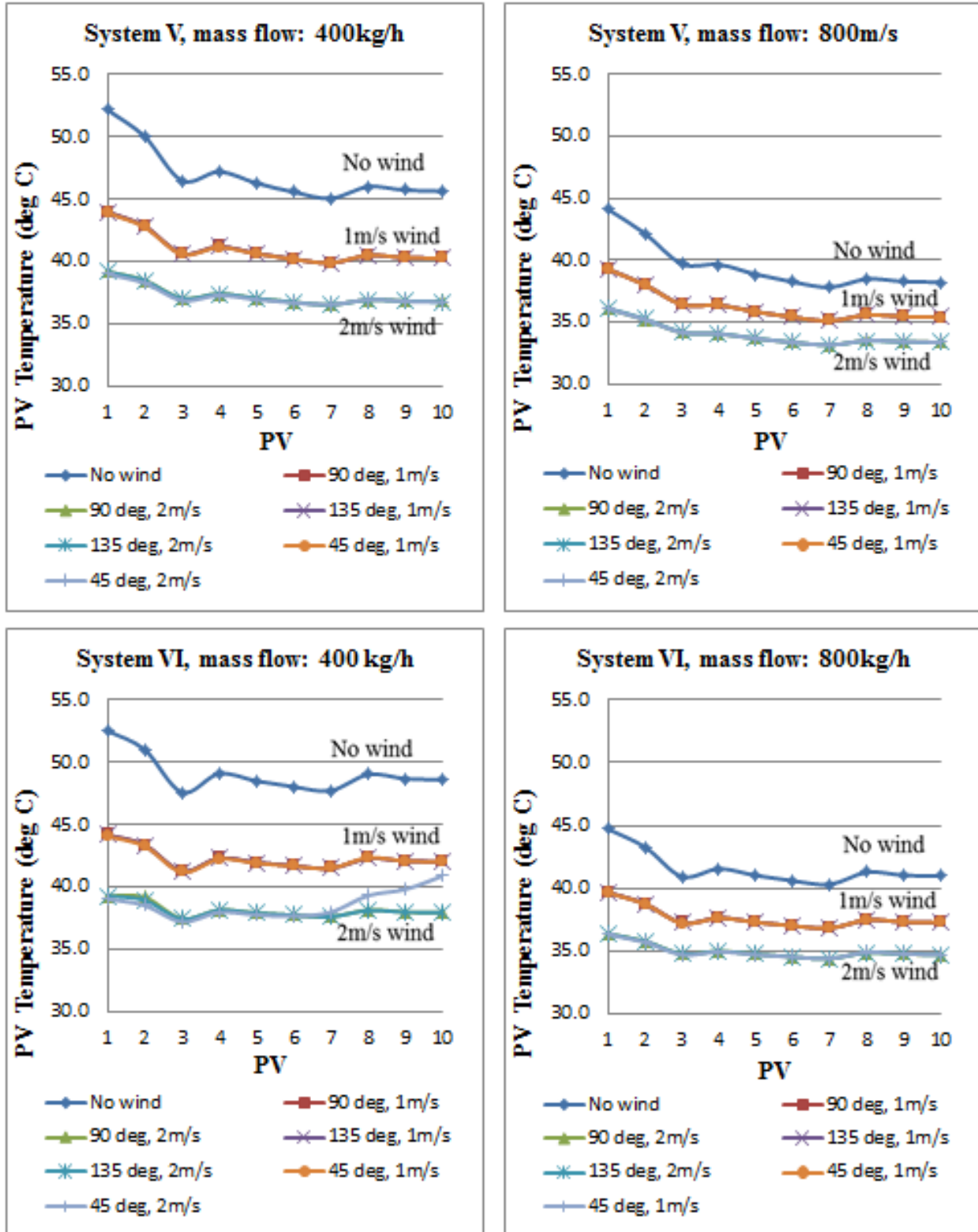


Figure 5.11: mum daily PV temperatures for Systems III and IV (multiple-inlet, optimized inlets) for summer conditions at total air mass flow rate of 400 kg/h and 800 kg/h.

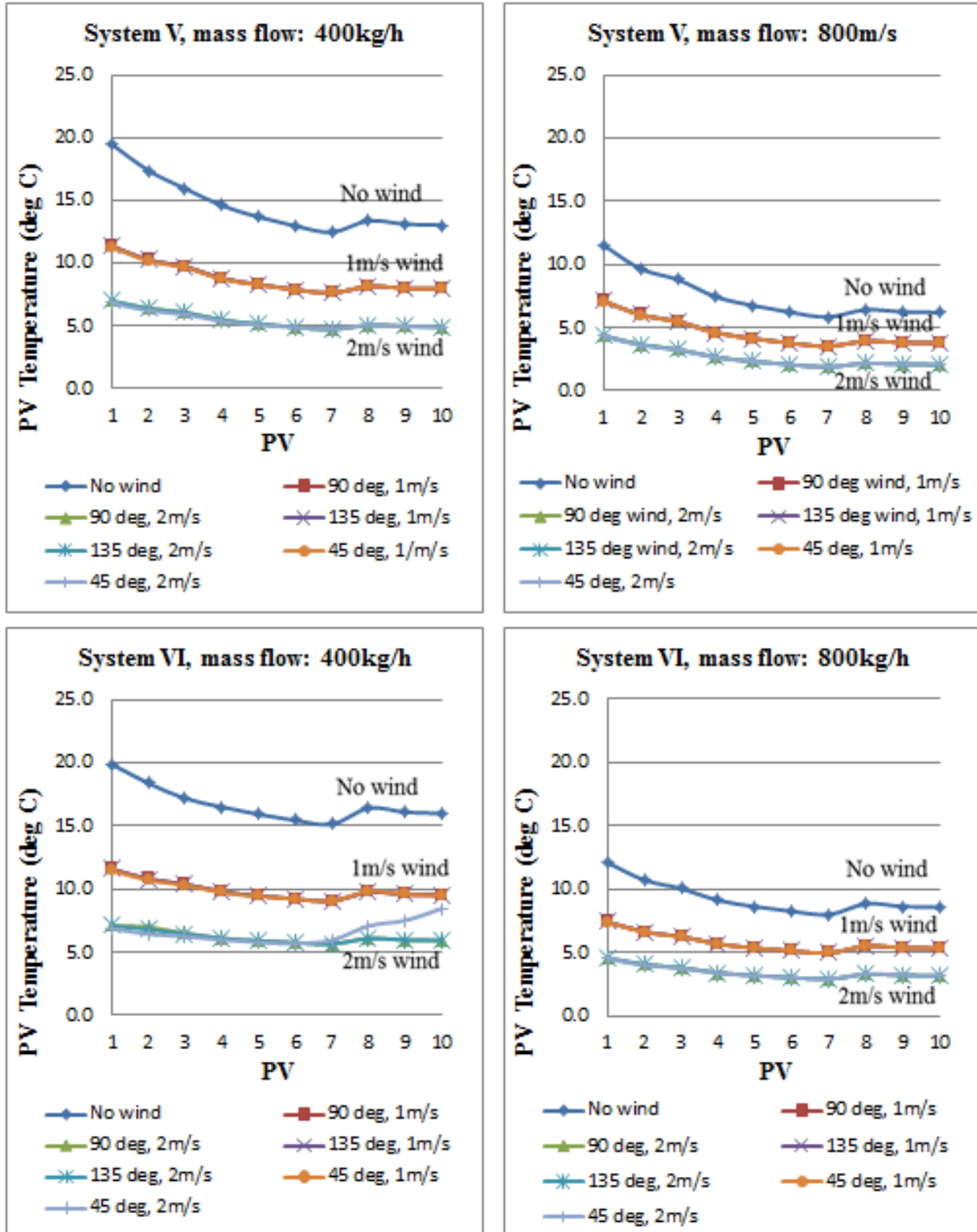


Figure 5.12: Maximum daily PV temperatures for Systems III and IV (multiple-inlet, optimized inlets) for winter conditions at total air mass flow rate of 400kg/h and 800 kg/h.

In order to compare the PV temperature uniformity for each system, the plots shown in Figures 5.13 and 5.14 were produced, each plot including the results of all six systems considered, at a specific total mass flow rate, at summer and winter and for all wind conditions. From the previous Figures (5.7 through 5.12), it is clear that wind direction has insignificant effect on the PV temperature distributions of the multiple inlet systems. Therefore, for the subsequent comparisons only a single wind direction was considered. For the optimized multiple-inlet system, the wind direction of 45° was assumed, since it produced the least uniform temperature distributions.

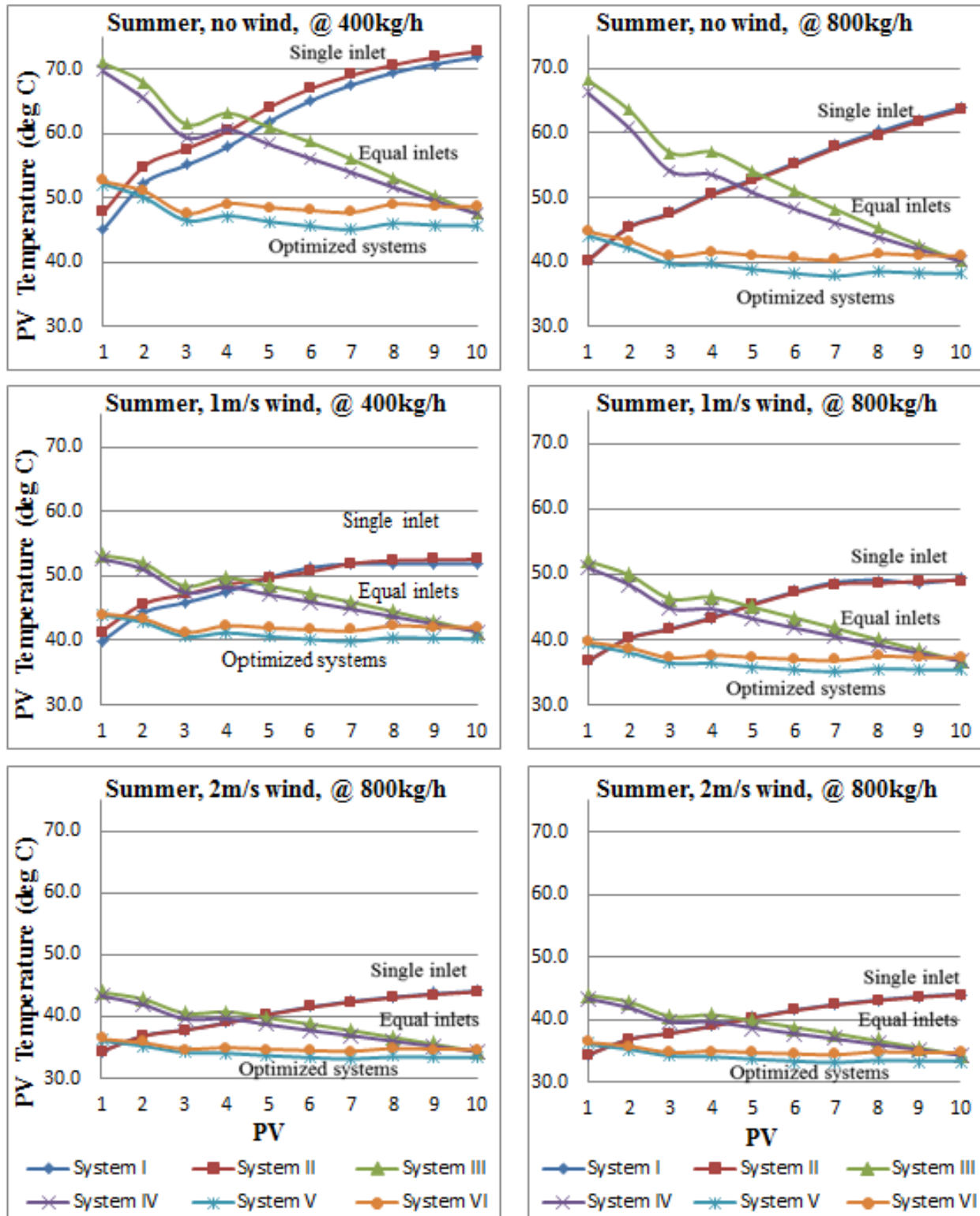


Figure 5.13: Maximum daily PV temperatures comparison for all systems, for summer conditions and 0m/s, 1m/s and 2m/s wind velocities at total air mass flow rate of 400kg/h and 800kg/h.

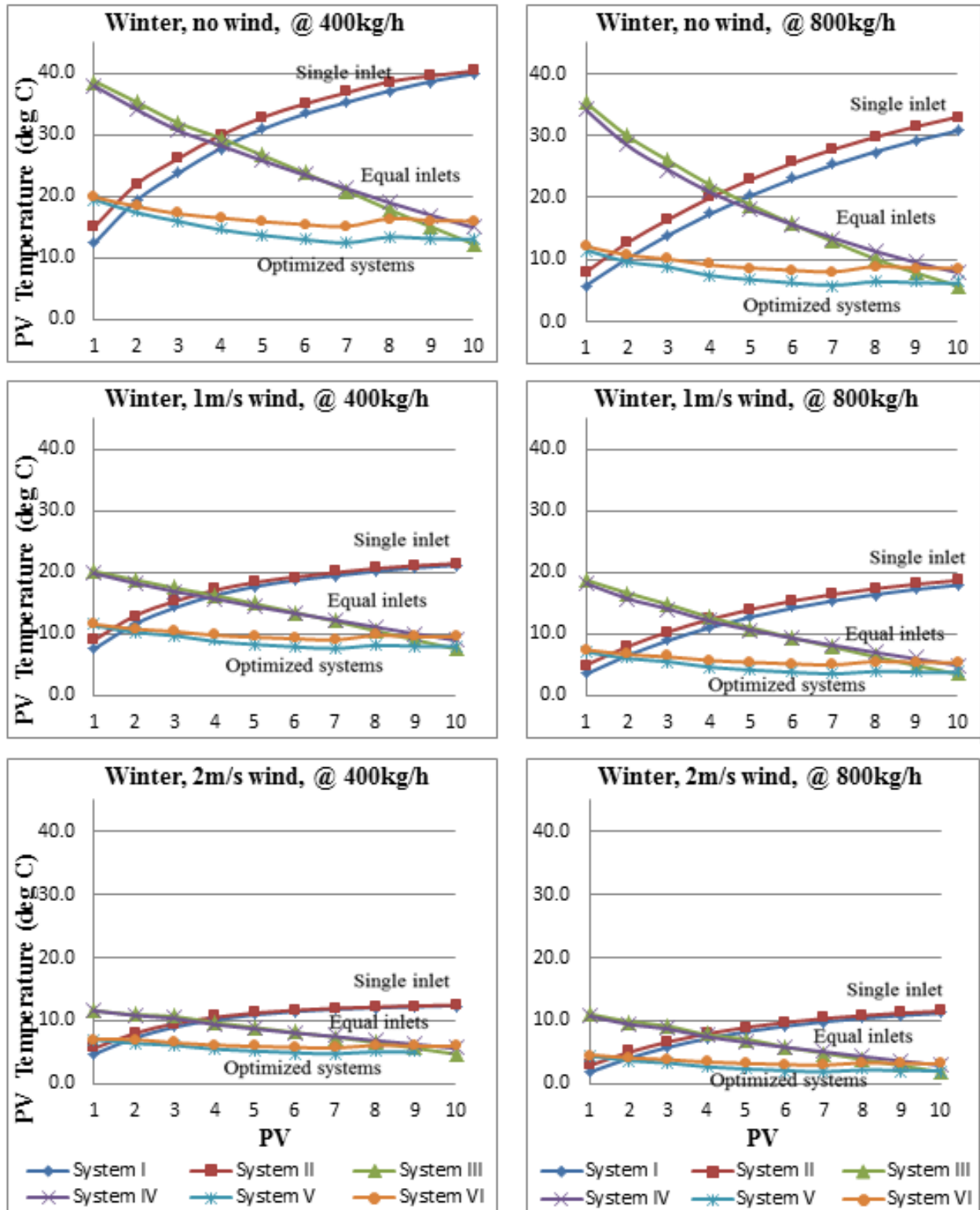


Figure 5.14: Maximum daily PV temperatures comparison for all systems, for winter conditions and 0m/s, 1m/s and 2m/s wind velocities at total air mass flow rate of 400 kg/h and 800kg/h.

Figures 5.13 and 5.14 show:

- Increase of the total air mass flow of the air collector results in lower PV temperatures, the differences being more prominent at conditions with no wind. However, with increasing wind velocity, external convection dominates and the differences are lower.
- Increasing wind velocity results in lower PV temperature distributions along the same string.
- The PV temperatures for the multiple inlet systems with equally sized inlets are in general slightly lower than for the single inlet system. The main difference is that the highest temperatures occur at the PV panels placed on the bottom, for which the inflow and resulting channel air flow is the smallest.
- In all cases, the optimized multiple-inlet systems result in uniform PV temperature distributions, with small temperature differences between panels and with the lowest overall PV temperatures.

- Electrical and combined electrical & thermal efficiency

Figures 5.15 and 5.16 present plots of the electrical and combined efficiencies of the systems, for the assumed cases of weather conditions. These efficiencies are daily, meaning that they are calculated according to the total electrical and thermal production of the systems and on the total solar irradiation incident on the installations.

The above efficiencies are defined as follows:

- Daily electrical efficiency: Total electrical energy produced over the total daily solar irradiation incident on the BIPV/T surface.
- Daily combined efficiency: The sum of the total daily electrical energy produced and thermal energy extracted and transferred to the air flowing inside the air channel over the total daily solar irradiation incident on the BIPV/T surface.

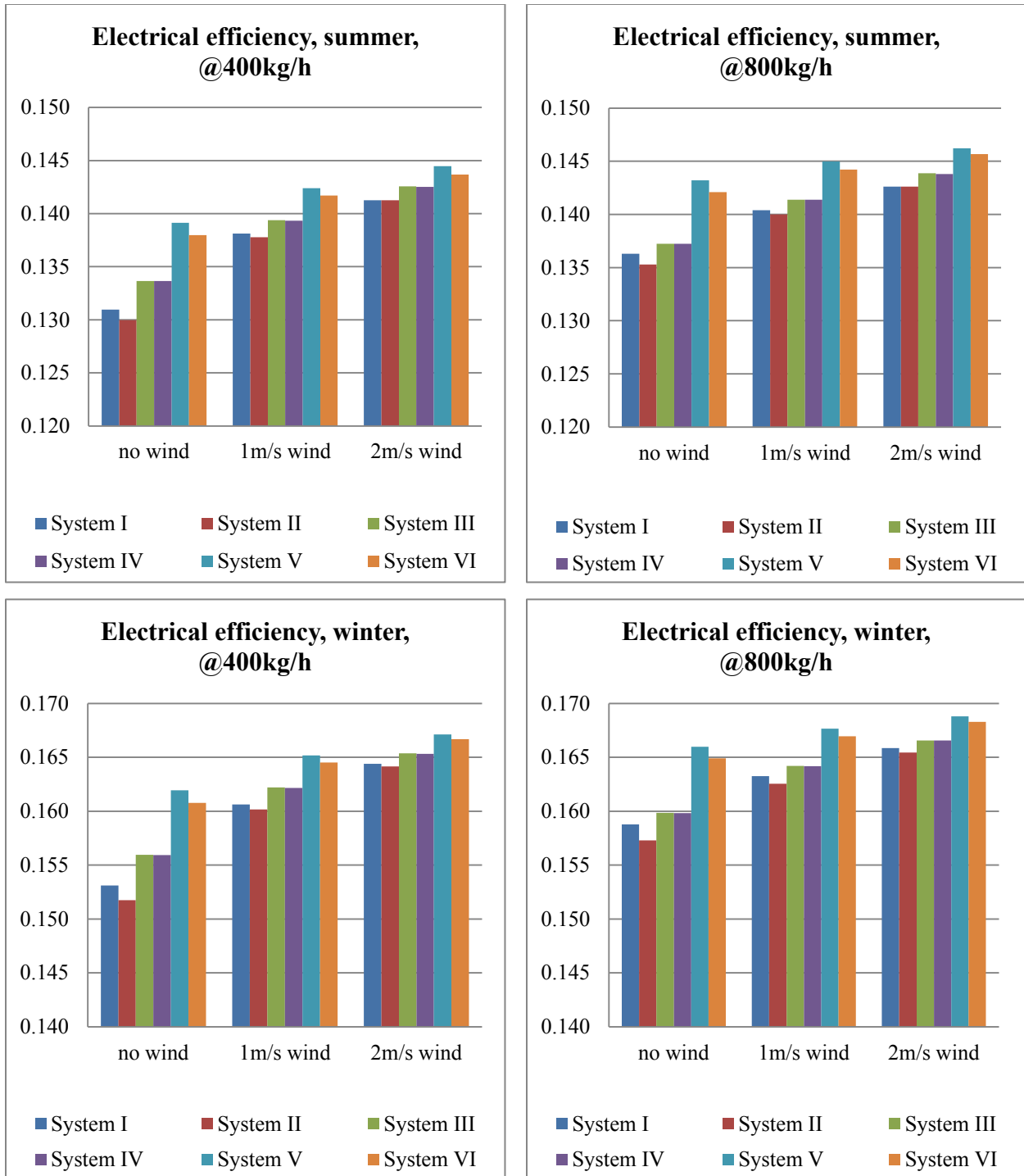


Figure 5.15: Electrical efficiency of the six systems for summer and winter conditions, with and without wind and at total air mass flow rate of 400 kg/h and 800 kg/h.

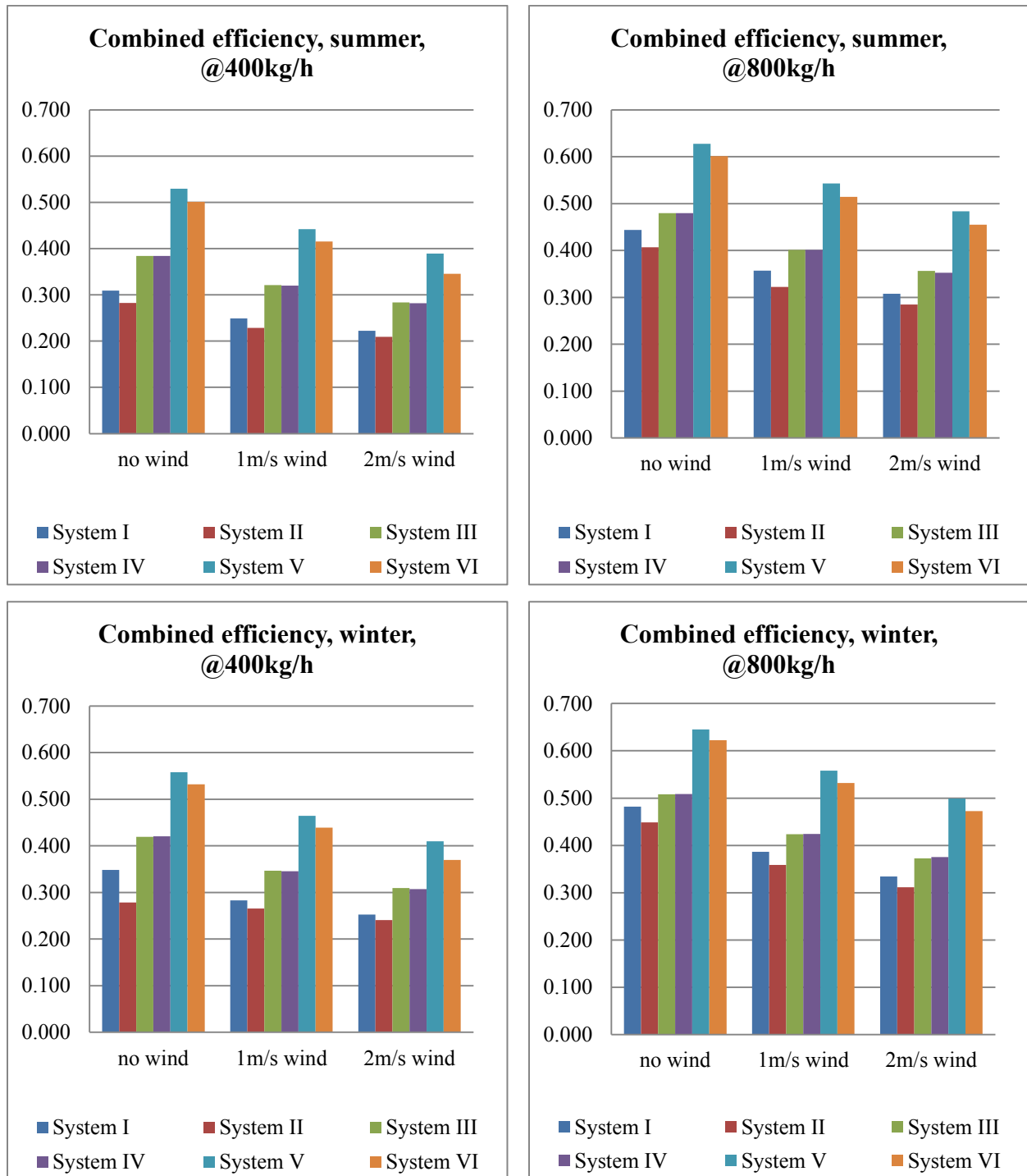


Figure 5.16: Combined electrical and thermal efficiency of the six systems for summer and winter conditions, with and without wind and at total air mass flow rate of 400 kg/h and 800 kg/h.

Based on these results, the following can be noted concerning the electrical and combined efficiencies of the assumed systems:

- The single inlet systems have the lowest overall performance, both electrically and thermally. The multiple-inlet systems with equally sized inlets perform slightly better than the single inlet systems, while the optimized multiple-inlet systems perform the best.
- Depending on the weather conditions, wind velocity and air collection rate, an optimized multiple-inlet system may have a marginally higher electrical efficiency of 0.3% - 1% and a considerably higher combined efficiency by 14% - 25%, primarily due to increase in the thermal efficiency. It should be noted that the fan consumption has not been addressed in this investigation and the net electrical production should be looked into for a more accurate comparison.
- The differences in the electrical efficiency of the systems are lower for increasing wind velocity and air collection rate.
- In accordance with previous studies, higher air collection rates results in higher thermal and therefore combined efficiencies. This is also the case for each system configuration, with the gap size of the air channel reduced, which results to higher air velocity inside the air channel and higher internal convection.

The optimized multiple-inlet system performs better both electrically and thermally in comparison to the single inlet system, under all the weather conditions assumed for these simulations, while maintaining the lowest PV temperatures and the least differences between the hottest and the coolest panels. The latter can be of major importance for large installation, since an optimized multiple-inlet system may lead to high system durability, while reducing issues such as differential expansion.

As was concluded from the previous part, a system optimized for uniform pressure conditions should perform well under all wind conditions. The localized compression or suction effects have an insignificant effect on the overall performance of the system.

6. Summary and conclusions

This thesis presents the development of a methodology for the modelling of multiple-inlet BIPV/T systems. These systems are expected to result in lower PV temperatures, as well as higher combined electrical and thermal efficiency, as compared to a single inlet system, due to the introduction of more than one intakes of fresh air. A flow model was created based on flow networking techniques for the modelling of inlet flows of a multiple-inlet system. This was partially validated by experimental flow measurements of a three-inlet prototype BIPV/T specimen. The flow model also considered the wind effects in the form of exterior pressures. A simple energy balance model was also developed, based on BIPV/T energy modelling, to account for the various cases of flow conditions for the inlets and the air channels of the system. It uses the results of the flow model as inputs for the flow of each control volume of the system.

These models were applied for the numerical investigation of variations of multiple-inlet BIPV/T systems considered for a potential retrofit project of an office building. These were compared with single inlet system designs for the same environmental conditions. The simulation results showed the following:

- A multiple-inlet system, the inlet flows of which have been optimized in order to achieve the highest heat extraction from all the PV modules of the system for no wind conditions, outperforms a single inlet system in terms of PV temperature uniformity, electrical efficiency and combined electrical and thermal efficiency, under all types of weather conditions assumed for this study.
- The temperature difference between the warmest and the coolest PV panels for the single inlet system may vary from 8 to 26°C, for a 2m/s wind and no wind conditions respectively, while the temperature of the warmest panel may exceed 70°C. The corresponding temperature difference for the optimized multiple-inlet system is 3 to 7°C, and the maximum PV temperature is 53°C. The much lower operating temperatures of an optimized system may be of significant importance for the durability and maintenance of large PV installations.
- A marginal increase of up to 1% in electrical efficiency was observed for the optimized system, as well as 14% to 25% higher combined electrical and thermal efficiency, in comparison to the single inlet system, depending on the weather conditions. The

difference in the combined efficiency is essentially due to the higher thermal efficiency of the optimized system. The thermal energy may not be all usable, except for fresh air heating in winter; however electricity is more useful than heat by a factor of about 3-4, as well as the expected higher durability of the system.

- The effect of wind direction on the flow distributions and as a result to the internal convection part of the energy balance was found to be insignificant for wind velocities up to 2m/s, regardless of the wind direction. Higher wind velocities would be expected to cause more considerable differences; however, with external convection dominating, the performance of all systems investigated would be similarly affected, in that the PV temperatures would be low and uniform, while the thermal gains would be minimal.

6.1 Contributions

1. A complete modelling procedure for the investigation of the performance of multiple inlet systems was developed for the first time. This could be used for any number of openings and PV strings and also lead to a standardised procedure for multiple-inlet BIPV/T modelling and design.
2. Through the numerical investigation of such systems, their expected performance has been studied and compared to that of existing single-inlet systems. Multiple-inlet systems can be designed by using the developed flow model for the sizing of the openings. A procedure was also suggested for the optimization of such systems, which may lead to enhanced electrical and thermal performance.
3. It is the first study that the actual flow distributions are used for such systems instead of the commonly assumed uniform inlet flow. Furthermore, the wind effects on these flow distributions were accounted for, for various wind directions and wind velocities.

6.2 Future work

The following are recommended future work in the investigation of multiple-inlet BIPV/T systems:

1. Full scale experimental investigation of multiple-inlet systems, under varying weather conditions, as well as varying geometric features of the inlets and the air channel of the system. This may help with further validation of the flow model, as well as the expected performance.
2. Combined experimental and CFD investigation of inlet configurations of varying geometric features. This will lead to more accurate correlations between pressure drop and flow through the inlets, which could be used for the resistance part of the flow model.
3. In conjunction with the previous steps, more accurate Nusselt number correlations could be developed for the energy modelling of the BIPV/T.
4. A detailed experimental investigation could lead to a dimensional analysis of the system, providing a more generalized correlation between the performance of the system, its geometric features, the total mass flow rate, etc. Such an analysis could make more clear the potential applications and limitations of a multiple-inlet BIPV/T system.

REFERENCES

- Aelenei, L., Pereira, R., Goncalves, H., Athienitis, A.K. (2013). International Conference on Solar Heating and Cooling for Buildings and Industry, 2013, Germany. *Energy Procedia* **48**, 474-483.
- Aly, M.A., Bitsuamlak, G. (2013). Aerodynamics of ground-mounted solar panels: Test model scale effects. *Journal of Wind Engineering and Industrial Aerodynamics* **123**, 250-260.
- Anderson, T.N., Duke, M., Morrison, G.L., Carson, J.K. (2008). Performance of a building integrated photovoltaic/thermal (BIPV/T) solar collector. *Solar Energy* **83**, 445-455.
- ASHRAE, 2009, -ASHRAE Handbook of Fundamentals, American Society of Heating, Refrigerating and Air-Conditioning Engineers, Atlanta, GA, USA
- Asfour, O.S., Gadi M.B. (2006). A comparison between CFD and Network models for predicting wind-driven ventilation in buildings. *Building and Environment* **42**, 4079-4085
- Athienitis, A.K., Bambara, J., O'Neill, B., Faille, J. (2010). A prototype photovoltaic/thermal system integrated with transpired collector. *Solar Energy* **85**, 139-153
- Aynsley, R.M. (1997). A resistance approach to analysis of natural ventilation airflow networks. *Journal of Wind Engineering and Industrial Aerodynamics* **67&68**, 711-719
- Balaras, C.A., Gaglia, A.G., Georgopoulou, E., Mirasgedis, S., Sarafidis, Y., Lalas, D.P. (2005) European residential buildings and empirical assessment of the Hellenic building stock, energy consumption, emissions and potential energy savings. *Building and Environment* **42**, 1298-1314
- Balocco, C. (2001). A simple model to study ventilated facades energy performance. *Energy and Buildings* **34**, 469-475
- Bambara, J. (2012). Experimental Study of a Façade-integrated Photovoltaic/thermal System with Unglazed Transpired Collector. M.A.Sc thesis: Concordia University, Montreal, Canada

Bambara, J., Athienitis, A.K., Karava, P. (2012) Performance Evaluation of a Building-Integrated Photovoltaic/Thermal System. International High Performance Buildings Conference, 2012, Purdue

Bergene, T., Lovvik O.M. (1995). Model calculation on a flat-plate solar heat collector with integrates solar cells. *Solar Energy* **55**, 453-462

Bigaila, E., Rounis, E.D., Luk, P., Athienitis, A.K. (2015). A study of a BIPV/T collector prototype for building façade applications. International Building Physics Conference, Turin, Italy

Brkic, D. (2008). An improvement of Hardy Cross method applied on looped spatial natural gas distribution networks. *Applied Energy* **86**, 1290-1300

Candanedo, L.M., Athienitis, A.K., Candanedo, J.A., O'Brien, W., Chen, Y. (2010) Transient and steady state models for open-loop air based BIPV/T systems, American Society of Heating, Refrigerating and Air-Conditioning Engineers. Transactions 2010, Vol.116, Part 1, 600-612

Candanedo, L.M., Athienitis, A.K., Park, K.W. (2011). Convective heat transfer coefficients in a building-integrated photovoltaic/thermal system. *ASME Journal of Solar Energy Engineering* **133**

Candanedo, L.M., O'Brien, W., Athienitis, A.K. (2009). Development of an air-based loop building-integrated photovoltaic/thermal system model, Glasgow, Scotland: IBPSA Conference

Charron, R., Athienitis, A.K. (2005). Optimization of the performance of double-facades with integrated photovoltaic panels and motorized blinds. *Solar Energy* **80**, 482-491

Chen, Y., Athienitis, A.K., Galal, K. (2010). Modeling, design and thermal performance of a BIPV/T system thermally coupled with a ventilated concrete slab in a low energy solar house: Part 1, BIPV/T system and house energy concept. *Solar Energy* **84**, 1892-1907

Delisle, V., Kummert, M. (2013). A novel approach to compare building integrated photovoltaics/thermal air collectors to side-by-side PV modules and solar thermal collectors. *Solar Energy* **100**, 50-65

Dymond, C., Kutscher, C. (1997). Development of a flow distribution and design model for transpired solar collectors. *Solar Energy* **60**, 291-300

Florschuetz, L.W. (1979). Extension of the Hottel-Whilier model to the analysis of combined photovoltaic/thermal flat plate collectors. *Solar Energy* **22**, 361-366

Getu, H., Yang, T., Athienitis, A.K., Fung, A. Computational fluid dynamics analysis of air-based building integrated photovoltaic thermal BIPV/T systems for efficient performance, e-Sim Conference, Ottawa, Canada, 2014.

Ghani, F., Duke, M., Carson, J.K. (2012). Effect of flow distribution on the photovoltaic performance of a building integrated photovoltaic/thermal (BIPV/T) collector. *Solar Energy* **86**, 1518-1530

Green, M., 1998. *Solar Cells: Operating Principles, Technology and System Applications*, University of New South Wales, Kensington, Australia

Hegazy, A.A., (1999). Comparative study of the performances of four photovoltaic/thermal solar air collectors. *Energy Conversion & Management* **41**, 861-881

Hunt, B. (1995). *Fluid Mechanics for Civil Engineers*. Department of Civil Engineering, University of Canterbury, Christchurch, New Zealand

Hutcheon, N.B., Handegord, G.O.P. 1995. *Building Science for a Cold Climate*. Third Edition. National Research Council Canada

https://en.wikipedia.org/wiki/Hardy_Cross_method

Inculet, D.R., Davenport, A.G. (1994). Pressure-equalized rainscreens: a study in the frequency domain. *Journal of Wind Engineering and Industrial Aerodynamics* **53**, 63-87

International Energy Agency, *Key World Energy Statistics*, 2014

International Energy Agency, Energy efficiency requirements in building codes, energy efficiency policies for new buildings, IEA Information paper, 2014

Kaldellis, J.K, Kapsali, M., Kavadias, K.A. (2014). Temperature and wind speed impact on the efficiency of PV installations. Experience obtained from outdoor measurements in Greece. *Renewable Energy* **66**, 612-624

Karava, P., Stathopoulos, T., Athienitis, A.K. (2003). Investigation of the performance of trickle ventilators. *Building and Environment* **38**, 981-993

Kato, S., Murakami, S., Takahashi, T., Gyobu, T. (1997). Chained analysis of wind tunnel test and CFD on cross ventilation of large-scale market building. *Journal of Wind Engineering and Industrial Aerodynamics* **67 & 68**, 573-587

Kutscher, C.F. (1994). Heat exchange effectiveness and pressure drop for air flow through perforated plates with and without crosswind. *Journal of Heat Transfer* **116**, 391-399

Ladas D.I., Stathopoulos, T. (2014). Performance of solar collectors on urban roofs under strong wind conditions, ICBEST conference, 2014, Germany

Li, S. Karava, P., Savory, E., Lin, W.E. (2013). Airflow and thermal analysis of flat and corrugated unglazed transpired solar collectors. *Solar Energy* **91**, 297-315

Lo, L.J., Banks, D., Novoselac, A. (2012). Combined wind tunnel and CFD analysis for indoor airflow prediction of wind-driven cross ventilation. *Building and Environment* **60**, 12-23

Lou, W., Huang, M., Zhang, M., Lin, N. (2012). Experimental and zonal modeling for wind pressures on double-skin facades of a tall building. *Energy and Buildings* **54**, 179-191

Mizraei, P.A., Paterna, E., Carmeliet, J. (2014). Investigation of the role of cavity airflow on the performance of building-integrated photovoltaic panels. *Solar Energy* **107**, 510-522

Natural Resources Canada, Office of Energy Efficiency. Comprehensive Energy Use Database:

http://oee.nrcan.gc.ca/corporate/statistics/neud/dpa/menus/trends/comprehensive/trends_com_ca.cfm, accessed June, 2015

Renewables 2014 Global Status Report, REN21, Renewable Energy Policy Network for the 21st Century

Rounis, E.D., Bigaila, E., Luk, P., Athienitis, A.K, Stathopoulos, T. Multiple-inlet BIPV/T modelling: wind effects and fan induced suction. (2015). A study of a BIPV/T collector prototype for building façade applications. International Building Physics Conference,

shapeways, 3D printed models, <http://www.shapeways.com>

Simiu, E., Scanlan, R.H. (1996). Wind Effects on Structures: Fundamentals and Applications to Design. John Wiley & Sons, Third Edition

Skoplaki, E., Palyvos, J.A. (2009). On the temperature dependence of photovoltaic module electrical performance. A review of efficiency/power correlations. Solar Energy **83**, 614-624

Soulis, I.B. Hydraulics. Democritean University of Thrace.

Stathopoulos, T. (1984). Design and fabrication of a wind tunnel for building aerodynamics. Journal of Wind Engineering and Industrial Aerodynamics **16**, 361-376

Tonui, J.K. & Tripanagnostopoulos, Y. (2006). Air-cooled PV/T solar collectors with low cost performance improvements. Solar Energy **81**, 498-511

Tonui, J.K., Tripanagnostopoulos, Y. (2006). Performance improvement of PV/T solar collectors with natural air flow operation. Solar Energy **82**, 1-12

US Energy Information Administration, Consumption surveys. Available at <http://www.eia.gov/consumption/>, accessed June, 2015

Vasan, N., Stathopoulos, T. (2014). Experimental study of wind effects on unglazed transpired collectors. Solar Energy **101**, 138-149

Volokh, K.Y. (2001). On the foundations of the Hardy Cross method. International Journal of Solid and Structures **39**, 4197-4200

Warren, M.R., James, P.H., Young, I.C. (1998). Handbook of the Heat Transfer, 3rd Edition

Yadav, A.S., Bhagoria, J.L. (2013). Heat transfer and fluid flow analysis of solar air heater: A review of CFD approach. Renewable and Sustainable Energy Reviews **23**, 60-79

Yang, R.J. (2014). Overcoming technical barriers and risks in the application of building integrated photovoltaics (BIPV): hardware and software strategies. Automation in Construction **51**, 92-102

Yang, T., Athienitis, A.K. (2014). A study of design options for a building integrated photovoltaic/thermal (BIPV/T) system with glazed air collector and multiple inlets. Solar Energy **104**, 82-92

APPENDIX I Flow distribution and PV temperatures of the optimized multiple-inlet systems (Systems V and VI)

This section presents the complete results for inlet flow distributions and PV panel temperatures for summer and winter for the optimized multiple inlet systems (System V and VI), for wind directions of 45°, 90° and 135°, and wind velocities 1m/s and 2m/s. Systems V and VI have decreasing inlet porosity, as presented in section 5.1 and shown in Figures 5.5 and 5.6.

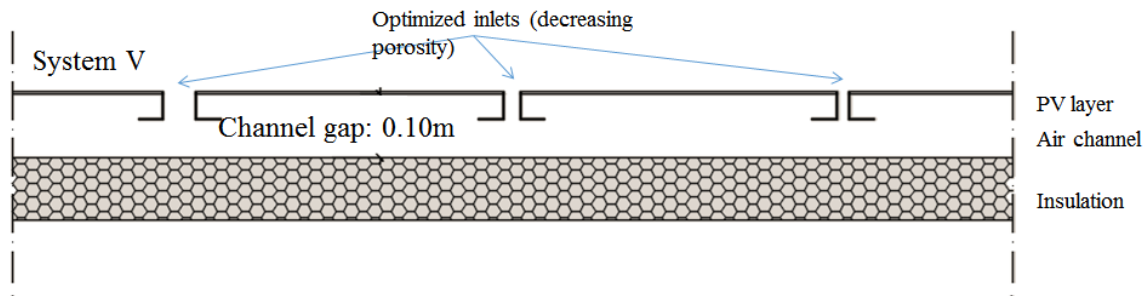


Figure 5.5: System V: Multiple-inlet system with optimized inlets (porosities as shown in Table 5.1) and channel gap size of 0.1m.

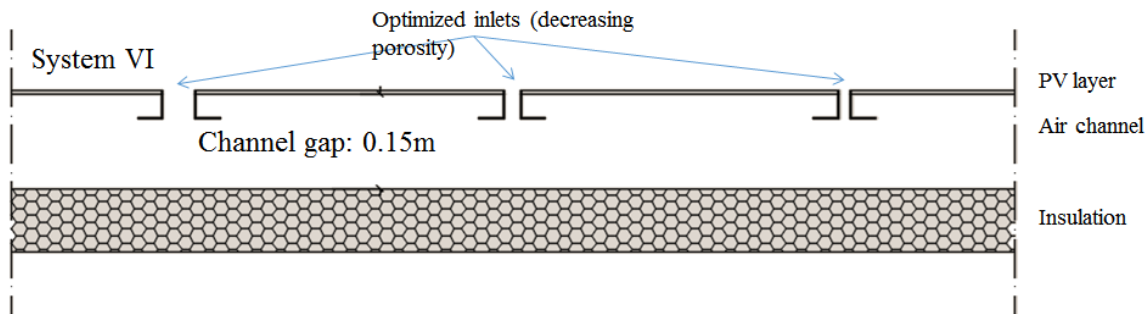


Figure 5.6: System VI: Multiple-inlet system with optimized inlets (porosities as shown in Table 5.1) and channel gap size of 0.15m.

Each of the following pages contains three tables, namely, the inlet flow distributions and the PV temperatures for summer and winter conditions, for a specific system, wind direction and velocity, and total mass flow rate. Each table presents the results for all 40 PV strings of the retrofit area.

System V, inlet flows for 1m/s wind, 45° and PV temperatures for summer and winter conditions at 400kg/h total air mass flow rate:

		Inlet Fflows (kg/h)																																					
Inlet	1	229	220	220	226	220	219	227	227	227	220	220	220	220	218	218	216	216	216	216	216	209	209	213	214	214	214	214	217	218	220	224	218	218	218	216	216	216	216
	2	39.3	43.7	43.6	38.7	43.7	43.4	38.7	38.7	38.7	43.7	43.7	43.7	43.7	43.2	43.2	42.8	42.8	42.8	42.8	42.8	47.2	47.2	42.2	42.3	42.4	42.4	42.4	42.9	43.2	43.5	38.2	43.2	43.2	43.2	42.9	42.9	42.8	42.7
	3	28	29.3	29.2	29.8	29.3	31.2	29.9	29.9	29.9	29.3	29.3	29.3	29.3	31.1	31.1	30.8	30.8	30.8	30.8	30.8	32.2	32.2	32.5	32.5	32.6	32.6	32.6	30.9	31.1	29.2	29.5	31.1	31.1	31.1	30.9	30.9	30.8	30.8
	4	36	38.6	38.5	37.4	38.6	38.5	37.5	37.5	37.5	38.6	38.6	38.6	38.6	38.3	38.3	39.6	39.6	39.6	39.6	39.6	40.6	40.6	40.8	40.9	40.9	40.9	40.9	39.7	38.3	38.5	38.7	38.3	38.3	38.3	39.7	39.7	39.6	39.5
	5	26.5	27	27	26.4	27.1	27	26.5	26.5	26.4	27	27	27	27	27.7	27.7	28.2	28.2	28.2	28.2	28.2	28.7	28.7	28.8	28.1	28.1	28.1	28.1	27.5	27.6	26.9	26.9	27.6	27.5	26.8	27.4	27.4	28.1	28.1
	6	22.4	22.4	22.8	22.6	22.4	22.3	22.2	22.2	22.2	22.4	22.4	22.4	22.4	22.8	22.8	23.1	23.1	23.1	23.1	23.1	23.2	23.2	23.3	23.3	22.9	22.9	22.9	23.1	22.7	22.9	23	22.7	22.8	22.9	23.1	23.2	23.1	23.5
	7	16.6	16.5	16.6	16.4	16.3	16.3	16.2	16.3	16.4	16.5	16.5	16.5	16.5	16.6	16.6	16.9	16.9	16.9	16.9	16.9	17	17	17	16.9	16.9	16.9	16.9	16.8	16.9	17	17	17.1	17.2	17.3	17.3	17.5		
	8	0.5	0.53	0.52	0.53	0.53	0.55	0.54	0.54	0.53	0.53	0.53	0.53	0.54	0.54	0.54	0.54	0.54	0.54	0.54	0.54	0.55	0.55	0.55	0.56	0.56	0.56	0.55	0.55	0.54	0.54	0.54	0.55	0.55	0.55	0.56	0.57	0.56	
	9	0.82	0.83	0.85	0.83	0.84	0.87	0.84	0.82	0.83	0.84	0.84	0.84	0.84	0.86	0.86	0.87	0.87	0.87	0.87	0.87	0.9	0.9	0.89	0.88	0.88	0.88	0.88	0.86	0.86	0.85	0.84	0.86	0.86	0.87	0.87	0.89	0.88	
	10	0.86	0.91	0.9	0.88	0.89	0.89	0.86	0.87	0.88	0.9	0.9	0.9	0.9	0.92	0.92	0.94	0.94	0.94	0.94	0.94	0.97	0.97	0.97	0.96	0.96	0.96	0.96	0.91	0.91	0.89	0.89	0.91	0.92	0.9	0.93	0.92	0.92	

		PV temperature (deg C), Summer																																						
PV module	1	43.6	43.8	43.8	43.7	43.8	43.9	43.7	43.7	43.7	43.8	43.8	43.8	43.8	43.9	43.9	44	44	44	44	44	44.2	44.2	44.1	44	44	44	44	43.9	43.9	43.9	43.7	43.9	43.9	43.9	43.9	44	44	44	
	2	42.6	42.7	42.7	42.6	42.7	42.7	42.6	42.6	42.6	42.7	42.7	42.7	42.7	42.7	42.7	42.8	42.8	42.8	42.8	42.8	42.8	42.9	42.9	42.9	42.9	42.9	42.9	42.8	42.7	42.7	42.7	42.7	42.7	42.7	42.7	42.8	42.8	42.8	42.8
	3	40.5	40.5	40.5	40.5	40.5	40.5	40.5	40.5	40.5	40.5	40.5	40.5	40.5	40.5	40.6	40.6	40.6	40.6	40.6	40.6	40.6	40.6	40.7	40.6	40.6	40.6	40.6	40.5	40.5	40.5	40.6	40.6	40.5	40.6	40.6	40.6	40.6		
	4	41.1	41.1	41.1	41.1	41.1	41.1	41.1	41.1	41.1	41.1	41.1	41.1	41.1	41.1	41.2	41.2	41.2	41.2	41.2	41.2	41.2	41.2	41.2	41.2	41.2	41.2	41.1	41.1	41.1	41.1	41.1	41.1	41.1	41.1	41.2	41.2	41.2	41.2	
	5	40.6	40.6	40.6	40.6	40.6	40.6	40.6	40.6	40.6	40.6	40.6	40.6	40.6	40.6	40.6	40.6	40.6	40.6	40.6	40.6	40.6	40.6	40.6	40.6	40.6	40.6	40.6	40.6	40.6	40.6	40.6	40.6	40.6	40.6	40.6	40.6	40.6	40.6	
	6	40.2	40.2	40.2	40.2	40.2	40.2	40.2	40.2	40.2	40.2	40.2	40.2	40.2	40.2	40.2	40.2	40.2	40.2	40.2	40.2	40.2	40.2	40.2	40.2	40.2	40.2	40.2	40.2	40.2	40.2	40.2	40.2	40.2	40.2	40.2	40.2	40.2	40.2	
	7	39.9	39.9	39.9	39.9	39.9	39.9	39.9	39.9	39.9	39.9	39.9	39.9	39.9	39.9	39.9	39.9	39.9	39.9	39.9	39.9	39.9	39.9	39.9	39.9	39.9	39.9	39.9	39.9	39.9	39.9	39.9	39.9	39.9	39.9	39.9	39.9	39.9	39.9	
	8	40.5	40.5	40.5	40.5	40.5	40.5	40.5	40.5	40.5	40.5	40.5	40.5	40.5	40.5	40.5	40.5	40.5	40.5	40.5	40.5	40.5	40.5	40.5	40.5	40.5	40.5	40.5	40.5	40.5	40.5	40.5	40.5	40.5	40.5	40.5	40.5	40.5	40.5	
	9	40.3	40.3	40.3	40.3	40.3	40.3	40.3	40.3	40.3	40.3	40.3	40.3	40.3	40.3	40.3	40.3	40.3	40.3	40.3	40.3	40.3	40.3	40.3	40.3	40.3	40.3	40.3	40.3	40.3	40.3	40.3	40.3	40.3	40.3	40.3	40.3	40.3	40.3	40.3
	10	40.3	40.2	40.2	40.3	40.3	40.3	40.3	40.3	40.3	40.3	40.3	40.3	40.3	40.3	40.2	40.2	40.2	40.2	40.2	40.2	40.2	40.2	40.2	40.2	40.2	40.2	40.2	40.2	40.2	40.2	40.2	40.2	40.2	40.2	40.2	40.2	40.2	40.2	40.2

		PV temperature (deg C), Winter																																						
PV module	1	11	11.3	11.3	11.1	11.2	11.3	11.1	11.1	11.1	11.3	11.3	11.3	11.3	11.3	11.3	11.4	11.4	11.4	11.4	11.4	11.6	11.6	11.5	11.4	11.4	11.4	11.4	11.3	11.3	11.1	11.3	11.3	11.3	11.3	11.4	11.4	11.4	11.4	
	2	10	10.1	10.1	10.1	10.1	10.2	10.1	10.1	10.1	10.1	10.1	10.1	10.1	10.2	10.2	10.3	10.3	10.3	10.3	10.3	10.3	10.3	10.3	10.3	10.3	10.3	10.2	10.2	10.1	10.2	10.2	10.2	10.2	10.2	10.2	10.2	10.3	10.3	
	3	9.56	9.63	9.64	9.59	9.62	9.63	9.58	9.58	9.59	9.63	9.63	9.63	9.63	9.65	9.65	9.71	9.71	9.71	9.71	9.71	9.71	9.75	9.75	9.76	9.75	9.74	9.74	9.74	9.69	9.66	9.64	9.65	9.66	9.66	9.65	9.7	9.7	9.71	9.72
	4	8.73	8.73	8.74	8.72	8.73	8.73	8.71	8.71	8.72	8.73	8.73	8.73	8.73	8.75	8.75	8.78	8.78	8.78	8.78	8.78	8.78	8.79	8.79	8.79	8.78	8.77	8.77	8.77	8.76	8.76	8.75	8.75	8.76	8.76	8.75	8.77	8.77	8.78	8.79
	5	8.26	8.26	8.27	8.26	8.26	8.26	8.25	8.25	8.25	8.26	8.26	8.26	8.26	8.27	8.27	8.28	8.28	8.28	8.28	8.28	8.28	8.28	8.28	8.29	8.28	8.28	8.28	8.28	8.27	8.28	8.28	8.28	8.28	8.28	8.29	8.29	8.29	8.3	
	6	7.89	7.89	7.89	7.89	7.89	7.89	7.89	7.89	7.89	7.89	7.89	7.89	7.89	7.89	7.9	7.9	7.9	7.9	7.9	7.9	7.9	7.9	7.9	7.9	7.9	7.9	7.9	7.9	7.9	7.9	7.9	7.9	7.9	7.9	7.9	7.9	7.9	7.9	7.9
	7	7.64	7.64	7.64	7.64	7.64	7.64	7.64	7.64	7.64	7.64	7.64	7.64	7.64	7.64	7.64	7.64	7.64	7.64	7.64	7.64	7.64	7.64	7.64	7.64	7.64	7.64	7.64	7.64	7.64	7.64	7.64	7.64	7.64	7.64	7.64	7.64	7.64	7.64	7.64
	8	8.2	8.18	8.19	8.18	8.18	8.16	8.17	8.17	8.18	8.18	8.18	8.18	8.18	8.17	8.17	8.17	8.17	8.17	8.17	8.17	8.16	8.16	8.16	8.16	8.16	8.16	8.16	8.16	8.16	8.17	8.17	8.17	8.16	8.16	8.16	8.16	8.15	8.15	8.15
	9	8.03	8.02	8.01	8.02	8.02	8	8.01	8.02	8.02	8.01	8.01	8.01	8.01	8.01	8.01	8	8	8	8	8	8	7.99	7.99	7.99	8	8	8	8	8.01	8.01	8.01	8.01	8	8	8	7.99	8	8	
	10	7.98	7.96	7.96	7.98	7.97	7.97	7.98	7.98	7.98	7.97	7.97	7.97	7.97	7.96	7.96	7.95	7.95	7.95	7.95	7.95	7.95	7.94	7.94	7.94	7.94	7.94	7.94	7.96	7.96	7.97	7.97	7.96	7.96	7.96	7.96	7.96	7.96	7.96	7.95

System V, inlet flows for 2m/s wind, 45° and PV temperatures for summer and winter conditions at 400kg/h total air mass flow rate:

		Inlet Fflows (kg/h)																																						
Inlet	1	273	236	235	262	237	230	264	263	263	236	236	236	236	226	226	218	218	218	218	218	218	190	190	206	209	210	210	218	221	226	234	234	218	225	227	220	219	218	217
	2	29.2	46.8	46.5	25	46.9	45.6	25.5	25.3	25.4	46.8	46.8	46.8	46.8	44.9	44.9	43.3	43.3	43.3	43.3	43.3	43.3	59.1	59.1	40.9	41.4	41.6	41.6	43.3	43.8	44.7	46.4	46.4	43.2	44.7	45	43.7	43.5	43.2	43
	3	19	24.8	24.5	27.7	24.9	32.7	27.8	27.7	27.7	24.7	24.7	24.7	24.7	32.3	32.3	31.1	31.1	31.1	31.1	31.1	31.1	36.4	36.4	37.2	37.5	37.6	37.6	31.1	31.5	32.2	24.3	24.3	31.1	32.1	32.4	31.4	31.3	31.1	30.9
	4	24.4	36.1	35.8	30.6	36.2	35.3	31.4	31.2	31.4	36.1	36.1	36.1	36.1	34.6	34.6	40	40	40	40	40	40	43.9	43.9	44.5	44.9	45.1	45.1	40	40.4	34.5	35.6	35.6	38.3	34.5	34.7	40.2	40.2	39.9	39.7
	5	23	24.3	24.1	22.9	24.4	23.9	22	21.9	21	24.2	24.2	24.2	24.2	26.6	26.6	28.8	28.8	28.8	28.8	28.8	28.8	30.8	30.8	31	28.3	28.4	28.4	28.8	25.9	26.1	23.9	23.9	27.6	26.2	22.7	26.4	25.4	29.3	29.2
	6	17.6	18.4	20.6	18.2	18.4	18	17.1	16.9	19.7	18.2	18.2	18.2	18.2	20.2	20.2	21.6	21.6	21.6	21.6	21.6	21.6	22.4	22.4	22.7	22.7	21	21	21.5	21.4	20.4	19.8	19.8	22.7	20	20.5	21.9	21.9	20.8	22.5
	7	10	10.4	9.09	10	9.61	11	9.79	10.4	7.95	11.4	11.4	11.4	11.4	12.9	12.9	14.4	14.4	14.4	14.4	14.4	14.4	14.7	14.7	14.9	14.2	14.2	14.7	14	14.4	13.1	13.1	17	14.9	15.4	9.78	16	14.3	14.5	
	8	1.13	1.04	3.04	1	0.75	0.46	0.91	0.27	1.06	0.51	0.51	0.51	0.51	0.45	0.45	0.45	0.45	0.45	0.45	0.45	0.45	0.5	0.5	0.48	0.52	0.53	0.53	0.5	0.51	0.47	0.63	0.63	0.54	0.47	0.52	2.9	0.54	0.79	0.75
	9	1.03	1.1	0.95	1.28	1.13	0.34	0.89	2.11	1.43	0.99	0.99	0.99	0.99	0.83	0.83	0.84	0.84	0.84	0.84	0.84	0.84	0.96	0.96	0.92	0.84	0.85	0.85	0.78	0.83	0.74	1.11	1.11	0.86	0.8	0.87	1.76	0.92	1.3	1.26
	10	1.07	0.99	0.91	0.86	0.91	2.88	1.06	1	0.98	1.18	1.18	1.18	1.18	1.02	1.02	1.07	1.07	1.07	1.07	1.07	1.07	1.22	1.22	1.17	1.11	1.12	1.12	1.02	0.87	0.78	1.19	1.19	0.91	0.88	0.81	1.75	0.88	1.34	1.5

		PV temperature (deg C), Summer																																						
PV module	1	38.2	38.8	38.8	38.4	38.8	38.9	38.4	38.4	38.4	38.8	38.8	38.8	38.8	39	39	39.1	39.1	39.1	39.1	39.1	39.1	39.7	39.7	39.4	39.3	39.3	39.3	39.1	39.1	39	38.9	38.9	39.1	39	39	39.1	39.1	39.1	39.2
	2	37.8	38.1	38.1	38	38	38.2	38	38	38	38.1	38.1	38.1	38.1	38.2	38.2	38.4	38.4	38.4	38.4	38.4	38.4	38.6	38.6	38.6	38.6	38.6	38.6	38.4	38.3	38.3	38.1	38.1	38.4	38.3	38.2	38.4	38.4	38.4	38.4
	3	36.6	36.7	36.8	36.7	36.7	36.8	36.6	36.6	36.6	36.8	36.8	36.8	36.8	36.8	36.8	37	37	37	37	37	37	37.1	37.1	37.1	37.1	37	37	37	36.9	36.8	36.8	36.8	37	36.8	36.8	36.9	36.9	37	37
	4	37.1	37.2	37.2	37.2	37.2	37.2	37.1	37.1	37.1	37.2	37.2	37.2	37.2	37.3	37.3	37.3	37.3	37.3	37.3	37.3	37.3	37.4	37.4	37.4	37.3	37.3	37.3	37.3	37.3	37.3	37.2	37.2	37.4	37.3	37.2	37.3	37.3	37.3	37.4
	5	36.9	36.9	36.9	36.9	36.9	36.9	36.8	36.9	36.9	36.9	36.9	36.9	36.9	36.9	36.9	37	37	37	37	37	37	37	37	37	37	37	36.9	36.9	37	36.9	36.9	36.9	36.9	37	36.9	37	36.9	37	37
	6	36.6	36.6	36.6	36.6	36.6	36.7	36.6	36.6	36.6	36.7	36.7	36.7	36.7	36.7	36.7	36.7	36.7	36.7	36.7	36.7	36.7	36.7	36.7	36.7	36.7	36.7	36.7	36.7	36.7	36.7	36.7	36.7	36.7	36.7	36.7	36.7	36.7	36.7	
	7	36.5	36.5	36.6	36.5	36.5	36.5	36.5	36.5	36.5	36.5	36.5	36.5	36.5	36.5	36.5	36.5	36.5	36.5	36.5	36.5	36.5	36.5	36.5	36.5	36.5	36.5	36.5	36.5	36.5	36.5	36.5	36.5	36.5	36.5	36.5	36.5	36.5	36.5	
	8	36.7	36.7	36.6	36.7	36.8	37	36.8	37.3	36.7	37	37	37	37	37	37	37	37	37	37	37	37	37	37	37	37	37	37	37	37	37	37	37	37	37	37	37	37	37	37
	9	36.7	36.7	36.7	36.7	36.7	37.2	36.8	36.6	36.7	36.8	36.8	36.8	36.8	36.8	36.8	36.8	36.8	36.8	36.8	36.8	36.8	36.8	36.8	36.8	36.8	36.8	36.8	36.8	36.8	36.8	36.8	36.8	36.8	36.8	36.8	36.8	36.8	36.8	36.8
	10	36.7	36.7	36.8	36.8	36.8	36.6	36.7	36.7	36.7	36.7	36.7	36.7	36.7	36.7	36.7	36.7	36.7	36.7	36.7	36.7	36.7	36.7	36.7	36.7	36.7	36.7	36.7	36.7	36.7	36.7	36.7	36.7	36.8	36.8	36.8	36.8	36.8	36.8	

		PV temperature (deg C), Winter																																							
PV module	1	6.18	6.71	6.73	6.33	6.7	6.8	6.31	6.32	6.32	6.71	6.71	6.71	6.71	6.71	6.86	6.86	6.98	6.98	6.98	6.98	6.98	6.98	7.46	7.46	7.18	7.14	7.12	7.12	6.99	6.95	6.87	6.74	6.74	6.99	6.87	6.85	6.95	6.97	6.99	7.01
	2	5.8	6.06	6.08	6	6.05	6.16	5.98	5.99	5.98	6.06	6.06	6.06	6.06	6.06	6.21	6.21	6.35	6.35	6.35	6.35	6.35	6.35	6.52	6.52	6.55	6.51	6.49	6.49	6.35	6.31	6.22	6.09	6.09	6.35	6.23	6.2	6.31	6.33	6.35	6.37
	3	5.63	5.81	5.84	5.73	5.8	5.83	5.71	5.72	5.71	5.82	5.82	5.82	5.82	5.89	5.89	6.03	6.03	6.03	6.03	6.03	6.03	6.14	6.14	6.16	6.12	6.1	6.1	6.03	5.99	5.9	5.85	5.85	6.04	5.91	5.88	5.99	6.01	6.03	6.05	
	4	5.29	5.31	5.34	5.29	5.3	5.31	5.26	5.27	5.27	5.31	5.31	5.31	5.31	5.38	5.38	5.44	5.44	5.44	5.44	5.44	5.44	5.48	5.48	5.48	5.44	5.42	5.42	5.44	5.39	5.39	5.35	5.35	5.47	5.39	5.36	5.4	5.42	5.44	5.47	
	5	5.03	5.04	5.07	5.04	5.03	5.05	5.02	5.03	5.04	5.05	5.05	5.05	5.05	5.08	5.08	5.11	5.11	5.11	5.11	5.11	5.11	5.13	5.13	5.13	5.12	5.11	5.11	5.12	5.11	5.1	5.09	5.09	5.15	5.1	5.11	5.11	5.13	5.12	5.14	
	6	4.85	4.85	4.85	4.85	4.84	4.86	4.84	4.85	4.83	4.86	4.86	4.86	4.86	4.87	4.87	4.88	4.88	4.88	4.88	4.88	4.88	4.89	4.89	4.89	4.88	4.88	4.88	4.88	4.88	4.88	4.88	4.88	4.88	4.88	4.88	4.88	4.88	4.88	4.88	
	7	4.76	4.76	4.78	4.76	4.76	4.76	4.76	4.76	4.77	4.75	4.75	4.75	4.75	4.74	4.74	4.74	4.74	4.74	4.74	4.74	4.74	4.75	4.75	4.75	4.74	4.75	4.75	4.74	4.74	4.74	4.74	4.74	4.75	4.74	4.74	4.74	4.74	4.74	4.74	
	8	4.91	4.93	4.8	4.94	5	5.16	4.96	5.38	4.93	5.11	5.11	5.11	5.11	5.15	5.15	5.15	5.15	5.15	5.15	5.15	5.15	5.12	5.12	5.13	5.1	5.1	5.1	5.12	5.11	5.13	5.05	5.05	5.09	5.14	5.1	4.81	5.09	4.99	5.01	
	9	4.93	4.92	4.94	4.89	4.91	5.33	4.96	4.84	4.87	4.95	4.95	4.95	4.95	4.99	4.99	4.99	4.99	4.99	4.99	4.99	4.99	4.96	4.96	4.97	4.99	4.98	4.98	5.01	4.99	5.02	4.92	4.92	4.98	5	4.98	4.85	4.96	4.89	4.9	
	10	4.91	4.93	4.95	4.96	4.95	4.79	4.92	4.92	4.93	4.9	4.9	4.9	4.9	4.93	4.93	4.92	4.92	4.92	4.92	4.92	4.92	4.89	4.89	4.9	4.91	4.91	4.91	4.93	4.96	4.99	4.89	4.89	4.95	4.96	4.98	4.83	4.96	4.87	4.85	

System V, inlet flows for 1m/s wind, 45° and PV temperatures for summer and winter conditions at 800kg/h total air mass flow rate:

		Inlet Fflows (kg/h)																																									
Inlet	1	438	434	434	437	434	434	437	437	437	434	434	434	434	434	433	433	432	432	432	432	432	428	428	431	431	431	431	432	432	433	434	434	433	433	433	432	432	432	432			
	2	83.5	85.7	85.7	83.3	85.7	85.6	83.3	83.3	83.3	85.7	85.7	85.7	85.7	85.7	85.5	85.5	85.3	85.3	85.3	85.3	85.3	87.6	87.6	85	85.1	85.1	85.1	85.3	85.4	85.5	85.7	85.7	85.5	85.5	85.5	85.5	85.4	85.3	85.3	85.3		
	3	60	60.6	60.6	60.9	60.6	61.6	60.9	60.9	60.9	60.6	60.6	60.6	60.6	61.5	61.5	61.4	61.4	61.4	61.4	61.4	61.4	62.1	62.1	62.2	62.3	62.3	62.3	61.4	61.4	61.5	60.6	60.6	61.5	61.5	61.5	61.4	61.4	61.4	61.4			
	4	77	78.3	78.3	77.7	78.3	78.3	77.7	77.7	77.7	78.3	78.3	78.3	78.3	78.3	78.2	78.2	78.8	78.8	78.8	78.8	78.8	79.3	79.3	79.4	79.5	79.5	79.5	78.8	78.9	78.2	78.3	78.3	78.2	78.1	78.2	78.9	78.8	78.8	78.8			
	5	55.2	55.4	55.4	55.1	55.5	55.4	55.2	55.2	55.2	55.4	55.4	55.4	55.4	55.8	55.8	56	56	56	56	56	56	56.3	56.3	56.3	56	56	56	56	55.7	55.7	55.4	55.4	55.7	55.7	55.3	55.6	55.6	56	56			
	6	46.4	46.4	46.6	46.5	46.4	46.3	46.3	46.3	46.3	46.4	46.4	46.4	46.4	46.6	46.6	46.7	46.7	46.7	46.7	46.7	46.7	46.8	46.8	46.8	46.8	46.6	46.6	46.7	46.7	46.6	46.6	46.6	46.6	46.6	46.7	46.8	46.7	46.9	46.9			
	7	34.7	34.6	34.7	34.6	34.5	34.5	34.5	34.5	34.6	34.6	34.6	34.6	34.7	34.7	34.8	34.8	34.8	34.8	34.8	34.8	34.8	34.8	34.8	34.9	34.8	34.8	34.8	34.9	34.8	34.8	34.8	34.8	34.9	34.9	35	35	35	35.1	35.1			
	8	1.1	1.12	1.11	1.11	1.12	1.13	1.12	1.12	1.11	1.12	1.12	1.12	1.12	1.12	1.12	1.12	1.12	1.12	1.12	1.12	1.12	1.13	1.13	1.13	1.13	1.13	1.13	1.13	1.13	1.13	1.12	1.12	1.13	1.13	1.13	1.13	1.13	1.13	1.13	1.13	1.14	1.13
	9	1.73	1.74	1.75	1.74	1.75	1.76	1.75	1.74	1.74	1.75	1.75	1.75	1.75	1.76	1.76	1.76	1.76	1.76	1.76	1.76	1.76	1.78	1.78	1.77	1.77	1.77	1.77	1.76	1.76	1.76	1.75	1.75	1.76	1.76	1.76	1.76	1.76	1.76	1.77	1.77	1.77	1.76
	10	1.84	1.86	1.86	1.84	1.85	1.85	1.83	1.84	1.84	1.85	1.85	1.85	1.85	1.86	1.86	1.87	1.87	1.87	1.87	1.87	1.87	1.89	1.89	1.89	1.88	1.88	1.87	1.86	1.86	1.85	1.85	1.86	1.86	1.86	1.87	1.87	1.87	1.87	1.87	1.87	1.87	1.87

		PV temperature (deg C), Summer																																											
PV module	1	39.2	39.2	39.2	39.2	39.2	39.2	39.2	39.2	39.2	39.2	39.2	39.2	39.3	39.3	39.3	39.3	39.3	39.3	39.3	39.3	39.3	39.3	39.3	39.3	39.3	39.3	39.3	39.3	39.3	39.2	39.2	39.3	39.3	39.3	39.3	39.3	39.3	39.3	39.3					
	2	38	38	38	38	38	38	38	38	38	38	38	38	38	38	38	38	38	38	38	38	38	38	38	38	38	38	38	38	38	38	38	38	38	38	38	38	38	38	38	38	38			
	3	36.4	36.4	36.4	36.4	36.4	36.4	36.4	36.4	36.4	36.4	36.4	36.4	36.4	36.4	36.4	36.4	36.4	36.4	36.4	36.4	36.4	36.4	36.4	36.4	36.4	36.4	36.4	36.4	36.4	36.4	36.4	36.4	36.4	36.4	36.4	36.4	36.4	36.4	36.4	36.4	36.4	36.4		
	4	36.3	36.3	36.3	36.3	36.3	36.3	36.3	36.3	36.3	36.3	36.3	36.3	36.3	36.3	36.4	36.4	36.4	36.4	36.4	36.4	36.4	36.4	36.4	36.4	36.4	36.4	36.4	36.4	36.4	36.3	36.3	36.3	36.3	36.3	36.3	36.3	36.3	36.3	36.4	36.4	36.4	36.4		
	5	35.8	35.8	35.8	35.8	35.8	35.8	35.8	35.8	35.8	35.8	35.8	35.8	35.8	35.8	35.8	35.8	35.8	35.8	35.8	35.8	35.8	35.8	35.8	35.8	35.8	35.8	35.8	35.8	35.8	35.8	35.8	35.8	35.8	35.8	35.8	35.8	35.8	35.8	35.8	35.8	35.8	35.8	35.8	
	6	35.4	35.4	35.4	35.4	35.4	35.4	35.4	35.4	35.4	35.4	35.4	35.4	35.4	35.4	35.4	35.4	35.4	35.4	35.4	35.4	35.4	35.4	35.4	35.4	35.4	35.4	35.4	35.4	35.4	35.4	35.4	35.4	35.4	35.4	35.4	35.4	35.4	35.4	35.4	35.4	35.4	35.4	35.4	
	7	35.1	35.1	35.1	35.1	35.1	35.1	35.1	35.1	35.1	35.1	35.1	35.1	35.1	35.1	35.1	35.1	35.1	35.1	35.1	35.1	35.1	35.1	35.1	35.1	35.1	35.1	35.1	35.1	35.1	35.1	35.1	35.1	35.1	35.1	35.1	35.1	35.1	35.1	35.1	35.1	35.1	35.1	35.1	
	8	35.6	35.6	35.6	35.6	35.6	35.6	35.6	35.6	35.6	35.6	35.6	35.6	35.6	35.6	35.6	35.6	35.6	35.6	35.6	35.6	35.6	35.6	35.6	35.6	35.6	35.6	35.6	35.6	35.6	35.6	35.6	35.6	35.6	35.6	35.6	35.6	35.6	35.6	35.6	35.6	35.6	35.6	35.6	35.6
	9	35.4	35.4	35.4	35.4	35.4	35.4	35.4	35.4	35.4	35.4	35.4	35.4	35.4	35.4	35.4	35.4	35.4	35.4	35.4	35.4	35.4	35.4	35.4	35.4	35.4	35.4	35.4	35.4	35.4	35.4	35.4	35.4	35.4	35.4	35.4	35.4	35.4	35.4	35.4	35.4	35.4	35.4	35.4	35.4
	10	35.4	35.4	35.4	35.4	35.4	35.4	35.4	35.4	35.4	35.4	35.4	35.4	35.4	35.4	35.4	35.4	35.4	35.4	35.4	35.4	35.4	35.4	35.4	35.4	35.4	35.4	35.4	35.4	35.4	35.4	35.4	35.4	35.4	35.4	35.4	35.4	35.4	35.4	35.4	35.4	35.4	35.4	35.4	35.4

		PV temperature (deg C), Winter																																											
PV module	1	7.03	7.09	7.09	7.04	7.09	7.1	7.04	7.04	7.04	7.09	7.09	7.09	7.09	7.1	7.1	7.12	7.12	7.12	7.12	7.12	7.12	7.17	7.17	7.14	7.13	7.13	7.13	7.12	7.11	7.1	7.09	7.09	7.1	7.1	7.1	7.11	7.11	7.12	7.12					
	2	5.98	6	6	6	6	6.01	5.99	5.99	5.99	6	6	6	6	6	6.02	6.02	6.03	6.03	6.03	6.03	6.03	6.05	6.05	6.05	6.05	6.05	6.05	6.03	6.03	6.02	6.01	6.01	6.02	6.02	6.02	6.03	6.03	6.03	6.03	6.03	6.03	6.03		
	3	5.45	5.47	5.47	5.46	5.47	5.47	5.46	5.46	5.46	5.47	5.47	5.47	5.47	5.47	5.47	5.49	5.49	5.49	5.49	5.49	5.49	5.5	5.5	5.5	5.5	5.49	5.49	5.49	5.48	5.47	5.47	5.47	5.48	5.48	5.47	5.48	5.48	5.47	5.48	5.49	5.49			
	4	4.6	4.6	4.61	4.6	4.6	4.6	4.6	4.6	4.6	4.6	4.6	4.6	4.6	4.6	4.61	4.61	4.61	4.61	4.61	4.61	4.61	4.62	4.62	4.62	4.61	4.61	4.61	4.61	4.61	4.61	4.61	4.61	4.61	4.61	4.61	4.61	4.61	4.61	4.61	4.61	4.61	4.61	4.62	
	5	4.14	4.14	4.14	4.14	4.14	4.14	4.14	4.14	4.14	4.14	4.14	4.14	4.14	4.14	4.14	4.15	4.15	4.15	4.15	4.15	4.15	4.15	4.15	4.15	4.15	4.15	4.14	4.14	4.15	4.15	4.14	4.14	4.14	4.14	4.14	4.15	4.15	4.15	4.15	4.15	4.15	4.15	4.15	
	6	3.79	3.79	3.79	3.79	3.78	3.79	3.78	3.78	3.79	3.79	3.79	3.79	3.79	3.79	3.79	3.79	3.79	3.79	3.79	3.79	3.79	3.79	3.79	3.79	3.79	3.79	3.79	3.79	3.79	3.79	3.79	3.79	3.79	3.79	3.79	3.79	3.79	3.79	3.79	3.79	3.79	3.79	3.79	
	7	3.54	3.54	3.54	3.54	3.54	3.54	3.54	3.54	3.54	3.54	3.54	3.54	3.54	3.54	3.54	3.54	3.54	3.54	3.54	3.54	3.54	3.54	3.54	3.54	3.54	3.54	3.54	3.54	3.54	3.54	3.54	3.54	3.54	3.54	3.54	3.54	3.54	3.54	3.54	3.54	3.54	3.54	3.54	3.54
	8	3.94	3.94	3.94	3.94	3.93	3.93	3.93	3.93	3.93	3.93	3.93	3.93	3.93	3.93	3.93	3.93	3.93	3.93	3.93	3.93	3.93	3.93	3.93	3.93	3.93	3.93	3.93	3.93	3.93	3.93	3.93	3.93	3.93	3.93	3.93	3.93	3.93	3.93	3.93	3.93	3.93	3.93	3.93	3.93
	9	3.82	3.82	3.82	3.82	3.82	3.82	3.82	3.82	3.82	3.82	3.82	3.82	3.82	3.82	3.82	3.82	3.82	3.82	3.82	3.82	3.82	3.82	3.81	3.81	3.81	3.81	3.81	3.81	3.82	3.82	3.82	3.82	3.82	3.82	3.82	3.82	3.82	3.82	3.82	3.82	3.82	3.82	3.82	3.82
	10	3.78	3.78	3.78	3.78	3.78	3.78	3.78	3.78	3.78	3.78	3.78	3.78	3.78	3.78	3.78	3.78	3.78	3.78	3.78	3.78	3.78	3.77	3.77	3.78	3.78	3.78	3.78	3.78	3.78	3.78	3.78	3.78	3.78	3.78	3.78	3.78	3.78	3.78	3.78	3.78	3.78	3.78	3.78	3.78

System VI, inlet flows for 1m/s wind, 45° and PV temperatures for summer and winter conditions at 400kg/h total air mass flow rate:

		Inlet Fflows (kg/h)																																								
Inlet	1	281.4	268.6	267.9	277.0	268.9	266.8	277.6	277.6	277.5	268.6	268.6	268.6	268.6	265.1	265.1	261.8	261.8	261.8	261.8	261.8	251.8	251.8	257.0	258.4	258.4	258.4	258.4	262.8	264.8	267.5	273.4	264.7	264.4	265.3	262.3	262.2	261.4	260.8			
	2	33.1	38.4	38.3	32.4	38.4	38.1	32.5	32.5	32.5	38.4	38.4	38.4	38.4	38.4	37.9	37.9	37.4	37.4	37.4	37.4	37.4	42.6	42.6	36.7	36.9	36.9	36.9	36.9	37.6	37.9	38.2	31.8	37.8	37.8	37.9	37.5	37.5	37.4	37.3		
	3	20.1	22.0	22.0	22.6	22.0	24.6	22.7	22.7	22.7	22.0	22.0	22.0	22.0	24.5	24.5	24.2	24.2	24.2	24.2	24.2	24.2	26.1	26.1	26.3	26.4	26.4	26.4	26.4	24.3	24.4	21.9	22.2	24.4	24.4	24.5	24.2	24.2	24.1	24.1		
	4	23.8	27.7	27.6	25.9	27.8	27.6	26.0	26.0	26.0	27.7	27.7	27.7	27.7	27.4	27.4	29.3	29.3	29.3	29.3	29.3	29.3	30.9	30.9	31.1	31.2	31.2	31.2	31.2	29.4	27.4	27.6	27.9	27.4	27.4	27.4	27.4	29.4	29.4	29.3	29.2	
	5	18.0	18.3	18.3	17.6	18.4	18.3	17.6	17.6	17.6	18.3	18.3	18.3	18.3	19.3	19.3	20.2	20.2	20.2	20.2	20.2	20.2	21.0	21.0	21.1	20.1	20.1	20.1	20.1	19.2	19.3	18.1	18.4	19.2	19.0	18.0	19.0	19.0	20.1	20.0		
	6	13.4	14.1	14.6	13.9	13.9	14.0	13.3	13.3	13.3	14.1	14.1	14.1	14.1	14.6	14.6	15.2	15.2	15.2	15.2	15.2	15.2	15.6	15.6	15.7	15.0	15.0	15.0	15.0	15.1	14.5	14.8	14.6	14.5	15.0	14.7	15.2	15.3	15.3	15.3	15.8	
	7	7.9	9.3	9.7	8.9	9.1	9.0	8.5	8.5	8.8	9.4	9.4	9.4	9.4	9.6	9.6	10.2	10.2	10.2	10.2	10.2	10.2	10.3	10.3	10.4	10.4	10.4	10.4	10.2	10.2	10.1	10.1	10.3	10.0	10.4	10.5	10.5	10.8	10.8	10.9	11.2	
	8	0.4	0.3	0.3	0.4	0.3	0.4	0.4	0.4	0.4	0.3	0.3	0.3	0.3	0.3	0.3	0.3	0.3	0.3	0.3	0.3	0.3	0.4	0.4	0.4	0.4	0.4	0.4	0.4	0.4	0.3	0.4	0.3	0.4	0.3	0.4	0.3	0.4	0.4	0.4	0.4	
	9	0.9	0.5	0.6	0.6	0.6	0.7	0.7	0.7	0.6	0.6	0.6	0.6	0.6	0.6	0.6	0.6	0.6	0.6	0.6	0.6	0.6	0.6	0.6	0.6	0.6	0.6	0.6	0.6	0.6	0.6	0.6	0.6	0.6	0.6	0.6	0.6	0.6	0.6	0.6	0.6	0.6
	10	1.0	0.7	0.6	0.7	0.6	0.6	0.6	0.6	0.7	0.6	0.6	0.6	0.6	0.6	0.7	0.7	0.7	0.7	0.7	0.7	0.7	0.8	0.8	0.7	0.7	0.7	0.7	0.7	0.6	0.6	0.6	0.7	0.6	0.6	0.6	0.6	0.6	0.6	0.6	0.6	0.6

		PV temperature (deg C), Summer																																											
PV module	1	43.7	44	44	43.8	44	44	43.8	43.8	43.8	44	44	44	44	44.1	44.1	44.1	44.1	44.1	44.1	44.1	44.4	44.4	44.3	44.2	44.2	44.2	44.1	44.1	44	43.9	44.1	44.1	44.1	44.1	44.1	44.1	44.1	44.2	44.2					
	2	43	43.2	43.2	43.1	43.2	43.2	43.1	43.1	43.1	43.2	43.2	43.2	43.2	43.2	43.2	43.3	43.3	43.3	43.3	43.3	43.3	43.4	43.4	43.4	43.4	43.4	43.4	43.3	43.3	43.2	43.2	43.3	43.3	43.2	43.3	43.3	43.3	43.3	43.3	43.3	43.3			
	3	41	41.1	41.1	41.1	41.1	41.1	41.1	41.1	41.1	41.1	41.1	41.1	41.1	41.2	41.2	41.2	41.2	41.2	41.2	41.2	41.3	41.3	41.3	41.3	41.3	41.3	41.2	41.2	41.1	41.1	41.2	41.2	41.2	41.2	41.2	41.2	41.2	41.2	41.2	41.2	41.2	41.2		
	4	42.2	42.2	42.2	42.2	42.2	42.2	42.2	42.2	42.2	42.2	42.2	42.2	42.2	42.2	42.2	42.3	42.3	42.3	42.3	42.3	42.3	42.3	42.3	42.3	42.3	42.3	42.2	42.2	42.2	42.2	42.2	42.2	42.2	42.2	42.2	42.3	42.3	42.3	42.3	42.3	42.3	42.3		
	5	41.9	41.9	41.9	41.9	41.9	41.9	41.9	41.9	41.9	41.9	41.9	41.9	41.9	41.9	41.9	41.9	41.9	41.9	41.9	41.9	41.9	41.9	41.9	41.9	41.9	41.9	41.9	41.9	41.9	41.9	41.9	41.9	41.9	41.9	41.9	41.9	41.9	41.9	41.9	41.9	41.9	41.9	41.9	
	6	41.6	41.6	41.6	41.6	41.6	41.6	41.6	41.6	41.6	41.6	41.6	41.6	41.6	41.6	41.6	41.6	41.7	41.7	41.7	41.7	41.7	41.7	41.7	41.7	41.7	41.7	41.7	41.7	41.7	41.7	41.7	41.7	41.7	41.7	41.7	41.7	41.7	41.7	41.7	41.7	41.7	41.7	41.7	
	7	41.5	41.5	41.5	41.5	41.5	41.5	41.5	41.5	41.5	41.5	41.5	41.5	41.5	41.5	41.5	41.5	41.5	41.5	41.5	41.5	41.5	41.5	41.5	41.5	41.5	41.5	41.5	41.5	41.5	41.5	41.5	41.5	41.5	41.5	41.5	41.5	41.5	41.5	41.5	41.5	41.5	41.5	41.5	41.5
	8	42.2	42.4	42.5	42.3	42.4	42.3	42.2	42.2	42.3	42.4	42.4	42.4	42.4	42.3	42.3	42.4	42.4	42.4	42.4	42.4	42.4	42.3	42.3	42.3	42.3	42.3	42.3	42.3	42.3	42.3	42.3	42.3	42.3	42.3	42.3	42.3	42.3	42.3	42.3	42.3	42.3	42.2	42.3	
	9	41.9	42.2	42.1	42.1	42.1	42	42	42	42	42.1	42.1	42.1	42.1	42.1	42.1	42.1	42.1	42.1	42.1	42.1	42.1	42	42	42	42.1	42.1	42.1	42.1	42.1	42.1	42.1	42.1	42.1	42.1	42.1	42.1	42.1	42.1	42.1	42.1	42.1	42.1	42.1	42.1
	10	41.8	42	42	42	42	42	42	42	42	42	42	42	42	42	42	42	42	42	42	42	42	41.9	41.9	41.9	42	42	42	42	42	42	42	42.1	42	42	42.1	42	42	42	42	42	42	42	42	42

		PV temperature (deg C), Winter																																										
PV module	1	11.1	11.4	11.4	11.2	11.4	11.5	11.2	11.2	11.2	11.4	11.4	11.4	11.4	11.5	11.5	11.6	11.6	11.6	11.6	11.6	11.8	11.8	11.7	11.6	11.6	11.6	11.5	11.5	11.4	11.3	11.5	11.5	11.5	11.6	11.6	11.6	11.6	11.6	11.6	11.6			
	2	10.5	10.6	10.6	10.6	10.6	10.7	10.6	10.6	10.6	10.6	10.6	10.6	10.6	10.7	10.7	10.8	10.8	10.8	10.8	10.8	10.9	10.9	10.9	10.9	10.9	10.9	10.8	10.7	10.6	10.7	10.7	10.7	10.7	10.7	10.7	10.8	10.8	10.8	10.8	10.8	10.8	10.8	
	3	10.2	10.3	10.3	10.2	10.3	10.3	10.2	10.2	10.2	10.3	10.3	10.3	10.3	10.3	10.3	10.4	10.4	10.4	10.4	10.4	10.4	10.4	10.4	10.4	10.4	10.4	10.3	10.3	10.3	10.3	10.3	10.3	10.3	10.3	10.3	10.4	10.4	10.4	10.4	10.4	10.4	10.4	10.4
	4	9.68	9.7	9.71	9.68	9.69	9.69	9.67	9.67	9.7	9.7	9.7	9.7	9.7	9.73	9.73	9.77	9.77	9.77	9.77	9.77	9.77	9.79	9.79	9.79	9.76	9.76	9.76	9.74	9.74	9.72	9.72	9.74	9.75	9.73	9.75	9.76	9.77	9.79	9.79	9.79	9.79		
	5	9.39	9.42	9.43	9.41	9.41	9.41	9.39	9.39	9.4	9.42	9.42	9.42	9.42	9.43	9.43	9.45	9.45	9.45	9.45	9.45	9.45	9.45	9.45	9.46	9.44	9.44	9.44	9.43	9.44	9.44	9.44	9.45	9.44	9.45	9.44	9.45	9.46	9.46	9.47	9.47	9.47	9.47	
	6	9.2	9.2	9.21	9.2	9.2	9.2	9.2	9.2	9.2	9.2	9.2	9.2	9.2	9.21	9.21	9.22	9.22	9.22	9.22	9.22	9.22	9.22	9.22	9.22	9.22	9.22	9.22	9.22	9.22	9.22	9.22	9.22	9.22	9.22	9.22	9.22	9.22	9.23	9.23	9.23	9.23	9.23	
	7	9.1	9.08	9.08	9.08	9.08	9.08	9.08	9.08	9.08	9.08	9.08	9.08	9.08	9.08	9.08	9.08	9.08	9.08	9.08	9.08	9.08	9.08	9.08	9.08	9.08	9.08	9.08	9.08	9.07	9.08	9.07	9.07	9.07	9.07	9.07	9.07	9.07	9.07	9.07	9.07	9.07	9.07	
	8	9.68	9.88	9.94	9.8	9.86	9.76	9.72	9.72	9.79	9.86	9.86	9.86	9.86	9.86	9.81	9.81	9.83	9.83	9.83	9.83	9.83	9.83	9.83	9.83	9.83	9.83	9.82	9.78	9.82	9.76	9.81	9.82	9.77	9.81	9.77	9.73	9.77	9.77	9.77	9.77	9.77		
	9	9.4	9.66	9.61	9.56	9.63	9.54	9.5	9.5	9.55	9.62	9.62	9.62	9.62	9.62	9.58	9.58	9.58	9.58	9.58	9.58	9.58	9.55	9.55	9.56	9.59	9.59	9.59	9.59	9.58	9.62	9.56	9.59	9.62	9.56	9.6	9.56	9.6	9.57	9.6	9.57	9.6	9.6	
	10	9.36	9.5	9.53	9.49	9.55	9.56	9.53	9.53	9.48	9.54	9.54	9.54	9.54	9.54	9.49	9.49	9.49	9.49	9.49	9.49	9.49	9.45	9.45	9.46	9.48	9.48	9.48	9.48	9.48	9.48	9.48	9.48	9.48	9.48	9.48	9.48	9.48	9.48	9.48	9.48	9.48	9.48	9.48

System VI, inlet flows for 2m/s wind, 45° and PV temperatures for summer and winter conditions at 400kg/h total air mass flow rate:

		Inlet Fflows (kg/h)																																					
Inlet	1	364	298	295	338	302	290	341	341	341	298	298	298	298	281	281	266	266	266	266	266	228	228	246	253	253	265	270	279	292	292	279	278	280	280	268	264	262	
	2	25.1	42.6	42.2	16	43.1	41.4	17.2	17.2	17.1	42.6	42.6	42.6	42.6	40.2	40.2	38.1	38.1	38.1	38.1	38.1	56	56	35.2	36.2	36.2	36.2	37.9	38.6	39.9	41.8	41.8	39.9	39.7	40.1	40.1	38.2	37.8	37.4
	3	5.67	15.4	14.9	19.8	16	26.7	20.2	20.2	20.2	15.4	15.4	15.4	15.4	25.9	25.9	24.6	24.6	24.6	24.6	24.6	31.5	31.5	32.2	32.6	32.6	32.6	24.5	24.9	25.7	14.4	14.4	25.7	25.6	25.9	25.9	24.7	24.4	24.1
	4	-9	23.8	23.3	15.3	24.4	23	16.1	16.1	16.1	23.8	23.8	23.8	23.8	21.6	21.6	29.7	29.7	29.7	29.7	29.7	35.4	35.4	36	36.5	36.5	36.5	29.6	30.1	21.3	22.9	22.9	21.2	21.1	21.5	21.5	29.9	29.6	29.3
	5	10.5	12.4	11.9	6.22	12.9	11.8	7.24	7.24	7.18	12.4	12.4	12.4	12.4	17.2	17.2	21	21	21	21	21	23.7	23.7	24	20.3	20.3	20.3	20.9	16.6	17	11.4	11.4	17	16.9	10.2	10.2	16	20.4	20.4
	6	5.25	6.9	11.2	9.05	7.58	6.66	2.63	2.63	2.55	6.87	6.87	6.87	6.87	10.5	10.5	13.2	13.2	13.2	13.2	13.2	15.1	15.1	15.4	12.7	12.7	12.7	13	12.6	10.3	10.9	10.9	10.2	10.2	10.7	10.7	13.2	13.2	15.4
	7	2.56	2.97	2.42	-1.4	-3.4	2.21	-0.7	-0.7	-1.2	3.02	3.02	3.02	3.02	4.79	4.79	6.56	6.56	6.56	6.56	6.56	8.07	8.07	8.18	5.86	5.86	5.86	6.16	5.68	4.46	4.72	4.72	5.34	6.68	6.04	6.04	7.44	8.66	10.1
	8	0	-0.1	1.08	-0.5	-0.6	-0.5	-1.1	-1.1	-0.3	-0.2	-0.2	-0.2	-0.2	-0.1	-0.1	0.16	0.16	0.16	0.16	0.16	0.12	0.12	0.11	1.44	1.44	1.44	0.22	0.05	1.33	0.96	0.96	0.18	0.37	0.3	0.3	1.46	0.56	0.33
	9	-1.5	-0.4	-0.8	-0.9	-0.8	-0.6	-1.4	-1.4	-0.8	-0.6	-0.6	-0.6	-0.6	-0.4	-0.4	0.8	0.8	0.8	0.8	0.8	3.14	3.14	3.65	0.13	0.13	0.13	2.53	1.8	0.09	0.55	0.55	0.48	0.42	4.6	4.6	0.29	0.63	0.48
	10	-2.6	-2	-1.2	-1.7	-0.7	-0.9	-1.1	-1.1	-1.5	-1.3	-1.3	-1.3	-1.3	-0.9	-0.9	-0.2	-0.2	-0.2	-0.2	-0.2	-0.8	-0.8	-0.9	0.88	0.88	0.88	0.03	0.1	0.74	0.19	0.19	1.21	0.92	0.15	0.15	1.27	0.55	0.76

		PV temperature (deg C), Summer																																							
PV module	1	38	38.8	38.8	38.3	38.7	38.9	38.2	38.2	38.2	38.8	38.8	38.8	38.8	39	39	39.2	39.2	39.2	39.2	39.2	39.8	39.8	39.5	39.4	39.4	39.4	39.2	39.2	39	38.9	38.9	39.1	39.1	39	39	39.2	39.3	39.3		
	2	37.7	38.2	38.3	38.1	38.2	38.4	38	38	38	38.2	38.2	38.2	38.2	38.5	38.5	38.7	38.7	38.7	38.7	38.7	38.7	39	39	39	38.9	38.9	38.9	38.7	38.7	38.5	38.3	38.3	38.5	38.5	38.5	38.5	38.7	38.7	38.8	
	3	36.7	37	37.1	36.9	37	37	36.8	36.8	36.8	37	37	37	37	37.1	37.1	37.3	37.3	37.3	37.3	37.3	37.5	37.5	37.5	37.4	37.4	37.4	37.4	37.3	37.2	37.1	37.1	37.2	37.2	37.2	37.2	37.2	37.3	37.4	37.4	
	4	39.1	37.8	37.8	37.7	37.7	37.8	37.6	37.6	37.6	37.8	37.8	37.8	37.8	37.9	37.9	38	38	38	38	38	38.1	38.1	38.1	38	38	38	38	38	37.9	37.9	37.9	37.9	38	37.9	37.9	38	38.1	38.1		
	5	37.6	37.7	37.7	37.6	37.6	37.7	37.6	37.6	37.6	37.7	37.7	37.7	37.7	37.7	37.7	37.8	37.8	37.8	37.8	37.8	37.9	37.9	37.9	37.8	37.8	37.8	37.8	37.8	37.8	37.8	37.8	37.8	37.8	37.8	37.8	37.8	37.8	37.8	37.8	
	6	37.6	37.6	37.6	37.5	37.5	37.6	37.6	37.6	37.6	37.6	37.6	37.6	37.6	37.6	37.6	37.6	37.6	37.6	37.6	37.6	37.7	37.7	37.7	37.7	37.7	37.7	37.7	37.7	37.7	37.6	37.6	37.7	37.7	37.7	37.7	37.7	37.7	37.7	37.7	
	7	37.6	37.6	37.6	40.3	40.3	37.6	40.4	40.4	40.4	37.6	37.6	37.6	37.6	37.6	37.6	37.6	37.6	37.6	37.6	37.6	37.6	37.6	37.6	37.6	37.6	37.6	37.6	37.6	37.6	37.6	37.6	37.6	37.6	37.6	37.6	37.6	37.6	37.6		
	8	40.4	40.4	37.8	42.1	42.2	40.4	42.2	42.2	42.2	40.4	40.4	40.4	40.4	40.4	40.4	38.6	38.6	38.6	38.6	38.6	38.8	38.8	38.9	37.7	37.7	37.7	38.4	39.4	37.7	37.8	37.8	38.5	38.1	38.3	38.3	37.7	38	38.2		
	9	42.2	42.2	40.5	43.3	43.3	42.2	43.3	43.3	43.3	42.2	42.2	42.2	42.2	42.2	42.2	37.9	37.9	37.9	37.9	37.9	37.9	37.9	37.6	37.6	37.6	38.7	38.7	38.7	37.7	37.7	39	38	38	38.1	38.1	37.6	37.6	38.3	37.9	38.1
	10	43.4	43.4	42.3	44.1	44.1	43.4	44.1	44.1	44.1	43.4	43.4	43.4	43.4	43.3	43.3	40.6	40.6	40.6	40.6	40.6	40.4	40.4	40.4	37.9	37.9	37.9	39.7	38.9	38	38.6	38.6	37.8	37.8	38.6	38.6	37.8	38	37.9		

		PV temperature (deg C), Winter																																					
PV module	1	5.98	6.69	6.73	6.25	6.65	6.78	6.22	6.22	6.22	6.69	6.69	6.69	6.69	6.89	6.89	7.07	7.07	7.07	7.07	7.07	7.58	7.58	7.33	7.24	7.24	7.24	7.09	7.03	6.92	6.76	6.76	6.92	6.93	6.9	6.9	7.06	7.1	7.13
	2	5.74	6.22	6.26	6.09	6.18	6.32	6.05	6.05	6.05	6.22	6.22	6.22	6.22	6.43	6.43	6.62	6.62	6.62	6.62	6.62	6.86	6.86	6.89	6.8	6.8	6.8	6.64	6.58	6.46	6.3	6.3	6.46	6.47	6.44	6.44	6.61	6.65	6.68
	3	5.73	6.1	6.15	5.93	6.06	6.11	5.89	5.89	5.89	6.11	6.11	6.11	6.11	6.22	6.22	6.41	6.41	6.41	6.41	6.41	6.58	6.58	6.6	6.51	6.51	6.51	6.43	6.37	6.24	6.19	6.19	6.25	6.26	6.23	6.23	6.4	6.44	6.48
	4	8.12	5.83	5.87	5.75	5.78	5.82	5.7	5.7	5.7	5.83	5.83	5.83	5.83	5.94	5.94	6.04	6.04	6.04	6.04	6.04	6.12	6.12	6.13	6.04	6.04	6.04	6.06	5.99	5.97	5.92	5.92	5.97	5.98	5.95	5.95	6.02	6.07	6.1
	5	5.7	5.72	5.77	5.71	5.67	5.71	5.64	5.64	5.65	5.72	5.72	5.72	5.72	5.77	5.77	5.84	5.84	5.84	5.84	5.84	5.84	5.88	5.88	5.89	5.84	5.84	5.85	5.84	5.8	5.81	5.81	5.81	5.82	5.86	5.86	5.87	5.87	5.9
	6	5.65	5.66	5.66	5.61	5.61	5.66	5.67	5.67	5.68	5.67	5.67	5.67	5.67	5.68	5.68	5.71	5.71	5.71	5.71	5.71	5.74	5.74	5.75	5.72	5.72	5.72	5.73	5.72	5.71	5.71	5.71	5.72	5.73	5.75	5.75	5.74	5.74	5.75
	7	5.67	5.68	5.71	7.96	7.97	5.71	8	8	8.01	5.68	5.68	5.68	5.68	5.66	5.66	5.67	5.67	5.67	5.67	5.67	5.68	5.68	5.68	5.69	5.69	5.69	5.69	5.69	5.7	5.69	5.69	5.69	5.68	5.71	5.71	5.69	5.67	5.67
	8	8	8.01	5.8	9.52	9.52	8.03	9.54	9.54	9.55	8.01	8.01	8.01	8.01	8	8	6.49	6.49	6.49	6.49	6.49	6.68	6.68	6.74	5.78	5.78	5.78	6.35	7.15	5.79	5.84	5.84	6.44	6.11	6.22	6.22	5.78	5.97	6.15
	9	9.54	9.55	8.1	10.6	10.6	9.57	10.6	10.6	10.6	9.55	9.55	9.55	9.55	9.55	9.55	9.55	9.55	9.55	9.55	9.55	9.55	9.55	9.55	9.55	9.55	9.55	9.55	9.55	9.55	9.55	9.55	9.55	9.55	9.55	9.55	9.55	9.55	9.55
	10	10.6	10.6	9.61	11.3	11.3	10.6	11.3	11.3	11.3	10.6	10.6	10.6	10.6	10.6	10.6	8.18	8.18	8.18	8.18	8.18	8.04	8.04	8.03	5.91	5.91	5.91	7.41	6.78	5.97	6.47	6.47	5.81	5.87	6.53	6.53	5.81	5.99	5.91

System VI, inlet flows for 1m/s wind, 45° and PV temperatures for summer and winter conditions at 800kg/h total air mass flow rate:

		Inlet Fflows (kg/h)																																								
Inlet	1	531	525	525	530	526	525	530	530	530	525	525	525	525	524	524	522	522	522	522	522	522	517	517	520	520	520	520	522	522	524	525	525	524	524	524	522	522	522	522		
	2	72.3	75	74.9	72	75	74.8	72.1	72.1	72.1	75	75	75	75	75	74.7	74.7	74.5	74.5	74.5	74.5	74.5	77.2	77.2	74.2	74.3	74.3	74.3	74.5	74.5	74.7	74.9	74.9	74.7	74.7	74.7	74.5	74.5	74.5	74.4		
	3	46.1	47	47	47.3	47	48.3	47.3	47.3	47.3	47	47	47	47	47	48.2	48.2	48.1	48.1	48.1	48.1	48.1	48.1	49	49	49.2	49.2	49.2	49.2	48.1	48.1	48.2	47	47	48.2	48.2	48.2	48.1	48.1	48.1	48.1	48
	4	55.7	57.5	57.5	56.6	57.5	57.5	56.7	56.7	56.7	57.5	57.5	57.5	57.5	57.4	57.4	58.3	58.3	58.3	58.3	58.3	58.3	59.1	59.1	59.2	59.3	59.3	59.3	58.3	58.3	57.4	57.5	57.5	57.4	57.4	57.4	58.4	58.3	58.3	58.3	58.3	
	5	38.6	39	39	38.6	39	39	38.6	38.6	38.6	39	39	39	39	39	39.5	39.5	39.9	39.9	39.9	39.9	39.9	39.9	40.4	40.4	40.4	39.9	39.9	39.9	39.9	39.1	39.5	38.9	38.9	39.5	39.4	38.9	39.4	39.3	39.9	39.9	39.9
	6	30.8	30.9	31.1	30.9	30.8	30.8	30.6	30.6	30.6	30.9	30.9	30.9	30.9	30.9	31.1	31.1	31.4	31.4	31.4	31.4	31.4	31.4	31.6	31.6	31.6	31.3	31.3	31.3	31.4	32	31.1	31.2	31.2	31.1	31.2	31.2	31.4	31.5	31.5	31.5	31.7
	7	21.9	21.9	22	21.8	21.8	21.7	21.7	21.7	21.8	21.9	21.9	21.9	21.9	22	22	22.3	22.3	22.3	22.3	22.3	22.3	22.3	22.3	22.3	22.3	22.3	22.3	22.3	22.3	22.3	22.2	22.2	22.3	22.3	22.3	22.4	22.5	22.5	22.6	22.7	
	8	0.72	0.74	0.72	0.74	0.74	0.76	0.75	0.75	0.73	0.74	0.74	0.74	0.74	0.75	0.75	0.74	0.74	0.74	0.74	0.74	0.74	0.75	0.75	0.75	0.76	0.76	0.76	0.75	0.7	0.75	0.75	0.75	0.75	0.76	0.76	0.75	0.76	0.75	0.76	0.77	0.76
	9	1.19	1.18	1.2	1.19	1.19	1.23	1.2	1.18	1.19	1.2	1.2	1.2	1.2	1.22	1.22	1.22	1.22	1.22	1.22	1.22	1.22	1.24	1.24	1.24	1.22	1.22	1.22	1.21	1.09	1.21	1.2	1.2	1.21	1.22	1.23	1.21	1.23	1.22	1.21		
	10	1.25	1.28	1.27	1.26	1.26	1.27	1.24	1.25	1.26	1.27	1.27	1.27	1.27	1.3	1.3	1.3	1.3	1.3	1.3	1.3	1.3	1.33	1.33	1.33	1.31	1.31	1.31	1.3	1.14	1.28	1.26	1.26	1.28	1.29	1.27	1.29	1.28	1.28	1.29		

		PV temperature (deg C), Summer																																									
PV module	1	39.5	39.6	39.6	39.5	39.6	39.6	39.5	39.5	39.5	39.6	39.6	39.6	39.6	39.6	39.6	39.6	39.6	39.6	39.6	39.6	39.7	39.7	39.7	39.7	39.7	39.7	39.6	39.6	39.6	39.6	39.6	39.6	39.6	39.6	39.6	39.6	39.6	39.6	39.6	39.6		
	2	38.7	38.7	38.7	38.7	38.7	38.7	38.7	38.7	38.7	38.7	38.7	38.7	38.7	38.7	38.7	38.7	38.7	38.7	38.7	38.7	38.8	38.8	38.8	38.8	38.8	38.7	38.7	38.7	38.7	38.7	38.7	38.7	38.7	38.7	38.7	38.7	38.7	38.7	38.7	38.7	38.7	38.7
	3	37.2	37.2	37.2	37.2	37.2	37.2	37.2	37.2	37.2	37.2	37.2	37.2	37.2	37.2	37.2	37.2	37.2	37.2	37.2	37.2	37.2	37.2	37.2	37.2	37.2	37.2	37.2	37.2	37.2	37.2	37.2	37.2	37.2	37.2	37.2	37.2	37.2	37.2	37.2	37.2	37.2	37.2
	4	37.6	37.6	37.6	37.6	37.6	37.6	37.6	37.6	37.6	37.6	37.6	37.6	37.6	37.6	37.6	37.6	37.6	37.6	37.6	37.6	37.6	37.6	37.6	37.6	37.6	37.6	37.6	37.6	37.6	37.6	37.6	37.6	37.6	37.6	37.6	37.6	37.6	37.6	37.6	37.6	37.6	37.6
	5	37.2	37.2	37.3	37.2	37.2	37.2	37.2	37.2	37.2	37.2	37.2	37.2	37.2	37.3	37.3	37.3	37.3	37.3	37.3	37.3	37.3	37.3	37.3	37.3	37.3	37.3	37.3	37.3	37.3	37.3	37.3	37.3	37.3	37.3	37.3	37.3	37.3	37.3	37.3	37.3	37.3	37.3
	6	37	37	37	37	37	37	37	37	37	37	37	37	37	37	37	37	37	37	37	37	37	37	37	37	37	37	37	37	37	37	37	37	37	37	37	37	37	37	37	37	37	37
	7	36.8	36.8	36.8	36.8	36.8	36.8	36.8	36.8	36.8	36.8	36.8	36.8	36.8	36.8	36.8	36.8	36.8	36.8	36.8	36.8	36.8	36.8	36.8	36.8	36.8	36.8	36.8	36.8	36.8	36.8	36.8	36.8	36.8	36.8	36.8	36.8	36.8	36.8	36.8	36.8	36.8	36.8
	8	37.5	37.5	37.5	37.5	37.5	37.5	37.5	37.5	37.5	37.5	37.5	37.5	37.5	37.5	37.5	37.5	37.5	37.5	37.5	37.5	37.5	37.5	37.5	37.5	37.5	37.5	37.5	37.5	37.5	37.5	37.5	37.5	37.5	37.5	37.5	37.5	37.5	37.5	37.5	37.5	37.5	37.5
	9	37.3	37.3	37.3	37.3	37.3	37.3	37.3	37.3	37.3	37.3	37.3	37.3	37.3	37.3	37.3	37.3	37.3	37.3	37.3	37.3	37.3	37.3	37.3	37.3	37.3	37.3	37.3	37.3	37.3	37.3	37.3	37.3	37.3	37.3	37.3	37.3	37.3	37.3	37.3	37.3	37.3	37.3
	10	37.2	37.2	37.2	37.2	37.2	37.2	37.3	37.2	37.2	37.2	37.2	37.2	37.2	37.2	37.2	37.2	37.2	37.2	37.2	37.2	37.2	37.2	37.2	37.2	37.2	37.2	37.2	37.2	37.2	37.2	37.2	37.2	37.2	37.2	37.2	37.2	37.2	37.2	37.2	37.2	37.2	37.2

		PV temperature (deg C), Winter																																									
PV module	1	7.34	7.4	7.41	7.36	7.4	7.41	7.36	7.36	7.36	7.4	7.4	7.4	7.4	7.4	7.42	7.42	7.44	7.44	7.44	7.44	7.5	7.5	7.47	7.46	7.46	7.46	7.44	7.44	7.42	7.41	7.41	7.43	7.43	7.42	7.44	7.44	7.44	7.44	7.45			
	2	6.59	6.62	6.62	6.61	6.62	6.63	6.61	6.61	6.61	6.62	6.62	6.62	6.62	6.64	6.64	6.66	6.66	6.66	6.66	6.66	6.66	6.68	6.68	6.69	6.68	6.68	6.66	6.66	6.64	6.63	6.63	6.64	6.64	6.64	6.66	6.66	6.66	6.66	6.66	6.66	6.66	
	3	6.24	6.26	6.26	6.25	6.26	6.26	6.24	6.24	6.24	6.26	6.26	6.26	6.26	6.27	6.27	6.29	6.29	6.29	6.29	6.29	6.29	6.3	6.3	6.3	6.29	6.29	6.29	6.29	6.28	6.27	6.26	6.26	6.27	6.27	6.27	6.28	6.28	6.29	6.29	6.29	6.29	
	4	5.68	5.68	5.69	5.68	5.68	5.68	5.68	5.68	5.68	5.68	5.68	5.68	5.68	5.69	5.69	5.7	5.7	5.7	5.7	5.7	5.7	5.7	5.7	5.71	5.7	5.7	5.7	5.7	5.69	5.69	5.69	5.69	5.69	5.69	5.69	5.69	5.69	5.69	5.69	5.69	5.69	5.69
	5	5.37	5.38	5.38	5.38	5.37	5.37	5.37	5.37	5.37	5.38	5.38	5.38	5.38	5.38	5.38	5.38	5.38	5.38	5.38	5.38	5.38	5.38	5.38	5.39	5.38	5.38	5.38	5.38	5.39	5.38	5.38	5.38	5.38	5.38	5.38	5.38	5.38	5.38	5.38	5.38	5.38	5.38
	6	5.15	5.14	5.15	5.14	5.14	5.14	5.14	5.14	5.14	5.15	5.15	5.15	5.15	5.15	5.15	5.15	5.15	5.15	5.15	5.15	5.15	5.15	5.15	5.15	5.15	5.15	5.15	5.15	5.15	5.15	5.15	5.15	5.15	5.15	5.15	5.15	5.15	5.15	5.15	5.15	5.15	5.15
	7	4.99	4.99	4.99	4.99	4.99	4.99	4.99	4.99	4.99	4.99	4.99	4.99	4.99	4.99	4.99	4.99	4.99	4.99	4.99	4.99	4.99	4.99	4.99	4.99	4.99	4.99	4.99	4.99	4.99	4.99	4.99	4.99	4.99	4.99	4.99	4.99	4.99	4.99	4.99	4.99	4.99	4.99
	8	5.57	5.56	5.57	5.56	5.56	5.54	5.55	5.55	5.56	5.56	5.56	5.56	5.56	5.55	5.55	5.55	5.55	5.55	5.55	5.55	5.55	5.55	5.55	5.55	5.55	5.55	5.55	5.54	5.54	5.54	5.55	5.58	5.55	5.55	5.55	5.55	5.54	5.54	5.55	5.54	5.54	5.54
	9	5.42	5.42	5.41	5.41	5.41	5.4	5.41	5.42	5.41	5.41	5.41	5.41	5.41	5.4	5.4	5.4	5.4	5.4	5.4	5.4	5.4	5.4	5.4	5.4	5.4	5.4	5.4	5.4	5.41	5.45	5.4	5.41	5.41	5.41	5.4	5.4	5.4	5.41	5.4	5.4	5.4	5.41
	10	5.37	5.36	5.36	5.37	5.37	5.37	5.37	5.37	5.37	5.37	5.37	5.37	5.37	5.36	5.36	5.35	5.35	5.35	5.35	5.35	5.35	5.35	5.35	5.35	5.35	5.35	5.35	5.36	5.41	5.36	5.37	5.37	5.36	5.36	5.36	5.36	5.36	5.36	5.36	5.36	5.36	5.36

System VI, inlet flows for 2m/s wind, 45° and PV temperatures for summer and winter conditions at 800kg/h total air mass flow rate:

		Inlet Fflows (kg/h)																																								
Inlet	1	563	538	537	555	538	534	556	556	556	538	538	538	538	538	531	531	524	524	524	524	524	524	504	515	515	517	517	517	517	524	526	530	536	547	530	530	531	525	525	523	522
	2	66.2	76.7	76.5	64.7	76.8	76.2	64.9	64.9	64.9	76.7	76.7	76.7	76.7	76.7	75.7	75.7	74.8	74.8	74.8	74.8	74.8	74.8	85.1	73.4	73.4	73.8	73.8	73.8	74.8	75.1	75.6	76.4	63.4	75.6	75.6	75.8	74.9	74.9	74.7	74.5	
	3	40	43.9	43.8	45.1	44	49.1	45.3	45.3	45.2	43.9	43.9	43.9	43.9	43.9	48.8	48.8	48.2	48.2	48.2	48.2	48.2	48.2	52.1	52.5	52.5	52.8	52.8	52.8	48.2	48.4	48.8	43.7	44.4	48.8	48.7	48.9	48.3	48.3	48.2	48.1	
	4	47.3	55.3	55.2	51.7	55.4	55.1	51.8	51.8	55.3	55.3	55.3	55.3	55.3	54.7	54.7	58.6	58.6	58.6	58.6	58.6	58.6	58.6	61.6	62	62	62.3	62.3	62.3	58.6	58.7	54.7	55.1	55.6	54.6	54.6	54.7	58.6	58.6	58.5	58.3	
	5	35.9	36.5	36.5	35.1	36.7	36.5	35.2	35.2	35.1	36.5	36.5	36.5	36.5	36.5	38.5	38.5	40.3	40.3	40.3	40.3	40.3	40.3	42	42.1	42.1	40.1	40.1	40.1	40.3	38.3	38.4	36.2	36.8	38.4	38.3	36	38	37.9	40	40	
	6	26.7	28.1	29.2	27.7	27.8	27.8	26.5	26.5	26.4	28.1	28.1	28.1	28.1	28.1	29.2	29.2	30.3	30.3	30.3	30.3	30.3	30.3	31	31.2	31.2	29.9	29.9	29.9	30.3	30	29	29.4	29	28.9	29.3	29.3	30.3	30.6	30.5	31.5	
	7	15.8	18.6	19.3	17.7	18	17.9	16.9	17	17.4	18.7	18.7	18.7	18.7	18.7	19.2	19.2	20.3	20.3	20.3	20.3	20.3	20.3	20.6	20.7	20.7	20.3	20.3	20.6	20.2	20	20.5	19.9	20.6	20.6	20.9	21.4	21.5	21.6	22.2		
	8	0.88	0.63	0.57	0.71	0.64	0.74	0.81	0.88	0.72	0.65	0.65	0.65	0.65	0.65	0.68	0.68	0.67	0.67	0.67	0.67	0.67	0.67	0.71	0.7	0.7	0.73	0.73	0.73	0.71	0.72	0.68	0.75	0.69	0.73	0.73	0.69	0.74	0.79	0.74		
	9	1.86	1.04	1.18	1.26	1.11	1.29	1.44	1.21	1.29	1.12	1.12	1.12	1.12	1.12	1.18	1.18	1.21	1.21	1.21	1.21	1.21	1.21	1.21	1.3	1.27	1.27	1.19	1.19	1.19	1.15	1.17	1.2	1.11	1.27	1.18	1.21	1.24	1.17	1.26	1.22	1.16
	10	1.9	1.39	1.29	1.39	1.22	1.17	1.27	1.38	1.43	1.25	1.25	1.25	1.25	1.25	1.34	1.34	1.41	1.41	1.41	1.41	1.41	1.41	1.53	1.5	1.5	1.43	1.43	1.43	1.38	1.25	1.28	1.17	1.36	1.29	1.31	1.21	1.29	1.24	1.25	1.32	

		PV temperature (deg C), Summer																																									
PV module	1	36	36.2	36.2	36.1	36.2	36.2	36.1	36.1	36.1	36.2	36.2	36.2	36.2	36.3	36.3	36.3	36.3	36.3	36.3	36.3	36.3	36.5	36.4	36.4	36.4	36.4	36.4	36.3	36.3	36.3	36.2	36.1	36.3	36.3	36.3	36.3	36.3	36.3	36.3	36.4		
	2	35.5	35.6	35.6	35.6	35.6	35.6	35.6	35.6	35.6	35.6	35.6	35.6	35.6	35.7	35.7	35.7	35.7	35.7	35.7	35.7	35.7	35.8	35.8	35.8	35.8	35.8	35.8	35.7	35.7	35.7	35.6	35.6	35.7	35.7	35.7	35.7	35.7	35.7	35.7	35.7	35.7	
	3	34.6	34.6	34.6	34.6	34.6	34.6	34.6	34.6	34.6	34.6	34.6	34.6	34.6	34.7	34.7	34.7	34.7	34.7	34.7	34.7	34.7	34.8	34.8	34.8	34.7	34.7	34.7	34.7	34.7	34.7	34.7	34.7	34.7	34.7	34.7	34.7	34.7	34.7	34.7	34.7	34.7	34.7
	4	34.9	34.9	34.9	34.9	34.9	34.9	34.9	34.9	34.9	34.9	34.9	34.9	34.9	34.9	34.9	34.9	34.9	34.9	34.9	34.9	34.9	35	35	35	34.9	34.9	34.9	34.9	34.9	34.9	34.9	34.9	34.9	34.9	34.9	34.9	34.9	34.9	34.9	34.9	34.9	35
	5	34.6	34.7	34.7	34.7	34.7	34.7	34.6	34.6	34.6	34.7	34.7	34.7	34.7	34.7	34.7	34.7	34.7	34.7	34.7	34.7	34.7	34.7	34.7	34.7	34.7	34.7	34.7	34.7	34.7	34.7	34.7	34.7	34.7	34.7	34.7	34.7	34.7	34.7	34.7	34.7	34.7	34.7
	6	34.5	34.5	34.5	34.5	34.5	34.5	34.5	34.5	34.5	34.5	34.5	34.5	34.5	34.5	34.5	34.5	34.5	34.5	34.5	34.5	34.5	34.5	34.5	34.5	34.5	34.5	34.5	34.5	34.5	34.5	34.5	34.5	34.5	34.5	34.5	34.5	34.5	34.5	34.5	34.5	34.5	34.5
	7	34.4	34.4	34.4	34.4	34.4	34.4	34.4	34.4	34.4	34.4	34.4	34.4	34.4	34.4	34.4	34.4	34.4	34.4	34.4	34.4	34.4	34.4	34.4	34.4	34.4	34.4	34.4	34.4	34.4	34.4	34.4	34.4	34.4	34.4	34.4	34.4	34.4	34.4	34.4	34.4	34.4	34.4
	8	34.8	34.9	35	34.9	34.9	34.9	34.8	34.8	34.9	34.9	34.9	34.9	34.9	34.9	34.9	34.9	34.9	34.9	34.9	34.9	34.9	34.9	34.9	34.9	34.9	34.9	34.9	34.9	34.9	34.9	34.9	34.9	34.9	34.9	34.9	34.9	34.9	34.9	34.9	34.9	34.9	34.9
	9	34.6	34.8	34.7	34.7	34.8	34.7	34.7	34.7	34.7	34.8	34.8	34.8	34.8	34.8	34.7	34.7	34.7	34.7	34.7	34.7	34.7	34.7	34.7	34.7	34.7	34.7	34.7	34.7	34.7	34.7	34.7	34.7	34.7	34.7	34.7	34.7	34.7	34.7	34.7	34.7	34.7	34.7
	10	34.6	34.7	34.7	34.7	34.7	34.7	34.7	34.7	34.7	34.7	34.7	34.7	34.7	34.7	34.7	34.7	34.7	34.7	34.7	34.7	34.7	34.7	34.6	34.6	34.6	34.7	34.7	34.7	34.7	34.7	34.7	34.7	34.7	34.7	34.7	34.7	34.7	34.7	34.7	34.7	34.7	34.7

		PV temperature (deg C), Winter																																								
PV module	1	4.31	4.49	4.5	4.37	4.49	4.52	4.36	4.36	4.36	4.49	4.49	4.49	4.49	4.54	4.54	4.59	4.59	4.59	4.59	4.59	4.59	4.74	4.66	4.66	4.64	4.64	4.64	4.59	4.58	4.55	4.51	4.42	4.55	4.55	4.54	4.58	4.59	4.6	4.61		
	2	3.87	3.97	3.98	3.94	3.96	4	3.93	3.93	3.93	3.97	3.97	3.97	3.97	4.02	4.02	4.07	4.07	4.07	4.07	4.07	4.07	4.13	4.14	4.14	4.12	4.12	4.12	4.07	4.06	4.02	3.98	3.99	4.03	4.03	4.02	4.06	4.06	4.08	4.09		
	3	3.67	3.74	3.75	3.71	3.74	3.74	3.7	3.7	3.7	3.74	3.74	3.74	3.74	3.77	3.77	3.82	3.82	3.82	3.82	3.82	3.82	3.86	3.86	3.86	3.84	3.84	3.84	3.82	3.8	3.77	3.76	3.76	3.77	3.78	3.76	3.81	3.81	3.82	3.83		
	4	3.36	3.37	3.38	3.36	3.37	3.37	3.35	3.35	3.35	3.37	3.37	3.37	3.37	3.39	3.39	3.42	3.42	3.42	3.42	3.42	3.42	3.43	3.44	3.44	3.41	3.41	3.41	3.42	3.4	3.4	3.39	3.39	3.4	3.4	3.39	3.41	3.41	3.42	3.43		
	5	3.16	3.18	3.18	3.17	3.17	3.17	3.16	3.16	3.16	3.18	3.18	3.18	3.18	3.19	3.19	3.2	3.2	3.2	3.2	3.2	3.2	3.2	3.2	3.2	3.19	3.19	3.19	3.19	3.19	3.19	3.19	3.19	3.19	3.19	3.19	3.19	3.19	3.19	3.19	3.19	3.19
	6	3.03	3.03	3.03	3.03	3.03	3.03	3.03	3.03	3.03	3.03	3.03	3.03	3.03	3.03	3.03	3.04	3.04	3.04	3.04	3.04	3.04	3.04	3.04	3.04	3.04	3.04	3.04	3.04	3.04	3.04	3.04	3.04	3.04	3.04	3.04	3.04	3.04	3.04	3.04	3.04	3.04
	7	2.96	2.94	2.94	2.95	2.94	2.95	2.95	2.95	2.95	2.94	2.94	2.94	2.94	2.94	2.94	2.94	2.94	2.94	2.94	2.94	2.94	2.94	2.94	2.94	2.94	2.94	2.94	2.94	2.94	2.94	2.94	2.94	2.94	2.94	2.94	2.94	2.94	2.94	2.94	2.94	2.94
	8	3.29	3.39	3.43	3.35	3.38	3.34	3.31	3.28	3.35	3.38	3.38	3.38	3.38	3.37	3.37	3.37	3.37	3.37	3.37	3.37	3.37	3.35	3.36	3.36	3.34	3.34	3.34	3.35	3.35	3.34	3.36	3.33	3.36	3.34	3.34	3.36	3.33	3.31	3.33		
	9	3.13	3.28	3.25	3.22	3.26	3.21	3.18	3.23	3.21	3.26	3.26	3.26	3.26	3.26	3.24	3.24	3.23	3.23	3.23	3.23	3.23	3.21	3.22	3.22	3.24	3.24	3.24	3.25	3.24	3.23	3.26	3.22	3.24	3.23	3.22	3.24	3.22	3.23	3.24		
	10	3.1	3.18	3.2	3.18	3.22	3.22	3.2	3.18	3.17	3.21	3.21	3.21	3.21	3.21	3.19	3.19	3.18	3.18	3.18	3.18	3.18	3.16	3.16	3.16	3.17	3.17	3.17	3.18	3.21	3.2	3.22	3.18	3.2	3.19	3.21	3.2	3.21	3.21	3.19		

System V, inlet flows for 1m/s wind, 90° and PV temperatures for summer and winter conditions at 400kg/h total air mass flow rate:

		Inlet FFlows (kg/h)																																								
Inlet	1	215	215	215	215	215	215	215	215	215	215	215	215	215	215	215	212	212	212	212	212	208	212	215	216	215	216	216	216	216	216	223	223	223	223	220	215	215	215	215		
	2	42.7	42.7	42.7	42.7	42.7	42.7	42.7	42.7	42.7	42.7	42.7	42.7	42.7	42.7	42.7	42.1	42.1	42.1	42.1	42.1	47.1	42.1	42.7	42.7	42.7	42.7	42.7	42.7	42.7	42.7	42.7	42.7	38	38	38	38	38	42.7	42.7	42.7	42.7
	3	30.7	30.7	30.7	30.7	30.7	30.7	30.7	30.7	30.7	30.7	30.7	30.7	30.7	30.7	30.7	32.4	32.4	32.4	32.4	32.4	32.1	32.4	30.7	30.8	30.7	30.8	30.8	30.8	30.8	30.8	29.4	29.4	29.4	29.4	27	30.7	30.7	30.7	30.7		
	4	39.5	39.5	39.5	39.5	39.5	39.5	39.5	39.5	39.5	39.5	39.5	39.5	39.5	39.5	39.5	40.7	40.7	40.7	40.7	40.7	40.5	40.7	39.5	39.5	39.5	39.5	39.5	39.5	39.5	39.5	38.5	38.5	38.5	38.5	37	39.5	39.5	39.5	39.5		
	5	28	28	28	28	28	28	28	28	28	28	28	28	28	28	28	28.6	28.6	28.6	28.6	28.6	28.6	28.6	28.1	28.1	28	28.1	28.1	28.1	28.1	28.1	27.6	27.6	27.6	27.6	29.4	28	28	28	28		
	6	23.6	23.6	23.6	23.6	23.6	23.6	23.6	23.6	23.6	23.6	23.6	23.6	23.6	23.6	23.6	23.8	23.8	23.8	23.8	23.8	23.7	23.8	23.6	23.5	23.6	23.5	23.5	23.5	23.5	23.5	23.4	23.4	23.4	23.4	29.7	23.6	23.6	23.6	23.6		
	7	17.7	17.7	17.7	17.7	17.7	17.7	17.7	17.7	17.9	17.7	17.7	17.7	17.7	17.7	17.7	17.8	17.8	17.8	17.8	17.8	17.7	17.6	17.6	17.5	17.7	17.5	17.5	17.5	17.5	17.5	17.5	17.5	17.5	17.5	17.5	17.3	17.7	17.7	17.7	17.7	
	8	0.57	0.57	0.57	0.57	0.57	0.57	0.57	0.57	0.56	0.57	0.57	0.57	0.57	0.57	0.57	0.58	0.58	0.58	0.58	0.58	0.58	0.56	0.56	0.56	0.56	0.56	0.56	0.56	0.56	0.55	0.55	0.55	0.55	0.31	0.57	0.57	0.57	0.57			
	9	0.88	0.88	0.88	0.88	0.88	0.88	0.88	0.88	0.88	0.88	0.88	0.88	0.88	0.88	0.88	0.9	0.9	0.9	0.9	0.9	0.9	0.9	0.89	0.87	0.87	0.87	0.87	0.87	0.87	0.87	0.84	0.84	0.84	0.84	0.4	0.88	0.88	0.88	0.88		
	10	0.93	0.93	0.93	0.93	0.93	0.93	0.93	0.93	0.93	0.93	0.93	0.93	0.93	0.93	0.93	0.96	0.96	0.96	0.96	0.96	0.98	0.95	0.93	0.92	0.94	0.92	0.92	0.92	0.92	0.92	0.92	0.92	0.89	0.89	0.89	0.89	0.41	0.93	0.93	0.93	0.93

		PV temperature (deg C), Summer																																									
PV module	1	44	44	44	44	44	44	44	44	44	44	44	44	44	44	44.1	44.1	44.1	44.1	44.2	44.1	44	44	44	44	44	44	44	44	44	44	44	44	44	44	44	44	44	44	44			
	2	42.8	42.8	42.8	42.8	42.8	42.8	42.8	42.8	42.8	42.8	42.8	42.8	42.8	42.8	42.8	42.9	42.9	42.9	42.9	42.9	42.9	42.8	42.8	42.8	42.8	42.8	42.8	42.8	42.8	42.7	42.7	42.7	42.7	42.8	42.8	42.8	42.8	42.8				
	3	40.6	40.6	40.6	40.6	40.6	40.6	40.6	40.6	40.6	40.6	40.6	40.6	40.6	40.6	40.6	40.7	40.7	40.7	40.7	40.7	40.7	40.6	40.6	40.6	40.6	40.6	40.6	40.6	40.6	40.6	40.6	40.6	40.6	40.6	40.6	40.6	40.6	40.6	40.6	40.6	40.6	
	4	41.2	41.2	41.2	41.2	41.2	41.2	41.2	41.2	41.2	41.2	41.2	41.2	41.2	41.2	41.2	41.2	41.2	41.2	41.2	41.2	41.2	41.2	41.2	41.2	41.2	41.2	41.2	41.2	41.2	41.2	41.2	41.2	41.2	41.2	41.2	41.2	41.2	41.2	41.2	41.2	41.2	
	5	40.6	40.6	40.6	40.6	40.6	40.6	40.6	40.6	40.6	40.6	40.6	40.6	40.6	40.6	40.6	40.6	40.6	40.6	40.6	40.6	40.6	40.6	40.6	40.6	40.6	40.6	40.6	40.6	40.6	40.6	40.6	40.6	40.6	40.6	40.6	40.6	40.6	40.6	40.6	40.6	40.6	
	6	40.2	40.2	40.2	40.2	40.2	40.2	40.2	40.2	40.2	40.2	40.2	40.2	40.2	40.2	40.2	40.2	40.2	40.2	40.2	40.2	40.2	40.2	40.2	40.2	40.2	40.2	40.2	40.2	40.2	40.2	40.2	40.2	40.2	40.2	40.2	40.2	40.2	40.2	40.2	40.2	40.2	
	7	39.9	39.9	39.9	39.9	39.9	39.9	39.9	39.9	39.9	39.9	39.9	39.9	39.9	39.9	39.9	39.9	39.9	39.9	39.9	39.9	39.9	39.9	39.9	39.9	39.9	39.9	39.9	39.9	39.9	39.9	39.9	39.9	39.9	39.9	39.9	39.9	39.9	39.9	39.9	39.9	39.9	
	8	40.5	40.5	40.5	40.5	40.5	40.5	40.5	40.5	40.5	40.5	40.5	40.5	40.5	40.5	40.5	40.5	40.5	40.5	40.5	40.5	40.5	40.4	40.5	40.5	40.5	40.5	40.5	40.5	40.5	40.5	40.5	40.5	40.5	40.5	40.5	40.5	40.5	40.5	40.5	40.5	40.5	40.5
	9	40.3	40.3	40.3	40.3	40.3	40.3	40.3	40.3	40.3	40.3	40.3	40.3	40.3	40.3	40.3	40.3	40.3	40.3	40.3	40.3	40.3	40.3	40.3	40.3	40.3	40.3	40.3	40.3	40.3	40.3	40.3	40.3	40.3	40.3	40.3	40.3	40.3	40.3	40.3	40.3	40.3	40.3
	10	40.2	40.2	40.2	40.2	40.2	40.2	40.2	40.2	40.2	40.2	40.2	40.2	40.2	40.2	40.2	40.2	40.2	40.2	40.2	40.2	40.2	40.2	40.2	40.2	40.2	40.2	40.2	40.2	40.2	40.2	40.2	40.2	40.2	40.2	40.2	40.2	40.2	40.2	40.2	40.2	40.2	40.2

		PV temperature (deg C), Winter																																										
PV module	1	11.4	11.4	11.4	11.4	11.4	11.4	11.4	11.4	11.4	11.4	11.4	11.4	11.4	11.4	11.5	11.5	11.5	11.5	11.6	11.5	11.4	11.4	11.4	11.4	11.4	11.4	11.4	11.4	11.2	11.2	11.2	11.2	11.2	11.4	11.4	11.4	11.4	11.4					
	2	10.3	10.3	10.3	10.3	10.3	10.3	10.3	10.3	10.3	10.3	10.3	10.3	10.3	10.3	10.4	10.4	10.4	10.4	10.4	10.3	10.4	10.3	10.3	10.3	10.3	10.3	10.3	10.3	10.2	10.2	10.2	10.2	10.3	10.3	10.3	10.3	10.3	10.3	10.3	10.3	10.3		
	3	9.7	9.7	9.7	9.7	9.7	9.7	9.7	9.7	9.7	9.7	9.7	9.7	9.7	9.7	9.7	9.8	9.8	9.8	9.8	9.8	9.8	9.7	9.7	9.7	9.7	9.7	9.7	9.7	9.7	9.7	9.7	9.7	9.7	9.7	9.7	9.7	9.7	9.7	9.7	9.7	9.7	9.7	
	4	8.8	8.8	8.8	8.8	8.8	8.8	8.8	8.8	8.8	8.8	8.8	8.8	8.8	8.8	8.8	8.8	8.8	8.8	8.8	8.8	8.8	8.8	8.8	8.8	8.8	8.8	8.8	8.8	8.8	8.8	8.8	8.8	8.8	8.8	8.8	8.8	8.8	8.8	8.8	8.8	8.8	8.8	
	5	8.3	8.3	8.3	8.3	8.3	8.3	8.3	8.3	8.3	8.3	8.3	8.3	8.3	8.3	8.3	8.3	8.3	8.3	8.3	8.3	8.3	8.3	8.3	8.3	8.3	8.3	8.3	8.3	8.3	8.3	8.3	8.3	8.3	8.3	8.3	8.3	8.3	8.3	8.3	8.3	8.3	8.3	
	6	7.9	7.9	7.9	7.9	7.9	7.9	7.9	7.9	7.9	7.9	7.9	7.9	7.9	7.9	7.9	7.9	7.9	7.9	7.9	7.9	7.9	7.9	7.9	7.9	7.9	7.9	7.9	7.9	7.9	7.9	7.9	7.9	7.9	7.9	7.9	7.9	7.9	7.9	7.9	7.9	7.9	7.9	
	7	7.6	7.6	7.6	7.6	7.6	7.6	7.6	7.6	7.6	7.6	7.6	7.6	7.6	7.6	7.6	7.6	7.6	7.6	7.6	7.6	7.6	7.6	7.6	7.6	7.6	7.6	7.6	7.6	7.6	7.6	7.6	7.6	7.6	7.6	7.6	7.6	7.6	7.6	7.6	7.6	7.6	7.6	
	8	8.1	8.1	8.1	8.1	8.1	8.1	8.1	8.1	8.1	8.1	8.1	8.1	8.1	8.1	8.1	8.1	8.1	8.1	8.1	8.1	8.1	8.1	8.1	8.1	8.1	8.1	8.1	8.1	8.1	8.1	8.1	8.1	8.1	8.1	8.1	8.1	8.1	8.1	8.1	8.1	8.1	8.1	
	9	8.0	8.0	8.0	8.0	8.0	8.0	8.0	8.0	8.0	8.0	8.0	8.0	8.0	8.0	8.0	8.0	8.0	8.0	8.0	8.0	8.0	8.0	8.0	8.0	8.0	8.0	8.0	8.0	8.0	8.0	8.0	8.0	8.0	8.0	8.0	8.0	8.0	8.0	8.0	8.0	8.0	8.0	8.0
	10	8.0	8.0	8.0	8.0	8.0	8.0	8.0	8.0	8.0	8.0	8.0	8.0	8.0	8.0	8.0	8.0	7.9	7.9	7.9	7.9	7.9	7.9	7.9	7.9	7.9	7.9	7.9	7.9	7.9	7.9	7.9	7.9	7.9	7.9	7.9	7.9	7.9	7.9	7.9	7.9	7.9	7.9	7.9

System V, inlet flows for 2m/s wind, 90° and PV temperatures for summer and winter conditions at 400kg/h total air mass flow rate:

		Inlet Fflows (kg/h)																																						
Inlet	1	215	215	215	215	215	215	215	215	215	215	215	215	215	215	215	203	203	203	203	203	187	204	215	216	215	216	216	216	216	216	251	251	251	251	250	215	215	215	215
	2	42.7	42.7	42.7	42.7	42.7	42.7	42.7	42.7	42.6	42.7	42.7	42.7	42.7	42.7	42.7	40.3	40.3	40.3	40.3	40.3	58.7	40.4	42.7	42.8	42.7	42.8	42.8	42.8	42.8	42.8	19.7	19.7	19.7	19.7	19.5	42.7	42.7	42.7	42.7
	3	30.7	30.7	30.7	30.7	30.7	30.7	30.7	30.7	30.7	30.7	30.7	30.7	30.7	30.7	30.7	36.9	36.9	36.9	36.9	36.9	36.1	36.9	30.7	30.8	30.7	30.8	30.8	30.8	30.8	30.8	25.4	25.4	25.4	25.4	25.3	30.7	30.7	30.7	30.7
	4	39.5	39.5	39.5	39.5	39.5	39.5	39.5	39.5	39.5	39.2	39.5	39.5	39.5	39.5	39.5	44.1	44.1	44.1	44.1	44.1	43.5	44.1	39.3	39.6	39.5	39.6	39.6	39.6	39.6	39.6	35	35	35	35	34.9	39.5	39.5	39.5	39.5
	5	28	28	28	28	28	28	28	28	28	27.7	28	28	28	28	28	30.3	30.3	30.3	30.3	30.3	30.2	30.4	27.9	28.3	28.1	28.3	28.3	28.3	28.3	28.3	26.4	26.4	26.4	26.4	26.2	28	28	28	28
	6	23.6	23.6	23.6	23.6	23.6	23.6	23.6	23.6	23.6	24.4	23.6	23.6	23.6	23.6	23.6	24.6	24.6	24.6	24.6	24.6	24.2	24.6	24.3	23.3	23.6	23.3	23.3	23.3	23.3	23.3	23.9	23.9	23.9	23.9	24.4	23.6	23.6	23.6	23.6
	7	17.7	17.7	17.7	17.7	17.7	17.7	17.7	17.7	18.7	17.7	17.7	17.7	17.7	17.7	17.7	18	18	18	18	18	17.7	17.5	17.7	16.9	17.6	16.9	16.9	16.9	16.9	16.9	17.3	17.3	17.3	17.3	17.9	17.7	17.7	17.7	17.7
	8	0.57	0.57	0.57	0.57	0.57	0.57	0.57	0.57	0.5	0.57	0.57	0.57	0.57	0.57	0.57	0.6	0.6	0.6	0.6	0.6	0.61	0.62	0.49	0.56	0.55	0.56	0.56	0.56	0.56	0.56	0.44	0.44	0.44	0.44	0.45	0.57	0.57	0.57	0.57
	9	0.88	0.88	0.88	0.88	0.88	0.88	0.88	0.88	0.77	0.88	0.88	0.88	0.88	0.88	0.88	0.96	0.96	0.96	0.96	0.96	0.96	0.97	0.82	0.86	0.84	0.86	0.86	0.86	0.86	0.86	0.62	0.62	0.62	0.62	0.65	0.88	0.88	0.88	0.88
	10	0.93	0.93	0.93	0.93	0.93	0.93	0.93	0.93	0.83	0.93	0.93	0.93	0.93	0.93	0.93	1.03	1.03	1.03	1.03	1.03	1.13	1.01	0.83	0.9	0.98	0.9	0.9	0.9	0.9	0.9	0.64	0.64	0.64	0.64	0.67	0.93	0.93	0.93	0.93

		PV temperature (deg C), Summer																																									
PV module	1	39.2	39.2	39.2	39.2	39.2	39.2	39.2	39.2	39.2	39.2	39.2	39.2	39.2	39.2	39.4	39.4	39.4	39.4	39.4	39.7	39.4	39.2	39.2	39.2	39.2	39.2	39.2	39.2	39.2	39.2	39.2	38.6	38.6	38.6	38.6	38.6	39.2	39.2	39.2	39.2		
	2	38.5	38.5	38.5	38.5	38.5	38.5	38.5	38.5	38.5	38.5	38.5	38.5	38.5	38.5	38.7	38.7	38.7	38.7	38.7	38.7	38.7	38.5	38.4	38.5	38.4	38.4	38.4	38.4	38.4	38.4	38.3	38.3	38.3	38.3	38.3	38.5	38.5	38.5	38.5			
	3	37	37	37	37	37	37	37	37	37	37	37	37	37	37	37.2	37.2	37.2	37.2	37.2	37.1	37.1	37	37	37	37	37	37	37	37	37	37	37	36.9	36.9	36.9	36.9	36.9	37	37	37	37	
	4	37.4	37.4	37.4	37.4	37.4	37.4	37.4	37.4	37.4	37.4	37.4	37.4	37.4	37.4	37.4	37.4	37.4	37.4	37.4	37.4	37.4	37.4	37.4	37.4	37.4	37.4	37.4	37.4	37.4	37.4	37.4	37.4	37.4	37.4	37.4	37.4	37.4	37.4	37.4	37.4	37.4	
	5	37	37	37	37	37	37	37	37	37	37	37	37	37	37	37	37	37	37	37	37	37	37	37	37	37	37	37	37	37	37	37	37	37	37	37	37	37	37	37	37	37	
	6	36.7	36.7	36.7	36.7	36.7	36.7	36.7	36.7	36.7	36.7	36.7	36.7	36.7	36.7	36.7	36.7	36.7	36.7	36.7	36.7	36.7	36.7	36.7	36.7	36.7	36.7	36.7	36.7	36.7	36.7	36.7	36.7	36.7	36.7	36.7	36.7	36.7	36.7	36.7	36.7	36.7	36.7
	7	36.5	36.5	36.5	36.5	36.5	36.5	36.5	36.5	36.5	36.5	36.5	36.5	36.5	36.5	36.5	36.5	36.5	36.5	36.5	36.5	36.5	36.5	36.5	36.5	36.5	36.5	36.5	36.5	36.5	36.5	36.5	36.5	36.5	36.5	36.5	36.5	36.5	36.5	36.5	36.5	36.5	36.5
	8	36.9	36.9	36.9	36.9	36.9	36.9	36.9	36.9	37	36.9	36.9	36.9	36.9	36.9	36.9	36.9	36.9	36.9	36.9	36.9	36.9	36.9	37	36.9	36.9	36.9	36.9	36.9	36.9	36.9	37	37	37	37	37	36.9	36.9	36.9	36.9			
	9	36.8	36.8	36.8	36.8	36.8	36.8	36.8	36.8	36.8	36.8	36.8	36.8	36.8	36.8	36.8	36.8	36.8	36.8	36.8	36.8	36.8	36.8	36.8	36.8	36.8	36.8	36.8	36.8	36.8	36.8	36.8	36.8	36.8	36.8	36.8	36.8	36.8	36.8	36.8	36.8	36.8	36.8
	10	36.8	36.8	36.8	36.8	36.8	36.8	36.8	36.8	36.8	36.8	36.8	36.8	36.8	36.8	36.8	36.7	36.7	36.7	36.7	36.7	36.7	36.7	36.8	36.8	36.7	36.8	36.8	36.8	36.8	36.8	36.8	36.8	36.8	36.8	36.8	36.8	36.8	36.8	36.8	36.8	36.8	36.8

		PV temperature (deg C), Winter																																							
PV module	1	7.0	7.0	7.0	7.0	7.0	7.0	7.0	7.0	7.0	7.0	7.0	7.0	7.0	7.0	7.2	7.2	7.2	7.2	7.2	7.5	7.2	7.0	7.0	7.0	7.0	7.0	7.0	7.0	7.0	6.5	6.5	6.5	6.5	6.5	7.0	7.0	7.0	7.0		
	2	6.4	6.4	6.4	6.4	6.4	6.4	6.4	6.4	6.4	6.4	6.4	6.4	6.4	6.4	6.6	6.6	6.6	6.6	6.6	6.6	6.6	6.4	6.4	6.4	6.4	6.4	6.4	6.4	6.4	6.2	6.2	6.2	6.2	6.2	6.4	6.4	6.4	6.4		
	3	6.1	6.1	6.1	6.1	6.1	6.1	6.1	6.1	6.1	6.1	6.1	6.1	6.1	6.1	6.1	6.2	6.2	6.2	6.2	6.2	6.2	6.1	6.1	6.1	6.1	6.1	6.1	6.1	6.1	6.0	6.0	6.0	6.0	6.0	6.1	6.1	6.1	6.1		
	4	5.5	5.5	5.5	5.5	5.5	5.5	5.5	5.5	5.5	5.5	5.5	5.5	5.5	5.5	5.5	5.5	5.5	5.5	5.5	5.5	5.5	5.5	5.5	5.5	5.5	5.5	5.5	5.5	5.5	5.5	5.5	5.5	5.5	5.5	5.5	5.5	5.5	5.5	5.5	5.5
	5	5.2	5.2	5.2	5.2	5.2	5.2	5.2	5.2	5.2	5.2	5.2	5.2	5.2	5.2	5.2	5.2	5.2	5.2	5.2	5.2	5.2	5.2	5.2	5.2	5.2	5.2	5.2	5.2	5.2	5.2	5.2	5.2	5.2	5.2	5.2	5.2	5.2	5.2	5.2	5.2
	6	4.9	4.9	4.9	4.9	4.9	4.9	4.9	4.9	4.9	4.9	4.9	4.9	4.9	4.9	4.9	4.9	4.9	4.9	4.9	4.9	4.9	4.9	4.9	4.9	4.9	4.9	4.9	4.9	4.9	4.9	4.9	4.9	4.9	4.9	4.9	4.9	4.9	4.9	4.9	4.9
	7	4.7	4.7	4.7	4.7	4.7	4.7	4.7	4.7	4.7	4.7	4.7	4.7	4.7	4.7	4.7	4.7	4.7	4.7	4.7	4.7	4.7	4.7	4.7	4.7	4.7	4.7	4.7	4.7	4.7	4.7	4.7	4.7	4.7	4.7	4.7	4.7	4.7	4.7	4.7	4.7
	8	5.1	5.1	5.1	5.1	5.1	5.1	5.1	5.1	5.1	5.1	5.1	5.1	5.1	5.1	5.1	5.1	5.1	5.1	5.1	5.1	5.1	5.1	5.1	5.1	5.1	5.1	5.1	5.1	5.1	5.1	5.1	5.1	5.1	5.1	5.1	5.1	5.1	5.1	5.1	5.1
	9	5.0	5.0	5.0	5.0	5.0	5.0	5.0	5.0	5.0	5.0	5.0	5.0	5.0	5.0	5.0	5.0	5.0	5.0	5.0	5.0	5.0	5.0	5.0	5.0	5.0	5.0	5.0	5.0	5.0	5.0	5.0	5.0	5.0	5.0	5.0	5.0	5.0	5.0	5.0	5.0
	10	4.9	4.9	4.9	4.9	4.9	4.9	4.9	4.9	4.9	5.0	4.9	4.9	4.9	4.9	4.9	4.9	4.9	4.9	4.9	4.9	4.9	4.9	4.9	4.9	4.9	4.9	4.9	4.9	4.9	4.9	4.9	4.9	4.9	4.9	4.9	4.9	4.9	4.9	4.9	4.9

System V, inlet flows for 2m/s wind, 90° and PV temperatures for summer and winter conditions at 800kg/h total air mass flow rate:

		Inlet Fflows (kg/h)																																							
Inlet	1	432	432	432	432	432	432	432	432	432	432	432	432	432	432	432	425	425	425	425	417	425	432	432	432	432	432	432	432	432	448	448	448	448	448	432	432	432	432		
	2	85.3	85.3	85.3	85.3	85.3	85.3	85.3	85.3	85.1	85.3	85.3	85.3	85.3	85.3	85.3	84	84	84	84	84	94.1	84	85.3	85.3	85.3	85.3	85.3	85.3	85.3	85.3	75.8	75.8	75.8	75.8	75.7	85.3	85.3	85.3	85.3	
	3	61.3	61.3	61.3	61.3	61.3	61.3	61.3	61.3	61.3	61.3	61.3	61.3	61.3	61.3	61.3	64.6	64.6	64.6	64.6	64.1	64.6	61.3	61.4	61.3	61.4	61.4	61.4	61.4	61.4	58.6	58.6	58.6	58.6	58.5	61.3	61.3	61.3	61.3		
	4	78.8	78.8	78.8	78.8	78.8	78.8	78.8	78.8	78.8	78.4	78.8	78.8	78.8	78.8	78.8	81.1	81.1	81.1	81.1	81.1	80.8	80.9	78.8	78.8	78.8	78.8	78.8	78.8	78.8	76.8	76.8	76.8	76.8	76.7	78.8	78.8	78.8	78.8		
	5	55.9	55.9	55.9	55.9	55.9	55.9	55.9	55.9	55.4	55.9	55.9	55.9	55.9	55.9	55.9	57.1	57.1	57.1	57.1	57.1	57	56.7	56	56.1	56	56.1	56.1	56.1	56.1	55	55	55	55	54.9	55.9	55.9	55.9	55.9		
	6	47	47	47	47	47	47	47	47	47	48.4	47	47	47	47	47	47.4	47.4	47.4	47.4	47.4	47.3	48.8	47	46.9	47	46.9	46.9	46.9	46.9	46.6	46.6	46.6	46.6	46.7	47	47	47	47		
	7	35.2	35.2	35.2	35.2	35.2	35.2	35.2	35.2	35.2	36.2	35.2	35.2	35.2	35.2	35.2	35.4	35.4	35.4	35.4	35.2	35.7	35.1	34.8	35.1	34.8	34.8	34.8	34.8	34.8	34.8	34.8	34.8	34.8	34.8	35.2	35.2	35.2	35.2		
	8	1.13	1.13	1.13	1.13	1.13	1.13	1.13	1.13	1.03	1.13	1.13	1.13	1.13	1.13	1.13	1.15	1.15	1.15	1.15	1.15	1.15	1.07	1.12	1.13	1.13	1.13	1.13	1.13	1.13	1.1	1.1	1.1	1.1	1.11	1.13	1.13	1.13	1.13		
	9	1.77	1.77	1.77	1.77	1.77	1.77	1.77	1.77	1.56	1.77	1.77	1.77	1.77	1.77	1.77	1.81	1.81	1.81	1.81	1.81	1.81	1.62	1.79	1.76	1.75	1.76	1.76	1.76	1.76	1.7	1.7	1.7	1.7	1.71	1.77	1.77	1.77	1.77		
	10	1.87	1.87	1.87	1.87	1.87	1.87	1.87	1.87	1.66	1.87	1.87	1.87	1.87	1.87	1.87	1.93	1.93	1.93	1.93	1.93	1.96	1.7	1.87	1.85	1.89	1.85	1.85	1.85	1.85	1.85	1.85	1.85	1.79	1.79	1.79	1.79	1.8	1.87	1.87	1.87

		PV temperature (deg C), Summer																																						
PV module	1	36.1	36.1	36.1	36.1	36.1	36.1	36.1	36.1	36.1	36.1	36.1	36.1	36.1	36.1	36.2	36.2	36.2	36.2	36.3	36.2	36.1	36.1	36.1	36.1	36.1	36.1	36.1	36.1	35.9	35.9	35.9	35.9	35.9	36.1	36.1	36.1	36.1		
	2	35.2	35.2	35.2	35.2	35.2	35.2	35.2	35.2	35.2	35.2	35.2	35.2	35.2	35.2	35.2	35.3	35.3	35.3	35.3	35.3	35.2	35.2	35.2	35.2	35.2	35.2	35.2	35.2	35.2	35.2	35.2	35.2	35.2	35.2	35.2	35.2	35.2	35.2	
	3	34.2	34.2	34.2	34.2	34.2	34.2	34.2	34.2	34.2	34.2	34.2	34.2	34.2	34.2	34.2	34.2	34.2	34.2	34.2	34.2	34.2	34.2	34.2	34.2	34.2	34.2	34.2	34.2	34.1	34.1	34.1	34.1	34.1	34.1	34.2	34.2	34.2	34.2	
	4	34.1	34.1	34.1	34.1	34.1	34.1	34.1	34.1	34.1	34.1	34.1	34.1	34.1	34.1	34.1	34.1	34.1	34.1	34.1	34.1	34.1	34.1	34.1	34.1	34.1	34.1	34.1	34.1	34	34	34	34	34	34.1	34.1	34.1	34.1		
	5	33.7	33.7	33.7	33.7	33.7	33.7	33.7	33.7	33.7	33.7	33.7	33.7	33.7	33.7	33.7	33.7	33.7	33.7	33.7	33.7	33.7	33.7	33.7	33.7	33.7	33.7	33.7	33.7	33.7	33.7	33.7	33.7	33.7	33.7	33.7	33.7	33.7	33.7	
	6	33.3	33.3	33.3	33.3	33.3	33.3	33.3	33.3	33.3	33.4	33.3	33.3	33.3	33.3	33.3	33.4	33.4	33.4	33.4	33.4	33.4	33.3	33.3	33.3	33.3	33.3	33.3	33.3	33.3	33.3	33.3	33.3	33.3	33.3	33.3	33.3	33.3	33.3	
	7	33.1	33.1	33.1	33.1	33.1	33.1	33.1	33.1	33.1	33.1	33.1	33.1	33.1	33.1	33.1	33.1	33.1	33.1	33.1	33.1	33.1	33.1	33.1	33.1	33.1	33.1	33.1	33.1	33.1	33.1	33.1	33.1	33.1	33.1	33.1	33.1	33.1	33.1	
	8	33.5	33.5	33.5	33.5	33.5	33.5	33.5	33.5	33.5	33.5	33.5	33.5	33.5	33.5	33.5	33.5	33.5	33.5	33.5	33.5	33.5	33.5	33.5	33.5	33.5	33.5	33.5	33.5	33.5	33.5	33.5	33.5	33.5	33.5	33.5	33.5	33.5	33.5	
	9	33.4	33.4	33.4	33.4	33.4	33.4	33.4	33.4	33.4	33.4	33.4	33.4	33.4	33.4	33.4	33.4	33.4	33.4	33.4	33.4	33.4	33.4	33.4	33.4	33.4	33.4	33.4	33.4	33.4	33.4	33.4	33.4	33.4	33.4	33.4	33.4	33.4	33.4	33.4
	10	33.3	33.3	33.3	33.3	33.3	33.3	33.3	33.3	33.3	33.4	33.3	33.3	33.3	33.3	33.3	33.3	33.3	33.3	33.3	33.3	33.3	33.3	33.3	33.3	33.3	33.3	33.3	33.3	33.3	33.3	33.3	33.3	33.3	33.3	33.3	33.3	33.3	33.3	

		PV temperature (deg C), Winter																																				
PV module	1	4.4	4.4	4.4	4.4	4.4	4.4	4.4	4.4	4.4	4.4	4.4	4.4	4.4	4.4	4.5	4.5	4.5	4.5	4.5	4.5	4.4	4.4	4.4	4.4	4.4	4.4	4.4	4.2	4.2	4.2	4.2	4.2	4.4	4.4	4.4	4.4	
	2	3.7	3.7	3.7	3.7	3.7	3.7	3.7	3.7	3.7	3.7	3.7	3.7	3.7	3.7	3.7	3.7	3.7	3.7	3.7	3.7	3.7	3.7	3.7	3.7	3.7	3.7	3.7	3.6	3.6	3.6	3.6	3.6	3.7	3.7	3.7	3.7	
	3	3.3	3.3	3.3	3.3	3.3	3.3	3.3	3.3	3.3	3.3	3.3	3.3	3.3	3.3	3.3	3.3	3.3	3.3	3.3	3.3	3.3	3.3	3.3	3.3	3.3	3.3	3.3	3.3	3.3	3.3	3.3	3.3	3.3	3.3	3.3	3.3	3.3
	4	2.7	2.7	2.7	2.7	2.7	2.7	2.7	2.7	2.7	2.7	2.7	2.7	2.7	2.7	2.7	2.7	2.7	2.7	2.7	2.7	2.7	2.7	2.7	2.7	2.7	2.7	2.7	2.7	2.7	2.7	2.7	2.7	2.7	2.7	2.7	2.7	2.7
	5	2.3	2.3	2.3	2.3	2.3	2.3	2.3	2.3	2.3	2.4	2.3	2.3	2.3	2.3	2.3	2.3	2.3	2.3	2.3	2.3	2.3	2.3	2.3	2.3	2.3	2.3	2.3	2.3	2.3	2.3	2.3	2.3	2.3	2.3	2.3	2.3	2.3
	6	2.1	2.1	2.1	2.1	2.1	2.1	2.1	2.1	2.1	2.1	2.1	2.1	2.1	2.1	2.1	2.1	2.1	2.1	2.1	2.1	2.1	2.1	2.1	2.1	2.1	2.1	2.1	2.1	2.1	2.1	2.1	2.1	2.1	2.1	2.1	2.1	2.1
	7	1.9	1.9	1.9	1.9	1.9	1.9	1.9	1.9	1.9	1.9	1.9	1.9	1.9	1.9	1.9	1.9	1.9	1.9	1.9	1.9	1.9	1.9	1.9	1.9	1.9	1.9	1.9	1.9	1.9	1.9	1.9	1.9	1.9	1.9	1.9	1.9	1.9
	8	2.2	2.2	2.2	2.2	2.2	2.2	2.2	2.2	2.2	2.2	2.2	2.2	2.2	2.2	2.2	2.2	2.2	2.2	2.2	2.2	2.2	2.2	2.2	2.2	2.2	2.2	2.2	2.2	2.2	2.2	2.2	2.2	2.2	2.2	2.2	2.2	2.2
	9	2.1	2.1	2.1	2.1	2.1	2.1	2.1	2.1	2.1	2.1	2.1	2.1	2.1	2.1	2.1	2.1	2.1	2.1	2.1	2.1	2.1	2.1	2.1	2.1	2.1	2.1	2.1	2.1	2.1	2.1	2.1	2.1	2.1	2.1	2.1	2.1	2.1
	10	2.1	2.1	2.1	2.1	2.1	2.1	2.1	2.1	2.1	2.1	2.1	2.1	2.1	2.1	2.1	2.1	2.1	2.1	2.1	2.1	2.1	2.1	2.1	2.1	2.1	2.1	2.1	2.1	2.1	2.1	2.1	2.1	2.1	2.1	2.1	2.1	2.1

System VI, inlet flows for 2m/s wind, 90° and PV temperatures for summer and winter conditions at 400kg/h total air mass flow rate:

		Inlet Fflows (kg/h)																																									
Inlet	1	260	260	260	260	260	260	260	260	260	260	260	260	260	260	260	242	242	242	242	242	224	243	261	262	261	262	262	262	262	262	262	262	319	319	319	319	319	260	260	260	260	
	2	37.2	37.2	37.2	37.2	37.2	37.2	37.2	37.2	37.1	37.2	37.2	37.2	37.2	37.2	37.2	37.2	34.7	34.7	34.7	34.7	34.7	55.7	34.7	37.3	37.4	37.2	37.4	37.4	37.4	37.4	37.4	37.4	37.4	-1.3	-1.3	-1.3	-1.3	-1.5	37.2	37.2	37.2	37.2
	3	24.1	24.1	24.1	24.1	24.1	24.1	24.1	24	24.1	24.1	24.1	24.1	24.1	24.1	24.1	31.9	31.9	31.9	31.9	31.9	31.3	32	24.1	24.1	24.1	24.1	24.1	24.1	24.1	24.1	24.1	24.1	16.2	16.2	16.2	16.2	16.2	24.1	24.1	24.1	24.1	
	4	29.2	29.2	29.2	29.2	29.2	29.2	29.2	29.2	29.1	29.2	29.2	29.2	29.2	29.2	29.2	29.2	35.7	35.7	35.7	35.7	35.7	35.1	35.7	29.2	29.3	29.2	29.3	29.3	29.3	29.3	29.3	29.3	29.3	23.5	23.5	23.5	23.5	23.5	29.2	29.2	29.2	29.2
	5	20	20	20	20	20	20	20	20	19.8	20	20	20	20	20	20	20	23.4	23.4	23.4	23.4	23.4	23.3	23.5	20	20.3	20	20.3	20.3	20.3	20.3	20.3	20.3	20.3	18.1	18.1	18.1	18.1	17.8	20	20	20	20
	6	16	16	16	16	16	16	16	15.9	16	16	16	16	16	16	16	16	17.7	17.7	17.7	17.7	17.7	17.3	17.7	16	15.4	16	15.4	15.4	15.4	15.4	15.4	15.4	12.9	12.9	12.9	12.9	13.8	16	16	16	16	
	7	11.5	11.5	11.5	11.5	11.5	11.5	11.5	12.6	11.5	11.5	11.5	11.5	11.5	11.5	11.5	11.5	12.2	12.2	12.2	12.2	12.2	11.7	11.3	11	10.3	11.3	10.3	10.3	10.3	10.3	10.3	10.6	10.6	10.6	10.6	9.5	11.5	11.5	11.5	11.5		
	8	0.38	0.38	0.38	0.38	0.38	0.38	0.38	0.35	0.38	0.38	0.38	0.38	0.38	0.38	0.38	0.38	0.44	0.44	0.44	0.44	0.44	0.43	0.49	0.32	0.37	0.36	0.37	0.37	0.37	0.37	0.37	0.21	0.21	0.21	0.21	0.48	0.38	0.38	0.38	0.38		
	9	0.61	0.61	0.61	0.61	0.61	0.61	0.61	0.59	0.61	0.61	0.61	0.61	0.61	0.61	0.61	0.61	0.73	0.73	0.73	0.73	0.73	0.69	0.75	0.74	0.58	0.53	0.58	0.58	0.58	0.58	0.58	0.6	0.6	0.6	0.6	0.84	0.61	0.61	0.61	0.61		
	10	0.64	0.64	0.64	0.64	0.64	0.64	0.64	0.66	0.64	0.64	0.64	0.64	0.64	0.64	0.64	0.64	0.79	0.79	0.79	0.79	0.79	1.02	0.76	0.67	0.59	0.79	0.59	0.59	0.59	0.59	0.59	0.67	0.67	0.67	0.67	0.87	0.64	0.64	0.64	0.64		

		PV temperature (deg C), Summer																																									
PV module	1	39.3	39.3	39.3	39.3	39.3	39.3	39.3	39.3	39.3	39.3	39.3	39.3	39.3	39.3	39.3	39.6	39.6	39.6	39.6	39.6	39.9	39.6	39.3	39.3	39.3	39.3	39.3	39.3	39.3	39.3	39.3	39.3	38.5	38.5	38.5	38.5	38.5	39.3	39.3	39.3	39.3	
	2	38.8	38.8	38.8	38.8	38.8	38.8	38.8	38.8	38.8	38.8	38.8	38.8	38.8	38.8	38.8	39.1	39.1	39.1	39.1	39.1	39.1	39.1	39.1	38.8	38.8	38.8	38.8	38.8	38.8	38.8	38.8	38.8	38.8	41.3	41.3	41.3	41.3	41.3	38.8	38.8	38.8	38.8
	3	37.4	37.4	37.4	37.4	37.4	37.4	37.4	37.4	37.4	37.4	37.4	37.4	37.4	37.4	37.4	37.6	37.6	37.6	37.6	37.6	37.6	37.6	37.6	37.4	37.4	37.4	37.4	37.4	37.4	37.4	37.4	37.4	37.4	37.3	37.3	37.3	37.3	37.3	37.4	37.4	37.4	37.4
	4	38.1	38.1	38.1	38.1	38.1	38.1	38.1	38.1	38.1	38.1	38.1	38.1	38.1	38.1	38.1	38.2	38.2	38.2	38.2	38.2	38.2	38.2	38.2	38.1	38.1	38.1	38.1	38.1	38.1	38.1	38.1	38	38	38	38	38	38.1	38.1	38.1	38.1		
	5	37.9	37.9	37.9	37.9	37.9	37.9	37.9	37.9	37.9	37.9	37.9	37.9	37.9	37.9	37.9	37.9	37.9	37.9	37.9	37.9	37.9	37.9	37.9	37.9	37.9	37.9	37.9	37.9	37.9	37.9	37.9	37.9	37.9	37.9	37.9	37.9	37.9	37.9	37.9	37.9	37.9	37.9
	6	37.7	37.7	37.7	37.7	37.7	37.7	37.7	37.7	37.7	37.7	37.7	37.7	37.7	37.7	37.7	37.7	37.7	37.7	37.7	37.7	37.7	37.7	37.7	37.7	37.7	37.7	37.7	37.7	37.7	37.7	37.7	37.7	37.7	37.7	37.7	37.7	37.7	37.7	37.7	37.7	37.7	37.7
	7	37.6	37.6	37.6	37.6	37.6	37.6	37.6	37.6	37.6	37.6	37.6	37.6	37.6	37.6	37.6	37.6	37.6	37.6	37.6	37.6	37.6	37.6	37.6	37.6	37.6	37.6	37.6	37.6	37.6	37.6	37.6	37.6	37.6	37.6	37.6	37.6	37.6	37.6	37.6	37.6	37.6	37.6
	8	38.1	38.1	38.1	38.1	38.1	38.1	38.1	38.1	38.1	38.1	38.1	38.1	38.1	38.1	38.1	38.1	38.1	38.1	38.1	38.1	38.1	38.1	38	38.2	38.1	38.1	38.1	38.1	38.1	38.1	38.1	38.1	38.1	38.4	38.4	38.4	38.4	38	38.1	38.1	38.1	38.1
	9	38	38	38	38	38	38	38	38	38	38	38	38	38	38	38	38	37.9	37.9	37.9	37.9	37.9	37.9	37.9	37.9	38	38	38	38	38	38	38	38	38	38	38	38	38	38	38	38	38	38
	10	37.9	37.9	37.9	37.9	37.9	37.9	37.9	37.9	37.9	37.9	37.9	37.9	37.9	37.9	37.9	37.9	37.9	37.9	37.9	37.9	37.9	37.9	37.9	37.9	38	37.9	38	38	38	38	38	38	38	38	38	38	38	38	38	38	38	38

		PV temperature (deg C), Winter																																									
PV module	1	7.1	7.1	7.1	7.1	7.1	7.1	7.1	7.1	7.1	7.1	7.1	7.1	7.1	7.1	7.1	7.4	7.4	7.4	7.4	7.6	7.4	7.1	7.1	7.1	7.1	7.1	7.1	7.1	7.1	7.1	7.1	6.5	6.5	6.5	6.5	6.5	7.1	7.1	7.1	7.1		
	2	6.7	6.7	6.7	6.7	6.7	6.7	6.7	6.7	6.7	6.7	6.7	6.7	6.7	6.7	6.7	6.9	6.9	6.9	6.9	6.9	6.9	6.9	6.9	6.7	6.7	6.7	6.7	6.7	6.7	6.7	6.7	6.7	6.7	6.7	6.7	6.7	6.7	6.7	6.7	6.7	6.7	6.7
	3	6.5	6.5	6.5	6.5	6.5	6.5	6.5	6.5	6.5	6.5	6.5	6.5	6.5	6.5	6.5	6.5	6.7	6.7	6.7	6.7	6.6	6.6	6.5	6.5	6.5	6.5	6.5	6.5	6.5	6.5	6.5	6.5	6.4	6.4	6.4	6.4	6.4	6.5	6.5	6.5	6.5	
	4	6.1	6.1	6.1	6.1	6.1	6.1	6.1	6.1	6.1	6.1	6.1	6.1	6.1	6.1	6.1	6.1	6.2	6.2	6.2	6.2	6.2	6.2	6.1	6.1	6.1	6.1	6.1	6.1	6.1	6.1	6.1	6.1	6.1	6.1	6.1	6.1	6.1	6.1	6.1	6.1	6.1	6.1
	5	5.9	5.9	5.9	5.9	5.9	5.9	5.9	5.9	5.9	5.9	5.9	5.9	5.9	5.9	5.9	5.9	5.9	5.9	5.9	5.9	5.9	5.9	5.9	5.9	5.9	5.9	5.9	5.9	5.9	5.9	5.9	5.9	5.9	5.9	5.9	5.9	5.9	5.9	5.9	5.9	5.9	
	6	5.8	5.8	5.8	5.8	5.8	5.8	5.8	5.8	5.8	5.8	5.8	5.8	5.8	5.8	5.8	5.8	5.8	5.8	5.8	5.8	5.8	5.8	5.8	5.8	5.8	5.8	5.8	5.8	5.8	5.8	5.8	5.8	5.8	5.8	5.8	5.8	5.8	5.8	5.8	5.8	5.8	5.8
	7	5.7	5.7	5.7	5.7	5.7	5.7	5.7	5.7	5.7	5.7	5.7	5.7	5.7	5.7	5.7	5.7	5.7	5.7	5.7	5.7	5.7	5.7	5.7	5.7	5.7	5.7	5.7	5.7	5.7	5.7	5.7	5.7	5.7	5.7	5.7	5.7	5.7	5.7	5.7	5.7	5.7	5.7
	8	6.1	6.1	6.1	6.1	6.1	6.1	6.1	6.1	6.1	6.1	6.1	6.1	6.1	6.1	6.1	6.1	6.0	6.0	6.0	6.0	6.1	6.0	6.2	6.1	6.1	6.1	6.1	6.1	6.1	6.1	6.1	6.1	6.4	6.4	6.4	6.4	6.0	6.1	6.1	6.1	6.1	
	9	6.0	6.0	6.0	6.0	6.0	6.0	6.0	6.0	6.0	6.0	6.0	6.0	6.0	6.0	6.0	6.0	6.0	6.0	6.0	6.0	6.0	6.0	6.0	6.0	6.0	6.0	6.0	6.0	6.0	6.0	6.0	6.0	6.0	6.0	6.0	6.0	6.0	6.0	6.0	6.0	6.0	6.0
	10	5.9	5.9	5.9	5.9	5.9	5.9	5.9	5.9	5.9	5.9	5.9	5.9	5.9	5.9	5.9	5.9	5.9	5.9	5.9	5.9	5.9	5.9	5.9	5.9	5.9	5.9	5.9	5.9	5.9	5.9	5.9	5.9	5.9	5.9	5.9	5.9	5.9	5.9	5.9	5.9	5.9	5.9

System V, inlet flows for 1m/s wind, 135° and PV temperatures for summer and winter conditions at 400kg/h total air mass flow rate:

		Inlet Fflows (kg/h)																																								
Inlet	1	215	215	219	215	215	217	215	224	216.2	216	215	215	215	215	215	215	215	215	215	212	212	212	215	215	215	215	215	216	216	216	216	219	220	215	215	215	215	215	215		
	2	42.7	42.7	43.3	42.7	42.7	43	42.7	38.1	42.85	42.8	42.7	42.7	42.7	42.7	42.7	42.7	42.7	42.7	42.7	42.5	42.1	42.1	42.1	42.7	42.7	42.7	42.7	42.7	42.8	42.8	42.9	42.9	43.3	38	42.7	42.7	42.7	42.6	42.7	42.7	
	3	30.7	30.7	29	30.7	30.7	31	30.7	29.4	30.86	30.8	30.7	30.7	30.7	30.7	30.7	30.7	30.7	30.7	30.7	30.6	32.4	32.4	32.4	30.7	30.7	30.7	30.7	30.7	30.8	30.8	30.9	30.9	29	27	30.7	30.7	30.7	30.7	30.7	30.7	
	4	39.5	39.5	38.3	39.5	39.5	38.1	39.5	38.6	39.64	39.6	39.5	39.5	39.5	39.5	39.5	39.5	39.5	39.5	39.5	39.3	40.7	40.7	40.7	39.5	39.5	39.5	39.5	39.5	39.6	39.6	39.6	39.6	38.3	37	39.5	39.5	39.5	39.3	39.5	39.5	
	5	28	28.1	27.5	28	28	27.4	28	28.6	27.34	28.1	28	28	28	28	28	28	28	28	28	28.7	28.6	28.6	28.6	28	28	28	28	28	28.1	28.1	27.4	27.4	27.5	29.4	28	28	28	27.8	28	28	
	6	23.6	23.6	23.4	23.6	23.6	23.3	23.6	22.2	23.18	23.1	23.6	23.6	23.6	23.6	23.6	23.6	23.6	23.6	23.6	24	23.8	23.8	23.8	23.6	23.6	23.6	23.6	23.6	23.6	23.1	23.1	23.2	23.2	23.4	29.7	23.6	23.6	23.6	24.3	23.6	23.6
	7	17.7	17.6	17.6	17.7	17.7	17.6	17.7	15.2	17.58	17.6	17.7	17.7	17.7	17.7	17.7	17.7	17.7	17.7	17.7	17.7	17.9	17.8	17.8	17.8	17.7	17.7	17.7	17.7	17.7	17.5	17.5	17.5	17.5	17.6	17.3	17.7	17.7	17.7	18.1	17.9	17.9
	8	0.56	0.56	0.55	0.57	0.57	0.56	0.57	0.79	0.572	0.57	0.57	0.57	0.57	0.57	0.57	0.57	0.57	0.57	0.57	0.56	0.58	0.58	0.58	0.57	0.57	0.57	0.57	0.57	0.56	0.56	0.56	0.56	0.55	0.31	0.57	0.57	0.57	0.53	0.56	0.56	
	9	0.87	0.89	0.85	0.88	0.88	0.88	0.89	1.41	0.864	0.86	0.88	0.88	0.88	0.88	0.88	0.88	0.88	0.88	0.88	0.87	0.9	0.9	0.9	0.88	0.88	0.88	0.88	0.88	0.87	0.87	0.87	0.87	0.85	0.4	0.88	0.88	0.89	0.77	0.88	0.88	
	10	0.94	0.93	0.9	0.93	0.93	0.9	0.92	1.47	0.92	0.92	0.93	0.93	0.93	0.93	0.93	0.93	0.93	0.93	0.93	0.95	0.96	0.96	0.96	0.93	0.93	0.93	0.93	0.93	0.92	0.92	0.92	0.92	0.9	0.41	0.93	0.93	0.92	0.82	0.93	0.93	

		PV temperature (deg C), Summer																																								
PV module	1	44	44	43.9	44	44	43.9	44	43.7	43.96	44	44	44	44	44	44	44	44	44	44	44.1	44.1	44.1	44	44	44	44	44	44	44	44	43.9	43.8	44	44	44	44	44	44			
	2	42.8	42.8	42.7	42.8	42.8	42.8	42.7	42.79	42.8	42.8	42.8	42.8	42.8	42.8	42.8	42.8	42.8	42.8	42.8	42.9	42.9	42.9	42.8	42.8	42.8	42.8	42.8	42.8	42.8	42.8	42.7	42.8	42.8	42.8	42.8	42.8	42.8	42.8	42.8	42.8	
	3	40.6	40.6	40.6	40.6	40.6	40.6	40.6	40.6	40.6	40.6	40.6	40.6	40.6	40.6	40.6	40.6	40.6	40.6	40.6	40.7	40.7	40.7	40.6	40.6	40.6	40.6	40.6	40.6	40.6	40.6	40.6	40.6	40.7	40.6	40.6	40.6	40.6	40.6	40.6	40.6	
	4	41.2	41.2	41.2	41.2	41.2	41.2	41.1	41.16	41.2	41.2	41.2	41.2	41.2	41.2	41.2	41.2	41.2	41.2	41.2	41.2	41.2	41.2	41.2	41.2	41.2	41.2	41.2	41.2	41.2	41.2	41.2	41.2	41.3	41.2	41.2	41.2	41.2	41.2	41.2	41.2	
	5	40.6	40.6	40.6	40.6	40.6	40.6	40.6	40.6	40.62	40.6	40.6	40.6	40.6	40.6	40.6	40.6	40.6	40.6	40.6	40.6	40.6	40.6	40.6	40.6	40.6	40.6	40.6	40.6	40.6	40.6	40.6	40.7	40.6	40.6	40.6	40.6	40.6	40.6	40.6		
	6	40.2	40.2	40.2	40.2	40.2	40.2	40.2	40.2	40.18	40.2	40.2	40.2	40.2	40.2	40.2	40.2	40.2	40.2	40.2	40.2	40.2	40.2	40.2	40.2	40.2	40.2	40.2	40.2	40.2	40.2	40.2	40.2	40.2	40.2	40.2	40.2	40.2	40.2	40.2	40.2	40.2
	7	39.9	39.9	39.9	39.9	39.9	39.9	39.9	39.9	39.88	39.9	39.9	39.9	39.9	39.9	39.9	39.9	39.9	39.9	39.9	39.9	39.9	39.9	39.9	39.9	39.9	39.9	39.9	39.9	39.9	39.9	39.9	39.9	39.9	39.9	39.9	39.9	39.9	39.9	39.9	39.9	39.9
	8	40.5	40.5	40.5	40.5	40.5	40.5	40.3	40.45	40.5	40.5	40.5	40.5	40.5	40.5	40.5	40.5	40.5	40.5	40.5	40.5	40.5	40.5	40.5	40.5	40.5	40.5	40.5	40.5	40.5	40.5	40.5	40.5	40.5	40.8	40.5	40.5	40.5	40.5	40.5	40.5	40.5
	9	40.3	40.3	40.3	40.3	40.3	40.3	40.1	40.29	40.3	40.3	40.3	40.3	40.3	40.3	40.3	40.3	40.3	40.3	40.3	40.3	40.3	40.3	40.3	40.3	40.3	40.3	40.3	40.3	40.3	40.3	40.3	40.3	40.3	40.8	40.3	40.3	40.3	40.3	40.3	40.3	40.3
	10	40.2	40.2	40.2	40.2	40.2	40.2	40.1	40.24	40.2	40.2	40.2	40.2	40.2	40.2	40.2	40.2	40.2	40.2	40.2	40.2	40.2	40.2	40.2	40.2	40.2	40.2	40.2	40.2	40.2	40.2	40.2	40.2	40.7	40.2	40.2	40.2	40.3	40.2	40.2	40.2	

		PV temperature (deg C), Winter																																							
PV module	1	11.4	11.4	11.3	11.4	11.4	11.3	11.4	11.1	11.4	11.4	11.4	11.4	11.4	11.4	11.4	11.4	11.4	11.4	11.4	11.5	11.5	11.5	11.4	11.4	11.4	11.4	11.4	11.4	11.4	11.3	11.2	11.4	11.4	11.4	11.4	11.4	11.4	11.4		
	2	10.3	10.3	10.2	10.3	10.3	10.2	10.3	10.2	10.2	10.3	10.3	10.3	10.3	10.3	10.3	10.3	10.3	10.3	10.3	10.4	10.4	10.4	10.3	10.3	10.3	10.3	10.3	10.3	10.3	10.2	10.2	10.2	10.3	10.3	10.3	10.3	10.3	10.3	10.3	10.3
	3	9.7	9.7	9.7	9.7	9.7	9.7	9.7	9.7	9.7	9.7	9.7	9.7	9.7	9.7	9.7	9.7	9.7	9.7	9.7	9.8	9.8	9.8	9.8	9.7	9.7	9.7	9.7	9.7	9.7	9.7	9.7	9.7	9.8	9.7	9.7	9.7	9.7	9.7	9.7	9.7
	4	8.8	8.8	8.8	8.8	8.8	8.8	8.8	8.8	8.8	8.8	8.8	8.8	8.8	8.8	8.8	8.8	8.8	8.8	8.8	8.8	8.8	8.8	8.8	8.8	8.8	8.8	8.8	8.8	8.8	8.8	8.8	8.9	8.8	8.8	8.8	8.8	8.8	8.8	8.8	
	5	8.3	8.3	8.3	8.3	8.3	8.3	8.3	8.3	8.3	8.3	8.3	8.3	8.3	8.3	8.3	8.3	8.3	8.3	8.3	8.3	8.3	8.3	8.3	8.3	8.3	8.3	8.3	8.3	8.3	8.3	8.4	8.3	8.3	8.3	8.3	8.3	8.3	8.3	8.3	8.3
	6	7.9	7.9	7.9	7.9	7.9	7.9	7.9	7.9	7.9	7.9	7.9	7.9	7.9	7.9	7.9	7.9	7.9	7.9	7.9	7.9	7.9	7.9	7.9	7.9	7.9	7.9	7.9	7.9	7.9	7.9	7.9	7.9	7.9	7.9	7.9	7.9	7.9	7.9	7.9	7.9
	7	7.6	7.6	7.6	7.6	7.6	7.6	7.7	7.6	7.6	7.6	7.6	7.6	7.6	7.6	7.6	7.6	7.6	7.6	7.6	7.6	7.6	7.6	7.6	7.6	7.6	7.6	7.6	7.6	7.6	7.6	7.6	7.6	7.6	7.6	7.6	7.6	7.6	7.6	7.6	7.6
	8	8.2	8.2	8.2	8.1	8.1	8.1	8.1	8.0	8.1	8.1	8.1	8.1	8.1	8.1	8.1	8.1	8.1	8.1	8.1	8.1	8.1	8.1	8.1	8.1	8.1	8.1	8.1	8.1	8.2	8.2	8.2	8.2	8.2	8.5	8.1	8.1	8.1	8.2	8.2	8.2
	9	8.0	8.0	8.0	8.0	8.0	8.0	8.0	7.9	8.0	8.0	8.0	8.0	8.0	8.0	8.0	8.0	8.0	8.0	8.0	8.0	8.0	8.0	8.0	8.0	8.0	8.0	8.0	8.0	8.0	8.0	8.0	8.0	8.4	8.0	8.0	8.0	8.0	8.0	8.0	8.0
	10	7.9	8.0	8.0	8.0	8.0	8.0	8.0	7.8	8.0	8.0	8.0	8.0	8.0	8.0	8.0	8.0	8.0	8.0	8.0	7.9	7.9	7.9	7.9	8.0	8.0	8.0	8.0	8.0	8.0	8.0	8.0	8.4	8.0	8.0	8.0	8.0	8.0	8.0	8.0	8.0

System V, inlet flows for 2m/s wind, 135° and PV temperatures for summer and winter conditions at 400kg/h total air mass flow rate:

		Inlet Fflows (kg/h)																																								
Inlet	1	215	215	230	215	215	223	215	250	219.6	217	215	215	215	215	215	215	215	215	212	203	203	203	215	215	215	215	215	215	217	217	219	219	230	250	215	215	215	215	215	215	
	2	42.7	42.7	45.5	42.7	42.7	44.2	42.7	19.4	43.54	43	42.7	42.7	42.7	42.7	42.7	42.7	42.7	42.7	42	40.3	40.3	40.3	42.7	42.7	42.7	42.7	42.7	42.7	43	43	43.4	43.4	45.5	19.5	42.7	42.7	42.7	42.7	42.6	42.6	
	3	30.7	30.7	23.5	30.7	30.7	31.8	30.7	25.3	31.29	30.9	30.7	30.7	30.7	30.7	30.7	30.7	30.7	30.7	30.3	36.9	36.9	36.9	30.7	30.7	30.7	30.7	30.7	30.7	31	31	31.2	31.2	23.5	25.3	30.7	30.7	30.7	30.7	30.7	30.7	
	4	39.5	39.3	34.7	39.5	39.5	33.9	39.5	34.8	40.17	39.8	39.5	39.5	39.5	39.5	39.5	39.5	39.5	39.5	39.5	38.8	44.1	44.1	44.1	39.5	39.5	39.5	39.5	39.5	39.5	39.8	39.8	40.1	40.1	34.7	34.9	39.5	39.5	39.5	39.5	39.2	39.2
	5	28.1	27.9	26.7	28	28	25.5	28	26.2	26.18	28.3	28	28	28	28	28	28	28	28	30.7	30.3	30.3	30.3	28	28	28	28	28	28	28.3	28.3	25.2	25.2	26.7	26.2	28	28	28	28	27.7	27.7	
	6	23.6	24.3	21.3	23.6	23.6	22.2	23.6	24.4	20.85	21.7	23.6	23.6	23.6	23.6	23.6	23.6	23.6	23.6	25.3	24.6	24.6	24.6	23.6	23.6	23.6	23.6	23.6	23.6	21.7	21.7	21.9	21.9	21.3	24.4	23.6	23.6	23.6	23.6	24.4	24.4	
	7	17.6	17.7	15.6	17.7	17.7	17.2	17.8	18	14.84	17.1	17.7	17.7	17.7	17.7	17.7	17.7	17.7	17.7	18.3	18	18	18	17.7	17.7	17.7	17.7	17.7	17.7	16.8	16.8	17	17	15.6	17.9	17.7	17.7	17.8	18	18.7	18.7	
	8	0.55	0.49	0.71	0.57	0.57	0.56	0.58	0.47	0.825	0.59	0.57	0.57	0.57	0.57	0.57	0.57	0.57	0.57	0.56	0.6	0.6	0.6	0.57	0.57	0.57	0.57	0.57	0.57	0.56	0.56	0.55	0.55	0.71	0.45	0.57	0.57	0.58	0.6	0.5	0.5	
	9	0.84	0.82	1.2	0.88	0.88	0.88	0.92	0.68	1.283	0.82	0.88	0.88	0.88	0.88	0.88	0.88	0.88	0.88	0.86	0.96	0.96	0.96	0.88	0.88	0.88	0.88	0.88	0.88	0.86	0.86	0.85	0.85	1.2	0.65	0.88	0.88	0.92	0.85	0.77	0.77	
	10	0.98	0.83	1.27	0.93	0.93	0.84	0.89	0.65	1.42	0.89	0.93	0.93	0.93	0.93	0.93	0.93	0.93	0.93	1.01	1.03	1.03	1.03	0.93	0.93	0.93	0.93	0.93	0.93	0.9	0.9	0.89	0.89	1.27	0.67	0.93	0.93	0.89	0.92	0.83	0.83	

		PV temperature (deg C), Summer																																							
PV module	1	39.2	39.2	38.9	39.2	39.2	39.1	39.2	38.6	39.11	39.2	39.2	39.2	39.2	39.2	39.2	39.2	39.2	39.3	39.4	39.4	39.4	39.2	39.2	39.2	39.2	39.2	39.2	39.1	39.1	38.9	38.6	39.2	39.2	39.2	39.2	39.2	39.2			
	2	38.5	38.5	38.2	38.5	38.5	38.3	38.5	38.3	38.37	38.4	38.5	38.5	38.5	38.5	38.5	38.5	38.5	38.5	38.7	38.7	38.7	38.5	38.5	38.5	38.5	38.5	38.5	38.4	38.4	38.4	38.4	38.2	38.3	38.5	38.5	38.5	38.5	38.5	38.5	
	3	37	37	36.9	37	37	36.9	37	36.9	36.94	37	37	37	37	37	37	37	37	37.1	37.2	37.2	37.2	37	37	37	37	37	37	37	37	37	36.9	36.9	37	37	37	37	37	37	37	37
	4	37.4	37.4	37.3	37.4	37.4	37.3	37.4	37.4	37.3	37.4	37.4	37.4	37.4	37.4	37.4	37.4	37.4	37.5	37.4	37.4	37.4	37.4	37.4	37.4	37.4	37.4	37.4	37.4	37.4	37.3	37.3	37.4	37.4	37.4	37.4	37.4	37.4	37.4	37.4	
	5	37	37	37	37	37	37	37	37	36.96	37	37	37	37	37	37	37	37	37.1	37	37	37	37	37	37	37	37	37	37	37	37	37	37	37	37	37	37	37	37	37	37
	6	36.7	36.7	36.7	36.7	36.7	36.7	36.7	36.7	36.7	36.7	36.7	36.7	36.7	36.7	36.7	36.7	36.7	36.7	36.7	36.7	36.7	36.7	36.7	36.7	36.7	36.7	36.7	36.7	36.7	36.7	36.7	36.7	36.7	36.7	36.7	36.7	36.7	36.7	36.7	36.7
	7	36.5	36.5	36.5	36.5	36.5	36.5	36.5	36.5	36.53	36.5	36.5	36.5	36.5	36.5	36.5	36.5	36.5	36.5	36.5	36.5	36.5	36.5	36.5	36.5	36.5	36.5	36.5	36.5	36.5	36.5	36.5	36.5	36.5	36.5	36.5	36.5	36.5	36.5	36.5	36.5
	8	36.9	37	36.8	36.9	36.9	36.9	36.9	37	36.8	36.9	36.9	36.9	36.9	36.9	36.9	36.9	36.9	36.9	36.9	36.9	36.9	36.9	36.9	36.9	36.9	36.9	36.9	36.9	36.9	36.9	36.9	36.8	37	36.9	36.9	36.9	36.9	37	37	
	9	36.8	36.8	36.7	36.8	36.8	36.8	36.8	36.9	36.7	36.8	36.8	36.8	36.8	36.8	36.8	36.8	36.8	36.8	36.8	36.8	36.8	36.8	36.8	36.8	36.8	36.8	36.8	36.8	36.8	36.8	36.8	36.7	36.9	36.8	36.8	36.8	36.8	36.8	36.8	36.8
	10	36.7	36.8	36.7	36.8	36.8	36.8	36.8	36.9	36.66	36.8	36.8	36.8	36.8	36.8	36.8	36.8	36.8	36.8	36.7	36.7	36.7	36.7	36.8	36.8	36.8	36.8	36.8	36.8	36.8	36.8	36.7	36.9	36.8	36.8	36.8	36.8	36.8	36.8	36.8	36.8

		PV temperature (deg C), Winter																																					
PV module	1	7.0	7.0	6.8	7.0	7.0	6.9	7.0	6.5	7.0	7.0	7.0	7.0	7.0	7.0	7.0	7.0	7.1	7.2	7.2	7.2	7.0	7.0	7.0	7.0	7.0	7.0	7.0	7.0	7.0	6.8	6.5	7.0	7.0	7.0	7.0	7.0	7.0	
	2	6.4	6.4	6.2	6.4	6.4	6.3	6.4	6.2	6.3	6.4	6.4	6.4	6.4	6.4	6.4	6.4	6.5	6.6	6.6	6.6	6.4	6.4	6.4	6.4	6.4	6.4	6.4	6.3	6.3	6.2	6.2	6.4	6.4	6.4	6.4	6.4	6.4	
	3	6.1	6.1	5.9	6.1	6.1	5.9	6.1	6.0	6.0	6.1	6.1	6.1	6.1	6.1	6.1	6.1	6.1	6.2	6.2	6.2	6.1	6.1	6.1	6.1	6.1	6.1	6.1	6.0	6.0	5.9	6.0	6.1	6.1	6.1	6.1	6.1	6.1	
	4	5.5	5.5	5.4	5.5	5.5	5.4	5.5	5.5	5.4	5.5	5.5	5.5	5.5	5.5	5.5	5.5	5.5	5.5	5.5	5.5	5.5	5.5	5.5	5.5	5.5	5.5	5.5	5.4	5.4	5.4	5.5	5.5	5.5	5.5	5.5	5.5	5.5	5.5
	5	5.2	5.2	5.1	5.2	5.2	5.2	5.2	5.2	5.1	5.1	5.2	5.2	5.2	5.2	5.2	5.2	5.2	5.2	5.2	5.2	5.2	5.2	5.2	5.2	5.2	5.2	5.1	5.1	5.1	5.1	5.1	5.2	5.2	5.2	5.2	5.2	5.2	5.2
	6	4.9	4.9	4.9	4.9	4.9	4.9	4.9	4.9	4.9	4.9	4.9	4.9	4.9	4.9	4.9	4.9	4.9	4.9	4.9	4.9	4.9	4.9	4.9	4.9	4.9	4.9	4.9	4.9	4.9	4.9	4.9	4.9	4.9	4.9	4.9	4.9	4.9	4.9
	7	4.7	4.7	4.8	4.7	4.7	4.7	4.7	4.7	4.8	4.7	4.7	4.7	4.7	4.7	4.7	4.7	4.7	4.7	4.7	4.7	4.7	4.7	4.7	4.7	4.7	4.7	4.7	4.7	4.7	4.7	4.7	4.7	4.7	4.7	4.7	4.7	4.7	4.7
	8	5.1	5.1	5.0	5.1	5.1	5.1	5.1	5.1	5.0	5.1	5.1	5.1	5.1	5.1	5.1	5.1	5.1	5.1	5.1	5.1	5.1	5.1	5.1	5.1	5.1	5.1	5.1	5.1	5.1	5.1	5.1	5.1	5.1	5.1	5.1	5.1	5.1	5.1
	9	5.0	5.0	4.9	5.0	5.0	5.0	5.0	5.0	4.9	5.0	5.0	5.0	5.0	5.0	5.0	5.0	5.0	5.0	5.0	5.0	5.0	5.0	5.0	5.0	5.0	5.0	5.0	5.0	5.0	4.9	5.1	5.0	5.0	5.0	5.0	5.0	5.0	
	10	4.9	5.0	4.9	4.9	4.9	5.0	5.0	5.0	4.9	5.0	4.9	4.9	4.9	4.9	4.9	4.9	4.9	4.9	4.9	4.9	4.9	4.9	4.9	4.9	4.9	4.9	4.9	5.0	5.0	5.0	5.0	4.9	5.0	4.9	4.9	5.0	4.9	5.0

System V, inlet flows for 2m/s wind, 135° and PV temperatures for summer and winter conditions at 800kg/h total air mass flow rate:

		Inlet Fflows (kg/h)																																							
Inlet	1	432	432	438	432	432	435	432	447	433.4	432	432	432	432	432	432	432	432	430	425	425	425	432	432	432	432	432	433	433	433	433	433	438	448	432	432	432	432	431	431	
	2	85.3	85.3	86.5	85.3	85.3	86	85.2	75.7	85.58	85.4	85.3	85.3	85.3	85.3	85.3	85.3	85.3	84.9	84	84	84	85.3	85.3	85.3	85.3	85.3	85.3	85.4	85.4	85.6	85.6	86.5	75.7	85.3	85.3	85.2	85.2	85.1	85.1	
	3	61.3	61.3	57.9	61.3	61.3	61.9	61.3	58.5	61.57	61.4	61.3	61.3	61.3	61.3	61.3	61.3	61.3	61.1	64.6	64.6	64.6	61.3	61.3	61.3	61.3	61.3	61.3	61.4	61.4	61.6	61.6	57.9	58.5	61.3	61.3	61.3	61.3	61.3	61.3	61.3
	4	78.8	78.8	76.3	78.8	78.8	76.1	78.8	76.7	79.07	78.9	78.8	78.8	78.8	78.8	78.8	78.8	78.8	78.4	81.1	81.1	81.1	78.8	78.8	78.8	78.8	78.8	78.8	78.9	78.9	79.1	79.1	76.3	76.7	78.8	78.8	78.8	78.7	78.4	78.4	
	5	56	56	54.8	55.9	55.9	54.7	55.9	54.9	54.55	56.1	55.9	55.9	55.9	55.9	55.9	55.9	55.9	57.3	57.1	57.1	57.1	55.9	55.9	55.9	55.9	55.9	56.1	56.1	54.6	54.6	54.8	54.9	55.9	55.9	55.9	55.9	55.4	55.4		
	6	47	47	46.5	47	47	46.3	47	46.7	46.12	46	47	47	47	47	47	47	47	47.8	47.4	47.4	47.4	47	47	47	47	47	47	46	46	46.1	46.1	46.5	46.7	47	47	47	47	48.4	48.4	
	7	35.1	35.1	35.1	35.2	35.2	35	35.3	35.2	34.97	34.9	35.2	35.2	35.2	35.2	35.2	35.2	35.2	35.5	35.4	35.4	35.4	35.2	35.2	35.2	35.2	35.2	34.8	34.8	34.8	34.8	35.1	35.2	35.2	35.2	35.3	35.3	36.2	36.2		
	8	1.13	1.12	1.11	1.13	1.13	1.13	1.14	1.11	1.146	1.15	1.13	1.13	1.13	1.13	1.13	1.13	1.13	1.13	1.15	1.15	1.15	1.13	1.13	1.13	1.13	1.13	1.13	1.13	1.13	1.11	1.11	1.13	1.13	1.14	1.15	1.03	1.03			
	9	1.75	1.79	1.72	1.77	1.77	1.76	1.79	1.73	1.737	1.74	1.77	1.77	1.77	1.77	1.77	1.77	1.77	1.76	1.81	1.81	1.81	1.77	1.77	1.77	1.77	1.77	1.76	1.76	1.76	1.76	1.72	1.71	1.77	1.77	1.79	1.75	1.56	1.56		
	10	1.89	1.87	1.81	1.87	1.87	1.82	1.85	1.78	1.85	1.85	1.87	1.87	1.87	1.87	1.87	1.87	1.87	1.91	1.93	1.93	1.93	1.87	1.87	1.87	1.87	1.87	1.86	1.86	1.85	1.85	1.81	1.8	1.87	1.87	1.85	1.87	1.66	1.66		

		PV temperature (deg C), Summer																																							
PV module	1	36.1	36.1	36	36.1	36.1	36.1	35.9	36.09	36.1	36.1	36.1	36.1	36.1	36.1	36.1	36.1	36.1	36.2	36.2	36.2	36.1	36.1	36.1	36.1	36.1	36.1	36.1	36.1	36	35.9	36.1	36.1	36.1	36.1	36.1	36.1	36.1			
	2	35.2	35.2	35.2	35.2	35.2	35.2	35.2	35.22	35.2	35.2	35.2	35.2	35.2	35.2	35.2	35.2	35.3	35.3	35.3	35.3	35.2	35.2	35.2	35.2	35.2	35.2	35.2	35.2	35.2	35.2	35.2	35.2	35.2	35.2	35.2	35.2	35.2	35.2		
	3	34.2	34.2	34.1	34.2	34.2	34.1	34.2	34.1	34.16	34.2	34.2	34.2	34.2	34.2	34.2	34.2	34.2	34.2	34.2	34.2	34.2	34.2	34.2	34.2	34.2	34.2	34.2	34.2	34.2	34.1	34.1	34.2	34.2	34.2	34.2	34.2	34.2	34.2		
	4	34.1	34.1	34	34.1	34.1	34	34.1	34	34.04	34	34.1	34.1	34.1	34.1	34.1	34.1	34.1	34.1	34.1	34.1	34.1	34.1	34.1	34.1	34.1	34.1	34	34	34	34	34	34.1	34.1	34.1	34.1	34.1	34.1	34.1		
	5	33.7	33.7	33.7	33.7	33.7	33.7	33.7	33.7	33.66	33.7	33.7	33.7	33.7	33.7	33.7	33.7	33.7	33.7	33.7	33.7	33.7	33.7	33.7	33.7	33.7	33.7	33.7	33.7	33.7	33.7	33.7	33.7	33.7	33.7	33.7	33.7	33.7	33.7		
	6	33.3	33.3	33.3	33.3	33.3	33.3	33.4	33.3	33.35	33.3	33.3	33.3	33.3	33.3	33.3	33.3	33.3	33.4	33.4	33.4	33.4	33.3	33.3	33.3	33.3	33.3	33.3	33.3	33.3	33.3	33.3	33.3	33.3	33.3	33.3	33.3	33.3	33.3	33.3	
	7	33.1	33.1	33.1	33.1	33.1	33.1	33.1	33.1	33.13	33.1	33.1	33.1	33.1	33.1	33.1	33.1	33.1	33.1	33.1	33.1	33.1	33.1	33.1	33.1	33.1	33.1	33.1	33.1	33.1	33.1	33.1	33.1	33.1	33.1	33.1	33.1	33.1	33.1	33.1	
	8	33.5	33.5	33.5	33.5	33.5	33.5	33.5	33.47	33.5	33.5	33.5	33.5	33.5	33.5	33.5	33.5	33.5	33.5	33.5	33.5	33.5	33.5	33.5	33.5	33.5	33.5	33.5	33.5	33.5	33.5	33.5	33.5	33.5	33.5	33.5	33.5	33.5	33.5	33.5	
	9	33.4	33.4	33.4	33.4	33.4	33.4	33.4	33.38	33.4	33.4	33.4	33.4	33.4	33.4	33.4	33.4	33.4	33.4	33.4	33.4	33.4	33.4	33.4	33.4	33.4	33.4	33.4	33.4	33.4	33.4	33.4	33.4	33.4	33.4	33.4	33.4	33.4	33.4	33.4	
	10	33.3	33.3	33.3	33.3	33.3	33.3	33.4	33.34	33.3	33.3	33.3	33.3	33.3	33.3	33.3	33.3	33.3	33.3	33.3	33.3	33.3	33.3	33.3	33.3	33.3	33.3	33.3	33.3	33.3	33.3	33.3	33.3	33.3	33.3	33.3	33.3	33.3	33.3	33.3	

		PV temperature (deg C), Winter																																							
PV module	1	4.4	4.4	4.3	4.4	4.4	4.4	4.2	4.4	4.4	4.4	4.4	4.4	4.4	4.4	4.4	4.4	4.4	4.5	4.5	4.5	4.4	4.4	4.4	4.4	4.4	4.4	4.4	4.3	4.2	4.4	4.4	4.4	4.4	4.4	4.4	4.4				
	2	3.7	3.7	3.6	3.7	3.7	3.6	3.7	3.6	3.6	3.7	3.7	3.7	3.7	3.7	3.7	3.7	3.7	3.7	3.7	3.7	3.7	3.7	3.7	3.7	3.7	3.7	3.6	3.6	3.6	3.6	3.7	3.7	3.7	3.7	3.7	3.7				
	3	3.3	3.3	3.3	3.3	3.3	3.3	3.3	3.3	3.3	3.3	3.3	3.3	3.3	3.3	3.3	3.3	3.3	3.3	3.3	3.3	3.3	3.3	3.3	3.3	3.3	3.3	3.3	3.3	3.3	3.3	3.3	3.3	3.3	3.3	3.3	3.3	3.3			
	4	2.7	2.7	2.7	2.7	2.7	2.7	2.7	2.7	2.7	2.7	2.7	2.7	2.7	2.7	2.7	2.7	2.7	2.7	2.7	2.7	2.7	2.7	2.7	2.7	2.7	2.7	2.7	2.7	2.7	2.7	2.7	2.7	2.7	2.7	2.7	2.7	2.7			
	5	2.3	2.3	2.3	2.3	2.3	2.3	2.3	2.3	2.3	2.3	2.3	2.3	2.3	2.3	2.3	2.3	2.3	2.4	2.3	2.3	2.3	2.3	2.3	2.3	2.3	2.3	2.3	2.3	2.3	2.3	2.3	2.3	2.3	2.3	2.3	2.3	2.3	2.4		
	6	2.1	2.1	2.1	2.1	2.1	2.1	2.1	2.1	2.1	2.1	2.1	2.1	2.1	2.1	2.1	2.1	2.1	2.1	2.1	2.1	2.1	2.1	2.1	2.1	2.1	2.1	2.1	2.1	2.1	2.1	2.1	2.1	2.1	2.1	2.1	2.1	2.1	2.1		
	7	1.9	1.9	1.9	1.9	1.9	1.9	1.9	1.9	1.9	1.9	1.9	1.9	1.9	1.9	1.9	1.9	1.9	1.9	1.9	1.9	1.9	1.9	1.9	1.9	1.9	1.9	1.9	1.9	1.9	1.9	1.9	1.9	1.9	1.9	1.9	1.9	1.9			
	8	2.2	2.2	2.2	2.2	2.2	2.2	2.2	2.2	2.2	2.2	2.2	2.2	2.2	2.2	2.2	2.2	2.2	2.2	2.2	2.2	2.2	2.2	2.2	2.2	2.2	2.2	2.2	2.2	2.2	2.2	2.2	2.2	2.2	2.2	2.2	2.2	2.2	2.2		
	9	2.1	2.1	2.1	2.1	2.1	2.1	2.1	2.1	2.1	2.1	2.1	2.1	2.1	2.1	2.1	2.1	2.1	2.1	2.1	2.1	2.1	2.1	2.1	2.1	2.1	2.1	2.1	2.1	2.1	2.1	2.1	2.1	2.1	2.1	2.1	2.1	2.1	2.1		
	10	2.1	2.1	2.1	2.1	2.1	2.1	2.1	2.1	2.1	2.1	2.1	2.1	2.1	2.1	2.1	2.1	2.1	2.1	2.1	2.1	2.1	2.1	2.1	2.1	2.1	2.1	2.1	2.1	2.1	2.1	2.1	2.1	2.1	2.1	2.1	2.1	2.1	2.1		

System VI, inlet flows for 1m/s wind, 135° and PV temperatures for summer and winter conditions at 800kg/h total air mass flow rate:

		Inlet Fflows (kg/h)																																									
Inlet	1	522	522	524	522	522	523	522	527	522	522	522	522	522	522	522	522	522	521	519	519	519	522	522	522	522	522	522	522	522	522	524	527	522	522	522	521	521					
	2	74.4	74.4	74.8	74.4	74.4	74.6	74.4	71.6	74.5	74.5	74.4	74.4	74.4	74.4	74.4	74.4	74.3	74.1	74.1	74.1	74.4	74.4	74.4	74.4	74.4	74.4	74.5	74.5	74.5	74.5	74.8	71.6	74.4	74.4	74.4	74.4	74.4	74.4				
	3	48	48	46.9	48	48	48.2	48	47	48.1	48.1	48	48	48	48	48	48	48	49.1	49.1	49.1	48	48	48	48	48	48	48	48.1	48.1	46.9	47	48	48	48	48	48	48	48	48			
	4	58.3	58.3	57.4	58.3	58.3	57.3	58.3	57.5	58.3	58.3	58.3	58.3	58.3	58.3	58.3	58.3	58.3	58.3	59.1	59.1	59.1	58.3	58.3	58.3	58.3	58.3	58.3	58.3	58.3	57.4	57.5	58.3	58.3	58.3	58.3	58.3	58.3	58.3	58.3			
	5	39.8	39.8	39.4	39.8	39.8	39.4	39.8	39.4	39.3	39.3	39.8	39.8	39.8	39.8	39.8	39.8	39.8	40.3	40.3	40.3	39.8	39.8	39.8	39.8	39.8	39.8	39.9	39.9	39.3	39.3	39.4	39.4	39.8	39.8	39.8	39.8	39.8	39.8	39.8			
	6	31.8	31.8	31.6	31.8	31.8	31.5	31.8	31.6	31.5	31.5	31.8	31.8	31.8	31.8	31.8	31.8	31.8	32.1	32	32	32	31.8	31.8	31.8	31.8	31.8	31.8	31.5	31.5	31.5	31.5	31.6	31.6	31.8	31.8	31.8	31.8	31.8	31.8	31.8		
	7	22.9	22.8	22.8	22.9	22.9	22.8	22.9	22.9	22.8	22.8	22.9	22.9	22.9	22.9	22.9	22.9	22.9	23	23	23	22.9	22.9	22.9	22.9	22.9	22.9	22.9	22.7	22.7	22.7	22.8	22.8	22.9	22.9	22.9	22.9	22.9	22.9	23	23	23	
	8	0.76	0.76	0.76	0.77	0.77	0.77	0.77	0.76	0.77	0.77	0.77	0.77	0.77	0.77	0.77	0.77	0.77	0.77	0.77	0.77	0.77	0.77	0.77	0.77	0.77	0.77	0.77	0.77	0.76	0.76	0.76	0.76	0.76	0.77	0.77	0.77	0.77	0.77	0.77	0.76	0.76	
	9	1.21	1.23	1.2	1.22	1.22	1.23	1.23	1.21	1.2	1.2	1.22	1.22	1.22	1.22	1.22	1.22	1.22	1.22	1.24	1.24	1.24	1.22	1.22	1.22	1.22	1.22	1.22	1.22	1.21	1.21	1.2	1.2	1.22	1.22	1.23	1.21	1.22	1.22	1.23	1.21	1.22	1.22
	10	1.3	1.29	1.26	1.29	1.29	1.27	1.27	1.25	1.27	1.27	1.29	1.29	1.29	1.29	1.29	1.29	1.29	1.29	1.31	1.31	1.31	1.29	1.29	1.29	1.29	1.29	1.29	1.28	1.28	1.28	1.28	1.26	1.26	1.29	1.29	1.27	1.28	1.29	1.29	1.27	1.28	1.29

		PV temperature (deg C), Summer																																													
PV module	1	39.6	39.6	39.6	39.6	39.6	39.6	39.6	39.6	39.6	39.6	39.6	39.6	39.6	39.6	39.6	39.6	39.6	39.7	39.7	39.7	39.7	39.6	39.6	39.6	39.6	39.6	39.6	39.6	39.6	39.6	39.6	39.6	39.6	39.6	39.6	39.6	39.6	39.6	39.6	39.6						
	2	38.7	38.7	38.7	38.7	38.7	38.7	38.7	38.7	38.7	38.7	38.7	38.7	38.7	38.7	38.7	38.7	38.8	38.8	38.8	38.8	38.7	38.7	38.7	38.7	38.7	38.7	38.7	38.7	38.7	38.7	38.7	38.7	38.7	38.7	38.7	38.7	38.7	38.7	38.7	38.7	38.7	38.7	38.7			
	3	37.2	37.2	37.2	37.2	37.2	37.2	37.2	37.2	37.2	37.2	37.2	37.2	37.2	37.2	37.2	37.2	37.2	37.2	37.2	37.2	37.2	37.2	37.2	37.2	37.2	37.2	37.2	37.2	37.2	37.2	37.2	37.2	37.2	37.2	37.2	37.2	37.2	37.2	37.2	37.2	37.2	37.2	37.2	37.2		
	4	37.6	37.6	37.6	37.6	37.6	37.6	37.6	37.6	37.6	37.6	37.6	37.6	37.6	37.6	37.6	37.6	37.6	37.6	37.6	37.6	37.6	37.6	37.6	37.6	37.6	37.6	37.6	37.6	37.6	37.6	37.6	37.6	37.6	37.6	37.6	37.6	37.6	37.6	37.6	37.6	37.6	37.6	37.6	37.6		
	5	37.3	37.3	37.3	37.3	37.3	37.3	37.3	37.3	37.3	37.3	37.3	37.3	37.3	37.3	37.3	37.3	37.3	37.3	37.3	37.3	37.3	37.3	37.3	37.3	37.3	37.3	37.3	37.3	37.3	37.3	37.3	37.3	37.3	37.3	37.3	37.3	37.3	37.3	37.3	37.3	37.3	37.3	37.3	37.3		
	6	37	37	37	37	37	37	37	37	37	37	37	37	37	37	37	37	37	37	37	37	37	37	37	37	37	37	37	37	37	37	37	37	37	37	37	37	37	37	37	37	37	37	37	37		
	7	36.8	36.8	36.8	36.8	36.8	36.8	36.8	36.8	36.8	36.8	36.8	36.8	36.8	36.8	36.8	36.8	36.8	36.8	36.8	36.8	36.8	36.8	36.8	36.8	36.8	36.8	36.8	36.8	36.8	36.8	36.8	36.8	36.8	36.8	36.8	36.8	36.8	36.8	36.8	36.8	36.8	36.8	36.8	36.8	36.8	
	8	37.4	37.5	37.5	37.4	37.4	37.4	37.4	37.5	37.4	37.4	37.4	37.4	37.4	37.4	37.4	37.4	37.4	37.4	37.4	37.4	37.4	37.4	37.4	37.4	37.4	37.4	37.4	37.4	37.4	37.4	37.5	37.5	37.4	37.4	37.4	37.4	37.4	37.4	37.4	37.4	37.4	37.4	37.4	37.4		
	9	37.3	37.3	37.3	37.3	37.3	37.3	37.3	37.3	37.3	37.3	37.3	37.3	37.3	37.3	37.3	37.3	37.3	37.3	37.3	37.3	37.3	37.3	37.3	37.3	37.3	37.3	37.3	37.3	37.3	37.3	37.3	37.3	37.3	37.3	37.3	37.3	37.3	37.3	37.3	37.3	37.3	37.3	37.3	37.3	37.3	37.3
	10	37.2	37.2	37.2	37.2	37.2	37.2	37.2	37.2	37.2	37.2	37.2	37.2	37.2	37.2	37.2	37.2	37.2	37.2	37.2	37.2	37.2	37.2	37.2	37.2	37.2	37.2	37.2	37.2	37.2	37.2	37.2	37.2	37.2	37.2	37.2	37.2	37.2	37.2	37.2	37.2	37.2	37.2	37.2	37.2	37.2	37.2

		PV temperature (deg C), Winter																																														
PV module	1	7.4	7.4	7.4	7.4	7.4	7.4	7.4	7.4	7.4	7.4	7.4	7.4	7.4	7.4	7.4	7.4	7.4	7.5	7.5	7.5	7.5	7.4	7.4	7.4	7.4	7.4	7.4	7.4	7.4	7.4	7.4	7.4	7.4	7.4	7.4	7.4	7.4	7.4	7.4	7.4	7.5	7.5					
	2	6.7	6.7	6.6	6.7	6.7	6.6	6.7	6.6	6.7	6.7	6.7	6.7	6.7	6.7	6.7	6.7	6.7	6.7	6.7	6.7	6.7	6.7	6.7	6.7	6.7	6.7	6.7	6.7	6.7	6.6	6.6	6.7	6.7	6.7	6.7	6.7	6.7	6.7	6.7	6.7	6.7	6.7	6.7	6.7	6.7		
	3	6.3	6.3	6.3	6.3	6.3	6.3	6.3	6.3	6.3	6.3	6.3	6.3	6.3	6.3	6.3	6.3	6.3	6.3	6.3	6.3	6.3	6.3	6.3	6.3	6.3	6.3	6.3	6.3	6.3	6.3	6.3	6.3	6.3	6.3	6.3	6.3	6.3	6.3	6.3	6.3	6.3	6.3	6.3	6.3	6.3	6.3	6.3
	4	5.7	5.7	5.7	5.7	5.7	5.7	5.7	5.7	5.7	5.7	5.7	5.7	5.7	5.7	5.7	5.7	5.7	5.7	5.7	5.7	5.7	5.7	5.7	5.7	5.7	5.7	5.7	5.7	5.7	5.7	5.7	5.7	5.7	5.7	5.7	5.7	5.7	5.7	5.7	5.7	5.7	5.7	5.7	5.7	5.7	5.7	
	5	5.4	5.4	5.4	5.4	5.4	5.4	5.4	5.4	5.4	5.4	5.4	5.4	5.4	5.4	5.4	5.4	5.4	5.4	5.4	5.4	5.4	5.4	5.4	5.4	5.4	5.4	5.4	5.4	5.4	5.4	5.4	5.4	5.4	5.4	5.4	5.4	5.4	5.4	5.4	5.4	5.4	5.4	5.4	5.4	5.4	5.4	
	6	5.2	5.2	5.2	5.2	5.2	5.2	5.2	5.2	5.2	5.2	5.2	5.2	5.2	5.2	5.2	5.2	5.2	5.2	5.2	5.2	5.2	5.2	5.2	5.2	5.2	5.2	5.2	5.2	5.2	5.2	5.2	5.2	5.2	5.2	5.2	5.2	5.2	5.2	5.2	5.2	5.2	5.2	5.2	5.2	5.2	5.2	5.2
	7	5.0	5.0	5.0	5.0	5.0	5.0	5.0	5.0	5.0	5.0	5.0	5.0	5.0	5.0	5.0	5.0	5.0	5.0	5.0	5.0	5.0	5.0	5.0	5.0	5.0	5.0	5.0	5.0	5.0	5.0	5.0	5.0	5.0	5.0	5.0	5.0	5.0	5.0	5.0	5.0	5.0	5.0	5.0	5.0	5.0	5.0	
	8	5.5	5.5	5.5	5.5	5.5	5.5	5.5	5.5	5.5	5.5	5.5	5.5	5.5	5.5	5.5	5.5	5.5	5.5	5.5	5.5	5.5	5.5	5.5	5.5	5.5	5.5	5.5	5.5	5.5	5.5	5.5	5.5	5.5	5.5	5.5	5.5	5.5	5.5	5.5	5.5	5.5	5.5	5.5	5.5	5.5	5.5	
	9	5.4	5.4	5.4	5.4	5.4	5.4	5.4	5.4	5.4	5.4	5.4	5.4	5.4	5.4	5.4	5.4	5.4	5.4	5.4	5.4	5.4	5.4	5.4	5.4	5.4	5.4	5.4	5.4	5.4	5.4	5.4	5.4	5.4	5.4	5.4	5.4	5.4	5.4	5.4	5.4	5.4	5.4	5.4	5.4	5.4	5.4	
	10	5.4	5.4	5.4	5.4	5.4	5.4	5.4	5.4	5.4	5.4	5.4	5.4	5.4	5.4	5.4	5.4	5.4	5.4	5.4	5.4	5.4	5.4	5.4	5.4	5.4	5.4	5.4	5.4	5.4	5.4	5.4	5.4	5.4	5.4	5.4	5.4	5.4	5.4	5.4	5.4	5.4	5.4	5.4	5.4	5.4	5.4	5.4

System VI, inlet flows for 2m/s wind, 135° and PV temperatures for summer and winter conditions at 800kg/h total air mass flow rate:

		Inlet Fflows (kg/h)																																								
Inlet	1	522	522	532	522	522	528	521	543	524	524	522	522	522	522	522	522	522	522	519	512	512	512	522	522	522	522	522	522	523	523	524	524	532	543	522	522	521	521	521	521	
	2	74.4	74.4	75.8	74.4	74.4	75.3	74.3	62.7	74.8	74.8	74.4	74.4	74.4	74.4	74.4	74.4	74.4	74	73	73	73	74.4	74.4	74.4	74.4	74.4	74.4	74.6	74.6	74.8	74.8	75.8	62.7	74.4	74.4	74.3	74.4	74.4	74.4	74.4	
	3	48	48	43.3	48	48	48.6	48	44	48.3	48.3	48	48	48	48	48	48	48	48	47.8	52.3	52.3	52.3	48	48	48	48	48	48.1	48.1	48.3	48.3	43.3	44	48	48	48	48	48	48	48	48
	4	58.3	58.3	54.6	58.3	58.3	54.4	58.1	55.2	58.6	58.6	58.3	58.3	58.3	58.3	58.3	58.3	58.3	58.3	58	61.7	61.7	61.7	58.3	58.3	58.3	58.3	58.3	58.3	58.5	58.5	58.6	58.6	54.6	55.2	58.3	58.3	58.1	58.3	58.2	58.2	58.2
	5	39.8	39.9	37.9	39.8	39.8	38	39.5	38.5	37.7	37.7	39.8	39.8	39.8	39.8	39.8	39.8	39.8	39.8	41.8	41.6	41.6	41.6	39.8	39.8	39.8	39.8	39.8	39.9	39.9	37.8	37.8	37.9	38.5	39.8	39.8	39.5	39.8	39.8	39.7	39.7	39.7
	6	31.8	31.8	31	31.8	31.8	30.5	32.5	30.5	30.5	30.5	31.8	31.8	31.8	31.8	31.8	31.8	31.8	33	32.6	32.6	32.6	31.8	31.8	31.8	31.8	31.8	30.5	30.5	30.5	30.5	31	30.5	31.8	31.8	32.5	31.8	31.8	31.8	31.8	31.8	
	7	22.8	22.6	22.6	22.9	22.9	22.4	23.5	22.2	22.6	22.6	22.9	22.9	22.9	22.9	22.9	22.9	22.9	23.4	23.2	23.2	23.2	22.9	22.9	22.9	22.9	22.9	22.2	22.2	22.3	22.3	22.6	22.1	22.9	22.9	23.5	23.1	23.4	23.4	23.4	23.4	
	8	0.75	0.73	0.73	0.77	0.77	0.78	0.72	0.81	0.79	0.79	0.77	0.77	0.77	0.77	0.77	0.77	0.77	0.77	0.8	0.8	0.8	0.8	0.77	0.77	0.77	0.77	0.77	0.76	0.76	0.75	0.75	0.73	0.79	0.77	0.77	0.72	0.8	0.74	0.74	0.74	
	9	1.18	1.27	1.14	1.22	1.22	1.26	1.13	1.34	1.15	1.15	1.22	1.22	1.22	1.22	1.22	1.22	1.22	1.21	1.29	1.29	1.29	1.22	1.22	1.22	1.22	1.22	1.21	1.21	1.19	1.19	1.14	1.29	1.22	1.22	1.13	1.18	1.21	1.21	1.21	1.21	
	10	1.34	1.3	1.19	1.29	1.29	1.22	1.1	1.3	1.23	1.23	1.29	1.29	1.29	1.29	1.29	1.29	1.29	1.29	1.38	1.37	1.37	1.37	1.29	1.29	1.29	1.29	1.29	1.26	1.26	1.24	1.24	1.19	1.35	1.29	1.29	1.1	1.28	1.3	1.3	1.3	

		PV temperature (deg C), Summer																																									
PV module	1	36.4	36.4	36.3	36.4	36.4	36.3	36.4	36.2	36.3	36.3	36.4	36.4	36.4	36.4	36.4	36.4	36.4	36.4	36.4	36.4	36.4	36.4	36.4	36.4	36.4	36.3	36.3	36.3	36.3	36.2	36.4	36.4	36.4	36.4	36.4	36.4	36.4	36.4	36.4	36.4		
	2	35.7	35.7	35.7	35.7	35.7	35.7	35.7	35.7	35.7	35.7	35.7	35.7	35.7	35.7	35.7	35.7	35.7	35.8	35.8	35.8	35.8	35.7	35.7	35.7	35.7	35.7	35.7	35.7	35.7	35.7	35.7	35.7	35.7	35.7	35.7	35.7	35.7	35.7	35.7	35.7	35.7	
	3	34.7	34.7	34.7	34.7	34.7	34.7	34.7	34.7	34.7	34.7	34.7	34.7	34.7	34.7	34.7	34.7	34.7	34.8	34.8	34.8	34.8	34.7	34.7	34.7	34.7	34.7	34.7	34.7	34.7	34.7	34.7	34.7	34.7	34.7	34.7	34.7	34.7	34.7	34.7	34.7	34.7	34.7
	4	35	35	34.9	35	35	34.9	35	34.9	34.9	34.9	35	35	35	35	35	35	35	35	35	35	35	35	35	35	35	35	34.9	34.9	34.9	34.9	34.9	34.9	35	35	35	35	35	35	35	35	35	35
	5	34.7	34.7	34.7	34.7	34.7	34.7	34.7	34.7	34.7	34.7	34.7	34.7	34.7	34.7	34.7	34.7	34.7	34.7	34.7	34.7	34.7	34.7	34.7	34.7	34.7	34.7	34.7	34.7	34.7	34.7	34.7	34.7	34.7	34.7	34.7	34.7	34.7	34.7	34.7	34.7	34.7	34.7
	6	34.5	34.5	34.5	34.5	34.5	34.5	34.5	34.5	34.5	34.5	34.5	34.5	34.5	34.5	34.5	34.5	34.5	34.5	34.5	34.5	34.5	34.5	34.5	34.5	34.5	34.5	34.5	34.5	34.5	34.5	34.5	34.5	34.5	34.5	34.5	34.5	34.5	34.5	34.5	34.5	34.5	34.5
	7	34.4	34.4	34.4	34.4	34.4	34.4	34.4	34.4	34.4	34.4	34.4	34.4	34.4	34.4	34.4	34.4	34.4	34.4	34.4	34.4	34.4	34.4	34.4	34.4	34.4	34.4	34.4	34.4	34.4	34.4	34.4	34.4	34.4	34.4	34.4	34.4	34.4	34.4	34.4	34.4	34.4	34.4
	8	34.8	34.9	34.9	34.8	34.8	34.8	34.9	34.8	34.8	34.8	34.8	34.8	34.8	34.8	34.8	34.8	34.8	34.8	34.8	34.8	34.8	34.8	34.8	34.8	34.8	34.8	34.8	34.8	34.8	34.8	34.8	34.8	34.8	34.8	34.8	34.8	34.8	34.8	34.8	34.8	34.8	34.8
	9	34.7	34.7	34.7	34.7	34.7	34.7	34.7	34.7	34.7	34.7	34.7	34.7	34.7	34.7	34.7	34.7	34.7	34.7	34.7	34.7	34.7	34.7	34.7	34.7	34.7	34.7	34.7	34.7	34.7	34.7	34.7	34.7	34.7	34.7	34.7	34.7	34.7	34.7	34.7	34.7	34.7	34.7
	10	34.7	34.7	34.7	34.7	34.7	34.7	34.7	34.7	34.7	34.7	34.7	34.7	34.7	34.7	34.7	34.7	34.7	34.7	34.7	34.7	34.7	34.7	34.7	34.7	34.7	34.7	34.7	34.7	34.7	34.7	34.7	34.7	34.7	34.7	34.7	34.7	34.7	34.7	34.7	34.7	34.7	34.7

		PV temperature (deg C), Winter																																								
PV module	1	4.6	4.6	4.5	4.6	4.6	4.6	4.5	4.6	4.6	4.6	4.6	4.6	4.6	4.6	4.6	4.6	4.6	4.6	4.7	4.7	4.7	4.6	4.6	4.6	4.6	4.6	4.6	4.6	4.5	4.4	4.6	4.6	4.6	4.6	4.6	4.6	4.6	4.6			
	2	4.1	4.1	4.0	4.1	4.1	4.0	4.1	4.0	4.1	4.1	4.1	4.1	4.1	4.1	4.1	4.1	4.1	4.1	4.2	4.2	4.2	4.1	4.1	4.1	4.1	4.1	4.1	4.1	4.1	4.0	4.0	4.1	4.1	4.1	4.1	4.1	4.1	4.1	4.1		
	3	3.8	3.8	3.8	3.8	3.8	3.8	3.8	3.8	3.8	3.8	3.8	3.8	3.8	3.8	3.8	3.8	3.8	3.9	3.9	3.9	3.9	3.8	3.8	3.8	3.8	3.8	3.8	3.8	3.8	3.8	3.8	3.8	3.8	3.8	3.8	3.8	3.8	3.8	3.8	3.8	
	4	3.4	3.4	3.4	3.4	3.4	3.4	3.4	3.4	3.4	3.4	3.4	3.4	3.4	3.4	3.4	3.4	3.4	3.5	3.5	3.5	3.5	3.4	3.4	3.4	3.4	3.4	3.4	3.4	3.4	3.4	3.4	3.4	3.4	3.4	3.4	3.4	3.4	3.4	3.4	3.4	3.4
	5	3.2	3.2	3.2	3.2	3.2	3.2	3.2	3.2	3.2	3.2	3.2	3.2	3.2	3.2	3.2	3.2	3.2	3.2	3.2	3.2	3.2	3.2	3.2	3.2	3.2	3.2	3.2	3.2	3.2	3.2	3.2	3.2	3.2	3.2	3.2	3.2	3.2	3.2	3.2	3.2	
	6	3.1	3.1	3.1	3.1	3.1	3.1	3.1	3.1	3.1	3.1	3.1	3.1	3.1	3.1	3.1	3.1	3.1	3.1	3.1	3.1	3.1	3.1	3.1	3.1	3.1	3.1	3.1	3.1	3.1	3.1	3.1	3.1	3.1	3.1	3.1	3.1	3.1	3.1	3.1	3.1	
	7	2.9	2.9	2.9	2.9	2.9	2.9	2.9	2.9	2.9	2.9	2.9	2.9	2.9	2.9	2.9	2.9	2.9	2.9	2.9	2.9	2.9	2.9	2.9	2.9	2.9	2.9	2.9	2.9	2.9	2.9	2.9	2.9	2.9	2.9	2.9	2.9	2.9	2.9	2.9	2.9	
	8	3.3	3.3	3.3	3.3	3.3	3.3	3.3	3.3	3.3	3.3	3.3	3.3	3.3	3.3	3.3	3.3	3.3	3.3	3.3	3.3	3.3	3.3	3.3	3.3	3.3	3.3	3.3	3.3	3.3	3.3	3.3	3.3	3.3	3.3	3.3	3.3	3.3	3.3	3.3	3.3	
	9	3.2	3.2	3.2	3.2	3.2	3.2	3.2	3.2	3.2	3.2	3.2	3.2	3.2	3.2	3.2	3.2	3.2	3.2	3.2	3.2	3.2	3.2	3.2	3.2	3.2	3.2	3.2	3.2	3.2	3.2	3.2	3.2	3.2	3.2	3.2	3.2	3.2	3.2	3.2	3.2	3.2
	10	3.2	3.2	3.2	3.2	3.2	3.2	3.2	3.2	3.2	3.2	3.2	3.2	3.2	3.2	3.2	3.2	3.2	3.2	3.2	3.2	3.2	3.2	3.2	3.2	3.2	3.2	3.2	3.2	3.2	3.2	3.2	3.2	3.2	3.2	3.2	3.2	3.2	3.2	3.2	3.2	3.2